THE UNIVERSITY OF HULL

# Fabrication of Novel Functional Anisotropic Micro-particles for Foam Stabilisation and Structuring in Food Formulations

being a Thesis submitted for the Degree of Doctor of Philosophy in the University of Hull

by

Andrew Lee Campbell, MChem (Hons)

June 2009

**ACKNOWLEDGEMENTS**

I would like to thank my supervisor, Dr Vesselin N. Paunov for his encouragement and help during the last three and a half years. Without the great ideas and guidance I would not have been able to produce this work. Many thanks. I would also like to give thanks to Dr Simeon Stoyanov for his support and useful discussions. I am grateful to the University of Hull for provision of a studentship and to the EPSRC, Unilever Research, Vlaardingen, The Netherlands and Chemistry Innovation Knowledge Transfer Network for provision and arrangement of funding for this work.

It has been both a pleasure and a privilege to work in the Surfactant and Colloid Group for the past years, and I express my sincere thanks to all members. In particular I would like to thank Will, Nae-Gyu and Ben for making me laugh, especially when things were not going well! Special thanks also to Anaïs, Mark, Emma, Jhonny, Ryo, Amro and Olivier for making the laboratories a nicer place to be. In addition I am grateful to Tim for technical assistance and advice over my research period in the group and to Janice Halder and especially Tony Sinclair for operating TEM and SEM apparatus respectively.

Finally I would like to thank my friends and family. Without your support I certainly would not have been able to get this far. So thank you Alan, Gill, Ben, Carl, Andrew, Θεώνη, Andrew, Philippa, Rishi, Karl, Adam, Alex, Jon and Michael. See you all soon.

## PUBLICATIONS AND PRESENTATIONS

The work presented in this thesis has given rise to the following articles and presentations in the journals and conferences listed below:

**'Scalable fabrication of anisotropic micro-rods from food-grade materials using an in-shear-flow dispersion solvent attrition technique'.** A.L. Campbell, B.L. Holt, S.D. Stoyanov, V.N. Paunov. *J. Mater. Chem.,* 2008, **18,** 4047.

**'Fabrication of functional anisotropic food-grade micro-rods with micro-particle inclusions with potential application for enhanced stability of food foams'.** A.L. Campbell, S.D. Stoyanov, V.N. Paunov. *Soft Matter,* 2009, **5,** 1019.

**'Novel multifunctional micro-ampules for structuring and encapsulation'**, A.L. Campbell, S. D. Stoyanov and V. N. Paunov, *Chem. Phys. Chem.*, 2009, accepted.

Poster entitled **'Fabrication of novel, food-grade micro-rods for stabilisation of edible foams'** at the annual CIKTN Associates Meeting, Vanbrugh College, University of York, March 2009.

Presentation entitled **'Novel anisotropic solid stabilisers from edible materials'** at the annual Surfactant and Colloid Group Workshop at the University of Hull, 2006.

Presentation entitled **'Fabrication of novel functional anisotropic micro-particles for foam stabilisation and structuring in food formulations'** at Unilever, Vlaardingen, The Netherlands, May 2009.

**ABSTRACT**

This thesis is concerned with the fabrication of novel food-grade anisotropic solid particles for foam stabilisation and applications in food formulations. Two main techniques were employed for the fabrication of these particles. Acidic hydrolysis of Nata de Coco bacterial cellulose was used to form cellulose nano-rods which were applied as a foam scaffolding material. Characterisation and modification of Nata de Coco nano-rods was also carried out. It was found that cellulose nano-rods modified with a surface layer of ethyl cellulose exhibited good foamability.

Secondly, a combination of in-shear-flow dispersion and solvent attrition techniques were employed to form micro-rods from the edible polymeric materials shellac, ethyl cellulose and zein. Characterisation of the properties of shellac, ethyl cellulose and zein micro-rods was carried out, together with assessments of their foam stabilisation ability. Stable aqueous foams were produced using shellac, ethyl cellulose and zein micro-rods as stabilisers, and ethyl cellulose micro-rods were also used to form water-in-oil emulsions.

An extension of this technique was used in the fabrication of novel functional anisotropic food-grade micro-rods with micro-particle inclusions giving altered morphology. Enhanced foamability and drainage retardation was achieved using lumpy yeast-shellac micro-rods to stabilise aqueous foams. The method was extended to the production of aqueous dispersions of ballooned micro-rods, formed by two different protocols.

This procedure also allowed the formation of novel, dual-function micro-rod capsules or ‘micro-ampules’ for stabilisation and encapsulation by inclusion of oils into the dispersed phase prior to micro-rod fabrication. The oils became trapped within the micro-rods resulting in micro-ampules with a range of morphologies which were characterised by fluorescence doping and microscopy.

**CONTENTS**

# CHAPTER 1 – INTRODUCTION: COLLOIDS, THEORY OF FOAMS, PARTICLE-STABILISED EMULSIONS AND FOAMS, AND FOOD COLLOIDS

This chapter will introduce the background necessary for the reader to be lead through the following experimental and results chapters. Starting with introductory theory and some typical examples, this section will then move on to some of the important features of colloidal systems. The introduction will then consider foams and particle-stabilised emulsions and foams. Discussion of the chosen materials for the research is presented in the introductory sections of the relevant results chapters. Finally, these systems will be considered within the context of food science applications, where the characteristics of surfactants, particles and protein-based stabilisation are introduced.

## 1.1. Introduction to colloids

Colloids are mixtures of two immiscible phases, a dispersion of one in the other, comprising a continuous phase, and a disperse phase. Particle size for the disperse phase ranges from a few nanometres up to several microns. Some typical examples of colloids together with their constituent dispersed and continuous phases are shown in table 1.1. Colloidal systems are characterised by their large interfacial area. This arises due to the finely-divided nature of the dispersed phase. For example, if the 1 mL oil phase of a 2 mL oil-in-water emulsion is sheared at high speed to form monodisperse drops with average diameter 1 micron, the resulting interfacial area between the two phases increases from approximately 1 $cm^2$ ($1x10^{-4}$ $m^2$ - dependent upon the shape of the vessel) to about 6 $m^2$ – a factor of 60,000 increase. This may be calculated as follows:

$$V_{oil\ drop} = \frac{4\pi r^3}{3} \quad [1.1]$$

$$S.A._{oil\ drop} = 4\pi r^2 \quad [1.2]$$

$$\frac{V_{oil\ phase}}{V_{oil\ drop}} = number\ of\ droplets \quad [1.3]$$

$$S.A._{oil\ drop} \times number\ of\ droplets = \text{total interfacial area} \quad [1.4]$$

where *V* represents volume, *S.A.* is surface area and *r* is the droplet radius, in this case, 0.5 µm. This large surface area can give colloidal materials interesting properties which can be very different to the bulk properties of the same materials.

| ***Continuous phase ↓*** | ***Dispersed phase →*** | **Gas** | **Liquid** | **Solid** |
|---|---|---|---|---|
| **Gas** | | ---------- | Aerosol (e.g. spray deodorant) | Solid aerosol (e.g. dust or smoke) |
| **Liquid** | | Foam (e.g. fire extinguisher foam, beer head) | Emulsion (e.g. cosmetics, foods-milk, butter, agrochemical formulations) | Sol (e.g. toothpaste, paint) |
| **Solid** | | Solid foam (e.g. bread, cake) | Solid emulsion (e.g. opal) | Solid dispersion (e.g. an alloy) |

**Table 1.1. Examples of different types of colloids together with their dispersed and continuous phases.**

The preparation of colloidal systems involves the creation of a large surface area, resulting in a large surface free energy. The surface tension or surface free energy is defined as the isothermal reversible work of forming unit area of interface. Surface free energy may be explained by considering the difference in energy between molecules at the surface and those in the bulk. If the interactions of the molecules in the pure liquid or solid bulk phase in equilibrium with its vapour are considered in terms of pair interaction energy $W_{AA}$ (the

microscopic interaction energies of pairs of like molecules A and A) then the energy $E_{A,bulk}$ per molecule in the bulk phase is

$$E_{A,bulk} = \frac{z_b}{2} W_{AA} \quad [1.5]$$

where $z_b$ is the number of nearest neighbours in the bulk phase. For molecules at the surface

$$E_{A,s} = \frac{1}{2} z_s W_{AA} \quad [1.6]$$

where $z_s$ is the number of nearest neighbours for a surface molecule. As $W_{AA}$ is negative and $z_b > z_s$, moving a molecule from the bulk to the surface increases the internal energy. In other words, work must be done to create new surface. The energy $E_s$ required to create an area $A$ is then

$$\frac{E_s}{A} = \left(\frac{E_{A,s} - E_{A,bulk}}{a_0}\right) = \frac{1}{2} \frac{W_{AA}(z_s - z_b)}{a_0} \quad [1.7]$$

where $a_o$ equals the area per molecule at the surface.[1]

Adsorption of surfactants or particles reduces the total surface energy. Surfactants are amphiphilic molecules which possess a hydrophilic head and hydrophobic tail and when adsorbed at a liquid interface, the molecule orientates with the hydrophilic group towards the aqueous phase. Usually the tail is a hydrocarbon chain, although for block copolymer surfactants (for example polyethylene oxide/polypropylene oxide (PEO/PPO)) the tail is simply the most hydrophobic part of the polymer, and there may be many sections of the polymer that adsorb, rather than a single tail. The surfactant head group may be formed from a variety of different chemistries. Anionic surfactants may have a sulphate group together with a stabilising metal cation (e.g. sodium dodecyl sulphate), cationic surfactants may have a quaternary ammonium ion together with a stabilising halogen anion (e.g. cetyl trimethylammonium bromide), whereas non-ionic surfactants can often feature a polyethylene oxide chain of varied length as the head group.

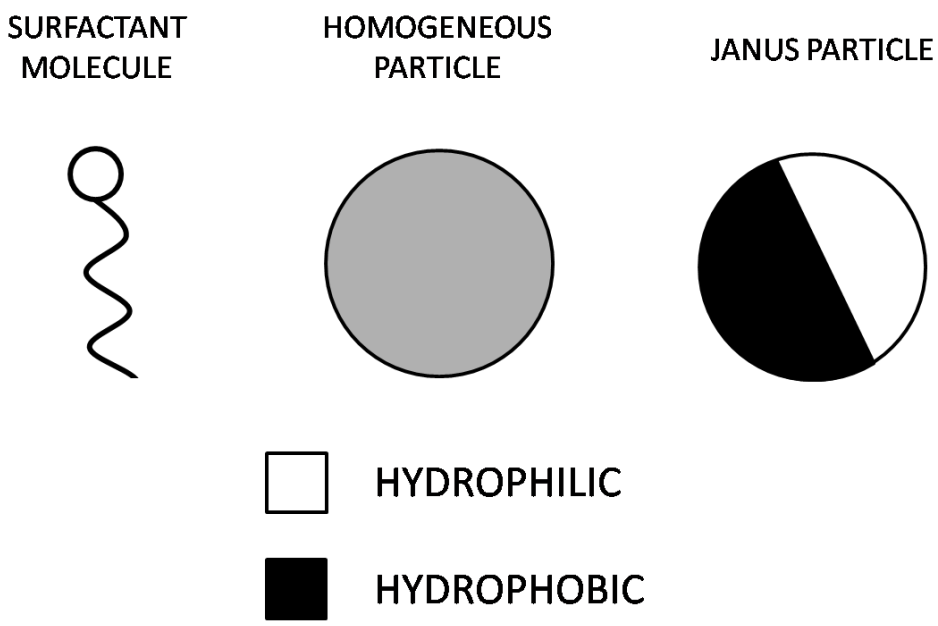


**Figure 1.1. Examples of surface-active agents used to stabilise emulsions and foams. Surfactant molecules commonly comprise a hydrophilic head group together with a hydrophobic tail and can adsorb at interfaces. Janus particles are solid particles, but with a similar amphiphilic structure, comprising two hemispheres of different wettabilities. Homogeneous particles use specific tuning of the chemistry of surface groups to vary wettability.**

Surfactants diffuse to the interface very quickly due to their small size, and are considered to adsorb and desorb on a rapid timescale.[2,3] As the concentration of surfactant added to a solution is increased, eventually the interface becomes saturated, and further surfactant molecules enter into the bulk solution. Above the critical micelle concentration the surfactant molecules self-assemble into structures and the hydrophobic tails can aggregate in the centre of the structure, shielding them from the hydrophilic bulk and creating a hydrophobic mini-environment within. The morphology of micelles is dependent upon the molecular structure of the component surfactant molecules. This aggregation process is driven by an entropic increase of the solvent.

Solid particles (fig. 1.1) stabilise in a different manner to molecular surfactants. Particles of the correct wettability (characterised by the 3 phase contact angle – section 1.3) adsorb at the interface due to the favourability of removing a relatively large area of high interfacial tension (high surface free energy). Due to the magnitude of this energy, they are often considered to be irreversibly adsorbed, and can be excellent stabilisers of emulsions and foams. A slightly different type of solid particle is the 'Janus' particle, so-named because it possesses two different faces like the Roman god Janus and many techniques exist for the preparation of these particles.[3-5] Janus particles exhibit an amphiphilic structure like molecular surfactants, with one hydrophobic side and one hydrophilic side, thus the particle should adsorb at the interface. In fact it has been shown by Binks and Fletcher[6] in a theoretical study that amphiphilic Janus particles can attach to an interface up to three times more strongly than equivalent homogeneously-coated surface-active particles at intermediate values of contact angle (~90º), with the greatest differences being observed at extreme contact angles, where homogeneously-coated particles tend to attach weakly. As well as for interfacial stabilisation purposes, particles with such anisotropy could have great potential use for the fabrication of colloidal/optical crystals and sensors.

### 1.1.1. Colloidal stability

A principal factor behind the behaviour of many colloidal systems originates from the electrical properties of the suspension. When a solid particle enters a polar medium such as water, it may obtain a surface charge. This occurs either by ion adsorption - unequal adsorption of counter-ions, ion dissolution - unequal loss of surface ions, or ionisation.[7] The result of this is an uneven distribution of co-ions and counter-ions in the immediate vicinity of the particle surface called the electrical double layer (EDL). It is called a double layer due to the two-tiered structure including a denser layer of counter-ions very near to the surface, together with a more diffuse outer region, comprising a mixture of co- and counter-ions. A schematic depiction of the structure of the EDL is shown in fig. 1.2.

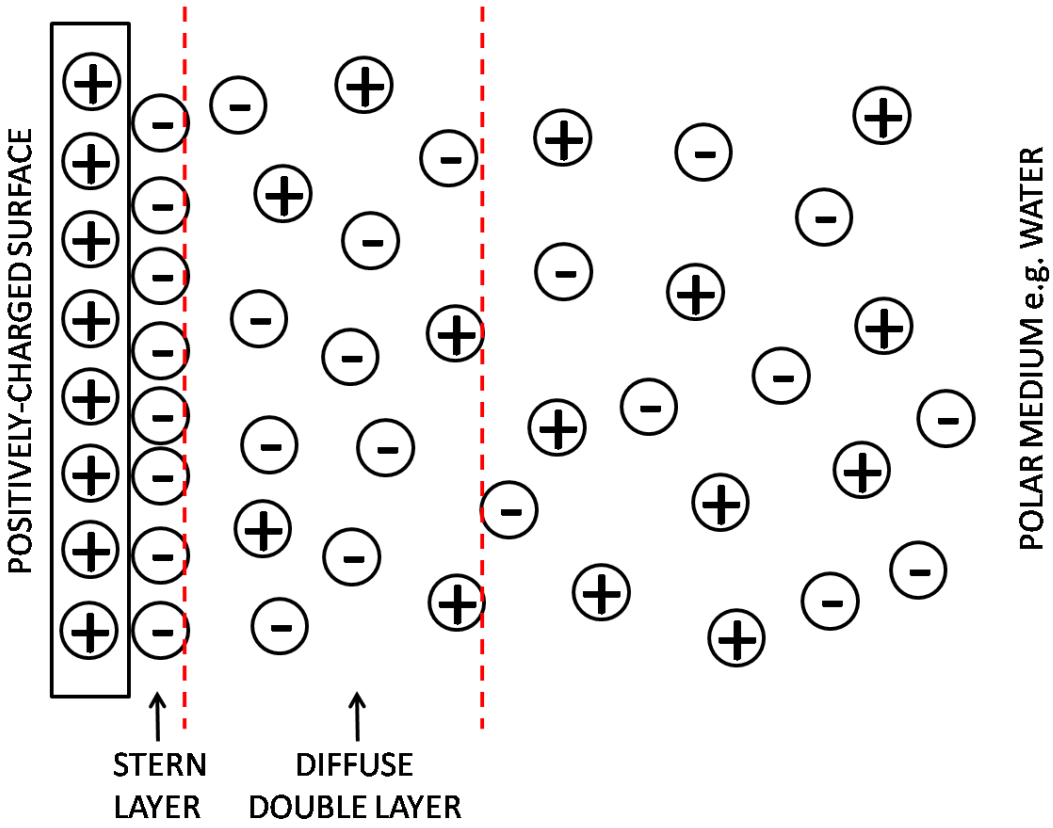


**Figure 1.2. Schematic representation of the Stern model of the electrical double layer, comprising a positively-charged flat surface, considered to be of infinite dimension and uniform charge, closely associated Stern layer of counter-ions and the diffuse double layer.**

The fixed, inner layer or Stern layer is a region of high potential, and the electrostatic force holding the charges there is such that some counter-ions may be considered to be attached and are not affected by thermal motion. The composition of the diffuse outer layer is governed by two competing factors, the electrostatic attraction of counter-ions to the oppositely-charged surface, and thermal motion, which leads to the ions being spread evenly throughout the medium. The electrical potential as a function of distance from the surface is shown in fig. 1.3.

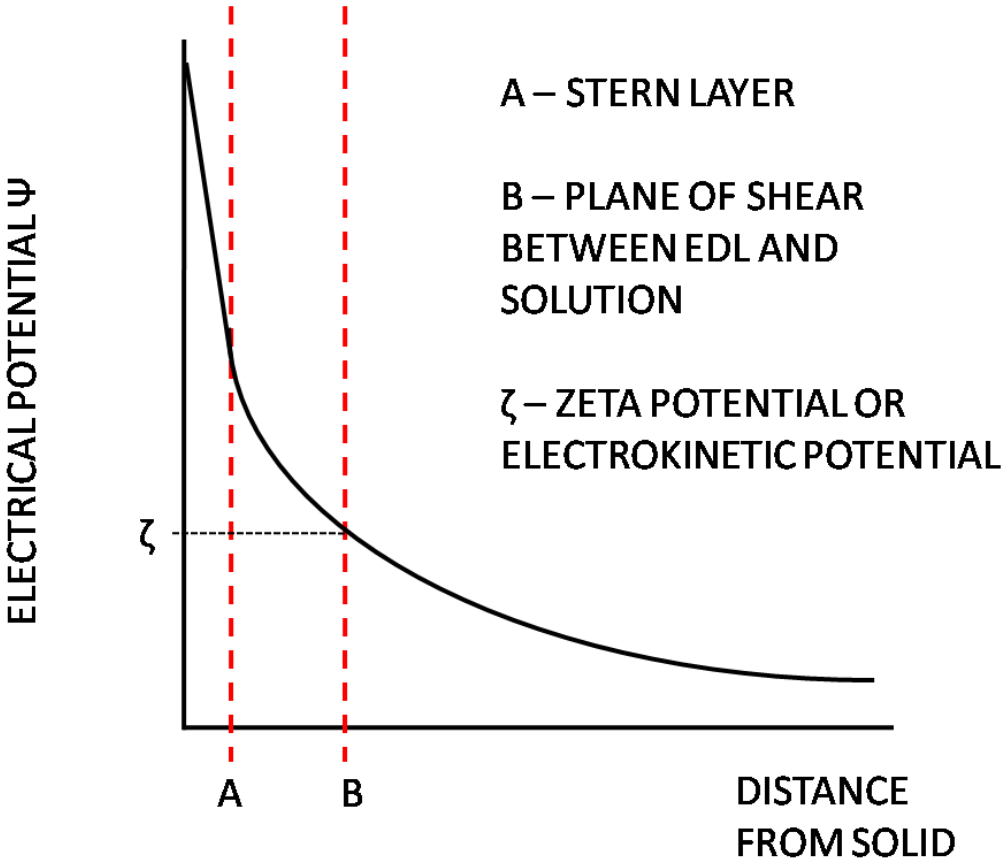


**Figure 1.3. Plot of electrokinetic potential vs. distance from the solid surface. Electrical potential decreases with distance from the surface. At the plane of shear between the solution and the solid surface's associated ionic environment, the electrical potential is referred to as the zeta potential or 'electrokinetic' potential.**

Within the diffuse part of the EDL, if we consider the ions to be point charges which obey a Poisson-Boltzmann distribution, then at a proximity to the surface where the electrical potential equals $\psi$, the number of positive or negative ions in a specific volume is described as follows:

$$n_+ = n_0 \exp(-ze\,\psi/kT) \qquad [1.8]$$

$$n_- = n_o \exp(+ze\,\psi/kT) \qquad [1.9]$$

where $n_o$ represents the bulk concentration of either species. If the surface is positively charged (as in fig. 1.4) then there will be excess negatively-charged ions in the solution in the vicinity, but further away the concentrations of positive and negative ions eventually become equal. The thickness of the diffuse double layer is of the order of the Debye screening length, $\kappa^{-1}$. The electrical potential at the plane of shear between the solution and the environment of associated ions which move with the solid (shown schematically in fig. 1.4) may be defined as the zeta ($\zeta$) potential. It can be measured by applying an electrical field to the colloidal dispersion and recording the mobility of the particles.

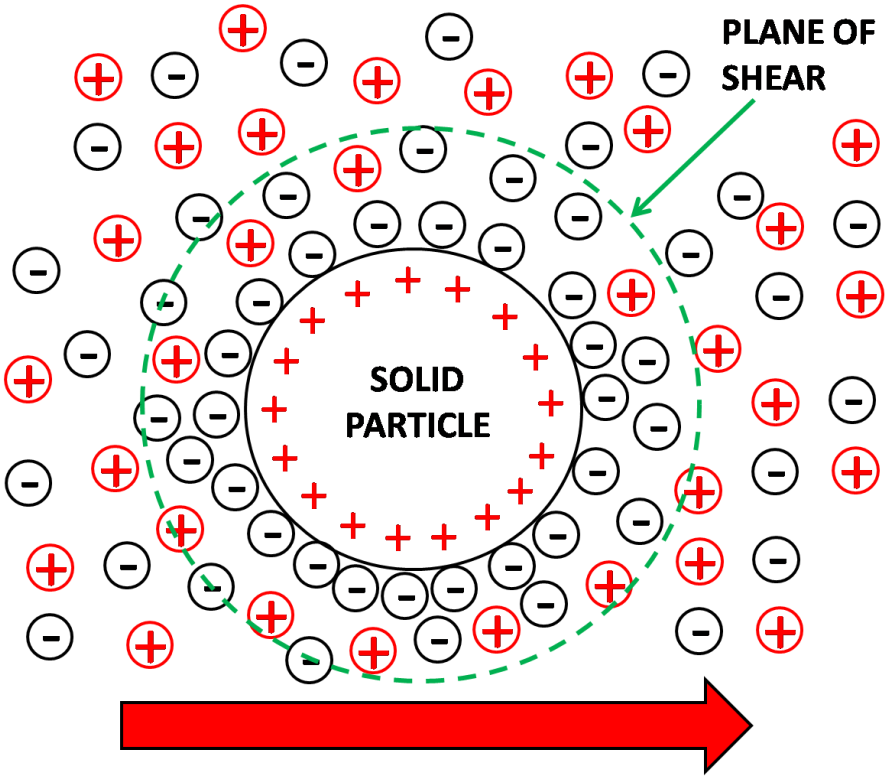


**Figure 1.4. A solid particle with positive surface charge moves through solution, taking with it its associated environment of counter-ions and diffuse outer layer of counter- and co-ions. The electrical potential at the plane of shear between this moving unit and the solution is referred to as the zeta potential.**

As the solid particles with acquired surface charge move around in a dispersion due to thermal motion – Brownian motion, they interact with other particles, and the resulting behaviour is complicated by the contribution of several effects. The DLVO theory was developed by Derjaguin and Landau[8], and by Verwey and Overbeek[9]; this theory aims to combine the electrostatic interactions of approaching particles (with their double layers) along with the van der Waals forces experienced, to enable some predictions to be made about the stability of a given system.

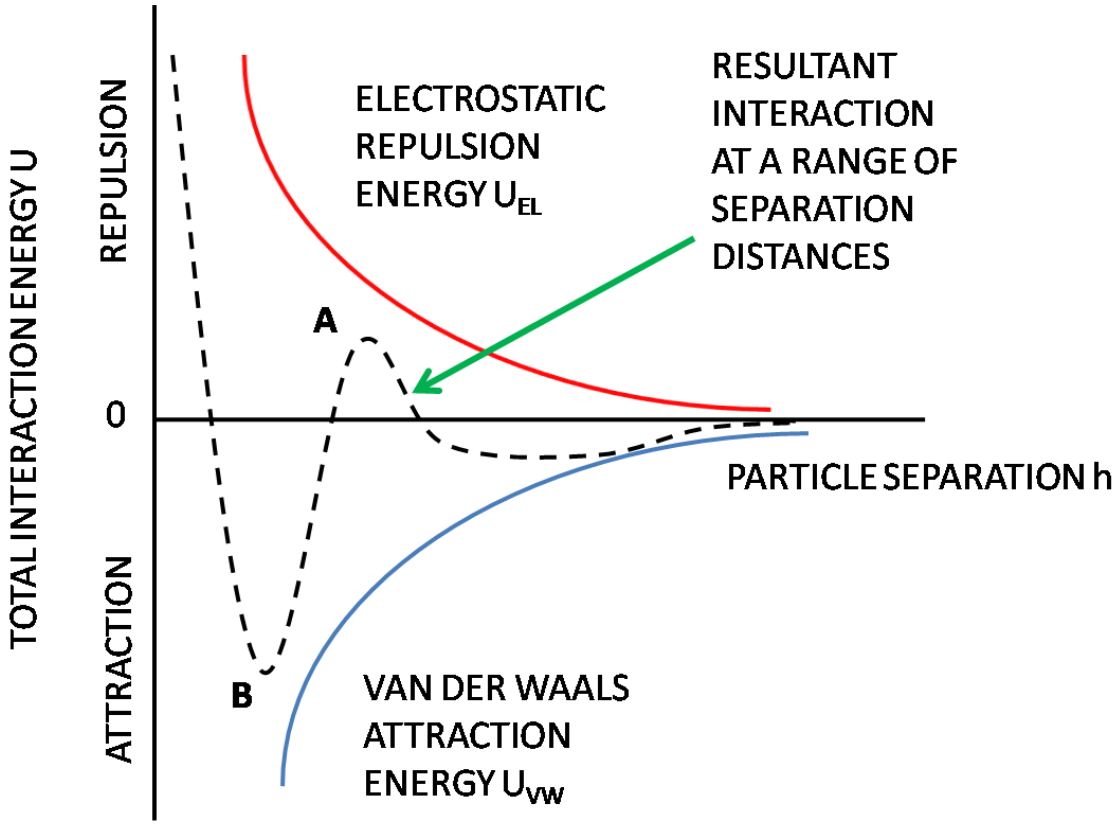


**Figure 1.5. Graph of interaction energy for two particles in suspension at a range of separations showing the electrostatic repulsion, the van der Waals attractive forces and the sum of both (broken black curve). Point A indicates the potential energy maximum below which the particles do not come together due to electrostatic repulsive forces, and the dispersion remains stable. If this peak can be overcome, then the attractive van der Waals forces bring the particles together, causing instability of the colloid (B).**

Van der Waals forces represent the average dipole-dipole interaction between molecules. They are comprised of contributions from three effects: orientation of molecules with permanent dipoles, induction interaction between one molecule with a permanent dipole and one with an induced dipole, and a dispersion interaction between two induced dipoles. The potential energy of interaction $U_{ab}(r)$ due to van der Waals forces between two molecules *a* and *b* separated by distance *r* is

$$U_{ab}(r) = -\frac{\alpha_{ab}}{r^6} \qquad [1.10]$$

where $\alpha_{ab}$ is a constant that characterizes the interaction. The van der Waals interaction between larger particles can be obtained by integrating the above equation over all couples of interacting molecules and then subtraction of the interaction energy at infinite separation between the particles. The result is particle geometry dependent.[15]

Addition of electrolyte causes screening of the electrostatic repulsion, but does not affect the van der Waals forces, giving a net attraction and leading to destabilisation of the colloid. Increasing the charge number of the ion (e.g. 2+, 3+) gives an even more powerful charge-screening effect (Schulze-Hardy rule – section 1.3.1).

## 1.2. Foams

A foam may be defined as a coarse dispersion of gas in a continuous phase (solid or liquid). Unlike for other colloidal systems like emulsions and sols, it is the continuous phase in foams which possesses colloidal dimensions. Due to the interfacial tension, foams are thermodynamically unstable, and if their lifetime is to be any more than transient, an extra, surface-active component should be added. Immediately after preparation, approximately spherical gas bubbles separated by thick layers of liquid are present. These rise rapidly by gravity, and in turn, the liquid which separates the gas bubbles towards the top of the foam drains by gravity. Eventually this leads to the formation of an arrangement of polyhedral gas cells, separated by thin liquid films. Both extremes are shown highly schematically in fig. 1.6.

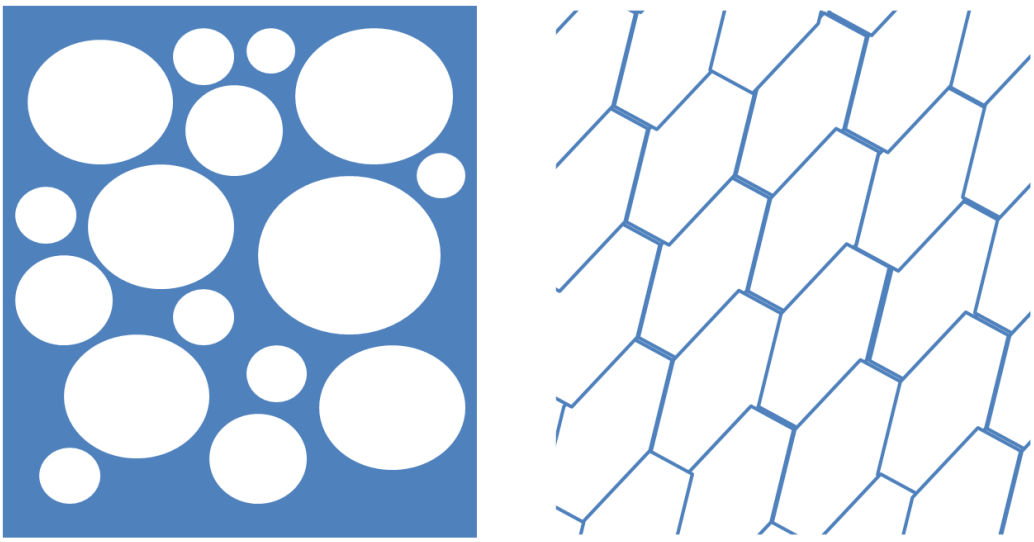

**Figure 1.6. Schematic diagram illustrating the dilute or 'wet' foam structure (left) of roughly spherical gas bubbles separated by thick liquid films and concentrated or 'dry' foam structure (right) of polyhedral gas cells separated by thin liquid films.**

Recently there has been great interest in aqueous foams stabilised by solid particles only[10-12,16-18, 23,24,29,30,33,34], and the aim of this study is to successfully stabilise aqueous foam using food-grade anisotropic solid particles. In view of this, the main factors affecting foam stability will be examined.

The principal processes of destabilisation in foams are drainage, disproportionation, thinning/rupture of the liquid films and bubble coalescence. Drainage involves the flow of continuous phase liquid through the network of thin films and Plateau borders which runs throughout the structure of a foam principally by gravity, and then by capillary suction within the Plateau borders (fig. 1.7).[13] One way that flow through the Plateau borders by gravity may be retarded is by increasing the viscosity of the continuous phase, so that the foam film thinning is heavily retarded and gas bubbles are separated by much thicker films.

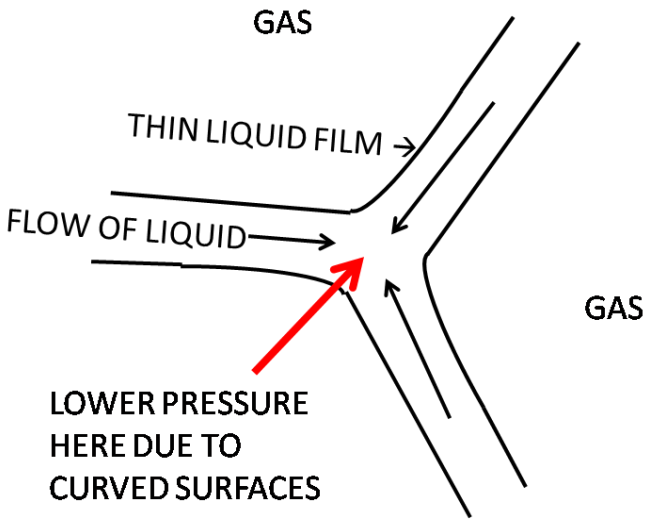


**Figure 1.7. Schematic diagram showing liquid flow in the region of a Plateau border. At the intersection of three thin liquid films (the Plateau border) curvature creates a pressure gradient which causes the liquid in the films to flow towards the Plateau border. This causes film thinning, and this thinning continues until counteracted by the disjoining pressure.**

In order to increase foam lifetimes, the rate of drainage of liquid through the foam films and Plateau borders must be reduced. During the drainage of a foam, the liquid films are subject to stresses which can cause a local increase in the surface area, and because the concentration of surface active solute there is unchanged at that moment, there is a local increase in the surface tension. In response to this surface tension gradient, surfactant molecules migrate to the area of higher tension to restore film equilibrium, and drag along an appreciable quantity of underlying continuous phase, restoring film thickness. This phenomenon is known as the Gibbs-Marangoni effect.[9]

A key factor in the destabilisation of foams, disproportionation is the transfer of gas from small to larger bubbles in the foam through the continuous phase, resulting in the shrinkage/disappearance of smaller bubbles.[19] This is analogous to the process of Ostwald ripening in emulsions.[14] Pressure difference across the bubble interface due to curvature may be described by the Young-Laplace equation

$$\Delta P = \gamma\left[\frac{1}{R_1} + \frac{1}{R_2}\right] \quad [1.11]$$

where ΔP represents the pressure difference across the curved interface, γ is the interfacial tension and $R_1$ and $R_2$ represent the two radii of curvature (of the inner and outer surfaces). At large interfacial curvatures the Laplace pressure promotes the solubility of the gas in the continuous phase. In the foam this causes a transfer of gas by diffusion from smaller bubbles to larger bubbles of lower surface curvature. This process is only halted when the films become flat. Increasing the surface viscosity and or surface elasticity by using high surfactant concentrations, and mixed surfactant systems at the interface gives a condensed film which can oppose the bubble dissolution.[15] This may also be achieved by adsorption of proteins or polymeric stabilisers. Kloek et al. comment however that interfacial viscosity may retard bubble dissolution, but it cannot stop it.[15] It has been demonstrated though, that solid particles are able to halt disproportionation all together[22] by jamming at the interface due to irreversible adsorption, preventing further bubble shrinkage. In this way, non-spherical bubbles have been produced.[21] For this reason solid particles have received a lot of attention in the pursuit for better foam stabilisers.

In order to further understand the forces acting within foams and the processes which occur during destabilisation, it is necessary to consider the interactions within the thin liquid films which comprise the bulk foam structure.[16] During the lifetime of a foam, the thin films which separate the polyhedral gas cells thin due to drainage of the continuous phase caused by gravity and capillary suction. It is when films thin too much that they become vulnerable to rupture. The film thinning is influenced by the disjoining pressure, Π. This excess pressure is composed of contributions from electrostatic and van der Waals interactions. The contribution of van der Waals disjoining pressure in a thin (plane–parallel film) is,

$$\Pi_{vw}(h) = -\frac{A_H}{6\pi h^3} \quad [1.12]$$

where $A_H$ is the Hamaker constant. The contribution of the electrostatic disjoining pressure is,

$$\Pi_{el} \approx 64 n_0 kT \gamma^2 e^{(-\kappa h)} \qquad [1.13]$$

where $n_0$ is the bulk concentration of the electrolyte ions and κ is the Debye-Hückel screening parameter which determines the range of electrostatic interactions in colloidal systems. $\Pi_{el}$ is repulsive for thin films of symmetrical surfaces. A typical example is the repulsion of opposing layers when ionic surfactant head groups are present.

In conclusion, the stabilisation of foams requires us to fabricate surface-active particles to adsorb at and preserve the gas-liquid interface, to control the liquid drainage, and to avoid close approach and contact of neighbouring gas bubbles. It is anticipated that anisotropic food-grade micro- and nano-particles could fulfil these criteria.

### 1.3. Particle-stabilised emulsions and foams

Macro-emulsions and foams are both thermodynamically unstable entities, which means that an extra component must be added that lowers the interfacial tension between the two fluid phases due to adsorption. The ability of solid particles to stabilise interfaces was first observed by Ramsden[17] and shortly afterwards, Pickering[18], and are known in the literature as 'Pickering emulsions'. Since then the field has grown considerably, and currently many reports detailing the phenomenal stability of particle stabilised emulsions and an increasing number on foams have been presented.[2,19-27] A critical parameter for the stabilising ability of small solid particles is the three phase contact angle the particle makes at the interface (fig. 1.8).

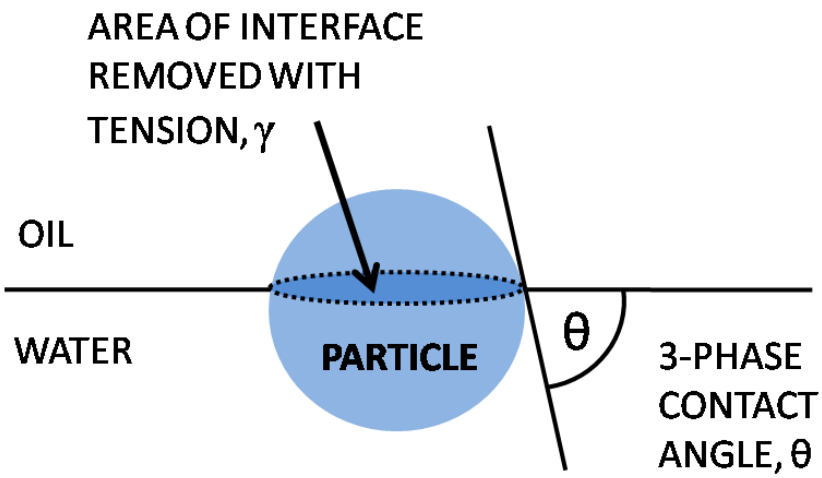


**Figure 1.8. Solid spherical particle adsorbed at the oil-water interface with three phase contact angle θ. This angle is commonly measured through the more polar fluid. Solid particles such as this remain attached to the liquid interface due to the relatively large area of high energy interface which has been removed upon their adsorption.**

The contact angle of a solid particle is related to the interfacial tensions (or surface free energies) between the three phases by Young's equation:

$$\gamma_{SV} = \gamma_{SL} + \gamma_{LV}\cos\theta \qquad [1.14]$$

where $\gamma_{SV}$, $\gamma_{SL}$ and $\gamma_{LV}$ are the interfacial tensions between the solid-vapour, solid-liquid and liquid-vapour interfaces respectively and θ is the three phase contact angle[28]. Normally this is measured through the more polar liquid. Particles with large contact angles (>90º) are deemed hydrophobic and tend to stabilise w/o systems, where particles with contact angles less than 90º are hydrophilic and tend to stabilise o/w systems. Contact angle is one of the important factors that determine the attachment energy of a colloidal particle; the other is particle size. Equation 1.15 shows that larger particles possess greater energies of detachment from the interface due to the larger area of high energy interface they can remove once adsorbed. Conversely, if we decrease the diameter of a colloidal particle down to approximately that of a surfactant molecule then the energy of attachment would drop

significantly, so that adsorption may be less favourable. The energy of removal of a spherical colloidal particle in the absence of gravity effects can be calculated as follows:

$$E = \pi r^2 \gamma_{\alpha\beta}(1 \pm \cos\theta)^2 \qquad [1.15]$$

where $r$ is the radius of a spherical particle, $\gamma_{\alpha\beta}$ is the interfacial tension of the phase α/phase β interface and θ is the three phase contact angle of the particle.[29] The sign in the brackets is positive for removal of the particle into the hydrophobic (gas or oil) phase and negative for removal into the aqueous phase. This thesis, however, is concerned with the fabrication of anisotropic (in shape) particles for foam stabilisation, and therefore clearly for geometric reasons the above equation for the energy of particle detachment from an interface does not hold. For a rod-shaped particle (with hemispherical ends), (pictured in fig. 1.9) the free energy of detachment into the water and oil phases is described in equations 1.16 and 1.17 respectively.[30]

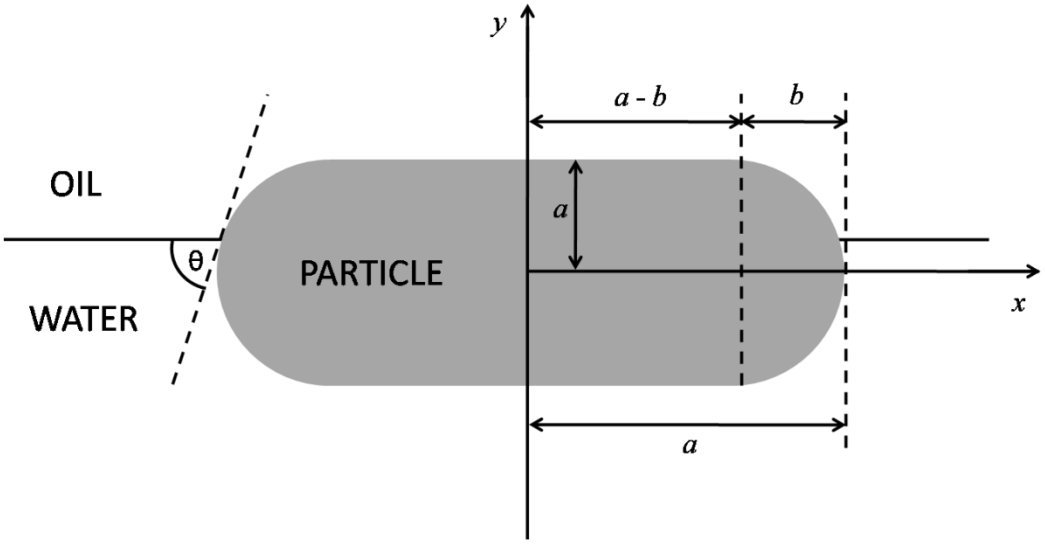


**Figure 1.9. Schematic diagram of a rod-shaped particle with hemispherical ends adsorbed at the oil-water interface with three phase contact angle, θ.[31]**

$$\Delta G_{dw} = \gamma_{ow} \pi b^2 (1\text{-}\cos\theta)^2 \left[1 + \frac{4\left(\frac{a}{b} - 1\right)(\sin\theta - \theta\cos\theta)}{\pi(1-\cos\theta)^2}\right] \quad [1.16]$$

$$\Delta G_{do} = \Delta G_{dw} + 4\pi\, \gamma_{ow}\, b^2 \cos\theta\, (a/b) \quad [1.17]$$

According to equations 1.16 and 1.17, rod-shaped particles adsorb more strongly at the interface than a spherical particle of the same volume: this can be attributed to increased interfacial coverage-per-volume of rod-like particles, assuming they adsorb parallel to the interface.[31] The efficacy of rod-shaped particles in stabilising aqueous foams has been demonstrated by Alargova et al.[32-24] They have shown that micron-sized hydrophobic polymer micro-rods are able to give outstanding levels of foam stability, giving resistance to foam drainage and coalescence, even under aggressive drying and vacuum conditions. Aside from increased surface area per unit volume (compared with similar particles of spherical shape) a principal reason for this enhanced stability is the ability of high aspect ratio particles to intertwine at the interface, giving additional steric stability and forming solid 'cages' upon drying. For this reason, the foams formed were deemed to be 'superstabilised'. The aim of this thesis is to develop hydrophobic micro-rods from food-grade materials which are capable of stabilising food foams.

### 1.3.1. Surface charge and background electrolyte

The importance of electrostatic phenomena on the stabilising effect of colloidal particles has been highlighted in numerous studies.[27,39-41] Stabilisation using solid particles involves the close approach and attachment of colloidal particles at interfaces, and so electrical double layer effects are extremely important to consider. It has already been stated that bulk electrolyte has the ability to screen electrostatic repulsions between charged particles, and the effect of ionic charge number is very pronounced (Schulze-Hardy rule). The 'critical coagulation concentration' (or C.C.C.) of electrolyte can be expressed as follows:

$$\text{C.C.C.} = \frac{84\varepsilon^3(kT)^5}{A_H^2 e^6 Z^6} \qquad [1.18]$$

where $\varepsilon$ is the dielectric constant of the continuous medium, $k$ is the Boltzmann constant, $T$ is the absolute temperature, $A_H$ is the Hamaker constant, $e$ is the electron charge and $Z$ is the counter-ion valency (e.g. 1, 2, 3). Equation 1.18 shows that increasing the charge number has a dramatic effect as it is raised to the sixth power. This effect was observed by Golemanov et al.[23], who used polystyrene latex particles with sulphate surface groups to stabilise water-in-oil emulsions. These systems did not conform to Bancroft's rule, where the stabiliser will be most soluble prior to emulsification in the continuous phase. Here it was found that emulsions containing $Na^+$, $Mg^{2+}$ and $Al^{3+}$ ions allowed stable water-in-oil emulsions to be formed with proportionally decreasing salt concentrations in agreement with the Schulze-Hardy rule. Conversely, Kostakis et al. found this effect not to be evident in silica nano-particle-stabilised aqueous foams which contain relatively high salt concentrations. However, they observed that NaCl between concentrations of 0.5 and 3 M seemed to increase the effective contact angle of hydrophilic silica particles, giving increased adsorption power. This was accompanied by the formation of so-called 'weak particle gels' formed by high concentrations of particles interacting in a network throughout the bulk system facilitated by the high salt concentrations. A number of studies have been conducted on foams and emulsions stabilised by charged colloidal particles.[35-37] Phase inversion of charged particle-stabilised emulsions can be induced[29] by altering the surface charge on the stabilizing particles by altering either the pH of the bulk or by addition of electrolyte, however this has been shown to be highly dependent on phase volumes used, and on the oil type.[38] If these conditions are not met, then demulsification can occur. Similarly, it is possible for foam-stabilising micro- and nano-particles to be rendered non-surface active and therefore totally ineffective by raising the system pH above their isoelectric points giving them overall negative charge. They are then repelled from the negatively-charged air/water interface, obstructing their adsorption.[30,31,39]

## 1.4. Stabilisation of emulsions and foams in food formulations

The aim of this thesis is to produce anisotropic micro-particles which could have great potential in the food industry, therefore it seems appropriate to give a brief introduction discussing some common food types which are based on foams and emulsions and how they may be stabilised. Emulsions and foams play a very important role in food formulations. Examples of food formulations which are based on emulsions and foams are many. Milk is an oil-in-water emulsion stabilised by casein micelles, whereas margarine is a water-in-oil emulsion stabilised by fat crystals. Bread, meringue and cake are all foams, however their shelf lives can be enhanced due to the solidification of the continuous phase that occurs through baking.[22] It has been noted however, that it is a challenge to maintain stability during these procedures even though the final product displays an elastic continuous phase which may halt disproportionation altogether.[40] Ice-cream is both an emulsion and a foam, stabilised by fat crystals, and is frozen, retarding the destabilisation processes.

Stabilisation of food formulations is complicated due to the confinement of using only ingredients which are food-grade. This means that many useful and effective additives which are used in other formulations may not be applicable. One specific example is cationic surfactants. The food grade ingredients which have been chosen for use in this study include shellac, bacterial cellulose, ethyl cellulose and zein. Shellac and zein are already commonly used as coatings for food and have been referred to as 'confectioner's glaze'. Nata de Coco is a popular delicacy in the Far East and Ethocel™ is a food-grade additive.[41]

The surface active agents which may be chosen for the stabilisation of foams or emulsions include small molecular surfactants, proteins (and polymers) and solid particles. Each of these materials possesses advantages and disadvantages. For example, small molecular surfactants such as Spans or Tweens are powerful emulsifiers due to their rapid diffusion to the interface. They do not however offer any considerable barrier to droplet close approach and coalescence. Proteins can fulfil both emulsifying and stabilising roles. Although their interfacial adsorption is slower than for small surfactant molecules, an adsorbed protein film at a liquid interface can provide a useful stabilizing surface layer for

enhanced stability. This barrier however, is not able to halt, but only retard disproportionation. Polymers may also give a useful steric barrier preventing the close approach of other drops/bubbles, and reducing the rate of destabilisation by remaining in the bulk, increasing the viscosity of the continuous phase. This retards foam drainage, and typical materials used for this purpose in food formulations include Gum Arabic, or polysaccharides such as carrageenan.

It has been demonstrated recently, that solid particles are able to adsorb (effectively irreversibly) to the liquid/vapour interface and offer complete stability against the process of disproportionation.[9] This is because during the shrinkage of a particle-stabilized bubble, when the interfacial area decreases to an extent where the interface becomes saturated, the shrinkage cannot continue, due to the irreversibly-adsorbed particles not being expelled from the interface. It has been noted, however, that many proteins may exist in the form of nano-particles, either due to self-assembly of molecules, or during processing.[42] This leads to a change in the behaviour of systems stabilised by proteins to that characteristic of emulsions and foams stabilised by conventional solid particles. A useful comparison between the action of surfactants, proteins and colloidal particles is presented by Tcholakova et al.[43] A further observation of systems stabilised by solid particles is the formation of networks of particles in the bulk – so-called 'weak particle gels'[22] which lend a further degree of kinetic stability to the formulations in which it is present. Similar to the effect of including a gelling hydrocolloid in the continuous phase, this slows down the drainage process, and hinders close approach of bubbles in foams.

In summary, stabilisation of food formulations is a complex field. The restrictions on ingredients which may be included together with systems which contain a number of phases or additives make it highly challenging. It is apparent that surface active colloidal particles offer a method to give enhanced levels of stabilisation, and it is anticipated that the novel, food-grade anisotropic particles which are the aim of this study may provide such high levels of foam (or emulsion) stability, in order to have potential utility in food formulations of the future.

## 1.5. Presentation of the thesis

This thesis is concerned with the fabrication of novel anisotropic solid particles from food-grade materials for the purpose of stabilisation of foams in food formulations. Two basic techniques have been used for their fabrication. Firstly, Nata de Coco bacterial cellulose was treated by sulphuric acid hydrolysis to produce cellulose nano-rods and the subsequent foamability testing and modification of this material is described in chapter 3.

The second technique was pioneered by Alargova et al. and is used as a base for the work in the remaining chapters. It is based on in-shear-flow dispersion solvent attrition and is used for the preparation of polymer micro-rods. Shellac, ethyl cellulose and zein are all used for the formation of surface-active micro-rods and their ability to stabilise aqueous foams is assessed in chapters 4, 5 and 6 respectively. A variety of pH and electrolyte combinations are investigated for the optimisation of these foams stabilised by micro-rods. The effectiveness of ethyl cellulose micro-rods for emulsion stabilisation is presented in chapter 5.

Using a modification of the technique described above, the fabrication of shellac and ethyl cellulose functional micro-rods containing particle inclusions is discussed in chapter 7. We envisage that micro-rods which stabilise foams could benefit from the presence of inclusions, to anchor the micro-rods in the foam structure, as well as creating obstructions to the liquid drainage within the foam. Further novel methods to produce functional anisotropic micro-rods are also presented here. Ballooned polymer micro-rods are formed by two different methods. The first involves the encapsulation of copper micro-particles within the micro-rods, before exposing the metal-containing rods to microwave radiation, giving localised heating around the encapsulated copper particles which in turn causes internal expansion which creates micro-lumps and cavities. The second involves the encapsulation of, and subsequent thermal degradation of sodium bicarbonate micro-crystals within ethyl cellulose micro-rods. This also results in the formation of ballooned polymer micro-rods.

Finally, micro-ampules have been fabricated by incorporation of oils into the micro-rod interiors. A variety of systems utilising different capsule wall (micro-rod) polymers, different encapsulated oils and also the effect of surfactants is investigated. It is anticipated

that this simple method of encapsulation could have great potential use in food and pharmaceutical industries. These materials can be used with multiple functions to stabilise and structure on one hand and encapsulate oils on the other.

Finally, conclusions from all work presented in this thesis are drawn, and suggestions for areas of useful future investigation are made.

### 1.5.1. Abbreviations

| Abbreviation | Definition |
|---|---|
| AC | alternating current |
| CMC | carboxymethyl cellulose, critical micelle concentration |
| $CO_2$ | carbon dioxide |
| DCDMS | dichlorodimethyl silane |
| DMSO | dimethylsulphoxide |
| DP | degree of polymerisation |
| DSA | drop shape analyser |
| EC | ethyl cellulose |
| FDA | Food and Drug Administration |
| GRAS | Generally Recognised As Safe |
| GTT | gel trapping technique |
| HCl | hydrochloric acid |
| HLB | hydrophile-lipophile balance |
| HPC | hydroxypropyl cellulose |
| HPMC | hydroxypropylmethyl cellulose |
| kDa | kilo-Dalton |
| KOH | potassium hydroxide |
| M | molar |
| MC | methyl cellulose |
| MCC | microcrystalline cellulose |

| | |
|---|---|
| MWNTs | multi-walled carbon nano-tubes |
| NaCl | sodium chloride |
| $NaHCO_3$ | sodium bicarbonate |
| NDC | Nata de Coco |
| PAH | poly(allylamine hydrochloride) |
| PDMS | poly dimethyl siloxane |
| PEO/PPO | poly ethylene oxide/poly propylene oxide |
| rpm | revolutions per minute |
| SEM | scanning electron microscopy |
| TEM | transmission electron microscopy |
| THF | tetrahydrofuran |
| w.r.t. | with respect to |
| ζ-potential | zeta potential |

### 1.6. References


[1] D. Fennell Evans, H. Wennerström, *The Colloidal Domain*, Wiley-VCH, New York, 1999.

[2] R. Aveyard, B.P.Binks, J.H. Clint. *Adv. Colloid Interface Sci.,* 2003, ***100-102,*** *503.*

[3] A. Perro, S. Reculusa, S. Ravaine, E. Bourgeat-Lami, E. Duguet. *J. Mater. Chem.,* 2005, **15,** 3745.

[4] V.N. Paunov, O.J. Cayre. *Adv. Mater.,* 2004, **16,** No. 9-10, 788.

[5] O. Cayre, V.N. Paunov, O.D. Velev. *J. Mater. Chem.*, 2003, **13,** 2445.

[6] B.P. Binks, P.D.I. Fletcher. *Langmuir,* 2001, **17,** 4708.

[7] D.J. Shaw. *Introduction to Colloid and Surface Chemistry,* 4th Ed., Elsevier, Oxford, 1992.

[8] B.V. Derjaguin, L.D. Landau. *Acta Physicochim. USSR,* 1941, **14,** 633.

[9] E.J.W. Verwey, J.Th.G. Overbeek. *Theory of Stability of Lyophobic Colloids.* Elsevier, Amsterdam. 1948.

[10] Z. Du, M.P. Bilbao-Montoya, B.P. Binks, E. Dickinson, R. Ettelaie, B.S. Murray. *Langmuir,* 2003, **19,** 3106

[11] M. Abkarian, A.B. Subramaniam, S-H. Kim, R.J. Larsen, S-M. Yang, H.A. Stone. *Physical Review Letters,* 2007, **PRL 99,** 188301-1

[12] T.S. Horozov. *Curr. Opin. Colloid Interface Sci.,* 2008, **13,** 134.

[13] D. Weaire, S. Hutzler. *The Physics of Foams,* Clarendon Press, Oxford, 1999.

[14] P. Taylor. *Adv. Colloid Interface Sci.,* 1998, **75,** 107.

[15] R.J. Pugh. *Adv. Colloid Interface Sci.,* 1996, **64,** 67.

[16] P.A. Kralchevsky, K.D. Danov, I.B. Ivanov in *Foams. Theory, Measurements, and Applications.* R.K. Prud'homme, S.A. Khan (Eds.), Marcel Dekker, New York, 1996.

[17] W. Ramsden. *Proc. Roy. Soc.,* 1903, **72,** 156.

[18] S.U. Pickering. *J. Chem, Soc.,* 1907, **91,** 2001.

[19] B.S. Murray, R. Ettelaie. *Curr. Opin. Colloid Interface Sci.,* 2004, **9,** 314.

[20] A.B. Subramaniam, M. Abkarian, L. Mahadevan, H.A. Stone. *Nature,* 2005, **438,** 930.

[21] U.T. Gonzenbach, A.R. Studart, E. Tervoort, L.J. Gauckler. *Angew. Chem., Int. Ed.,* 2006, **45,** 3526.

[22] E. Dickinson, R. Ettelaie, T. Kostakis, B.S. Murray. *Langmuir*, 2004, **20,** 8517.

[23] B.P. Binks, J.A. Rodrigues. *Angew. Chem., Int. Ed.,* 2005, **44,** 441.

[24] K. Golemanov, S. Tcholakova, P.A. Kralchevsky, K.P. Ananthapadmanabhan, A. Lips. *Langmuir,* 2006, **22,** 4968.

[25] B.P. Binks, R. Murakami, *Nature Mater.,* 2006, **5,** 865.

[26] T. Kostakis, R. Ettelaie, B.S. Murray. *Langmuir,* 2006, **22,** 1273.

[27] B.P. Binks, T.S. Horozov. *Angew. Chem., Int. Ed.,* 2005, **44,** 3722.

[28] W.J. Popiel. *Introduction to Colloid Science,* Exposition Press, Hicksville, NY, 1978.

[29] B.P. Binks. *Curr. Opin. Colloid Interface Sci.*. 2002, **7,** 21.

[30] B.P. Binks, T.S. Horozov. In *Colloidal Particles at Liquid Interfaces,* Chapter 1, Cambridge University Press, 2006.

[31] Y. Nonomura, S. Komura, K. Tsujii. *J. Oleo Sci., 2004*, **53,** No. 12, 607.

[32] R.G. Alargova, D.S. Warhadpande, V.N. Paunov, O.D. Velev. *Langmuir,* 2004, **20,** 10371.

[33] R.G. Alargova, K.H. Bhatt, V.N. Paunov, O.D.Velev, *Adv. Mater.,* 2004, **16,** 1653.

[34] R.G. Alargova, V.N. Paunov, O.D.Velev, *Langmuir,* 2006, **22,** 765.

[35] B.P. Binks, J.A. Rodrigues. *Angew. Chem.,* 2005, **44,** 441.

[36] B.P. Binks, R. Murakami, S.P. Armes, S. Fujii, A. Schmid. *Langmuir,* 2007, **23,** 8691.

[37] S.L. Kettlewell, A. Schmid, S. Fujii, D. Dupin, S.P. Armes. *Langmuir,* 2007, **23,** 11381.

[38] E.S. Read, S. Fujii, J.I. Amalvy, D.P. Randall, S.P. Armes. *Langmuir,* 2004, **20,** 7422.

[39] B.P. Binks, B. Duncumb, R. Murakami. *Langmuir,* 2007, **23,** 9143.

[40] E. Allen Foegeding, P.J. Luck, J.P. Davis. *Food Hydrocolloids,* 2006, **20,** 284.

[41] R. Anton, S. Barlow, D. Boskou, L. Castle, R. Crebelli, W. Dekant, K-H. Engel, S. Forsythe, W. Grunow, J.-C. Larsen, C. Leclercq, W. Mennes, M-R. Milana, I. Rietjens, K. Svensson, P. Tobback, F. Toldra. *Eur. Food Standards Agency J.* 2004, **1.**

[42] E.Dickinson in *Colloidal Particles at Liquid Interfaces,* Chapter 8, B.P. Binks, T.S. Horozov. (Eds.), Cambridge University Press, 2006.

[43] S. Tcholakova, N.D. Denkov, A. Lips. *Phys. Chem. Chem. Phys.,* 2008, **10,** 1627.

# CHAPTER 2 – EXPERIMENTAL

## 2.1. Materials

### 2.1.1. Water

Milli-Q water was used in all experiments where water was required. The water is purified by reverse osmosis by passage through the Millipore system. The resistivity of the water was always above 18 $M\Omega.cm^{-1}$ and the conductivity was measured at 2.04 $mS.cm^{-1}$.

### 2.1.2. Organic solvents

These materials were mainly used in the disperse phase solutions for production of polymer micro-rods, but others were used in the production of water-in-oil emulsions that were stabilized by ethyl cellulose micro-rods. A list of the solvents, together with purity and information on suppliers is shown in table 2.1.

| Material | Purity | Manufacturer | Use(s) |
|---|---|---|---|
| Ethanol | 99.99% (HPLC grade) | Fisher Scientific | Dissolution of shellac, ethyl cellulose and zein* (*including 10% water) |
| Acetone | 99.98% | Fisher Scientific | Dissolution of ethyl cellulose |
| Tetrahydrofuran | >99.5% | Fisher Scientific | |
| Propan-1-ol | >99.5% | BDH Laboratories | Dissolution of Zein (including 10% water) |
| Propan-2-ol | 99.98% (HPLC grade) | Fisher Scientific | |
| Undecane | >99% | Aldrich | Emulsion continuous phase |
| Heptane | 99.99% (HPLC grade) | Aldrich | |
| Octane | | Aldrich | |

**Table 2.1. Relevant information on organic solvents used within this thesis.**

### 2.1.3. Cellulose, cellulose derivatives, protein based material and waxes

These materials were used in the formation of micro- and nano-rods (bacterial cellulose) either by the use of an in-shear-flow dispersion solvent attrition technique or by acidic hydrolysis in the case of bacterial cellulose. A list of the materials is shown in table 2.2.

| **Material** | **Manufacturer** | **Use(s)** |
|---|---|---|
| Nata de Coco | Supplied by Unilever Food Technology, Vlaardingen, The Netherlands | Formation of nano-fibres |
| Ethyl cellulose (48 – 49.5 wt.% ethoxyl content; viscosity 3 – 5.5 mPa.s in toluene 80:20 at 25 ºC) | Fluka | Production of micro-rods |
| Methyl cellulose (Methocel™) | Dow Chemical Company | Formation of ethyl cellulose micro-rods containing Methocel™ |
| Zein | Freeman Industries Ltd. | Production of micro-rods |
| Shellac | Temuss Ltd, Canada | Production of micro-rods |

**Table 2.2. Relevant information on materials used to form nano- and micro-rods within this thesis.**

### 2.1.4. Micro-particles and yeast cells

Micro-particles and yeast cells were used as the inclusions in functional micro-rods, whilst exposure of entrapped copper micro-particles to microwave radiation and thermal degradation of sodium bicarbonate led to the production of 'ballooned' micro-rods. Information on these materials is included in table 2.3.

| Material | Batch information | Manufacturer | Use(s) |
|---|---|---|---|
| **Yeast (baker's)** | N/A | Sainsbury's | Lumpy shellac and ethyl cellulose micro-rods |
| **Aeroperl R806/30** | Lot no. 9110122 | Degussa | |
| **Sporopollenin *(lycopodium clavatum)*** | N/A | Polysciences | |
| **Pollen grains *(lycopodium clavatum)*** | N/A | Unknown | |
| **Magnetite particles** | Unknown | Synthesised as shown in ref 1 | Magnetic shellac and ethyl cellulose micro-rods |
| **Copper micro-particles <10 μm** | N/A | Sigma Aldrich | Ballooned micro-rods |
| **Sodium bicarbonate (crushed)** | 99.83% | Fisher | |

**Table 2.3. Relevant information on micro-particles used within this thesis.**

### 2.1.5. Surfactants, oils encapsulated within 'micro-rod capsules' and fluorescent probes

The surfactants and oils listed below (table 2.4) were used in the production of micro-rod capsules. Fluorescent dopants are used throughout this work to aid visualisation of all micro-rods and novel particles on which they are based.

| Material | Purity | Manufacturer | Use(s) |
|---|---|---|---|
| **Tween 20** | Unknown | Aldrich | Altering interfacial tension during formation of micro-rod capsules |
| **Tween 60** | Unknown | Aldrich | |
| **Span 85** | Unknown | Sigma | |
| **Dimethylsulphoxide** | >99% | BDH 'GPR' | Oils for encapsulation within micro-rod capsules |
| **Isopropyl myristate** | | Aldrich | |
| **Sunflower oil** | Unknown | Unknown, bought from Asda supermarket | |
| **Tricaprylin** | >99% | Aldrich | |
| **Cod liver oil** | Unknown | Unknown, bought from Boots Ltd. | |
| **Nile Red** | Unknown | Sigma | Visualisation of ethyl cellulose structures, ballooned micro-rods and micro-rod capsules |
| **Perylene** | Unknown | Sigma | |
| **Fluorescein (disodium salt)** | $H_2O$ content 6.8% | Sigma | |

**Table 2.4. Relevant information on surfactants and fluorescent probes used within this thesis.**

### 2.1.6. Other materials

A summary of information for the remaining materials used in this thesis is shown below in table 2.5.

| Material | Purity | Manufacturer | Use(s) |
|---|---|---|---|
| **Glycerol** | 99+ % | Alfa Aesar | Constituent of continuous phase for micro-rod production |
| **Ethylene glycol** | >99% | Fisher | Constituent of non-aqueous continuous phase for micro-rod production |
| **Hydrochloric acid** | 37% w/w | Fisher | Production of low pH solutions |
| **Sulphuric acid** | 98% w/w | Fisher | Hydrolysis of bacterial cellulose |
| **Potassium hydroxide** | ≥99% | BDH Laboratories 'AnalaR' | Production of high pH solutions |
| **Sodium hydroxide** | ≥99% | BDH Laboratories 'AnalaR' | |
| **Sodium chloride** | ≥99.5% | BDH Laboratories 'AnalaR' | Addition of electro-lyte in micro-rod foaming tests |
| **Urea** | 99.76% | Fisher | Chaotropic agent to disrupt H-bonding |
| **Gellan (Kelcogel)** | Lot no. S_1L1962A | CP Kelco | Gel trapping technique |
| **Polydimethylsiloxane Sylgard 184** | N/A | Dow Corning | |

**Table 2.5. Relevant information on other materials used within this thesis.**

## 2.2. Instruments

### 2.2.1. Microscopes

#### 2.2.1.1. Olympus BX51 fluorescence microscope

This microscope was most frequently used for visual observation during this work. It is fitted with 4x, 10x, 50x and 100x objectives together with 20x and 40x LWD (long working distance) objectives. The eyepiece gives 10x magnification together with dioptre adjustment for spectacle wearers. The apparatus is also fitted with an electronic focussing stage (Prior PROSCAN) which allows 3D reconstruction images produced by combining multiple exposures recorded at the same location on the slide but at different focal planes controlled by the stage. The microscope is fitted with a mercury lamp and a range of different filter sets used to visualise fluorescent dopants which are visible at different wavelengths. Images were recorded using an Olympus DP70 10 megapixel camera and ImagePro Plus software.

#### 2.2.1.2. Olympus BX51M reflected light microscope

Reflected light images were recorded using an Olympus BX51M microscope fitted with 5x, 10x and 20x objectives. The eyepiece on this microscope provides 10x magnification also. Images were recorded using an Olympus DP50 6 megapixel camera and ImagePro Plus software from MediaCybernetics.

#### 2.2.1.3. Nikon transmitted light microscope

A Nikon optical microscope fitted with 4x, 10x, 40x and 100x objectives was also used for recording images of micro-rods and micro-particles. This micro-scope was equipped with a Q-Imaging digital camera and a 10x eyepiece.

#### 2.2.1.4. SEM

A Zeiss EVO60 scanning electron microscope was used to examine bacterial cellulose fibres and other micro-rods and particles. Prior to viewing, samples (on 100 $mm^2$ glass squares, rinsed in ethanol and dried with jet of clean air) were coated with a several

nanometre thick layer of either carbon or gold/palladium to increase backscatter of electrons for viewing efficiency. Advantages of a gold/palladium coating are:

- Good backscatter
- High signal to noise ratio
- High contrast
- Fast process

The disadvantage of this coating is that texture is visible in this coating at extreme magnifications. To avoid this, a thin layer of carbon may be used instead, giving a very smooth coating for high magnification uses. Disadvantages of a carbon coating are:

- Poor backscatter compared to Au/Pd
- Poorer signal to noise ratio due to signal amplification
- Longer process to coat the samples

Different viewing angles are available, for example, to highlight the contact angle of an embedded particle which has been trapped by the GTT[6].

### 2.2.2. Mixing apparatus

#### 2.2.2.1. High shear mixing

An IKA Ultra Turrax T25 Basic mixer from Janke and Kunkel was used when high speed shear mixing was required. Mixing speed could be varied from 11,000 up to 24,000 rpm. A mixing impeller head of 18 mm diameter was used in most cases. This apparatus was used to form water-in-oil emulsions stabilised by ethyl cellulose micro-rods and also in the attempted down-sizing of ethyl cellulose micro-rods.

#### 2.2.2.2. Precision stirrer

For the production of polymer micro-rods via an in-shear-flow dispersion solvent attrition technique, a Cole Parmer Digital Reversing Mixer was employed. This mixer combines precise digital control of speed (between 0 and 2,010 rpm) with the ability to reverse direction and perform cycles of mixing regimes. The mixer gives excellent control of shear

rate produced due to the constant torque generated. Due to the importance of shear rate on the properties of resultant polymer micro-rods, this apparatus is well suited to the task. The mixer and head used are shown in fig. 2.1. The separation between the outside of the mixing head and the inside wall of the beaker was approximately 6 mm.

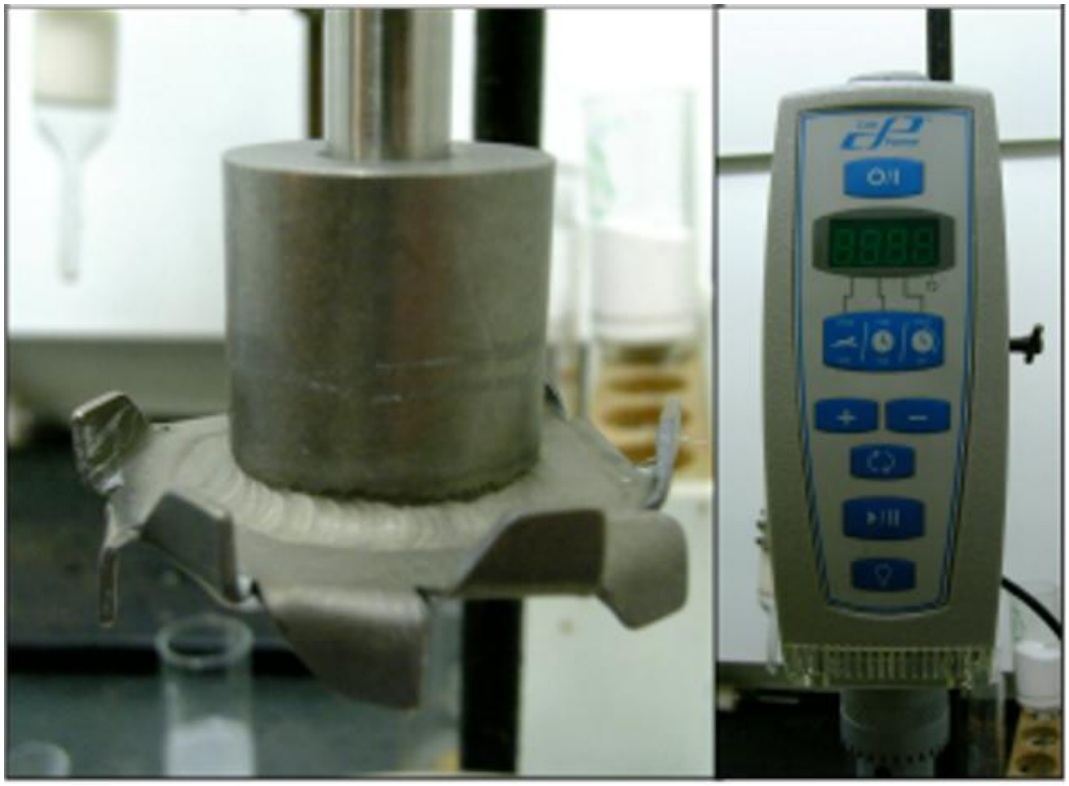

**Figure 2.1. Cole Parmer Digital Reversing Mixer and mixing head. The head fits into a 250 mL beaker, leaving channels approximately 6 mm in diameter in between the edge of the head and the inside of the beaker where dispersed phase polymer solutions are injected to form micro-rods.**

### 2.2.3. Heating devices

#### 2.2.3.1. Oven

An LTE Scientific UNITEMP drying cabinet was used for the purposes of drying glassware and storing gellan solutions above gelling temperature prior to usage. The unit was set to operate at 50 ºC normally.

#### 2.2.3.2. Stirrer hotplates

An IKA RH-KT/C stirrer hotplate from Janke and Kunkel was used for heating and stirring. This apparatus was mainly used for the dissolution of polymers into dispersed phase solutions for micro-rod production but also for a variety of other uses including hydrolysis of bacterial cellulose and thermal degradation of ethyl cellulose micro-rods containing sodium bicarbonate.

#### 2.2.3.3. Water bath

A Grant LTD 6 G thermostat water bath was used for heating and dissolving gellan. This unit is capable of maintaining temperatures from -20 ºC up to 100 ºC.

#### 2.2.3.4. Microwave source

A Toshiba 650 W domestic microwave oven was used for microwave treatment of ethyl cellulose micro-rods containing copper micro-particle inclusions.

### 2.2.4. Ultrasonic devices

#### 2.2.4.1. Branson sonicator

When high power ultrasound was required to disperse materials in viscous dispersed phase solutions for example, a Branson Digital Sonifier Model 450 was used. Fitted with a tip of 5 mm diameter, the maximum power of this apparatus is 400 W and it is also capable of pulsing. When higher power levels or extended periods of sonication were necessary it was useful to include an ice bath to prevent excessive heating of the sample.

#### 2.2.4.2. Ultrasonic bath

When lower power ultrasound was a necessity, a Decon FS3006 ultrasonic bath was used. Temperature and sonication time may be set as desired. This apparatus was used to clean mixer heads and glassware.

### 2.2.5. Particle sizing & zeta potential measurement

#### 2.2.5.1. Malvern Zetasizer 3000 HS

A Malvern Zetasizer 3000 HS (Malvern Instruments Ltd, UK) was used to record the size and zeta potentials of a range of micro- and nano-particles, rods and fibres. The apparatus is fitted with a 532 nm wavelength diode laser operating at 50 mW, and an aqueous dip cell was most frequently used (for zeta potential measurement), so samples were introduced in a cuvette (1 mL for zeta potential measurements, 2 mL for size measurements).

### 2.2.6. Other equipment

#### 2.2.6.1. Eppendorf micropipettes

For fast and efficient measurement of precise liquid volumes, Eppendorf research micropipettes from 0.1 µL up to 5000 µL were used. A 1000 µL micropipette was used to inject dispersed phase solutions into the continuous phase under shear for polymer micro-rod production.

#### 2.2.6.2. Centrifuges

When small sample volumes (up to 1.5 mL) were used, an Eppendorf Minispin Plus was employed, with a maximum available speed of 14,500 rpm. When it was necessary to centrifuge larger samples, a Baird and Tatlock Auto Bench Centrifuge Mark IV was used. This unit has a maximum speed of 6,000 rpm.

#### 2.2.6.3. Spin coater

A Cookson Electronics Spin-coater model P6700 with Busch vacuum pump was used to spin coat glass slides with polymer prior to examination with drop shape analysis apparatus (section 2.2.6.6) to determine the contact angle of water drops on the polymers. Spinning speeds from 100 up to 8,000 rpm are available.

#### 2.2.6.4. Conductivity measurement

A Jenway 4510 conductivity meter and probe was used to measure emulsion continuous phase conductivity amongst other tasks.

#### 2.2.6.5. pH measurement

A Fisherbrand Hydrus 400 was used to measure the pH of solutions used in foaming experiments where the effect of a range of pH values on foamability of micro-rods was investigated.

#### 2.2.6.6. Drop shape analysis

A Krüss drop shape analysis system DSA 10 was used to examine the contact angles of water drops resting on layers of shellac, zein and ethyl cellulose in order to compare relative hydrophobicities. The instrument consists of a chamber (where either measurements in air or under liquids may be carried out) and suspended syringe for dispensing precise volumes of liquid and a video camera system (stills may also be made, from which calculations of contact angles can be deduced). The calculation made by the apparatus software uses the Young-Laplace equation (chapter 1).

## 2.3. Methods

### 2.3.1. Preparation of cellulose nano-rods from Nata de Coco gelatinous cubes

A solution of sulphuric acid (50 wt.%) in water (Milli-Q, purified by reverse osmosis) was prepared (100 g total weight, in 250 mL beaker). Gelatinous Nata de Coco cubes were sliced into small pieces using a scalpel and added to the acid solution. The acidic

suspension was heated and stirred (IKA magnetic stirrer hotplate, 60 °C, 2.5 hr) in order to hydrolyse the nano-rods. Upon the completion of the hydrolysis, the suspension was allowed to cool to near room temperature (still stirring) and then centrifuged (Eppendorf Mini Spin, 14,500 rpm, 5 min). After centrifuging, the acidic supernatant was removed and replaced with Milli-Q water. This process was repeated 5 times until the pH of the suspension increased sufficiently for the reaction to stop. The contents of the centrifuge vials were then re-combined and the cellulose nano-rods re-dispersed using ultrasound (Branson Sonifier, 50% intensity, 2 min, 0.5 sec on, 0.5 sec off). Zeta potential and particle size distribution data for the resultant nano-rods is presented in chapter 3.

#### 2.3.1.1. Surface modification of sulphuric acid-hydrolysed Nata de Coco nano-fibres with ethyl cellulose and shellac wax

Surface modification of Nata de Coco nano-fibres was achieved by a solvent change technique where nano-fibres were suspended in a solution of the desired modification material (e.g. shellac in ethanol or ethyl cellulose in acetone) of low viscosity, typically 1 wt.%. Milli-Q water was added to this stirring suspension gradually (dropwise) to induce precipitation of the dissolved modification materials onto the nano-fibres resulting in a thin surface coating. Resultant modified nano-fibres were warmed with stirring to evaporate volatile solvent before optical examination.

#### 2.3.1.2. Surface modification of sulphuric acid-hydrolysed Nata de Coco nano-fibres with polyelectrolyte

Poly (allylamine hydrochloride) was used to positively charge the nano-fibres to see if this would enhance the foamability of the nano-fibres. The polyelectrolyte was introduced to the nano-fibres as follows. An aqueous suspension of sulphuric acid hydrolysed Nata de Coco nano-fibres (0.5 wt.%) was added slowly (dropwise, 30 min) to a stirring solution of poly (allylamine hydrochloride) (3 mg/mL). Once all the NDC was added the suspension was washed in Milli-Q water by repeated centrifugation and supernatant replacement to

remove excess polyelectrolyte. The zeta-potential of the modified nano-fibres was then measured (Malvern Zetasizer 3000 HS) and results are presented in chapter 3.

### 2.3.2. Preparation of ethyl cellulose nano-particles

A solution of ethyl cellulose in acetone (1 wt.%) was prepared. To this, an equal volume of Milli-Q water was added rapidly at room temperature. The mixture was then heated with stirring to evaporate the acetone and leave a 1 wt.% aqueous suspension of ethyl cellulose nano-particles. Resultant nano-particle diameter was evaluated at 155±10 nm using Malvern Zetasizer 3000HS.

### 2.3.3. Purification of shellac

Shellac was ground (pestle and mortar) and added to ethanol at weight percentages between 5 – 50%. The mixtures were heated (~70 °C) and stirred using a magnetic stirrer to dissolve the shellac. Whilst still warm, the honey-like, viscous liquid was poured into soda glass vials and centrifuged (5 min, 2000 rpm, Baird and Tatlock Auto Bench Centrifuge Mark 4) to sediment any impurities. The clear upper phase (about 80% of the sample) was separated from the impurities, and used to produce shellac micro-rods.

### 2.3.4. Preparation of shellac micro-rods by an in-shear-flow dispersion solvent attrition technique

This method was pioneered by Alargova et al. and has been used successfully for the production of polymer micro-rods[2,3,4]. In our study, we present for the first time novel food-grade and novel, functional micro-rods produced using this technique. For the continuous phase, a mixture of 85% glycerol and 15% Milli-Q water (v/v, 50 mL) was added to a 250 mL beaker. A Cole Parmer Digital Reversing Mixer (Servodyne Ltd.) was used for the production of polymer micro-rods. The mixer head was dipped into this mixture so that the blades on the outside of the head were submersed. The mixer speed was set, and shellac in ethanol solutions between 5 and 50 wt.% were injected (1 mL, Eppendorf micropipette)

into the area between the outside of the mixer head and the inside of the beaker where it is thought maximum shear occurs. After 10 min of stirring, the aqueous glycerol micro-rod suspension was diluted with Milli-Q water and filtered (Whatman No.1 filter papers). The micro-rods were repeatedly washed with Milli-Q water (4 times) using filtration to remove glycerol and then examined by optical microscopy and their foamability assessed.

### 2.3.5. Preparation of ethyl cellulose micro-rods by an in-shear-flow solvent attrition dispersion technique

These particles were produced using a procedure the same as that described in the previous section except for the use of dispersed phase solutions as follows. Ethyl cellulose (48 – 49.5 wt.% ethoxyl content; viscosity 3 – 5.5 mPa s in toluene 80:20 at 25 ºC) was dissolved by gentle heating (hotplate stirrer, 45 – 65 ºC, depending on solvent) and stirring with a magnetic stirrer bar at the following weight percentages.

| **Solvent** | **Wt.% of EC solubilised** |
|---|---|
| Ethanol | 5 – 30 |
| Acetone | 5 – 30 |
| Tetrahydrofuran | 5 – 15 |

**Table 2.6. Details of solutions of ethyl cellulose in various solvents.**

### 2.3.6. Preparation of zein micro-rods by an in-shear-flow solvent attrition dispersion technique

These particles were produced using a procedure the same as that described in the previous section except for the use of disperse phase solutions as follows. It is well documented that zein is soluble in aqueous alcohol solutions[5] and it was found that the best micro-rods were produced when ethanol, propan-1-ol or propan-2-ol was combined with 10% Milli-Q water with zein loadings around 40 – 50 wt.%. The solutions must be used within a few days however, due to the tendency of zein solutions in water-alcohol mixtures to gel.

### 2.3.7. Preparation of polymer micro-rods with inclusions

#### 2.3.7.1. Shellac micro-rods with yeast cells

Yeast cells (baker's yeast, 0.2 g) were hydrated by addition of Milli-Q water. The mixture was then centrifuged and the aqueous supernatant removed and replaced with ethanol. The suspension of yeast cells in a water/ethanol mixture was then mixed thoroughly using firstly an IKA Minishaker, and, if necessary, ultrasound. The process of centrifugation and replacement of the supernatant (with ethanol) was repeated 4 more times to ensure the removal of a satisfactory amount of water. The supernatant was removed finally, and the yeast 'slurry' was transferred into 1 mL of shellac in ethanol solution. This was stirred and sonicated to make a homogeneous dispersed phase for the production of lumpy micro-rods. From this point, the dispersed phase was injected into the stirring continuous phase as described in section 2.3.4, and after formation, the micro-rods were washed and isolated by filtering exactly the same as for regular shellac and ethyl cellulose micro-rods. 'Lumpy' micro-rods were then characterised by optical microscopy. The foamability of these micro-rods was also assessed.

#### 2.3.7.2. Micro-rods containing large 'inclusions'

In order to produce shellac or ethyl cellulose micro-rods containing large 'inclusions' e.g. sporopollenin or Aeroperl$^{TM}$ aerated silica, the particles were added to the dispersed phase solution and sonicated (Branson Digital Sonicator Model 450, 10 – 35% intensity, for 90 s) to disperse the particles homogeneously prior to injection into the continuous phase under shear to form lumpy micro-rods. The remainder of the procedure is the same as that described in section 2.3.4.

#### 2.3.7.3. Ethyl cellulose ‘ballooned’ micro-rods with copper particle ‘inclusions’

Ballooned micro-rods from ethyl cellulose were produced by adding 0.25 g copper micro-particles to 1 mL of 30% ethyl cellulose in acetone (columned twice with $Al_2O_3$) solution. This was sonicated to homogenise it, and then added slowly to the continuous phase (85% glycerol, 15% Milli-Q water (v/v) under stirring (2,000 rpm, 10 min) to form micro-rods. The micro-rods were washed and isolated as normal by filtration (Whatman No.1 filter paper). Aqueous suspensions of micro-rods were then exposed to microwave radiation (Toshiba 650 W domestic microwave oven) and observed by optical microscopy to investigate the effects.

#### 2.7.3.4. Ethyl cellulose ‘ballooned’ micro-rods with sodium bicarbonate

Ethyl cellulose ballooned micro-rods were produced by adding 0.25 g $NaHCO_3$ crystals to 1 mL of 30% ethyl cellulose in acetone (columned twice with $Al_2O_3$) solution. This was sonicated to homogenise it, and then added slowly to the continuous phase (75% glycerol, 25% ethylene glycol, v/v) under stirring (2,000 rpm) for 10 min. A small sample of this suspension was taken for observation. The micro-rods (still remaining in the non-aqueous continuous phase) were then transferred to a hotplate stirrer where they were heated to 170 °C for 30 min (with stirring, 300 rpm) in order to thermally decompose the sodium bicarbonate and produce so-called ‘ballooned micro-rods’ containing $CO_2$ gas. Following the heat treatment, the micro-rods were washed with Milli-Q water by filtration (Whatman No.1 filter paper) to remove excess glycerol and analysed by optical and fluorescence microscopy.

### 2.3.8. Preparation of magnetic micro-rods

Magnetic shellac micro-rods were produced by addition of a high concentration suspension of magnetic nano-particles* in ethanol to a pre-prepared shellac in ethanol solution followed by sonication to thoroughly disperse the nano-particles. This resulted in a 50 wt.% solution

of shellac in ethanol with 3 wt.% (with respect to shellac weight) of suspended magnetic nano-particles within. This was added to glycerol (85%, aq) undergoing stirring (1000 rpm, Cole Palmer mixer) for 10 min. The magnetic micro-rod suspension was then filtered (Whatman No. 1 filter paper, 240 mm), washed (Milli-Q water, x4) and then characterised by optical microscopy.

*Magnetic nano-particles were produced using the method of Maity et al.[1]

### 2.3.9. Foam scaffolding

Aqueous suspensions of sulphuric acid hydrolysed cellulose nano-rods and ethyl cellulose nano-particles were combined in various ratios and foams were produced by hand-shaking. Graduated test tubes were used for foaming experiments, and these comprised 10 mL liquid and 0.5 wt.% total solids (the ratio of ethyl cellulose nano-particles to Nata de Coco was altered between 1:10 and 10:1). Results are presented in chapter 3. Foams heights were measured in a 15 cm long graduated cylinder (with approximately 10 mm internal diameter) using a ruler.

### 2.3.10. Preparation of micro-ampules

In order to produce micro-ampules, the oil targeted for encapsulation (and fluorescent dopant if necessary) was added to the dispersed phase solution and mixed thoroughly prior to addition to the continuous phase under shear (rest of procedure same as that for shellac, ethyl cellulose and zein micro-rods). Typically, ratios of polymer to encapsulated oil of 75:25 to 50:50 (together with 0.001 wt.% Nile Red fluorescent dopant) were used.

### 2.3.11. Preparation of water-in-oil emulsions stabilised by ethyl cellulose micro-rods

Milli-Q water, ethyl cellulose micro-rods* and oil were weighed into a soda glass vial (in that order) before being sheared at 11,000 rpm for 2 min (IKA Ultra Turrax T25 basic, 18

mm diameter impeller) to produce an emulsion. The conductivity of these water-continuous systems was typically around 0.2 μS $cm^{-1}$. The emulsions were then observed by optical microscopy. Oils such as octane, heptane and undecane were used as the continuous phase for emulsion production depending on whether evaporation of the continuous phase was desired.

*Weighed as a dry powder, micro-rods produced as described in section 2.3.5 from an acetone dispersed phase and subsequently oven-dried at 50 ºC overnight prior to use in this method.

### 2.3.12. Gel trapping technique for analysis of the adsorption of micro-rods at the air-liquid interface

A 0.5 wt.% solution of gellan in Milli-Q water was prepared by heating (90 ºC) and stirring before filtration (Strata $C_{18}$-E column from Phenomenex) for the removal of surface-active impurities. Filtration was carried out at 40 – 50 ºC to prevent gelling of the gellan solution during its passage through the column. This was achieved using an arrangement of heat guns to warm the column. Finally, the filtered gellan was heated to evaporate excess water, bringing the concentration of the solution up to 2 wt.% (for use in the GTT). A small amount of this solution was placed in a dish, and to it, a drop of water containing micro-rods (either shellac or zein) was introduced. In a modification to the method of Paunov[6], a spreading solvent (such as IPA) was not used, due to the solubility of the polymers used for micro-rod production in such solvents. Once the gellan solution had set (at room temperature), a layer of PDMS was poured over the top, and once again allowed to set. Once set, this layer was imaged by SEM and the results are presented in chapters 4 and 6.

### 2.3.13. Procedure for foamability and foam stability tests

Typically 10 mL suspensions of particles in Milli-Q water were added to glass tubes approximately 150 mm in length, with 10 mm internal diameters. Weight percentages of particles were varied depending on the particular study, but normally 1 – 5 wt.% were

employed. After hand-shaking vertically 20 times, the foam height was monitored over time using a ruler. Experiments were typically repeated 3 times. The error in the measured foam height was estimated to be half the maximum bubble diameter. The separate replicates generally agreed to within this error.

## 2.4. References


[1] Maity D, Agrawal D.C. *J. Magnetism and Magnetic Materials*, 2007, **46,** 308.

[2] R.G. Alargova, D.S. Warhadpande, V.N. Paunov, O.D. Velev. *Langmuir,* 2004, **20,** 10371.

[3] R.G. Alargova, K.H. Bhatt, V.N. Paunov, O.D.Velev, *Adv. Mater.*, 2004, **16,** 1653.

[4] R.G. Alargova, V.N. Paunov, O.D.Velev, *Langmuir,* 2006, **22,** 765.

[5] J.W. Lawton, *Cereal Chem.*, 2002, **79,** 1.

[6] V.N. Paunov. *Langmuir,* 2003, **19,** 7970.

# CHAPTER 3 – BACTERIAL CELLULOSE NANO-RODS: PREPARATION, CHARACTERISATION AND MODIFICATION FOR FOAM STABILISATION

## 3.1. Cellulose: chemical structure, origins and uses. Why use Nata de Coco?

Cellulose is the world's most abundant biopolymer and gives structure to the cell walls of plants. Table 3.1 shows some examples of the cellulose content of various agricultural sources.

| *Source* | *Cellulose content (oven-dry wt. %)* |
|---|---|
| ***Bluegrass*** | ***28*** |
| ***Clover*** | ***26*** |
| ***Corn*** | ***43*** |
| ***Cotton*** | ***91*** |
| ***Oats*** | ***18*** |
| ***Peanuts*** | ***49*** |
| ***Rice*** | ***42*** |
| ***Soybeans*** | ***32*** |
| ***Sugarcane*** | ***48*** |
| ***Wheat*** | ***50*** |

**Table 3.1. Cellulose content of various agricultural sources.[1]**

In this chapter we are concerned with bacterial cellulose, which is produced by the gram-negative bacterium *Acetobacter xylinum*.[2] Nata de Coco bacterial cellulose has been consumed in Malaysia and the Far East as a confectionary delicacy for many years although its popularity has declined more recently. Bacterial cellulose is superior in many ways to cellulose produced by plants, because it has a finer structure, greater purity, higher levels of biodegradability and far greater mechanical strength.[3]

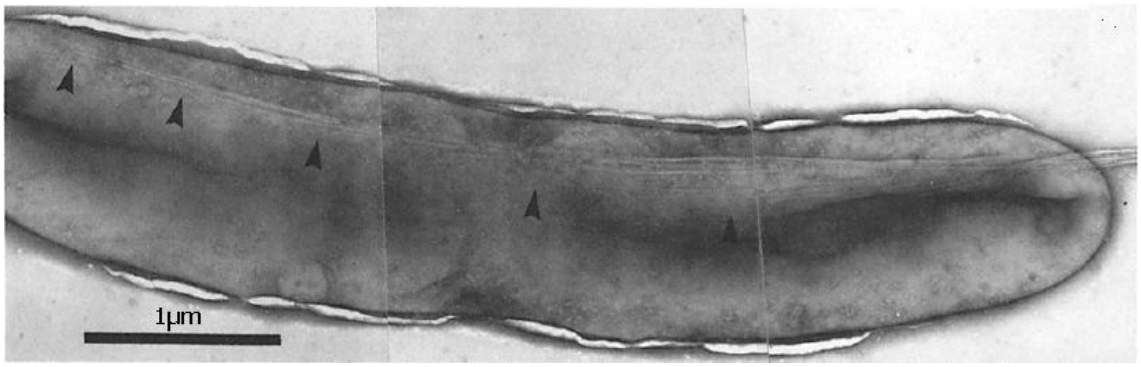


**Figure 3.1. *A. xylinum* cell synthesizing cellulose microfibrils, starting at multiple points along the cell (black arrows).[4]**

*A. xylinum* synthesizes a cellulose ribbon and this is composed of many smaller microfibrils that originate at multiple points along the length of the cell (fig. 3.1). The microfibrils formed then combine or 'fasciate' to form the twisting ribbon of bacterial cellulose in the form of a pellicle in the incubation medium. It has been shown by Haigler et al. that cellulose ribbon assembly may be disrupted or altered by addition of small amounts of various cellulose derivatives to the incubation medium.[4] Methylcellulose, hydroxypropylcellulose (HPC) and hydroxypropylmethylcellulose (HPMC) have been used for this purpose, but it was found that carboxymethylcellulose (CMC) was the most effective. Addition of 0.1% CMC to the incubation medium inhibited normal fasciation of microfibrils into the twisting ribbon of cellulose, and the difference between a control and a sample treated with CMC is clearly visible (figs. 3.2 and 3.3). The inhibition of aggregation of fibrils containing CMC is caused by carboxylic acid groups repelling one another.[5]

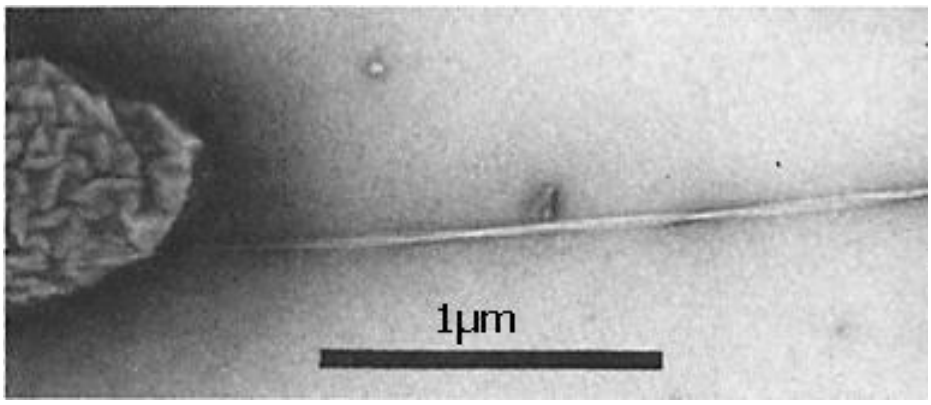


**Figure 3.2. Cellulose ribbon formed by *A. xylinum*.[4]**

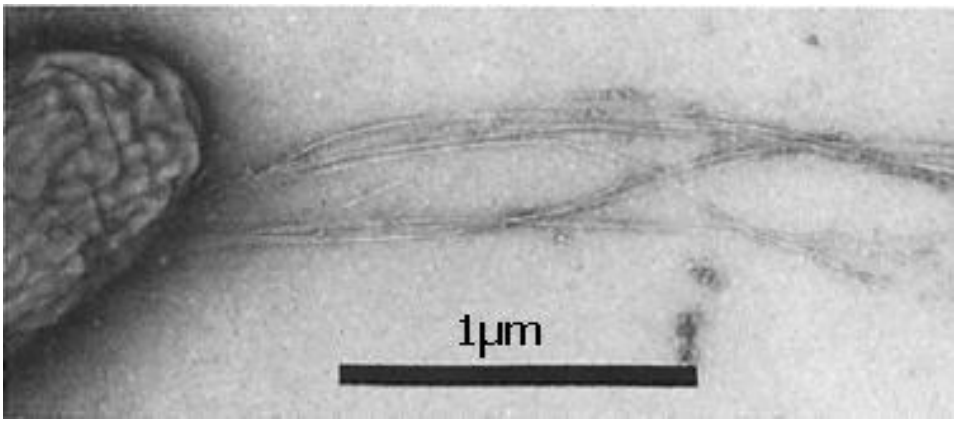


**Figure 3.3. Individual bacterial cellulose microfibrils which have not fasciated, due to the addition of CMC.**[4]

The *in vivo* process of cellulose biosynthesis by *A. xylinum* has been studied in detail. Malcolm Brown Jr et al. reveal some intricate facets of the process using darkfield light microscopy.[6] They found that the twisting cellulose ribbon was produced at a rate of 2 µm $min^{-1}$, and that the ribbon itself was composed from 46 separate microfibrils. This corresponds to the row of synthetic sites situated along the long axis of the rod-shaped *A. xylinum* cell, numbering approximately 50, and this was visualized using freeze-etching and electron microscopy.

Although cellulose may be derived from a variety of sources (see section 3.1), its molecular structure (fig. 3.4) is invariant of the source. *β*-Glucopyranose units are linked to one another via an ether bridge from carbon no.1 of one molecule to carbon no.4 of an adjacent molecule.[7]

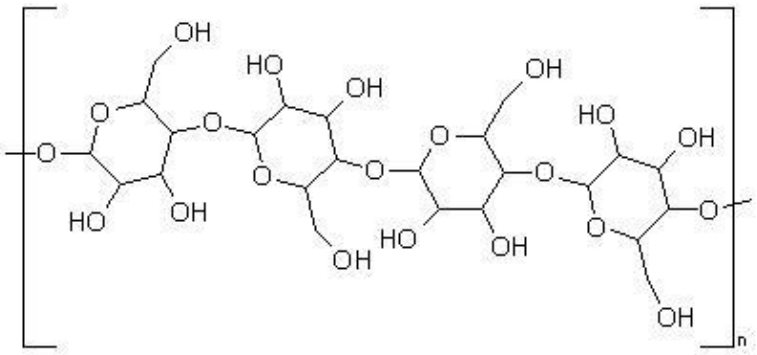


**Figure 3.4. Chemical structure of a section of the cellulose polymeric chain *β*-Glucopyranose units are linked to one another via an ether bridge from carbon no.1 of one molecule to carbon no.4 of an adjacent molecule.**

The $\beta$-linkage causes the cellulose chains to adopt a rigid and extended conformation which allows strong fibres to be formed. Because each successive monomeric unit of the cellulose chain is oriented upside down relative to its neighbours, extensive hydrogen bonding between adjacent chains occurs[8], which faciliates the formation of microfibrils. The microfibrils are twisted and these in turn associate to form much larger fibres. On a molecular level[9], the rings of the cellulose chain are found to be in the chair conformation, and in native cotton cellulose, the degree of polymerisation in the chains is approximately 15,000. This is high, and a figure of 13,000 is reported by Fleming et al.[9] Bacterial cellulose by comparison has been reported[10] to have a D.P. of around 2,000 – 6,000.

There are a variety of polymorphs of cellulose (I, II, $III_I$, $III_{II}$, $IV_I$ and $IV_{II}$) and these may all be interconverted.[10] Native cellulose is present as cellulose I (although this is not the most stable polymorph) and this can be converted to cellulose II by a process called mercerization (swelling in sodium hydroxide and subsequent cleaning). From celluloses I and II, celluloses III and IV are produced by processes of liquid ammonia treatment and heating in glycerol respectively, with cellulose $III_I$ being produced by liquid ammonia treatment of cellulose I for example. It is then reported that there are two different polymorphs of cellulose I itself, cellulose $I_\alpha$ and $I_\beta$. These two polymorphs are found in different ratios within different organisms, and have different hydrogen-bonding patterns.[10]

The structure of cellulose has been shown by x-ray diffraction to be mainly crystalline. Cellulose derived from different sources shows varying degrees of crystallinity.[11,12] However, the structure is actually composed of a mixture of highly crystalline and more amorphous areas. This random distribution of crystalline and amorphous areas in the cellulose bulk structure leads to an irregular surface. It is the amorphous regions of the structure which are of lower density and are susceptible to attack by enzymes or hydrolysis allowing one to modify the cellulose for a variety of applications.

Cellulose readily absorbs moisture from the atmosphere, and so a sample of cellulose which has been thoroughly dried (in an oven for example) will, when returned to a natural environment re-equilibrate itself with the ambient moisture level. Cellulose nano-rods are extremely strong and they are increasingly being incorporated in composite materials for reinforcement purposes. These natural fibres could be used in polymer composites as a replacement for inorganic fibres and have advantages such as

light weight and low cost.[13] Orts et al. comment on the effect of addition of cellulose microfibrils on the properties of polymer nano-composites.[14] Cellulose microfibrils have an axial Young's modulus potentially stronger than steel and thus present potential for reinforcement of materials. It was found that a 5-fold increase in Young's modulus of starch plastics could be achieved by addition of 10.3% (w/w) cotton cellulose microfibrils.[14] Microfibrils derived from tunicin cellulose are reported to provide even greater reinforcement of composites. This is because tunicin microfibrils are large and regular in morphology; however, harvesting difficulties require a more practical solution, as cellulose derived from native cotton is both abundant and comparatively easy to harvest.

### 3.2. Hydrolysis of bacterial cellulose

To produce fibres with dimensions and aspect ratio that would be applicable for interfacial stabilisation, the cellulose must be modified. This can be achieved by hydrolysis using concentrated mineral acids such as sulphuric acid and hydrochloric acid. The result of this is the formation of discreet cellulose fibres or microcrystallites. These micro-particles exhibit the rod-like shape which makes them very suitable for stabilisation of foams.

The first report[15] of acid treatment of cellulose to produce such crystallites was by Rånby in 1951. Here, microcrystallites of wood cellulose and viscose rayon were produced and characterised. Fig. 3.5 shows a schematic diagram of the effect of hydrolysis in sulphuric acid on Nata de Coco bacterial cellulose. The cellulose is exposed to concentrated acid, and when the desired period of hydrolysis is complete, the fibres produced are washed in pure water. This can be done by sedimentation/centrifugation cycles or by dialysis. The fibres are then re-dispersed using ultrasound, taking care not to allow excessive heating of the sample, as this could affect the integrity of surface groups present which charge-stabilise the suspension.[16] Nano-rods of approximately 1 μm in length and 50 nm in diameter were produced due to amorphous regions of the cellulose network being hydrolysed leading to shortening of the cellulose polymer chains.

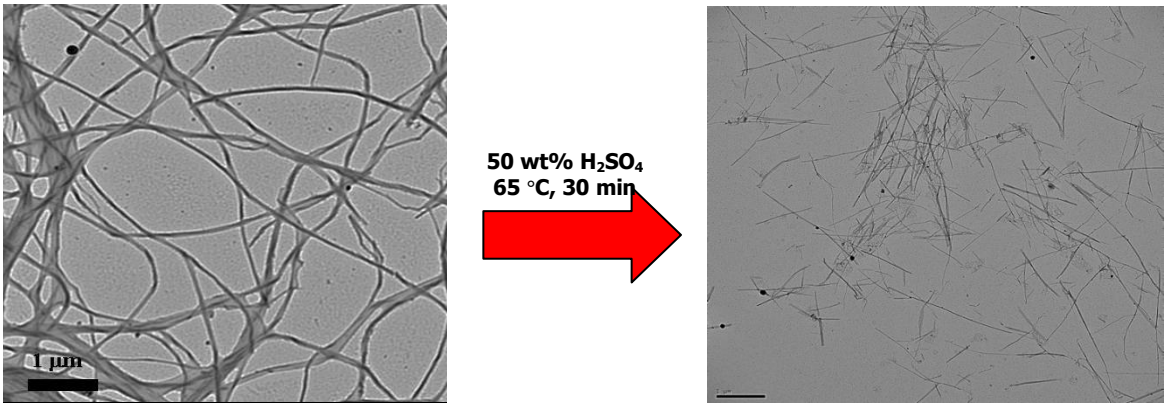


**Figure 3.5 Effect of acidic hydrolysis on bacterial cellulose structure, where amorphous regions of the cellulose chain are broken down to form discrete nano-rods. Scale bars are 1µm.**

The amorphous areas lack the extensive ordering of the majority of the crystal lattice structure, which is insoluble in water and resists attack from reagents.[8]

Dong et al. explore the effects of varying the preparation conditions for sulphuric acid hydrolysis of cotton cellulose on the properties of the microcrystallites obtained.[17] Whatman filter paper (which had been ground down to powder) was used to prepare the cellulose suspensions, and a 64% w/v aqueous solution of sulphuric acid was used to hydrolyse the cellulose.[18] Firstly, the effect of hydrolysis temperature was investigated; at a low temperature of 26 °C it was found that an extended period of time was required for microcrystallites to be formed. At 65 °C, the hydrolysis time had to be shortened to only 15 min to avoid the formation of a viscous black suspension. At 45 °C the process could be controlled well, and a chiral nematic phase was produced.[18] The effect of hydrolysis time was also reported, and a correlation was obtained where an increase in hydrolysis time lead to a decrease in microcrystallite size (fig. 3.6). Increasing the hydrolysis time also lead to an increased sulphate content being measured by conductometric titration.

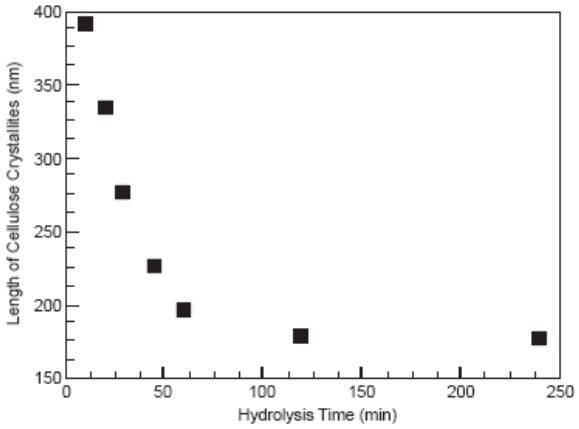


**Figure 3.6. Decrease in cellulose crystallite length with increased hydrolysis time.[18]**

The process of hydrolysis of cellulose with hydrochloric acid is extremely important for the production of various grades of microcrystalline cellulose (MCC).[10] Araki et al. compare hydrolysis of cellulose with HCl together with the characteristics of the resultant microcrystalline cellulose suspension with an equivalent system where sulphuric acid is used.[17] The different chemical treatments lead to different leftover groups on the surface of the microcrystallites after hydrolysis[18], and this in turn affects their properties. It is reported[17] that when HCl is used, strong and weak acid groups are present at 0 and <18 mmol $kg^{-1}$ respectively on the cellulose microcrystallites produced, whereas with $H_2SO_4$, strong and weak acid groups are present at 84 and 26 mmol $kg^{-1}$. These figures were revealed by conductometric titration and the greater number of strong acid groups on the cellulose hydrolysed by $H_2SO_4$ gives rise to a suspension that is electrostatically stabilised to a considerably greater extent than an equivalent suspension produced from HCl hydrolysis. The lack of electrostatic stabilisation in the suspension produced from HCl gives rise to aggregation of the fibres, and a variety of aggregate sizes are possible. This in turn leads to complex rheological behaviour and thixotropy at higher concentrations.[17]

Cellulose nano-rods exhibit many interesting properties, but perhaps the most noteworthy is the formation of so-called colloid crystals. Stable suspensions of cellulose microcrystallites formed by sulphuric acid hydrolysis may exhibit birefringence.[19] Because the fibres are rod-like in shape, they have a tendency to align under certain conditions and this gives rise to the phenomenon. The preparation conditions for these systems are critical however, and Dong et al. report on the effects of varying the conditions on the formation of such colloid crystals of cellulose.[18] It was found that

above a critical concentration of the microcrystallites, a chiral nematic ordered phase was formed which displayed properties similar to that of a cholesteric liquid crystal.[18] It was also shown that there was a size distribution within the suspension, and fractionation was observed, where the longer fibres formed an anisotropic phase at the base of the vessel, and the shorter fibres were present in an isotropic phase above. Longer fibres found within the isotropic portion of the system migrated to the liquid crystalline phase[18] because it was more favourable for them to be in the highly ordered region.

As discussed, the conditions required for ordered phase formation are highly sensitive, and a number of parties have carried out work to investigate this.[18-23] Araki et al. observed dramatic changes in the phase separation behaviour of suspensions of rod-like hydrolysed bacterial cellulose microcrystallites through the addition of trace amounts of electrolyte.[21] A spontaneous nematic phase was observed; a result of parallel alignment of the microcrystallites. Addition of <1 mM NaCl led to the formation of a chiral nematic phase however.[21] A possible reason for this is that in an aqueous suspension, ionised sulphate groups at the microcrystallite surface promote repulsion between the microcrystallites, and this effectively renders the twisted fibres as cylinders. These cylinders then pack like rod-shaped liquid crystal molecules forming a nematic liquid phase. When trace quantities of salt are added to the system the electrostatic repulsion is reduced, and the twisted fibres are able to pack more closely in a screw-like manner (fig. 3.7) creating a chiral nematic phase.[21] Interestingly, much lower concentrations of bacterial cellulose were required to produce birefringent suspensions compared with similar systems using native cotton cellulose.[21]

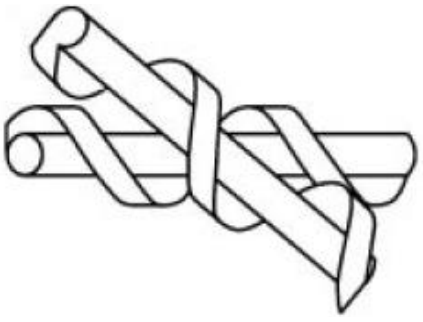

**Figure 3.7. Schematic of screw like packing of cellulose microcrystallites which could lead to chirality.[10]**

The useful characteristics of cellulose give it many industrial applications. It is non-toxic, and so MCC is frequently found in food and pharmaceutical products. For example, it has been used routinely as a tablet excipient, and also as a fat substitute in dairy-based products.[10]

Birefringent properties of suspensions of the cellulose nano-rods hydrolysed with sulphuric acid[20] can be preserved upon drying to produce solid films which reflect circularly polarized light.[24] The chiral nematic pitch and the wavelength of the reflected light can be controlled by varying the electrolyte concentration in the system prior to evaporation. The films can reflect visible light of colour dependent upon the viewing angle.[25] These films could be used for applications ranging from security features on bank notes to passports.[25]

This chapter is concerned with the acidic hydrolysis of Nata de Coco bacterial cellulose, together with characterisation, modification and foam-stabilising applications of the resultant nano-rods.

### 3.3. Characterisation of nano-rods fabricated from bacterial cellulose

Nata de Coco bacterial cellulose was hydrolysed using sulphuric acid using a process described in chapter 2 to produce cellulose nano-rods which are further utilised for foam stabilisation.

Colour changes observed during hydrolysis (fig. 3.8) are due to side reactions such as dehydration.[18] Generally, the colour of the reaction mixture varies from colourless to pale yellow or pale orange, changing to orange, red, then brown, and if the reaction is allowed to continue, the suspension becomes highly dehydrated and a black foamy slurry is formed.

**Figure 3.8. Colour change from pale peach to deep red of acidic suspension during hydrolysis over 90 min (50 g of 40 wt. % $H_2SO_4$ (aq) with 3 g gelatinous Nata de Coco bacterial cellulose).**

It is worth mentioning that the temperature at which the hydrolysis was carried out made a large difference to the timing of colour changes during the reaction. If a 50 wt.% acid solution was used, and the hydrolysis was carried out at 85 ˚C, the colour change from colourless to brown occurs in ten minutes. However, if the hydrolysis is carried out at 45 ˚C, the solution changes from colourless to pale orange over 45 minutes, and the hydrolysis takes in excess of 6 hours to complete. Following hydrolysis and subsequent dispersion of the nano-rods in Milli-Q water (after a number of centrifugation/supernatant replacement cycles), characterisation using laser diffraction particle sizing and microscopy (TEM & SEM) was carried out. Due to the small diameters of the nano-rods produced, optical microscopy was not used.

### 3.3.1. Particle size distribution

A dilute aqueous suspension of acid hydrolysed Nata de Coco nano-rods was used to measure the average particle size. Dimensions of the nano-rods were found to be around 400 nm (Malvern Zetasizer 3000HS). This apparatus is described in further detail in the experimental section, chapter 2. It should be noted that this figure must only be used as a guide, because the mathematical model incorporated within the software of the machine bases an assumption that the particles (or droplets) being measured are spheres. Clearly this is not the case – the bacterial cellulose nano-rods are likely to have very high aspect ratios. The value produced by the apparatus may lie between that of the length and the diameter of the nano-rods. Fig. 3.9 illustrates a typical size distribution obtained showing 3 runs giving an average reading of approximately 400 nm. Evidence of sedimentation of the larger cellulose nano-rods was also seen. Measurements were taken of one sample at 0, 30 and 60 min., and the shifting of the peaks shown in fig. 3.10 (red = initial, blue = 30 min & green = 60 min). The peak shifts to a smaller value after the larger particles in the sample sediment to the bottom of the cuvette where they are not measured. Fig. 3.11 shows 3 readings of the same sample after 24 hours. The peaks are virtually identical suggesting that the sedimentation process of the coarse part of the nano-rods is complete.

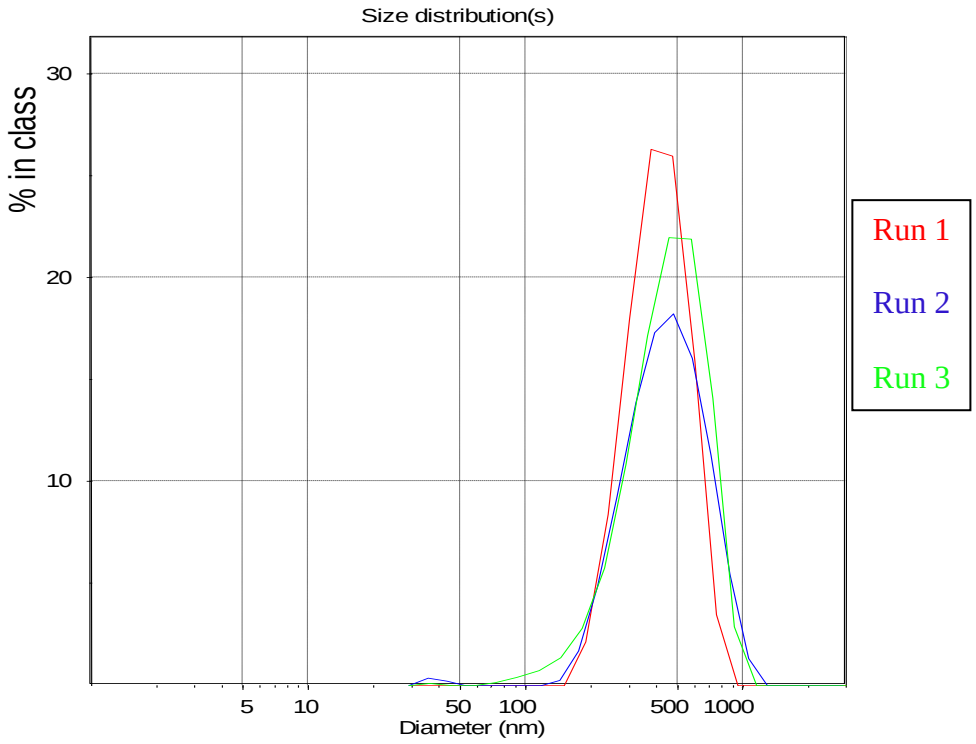


**Figure 3.9. Particle size distribution of dilute suspension of Nata de Coco nano-rods one hour after hydrolysis for 1 hr at 60 °C in 50 wt% $H_2SO_4$ (aq). Three successive runs recorded immediately after one another. Average size recorded between 400 and 500 nm.**

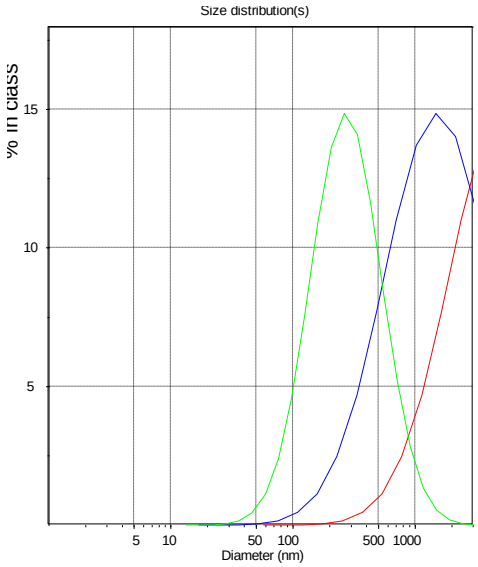


**Figure 3.10. Shifting effect of particle size distribution with time; red – initial, blue – 30min later and green – 1hr later.**

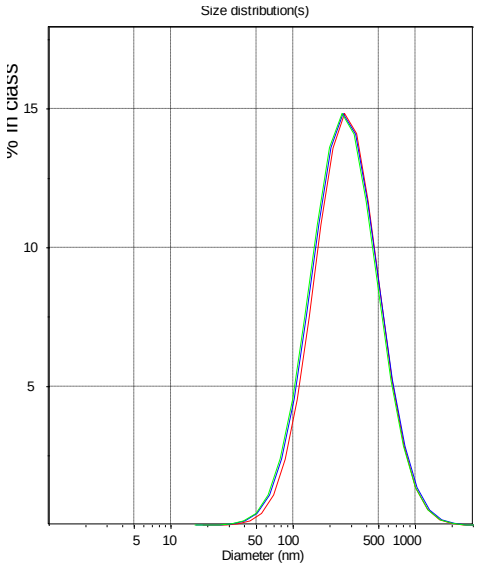


**Figure 3.11. Particle size distribution after 24hr settling time; measurements were spaced as in the figure to the left, but no shifting of the distribution is seen.**

### 3.3.2. ζ-potential measurement

We characterised the zeta-potential of an aqueous suspension of sulphuric acid hydrolysed Nata de Coco nano-rods prepared as described in chapter 2 (fig. 3.12).

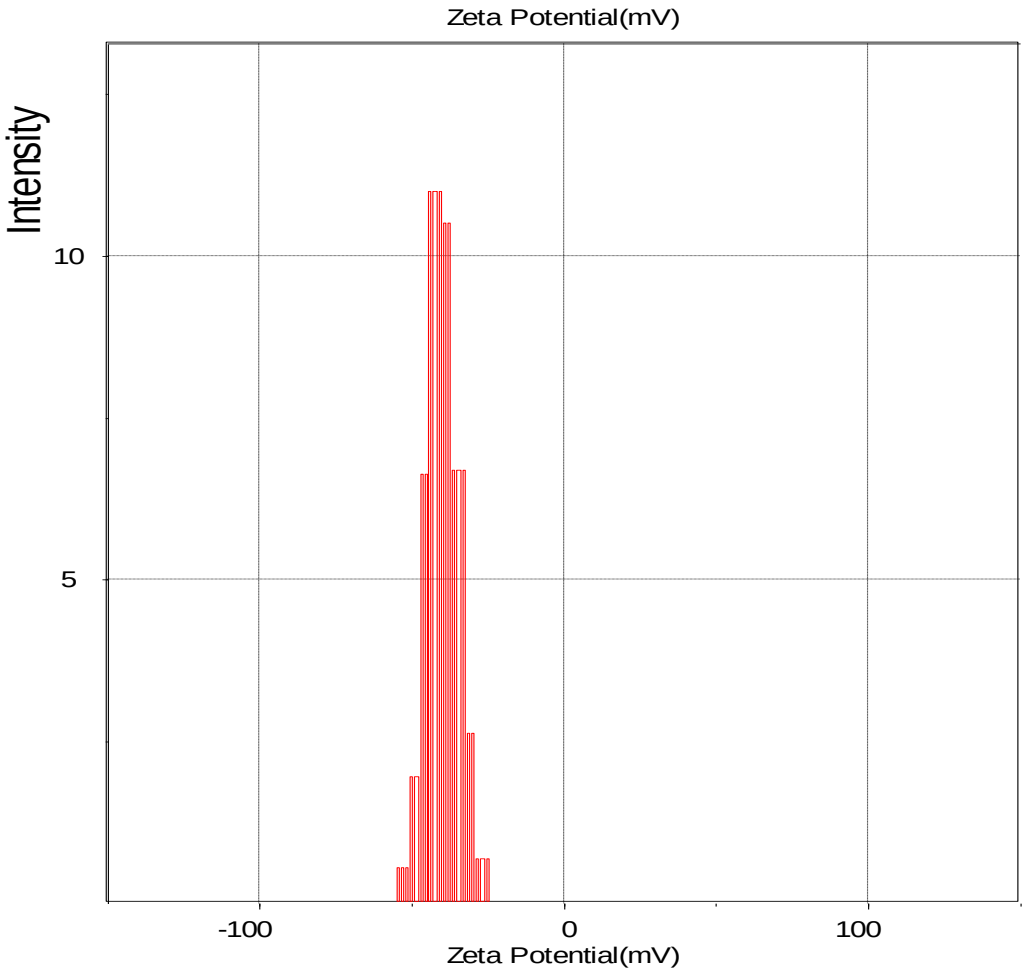


**Figure 3.12. Zeta potential of a dilute aqueous suspension of unmodified sulphuric-acid hydrolysed Nata de Coco nano-rods.**

The zeta potential was evaluated at –39 ±5 mV representing the partial substitution of the surfaces of the nano-rods with negatively-charged sulphuric acid ester groups.

#### 3.3.2.1. Effect of increased hydrolysis temperature

It was decided to investigate the effect of altering the temperature of hydrolysis on the properties of the fibres produced. The hydrolysis was carried out at temperatures

between 60 ˚C and 80 ˚C and the hydrolysis time was fixed to 1 hour at a sulphuric acid concentration of 40 wt.%.

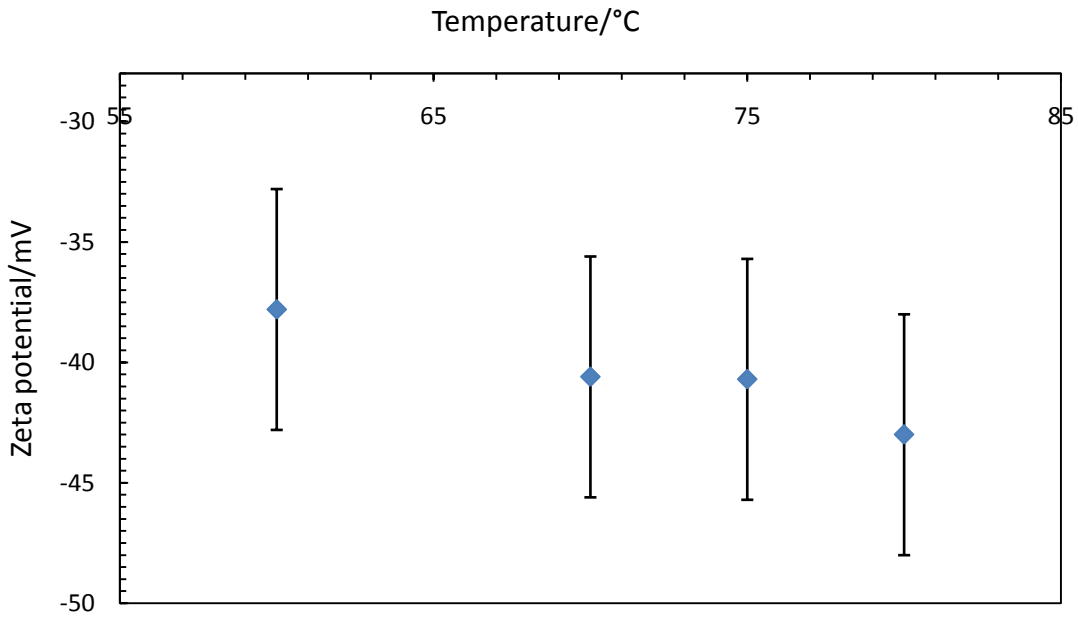


**Figure 3.13. Effect of temperature during sulphuric acid hydrolysis of Nata de Coco bacterial cellulose for 1 hr. using 40 wt.% $H_2SO_4$.**

The increased temperature of hydrolysis of the cellulose led to the recording of greater negative zeta-potential of the resulting nano-rods. This suggests that more negatively-charged strong acid groups were grafted to the cellulose backbone during sulphuric acid hydrolysis at higher temperatures. However, excessive heat during the nano-fibre re-dispersion process should be avoided[17] as electrostatically-stabilising strong acid groups can be hydrolysed during excessive sonication.

### 3.3.2.2. Effect of increased hydrolysis sulphuric acid concentration

The effect of altering the hydrolysis sulphuric acid concentration on the properties of the resultant nano-rods was investigated. Concentrations of sulphuric acid between 30 wt.% and 60 wt.% were used, the hydrolysis time was fixed to 1 hour and the hydrolysis temperature used was 60 ˚C.

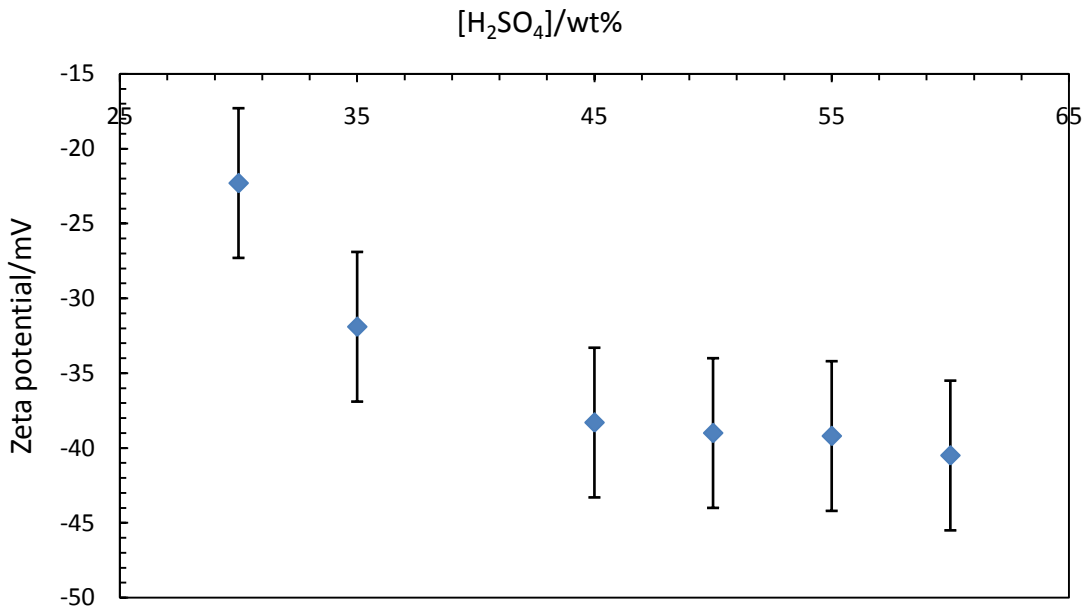


**Figure 3.14. Effect of increased acid concentration on the zeta potential of resultant Nata de Coco nano-rods after hydrolysis at 60 ºC for 1 hr. Here, higher acid concentrations led to increasingly negative zeta potential values, suggesting that more sulphate ester groups were grafted on to the surfaces of the cellulose nano-rods.**

As seen in fig. 3.14, the negative zeta potential of the cellulose nano-rods increases in magnitude with the $H_2SO_4$ concentration used for hydrolysis. This is probably due to an increased number of negatively charged sulphate ester groups being grafted to the cellulose backbones of the resulting nano-fibres giving an increasingly negative zeta potential.

### 3.3.3. Scanning electron microscopy

Bacterial cellulose nano-rods produced by sulphuric acid hydrolysis were analysed by scanning electron microscopy (SEM). SEM relies on the topography or height of the sample to give an image with contrast, and the height of the nano-rods is likely to have only been a few tens of nanometres. The image contrast is low due to the deposited layer of carbon coating on the sample.

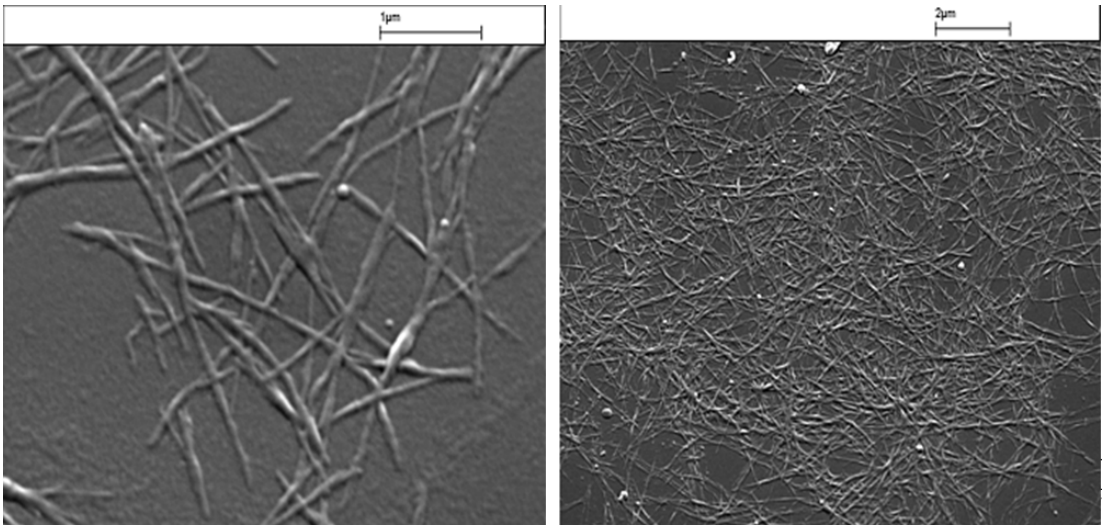


**Figure 3.15. SEM images of Nata de Coco nano-rods produced by sulphuric acid hydrolysis of gelatinous cubes of Nata de Coco bacterial cellulose. Left scale bar is 1 µm, right scale bar is 2 µm.**

Scanning electron microscopy shows the nano-rods to be relatively straight, with lengths varying between 1 and a few microns. The upper limit of nano-fibre length is not known, although there are likely to be some relatively long fibres which have not been ‘cut’ during the hydrolysis. Generally nano-rods are below 5 µm in length. The diameters of the cellulose nano-rods are estimated to be between 50 and 100 nm.

### 3.3.4. Transmission electron microscopy

A better idea of the true dimensions of the fibres was obtained by transition electron microscopy imaging (TEM). Fig. 3.16 shows a typical TEM image of cellulose nano-rods after sulphuric acid hydrolysis.

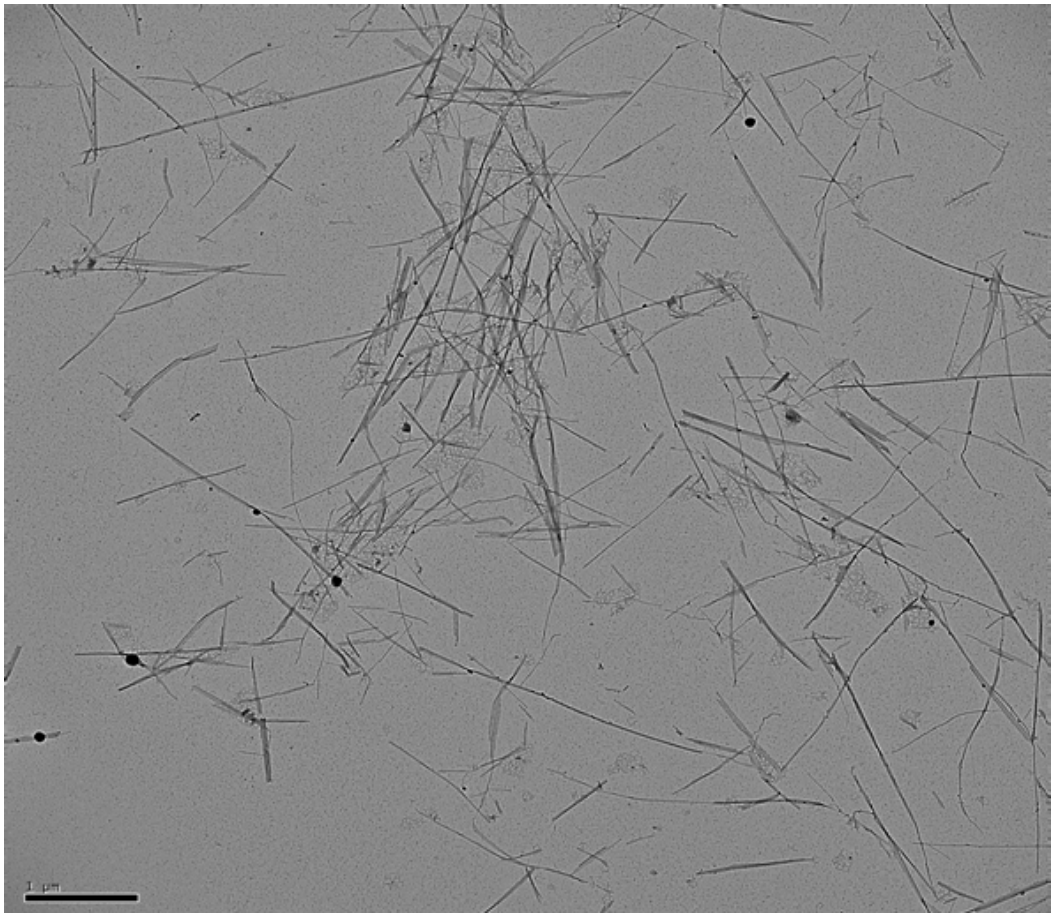

**Figure 3.16. TEM image of cellulose nano-rods produced by hydrolysis of gelatinous cubes of Nata de Coco bacterial cellulose in 45 wt.% sulphuric acid for 1 hr at 60 °C. Scale bar is 1 µm.**

It has been reported in the literature[10,21] that twists in the cellulose fibres facilitate the chiral nematic phase formed by cellulose fibres under precise conditions by encouraging screw-like packing of the fibres. Fig. 3.17 shows these twists clearly as indicated by the white arrows.

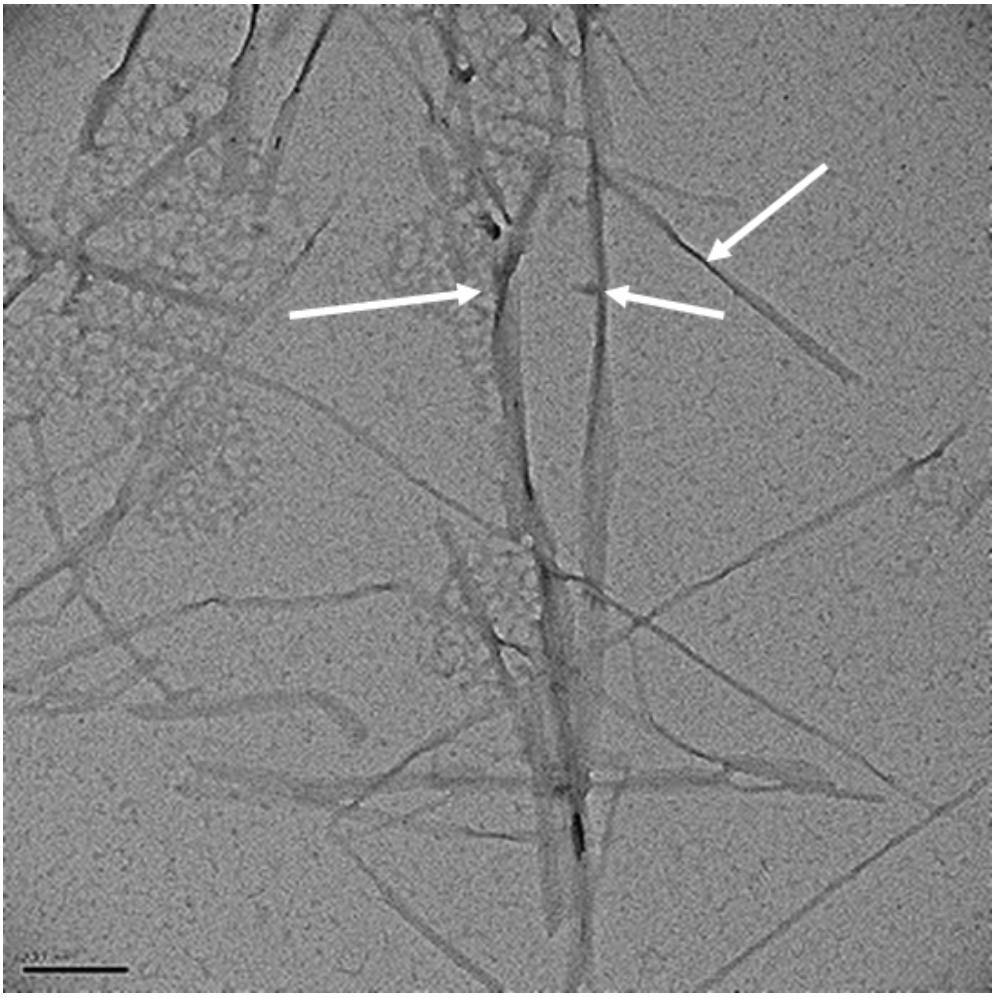

**Figure 3.17. TEM image of sulphuric acid hydrolysed cellulose nano-rods showing twists in fibres (arrows). Cellulose ribbons are estimated to be around 10 nm in thickness and up to 50 nm in diameter. Scale bar is 200 nm.**

The previous three images give an impression of the nano-fibre lengths on average being around 1-2 μm, and diameters are in the order of 50 nm. It was also noticed how transparent the nano-rods appeared using TEM, especially when high magnifications were used, and this made focussing on them very difficult. The nano-rods were clearly much too small to be seen under an optical microscope, and detailed analysis of dimensions (using Image-Pro Plus software) was not carried out.

### 3.4. Foamability of cellulose nano-rods

Bacterial cellulose nano-rod suspensions between 0.5 and 2 wt.% in Milli-Q water were prepared to assess their foamability. All Nata de Coco nano-fibres used for foamability studies were produced by sulphuric acid hydrolysis for 1 hr at 60 °C using 45 wt.% $H_2SO_4$. Approximately 10 g of gelatinous Nata de Coco cubes were required to obtain 0.2 g of dry nano-fibres.

It was found that no foam could be formed at any of the nano-fibre concentrations, and increasing the concentration further to try and facilitate foaming would have lead to gelling of the suspension, and thus no foam could be produced then due to the difficulty of shearing (as hand shaking was used to produce foam) at this viscosity. It was decided that surface-modification of the nano-rods would be necessary to increase their surface activity by lowering the hydrophilicity (caused by the surface –OH and sulphate groups).

### 3.5. Surface modification of cellulose nano-rods

#### 3.5.1. Modification of cellulose nano-rods with polyelectrolyte

In order to invert the surface charge of the cellulose nano-rods from negative to slightly positive, the cationic polyelectrolyte poly (allylamine hydrochloride) or PAH was used. This polyelectrolyte has a molecular weight of approximately 70,000 g $mol^{-1}$ and should coat the nano-rods in a positively-charged 'jacket'. A 3 mg/mL solution of PAH in Milli-Q water was prepared. This was placed on a magnetic stirrer, and set stirring at 750 rpm. At 1 wt.% in Milli-Q water, the fibres formed a very viscous suspension, so the suspension was diluted 50:50 with Milli-Q water prior to addition to the stirring solution to aid adequate dispersion and even coverage of the fibres in polyelectrolyte.

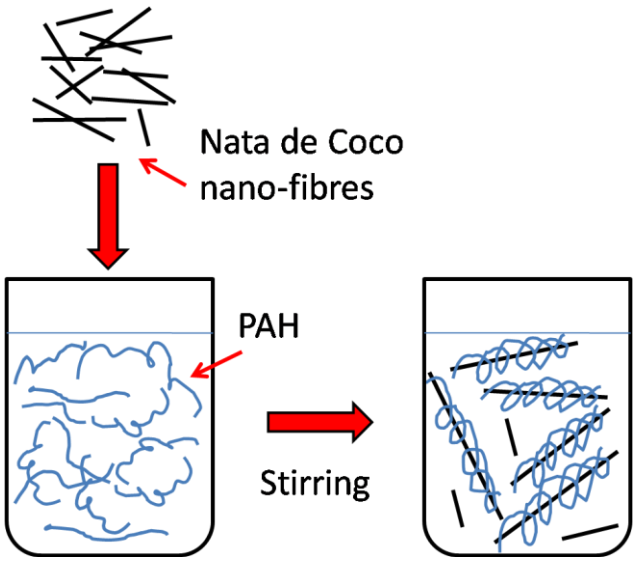


**Figure 3.18. Schematic diagram representing the 'wrapping' of cationic polyelectrolyte (poly (allylamine hydrochloride)) around the negatively-charged cellulose nano-rods to reverse their surface charge.**

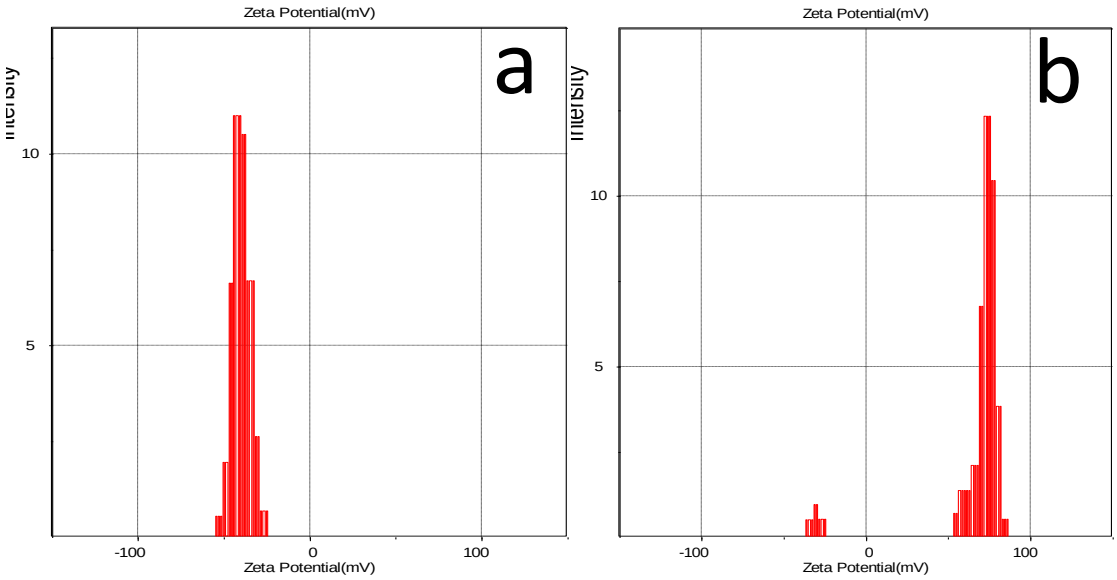


**Figure 3.19. ζ-potential measurement of an aqueous suspension of cellulose nano-rods before (a) and after (b) treatment with The mathematical model used to evaluate the ζ-potential of these particles is based on spheres rather than rod-shapes. With this in mind, we use this technique only to show a qualitative change from negative to positive surface charge.**

The suspension was added very slowly (dropwise, 30 min) to the polyelectrolyte solution with intensive stirring to facilitate even coverage. After addition, the polyelectrolyte-coated nano-rods were washed after centrifugation and replacement of the supernatant with Milli-Q water. This was repeated 5 times to ensure that minimal free polyelectrolyte remained in the sample which could affect the zeta potential recorded for the modified fibres. The nano-fibre suspension was concentrated to approximately 0.5 wt.% to assess its foamability but no foaming was observed. The zeta potential of the modified fibres was evaluated, and compared to that recorded for an aqueous suspension of unmodified cellulose nano-rods (fig. 3.19). A clear shift from around -40 mV to +66 mV was observed indicating that the nano-rods had been successfully coated together with a small remnant peak at around -40 mV indicating that there could be a small fraction of uncoated nano-rods left over after the procedure. We checked that the zeta potential of PAH alone is around +160 mV. Therefore despite apparently successfully coating the nano-rods with polyelectrolyte, this technique did not produce surface-active nano-rods. Reducing the charge to close to neutrality could potentially be more successful.

### 3.5.2. Modification of cellulose nano-rods with shellac

In order to increase the surface hydrophobicity and in doing so the surface-activity of cellulose nano-rods, a dispersion of nano-rods was coated in a layer of shellac. Shellac was chosen due to its surface-activity (see chapter 4), food grade status and mechanical strength. The shellac was deposited onto the surfaces of the nano-rods by inducing precipitation from a solution in which the nano-rods were suspended, by a solvent-change technique. The procedure is described fully in the experimental chapter 2. Following the precipitation of the shellac, the suspension was washed in Milli-Q water to remove ethanol, examined microscopically (SEM and TEM) and the foamability of the modified nano-rods was assessed. Scanning electron microscopy revealed little detail as to whether the nano-rods had a deposited surface layer of shellac. Fig. 3.20 shows a bed of interwoven nano-rods, together with some larger ‘globules’ or spheroidal precipitated particles of shellac. More insightful images were obtained using transmission electron microscopy. Figs. 3.21 and 3.22 show cellulose nano-rods which appear to have a coating of shellac. This was accompanied by a noticeable decrease in the transparency of the nano-rods at higher magnifications (compared with fig. 3.17). At

extreme magnification (fig. 3.23), a multi-layered structure was evident, similar to that seen in multi-wall carbon nano-tubes (MWNTs).

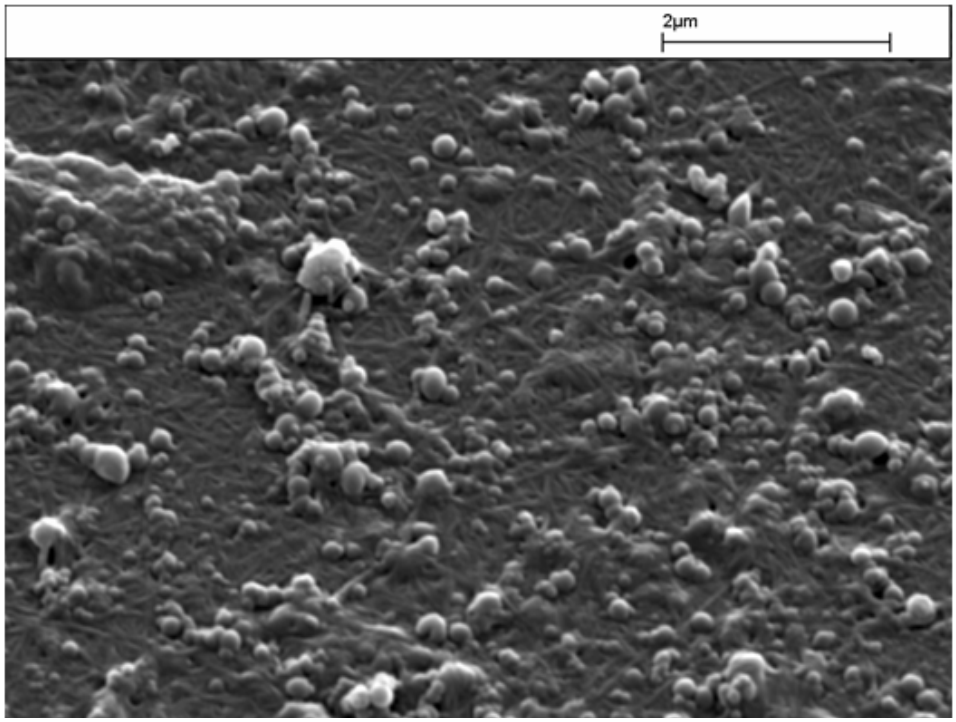


**Figure 3.20. SEM image of cellulose nano-rods and excess precipitated shellac wax particles. Surface coating of wax on nano-rods is not evident using this technique.**

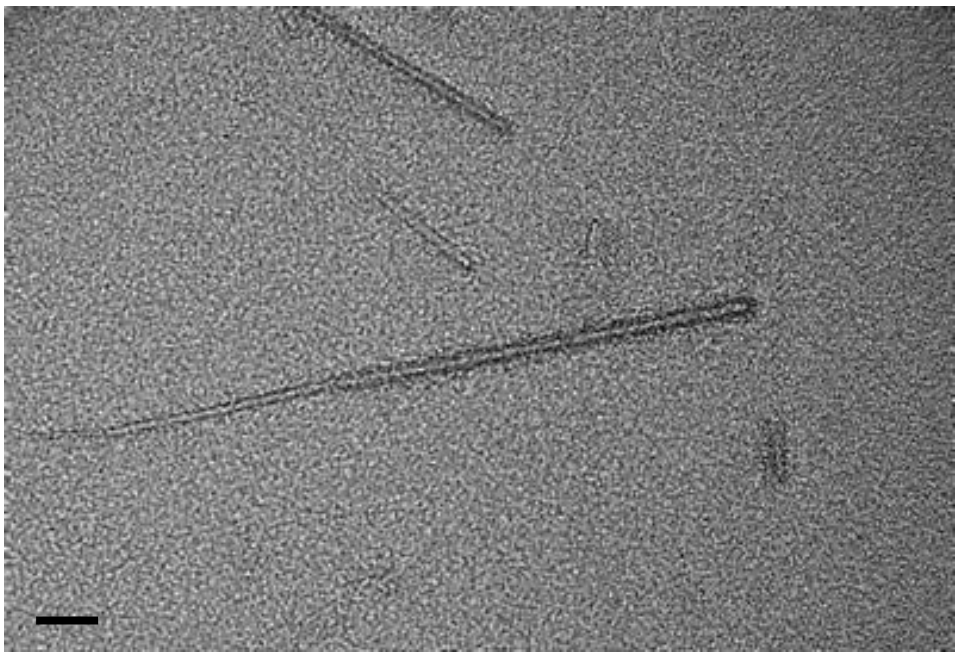

**Figure 3.21. TEM image of cellulose nano-rods treated with shellac wax. Scale bar is 20 nm.**

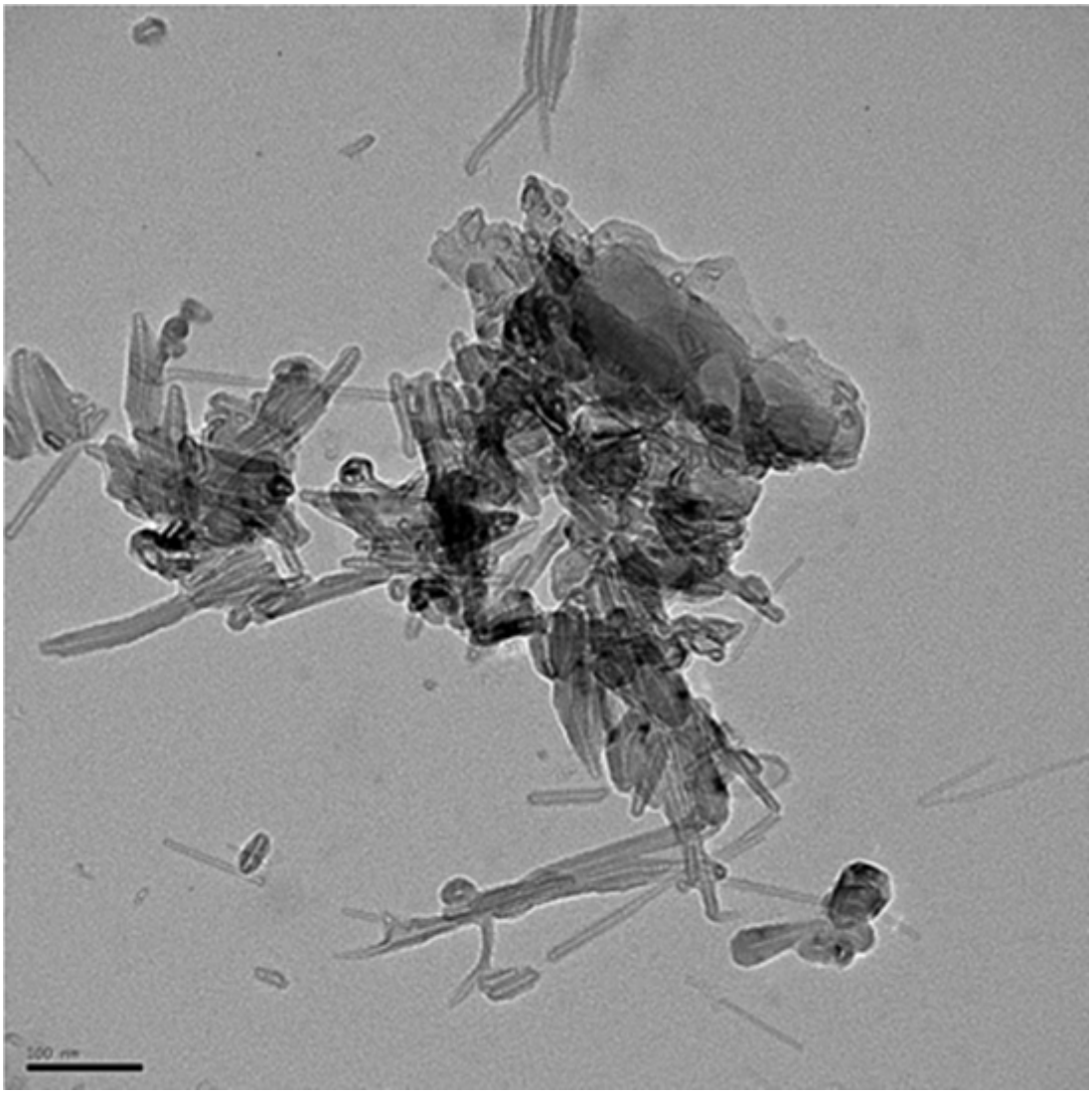


**Figure 3.22. An aggregate of shellac-coated cellulose nano-rods. This shows that the material has sticky properties. Scale bar is 100 nm.**

A hand-shaken aqueous suspension of 0.5 wt.% shellac-coated cellulose nano-rods exhibited relatively poor foamability. The foamability could be attributed solely to the discreet shellac globules observed by SEM (fig. 3.20).

In the following chapter the foamability of anisotropic rods comprised of shellac wax alone will be examined in the pursuit to produce food-grade anisotropic micro-rods which are capable of stabilising aqueous foams.

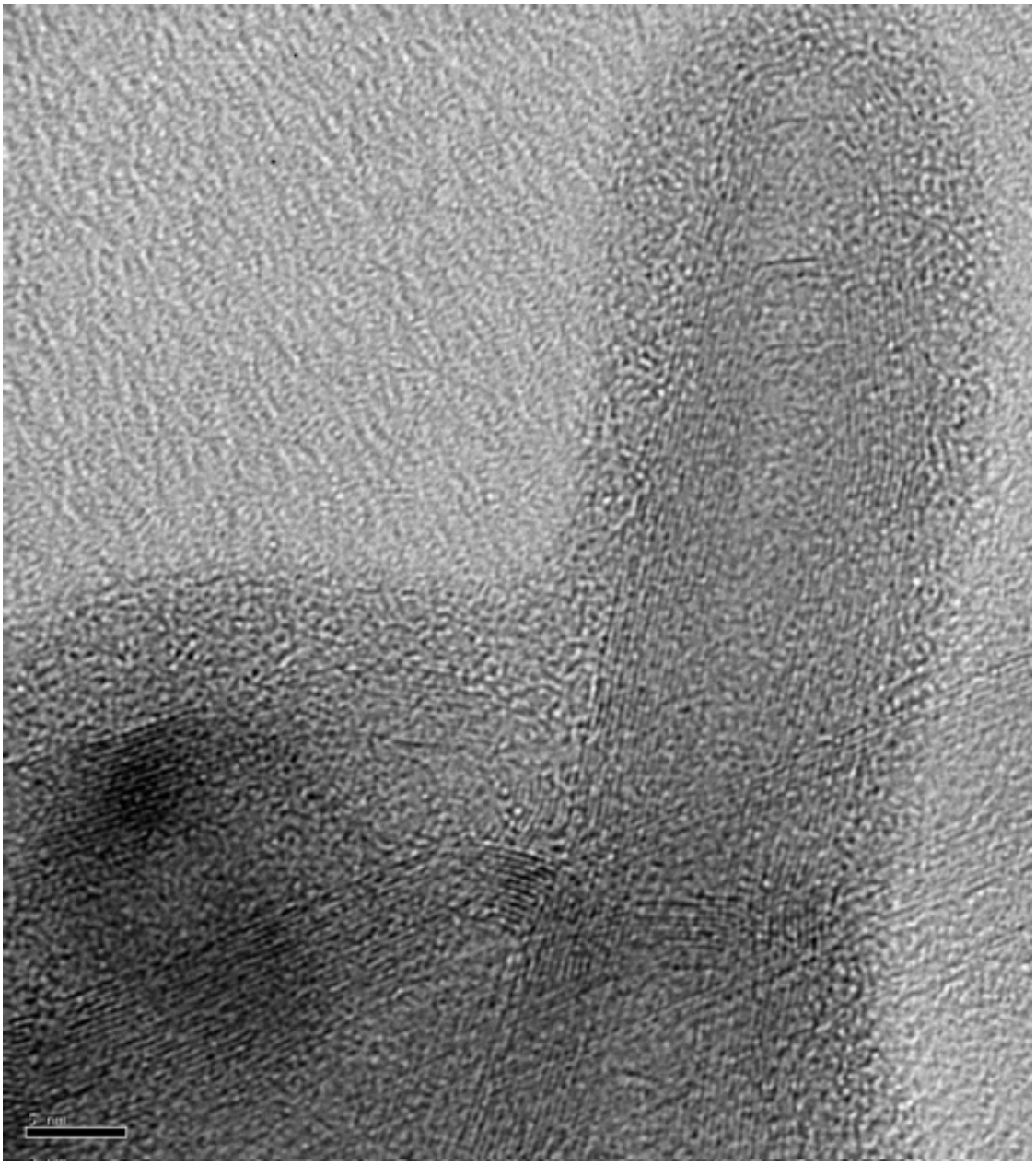

**Figure 3.23. Extreme magnification TEM image of the tip of a shellac-coated cellulose nano-rod, which exhibits a multi-layered appearance, similar to that observed in multi-wall carbon nano-tubes. Scale bar is 5 nm.**

### 3.5.3. Modification of cellulose nano-rods with ethyl cellulose

Ethyl cellulose was used to coat the surfaces of cellulose nano-rods. Ethyl cellulose is surface-active and is an approved food additive[25], used as a coating agent and a tablet excipient. It was expected that specific hydrogen bonding between the bacterial

cellulose nano-rods and the ethyl cellulose should allow successful coating of the nano-rods, and may give them enhanced foamability.

Hydrolysed Nata de Coco nano-rods modified with ethyl cellulose were prepared as described in chapter 2. Cellulose nano-rods were present at 0.5 wt.% together with an equal weight of ethyl cellulose, and the suspension was hand-shaken 20 times along with a control of just 0.5 wt.% ethyl cellulose to produce foams, and the evolution of foam height with time for both samples is presented in fig. 3.24. Error in measurement of foam height considered to be ± 2 mm and is based on the measurement from the top to the bottom of the foam, through the centres of the bubbles. A further aspect of measurement error is that the bubbles are smaller at the start and thus the error is also smaller. When bubbles coarsen over time, the magnitude of the error in measurement also increases. Errors based on three repetitions of the procedure.

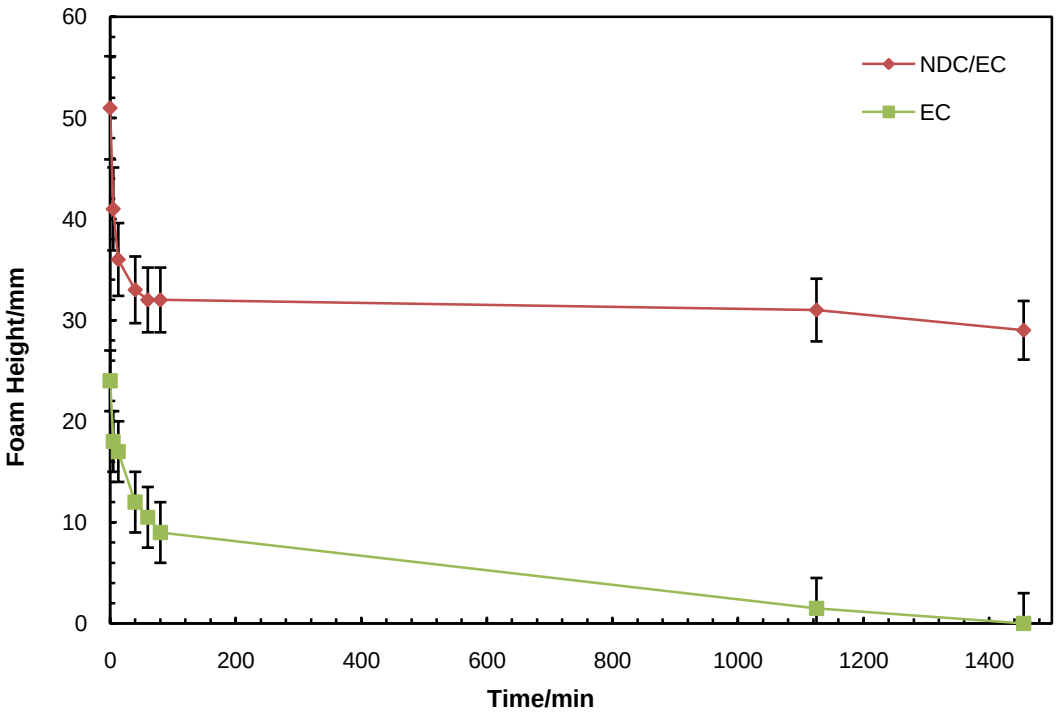


**Figure 3.24. Change in foam height over time of aqueous foams, one stabilised by ethyl cellulose nano-particles only, and one by acid-hydrolysed cellulose nano-rods surface-modified with a coating of ethyl cellulose.**

The stability of the foam where both cellulose nano-rods and ethyl cellulose are present is far greater than the foam where only ethyl cellulose nano-particles are present. This suggests that surface-active ethyl cellulose gives good foamability, but the steric

advantages of the nano-rods (over nano-spheres or nano-particles of low aspect ratio) including increased interfacial area coverage (per volume) and ability to intertwine at the interface are required to give enhanced stability over the longer term. It was decided to investigate the effect of varying the ratio of ethyl cellulose to Nata de Coco nano-rods. Ratios of 1:1, 1:5 and 1:20 were used (EC: NDC).

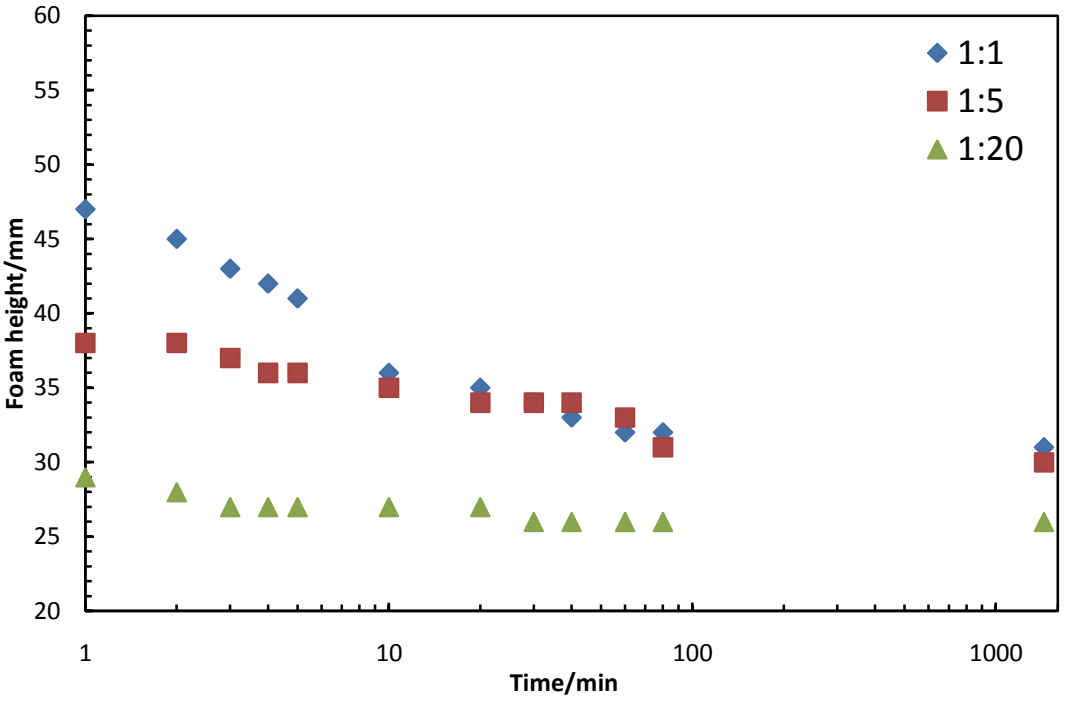


**Figure 3.25. Effect of varying the ethyl cellulose to cellulose nano-fibre ratio in ethyl cellulose coated cellulose nano-rods on foamability and stability of aqueous foams containing 0.5 wt.% modified nano-rods.**

The graph shows that an increase in ethyl cellulose to nano-rods weight ratio increases the foamability and to a lesser extent, the stability too. A distinct levelling out can be seen after approximately 30 minutes when foam height is plotted against time, showing the initial aqueous drainage from the foam.

### 3.5.3.1. Effect of variation of weight percentage of nano-rods

To ascertain the effect of concentration of the surface-modified nano-rods on the foamability and stability of the resulting aqueous foams together with the effect of varying the ratio of modifier to fibre substrate, nano-rods of 1:1, 1:5 and 1:20 ethyl

cellulose: Nata de Coco ratio were used to produce foams at 0.1, 0.2, 0.3, 0.4 and 0.5 wt.% content. Figs. 3.26 – 3.28 show the effect of varying the weight percentage of stabilising surface-modified Nata de Coco nano-rods at 1:1, 1:5 and 1:20 EC: NDC ratios respectively.

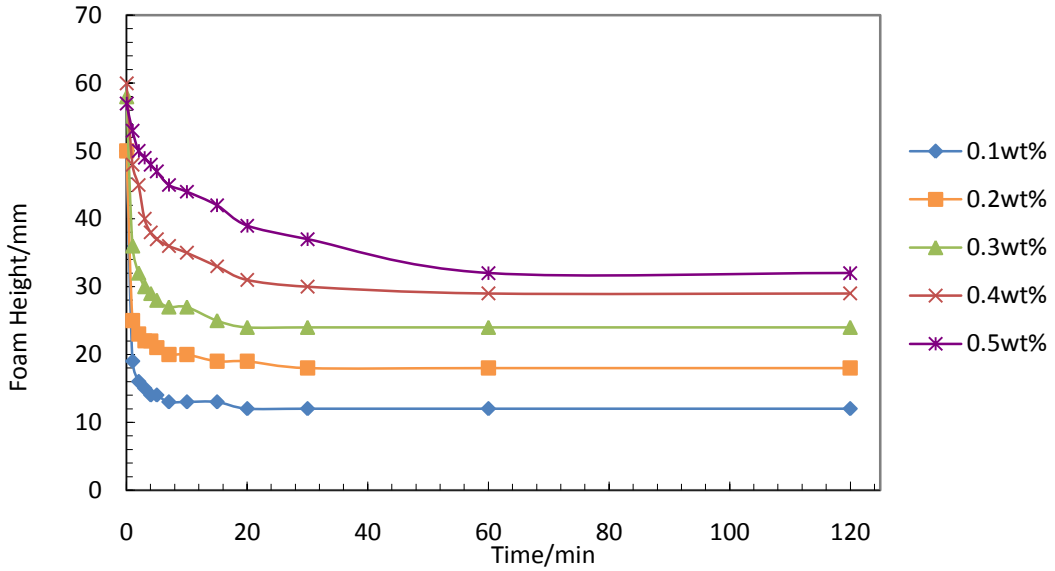


**Figure 3.26. Effect of increasing concentration of ethyl cellulose-coated cellulose nano-rods with 1:1 ethyl cellulose/cellulose ratio on foamability and foam stability.**

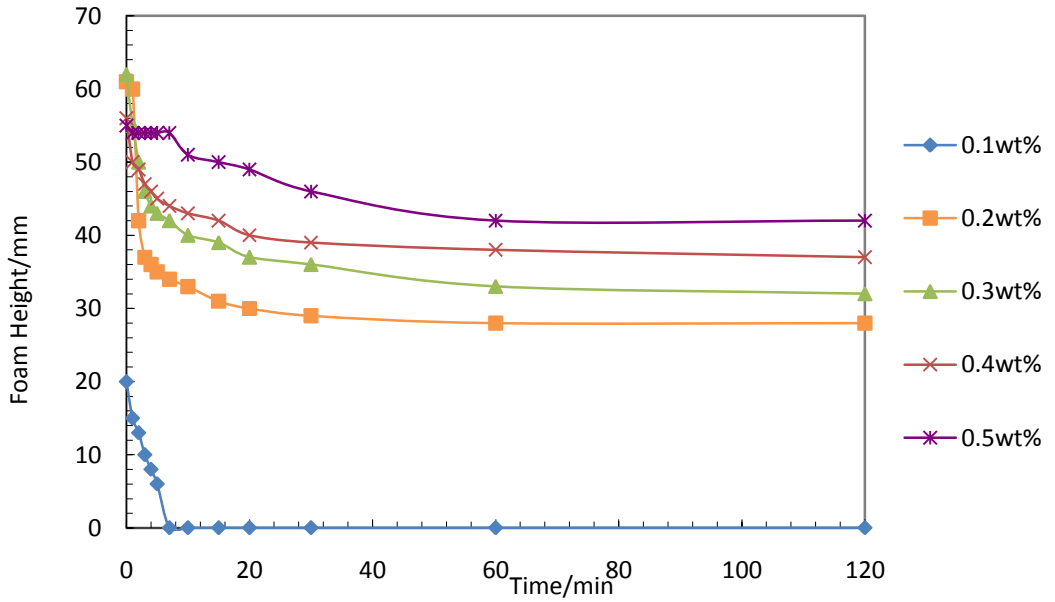


**Figure 3.27. Effect of increasing concentration of ethyl cellulose-coated cellulose nano-rods with 1:5 ethyl cellulose/cellulose ratio on foamability and foam stability.**

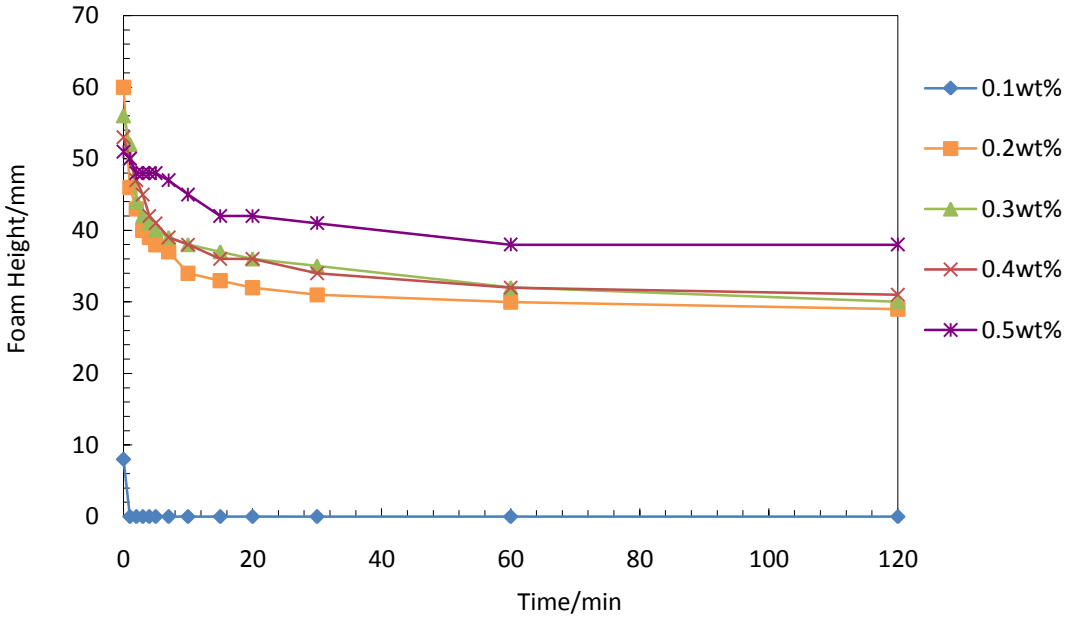


**Figure 3.28. Effect of increasing concentration of ethyl cellulose-coated cellulose nano-rods with 1:20 ethyl cellulose/cellulose ratio on foamability and foam stability.**

These plots all show that below 0.2 wt.% the continuous phase viscosity is not sufficient to slow down the destabilisation mechanisms present in the foams, namely creaming of bubbles and the ensuing close approach and coalescence and also liquid drainage. The foams had low volume, but it may be possible to produce far superior foams both in terms of volume and stability by utilising ethyl cellulose particles alone.

## 3.6. Foam scaffolding and composite foams

### 3.6.1. The idea of foam scaffolding – synergy between cellulose nano-rods and ethyl cellulose nano-particles

It is possible to create exceptionally stable foam formulations by stabilisation of the air-liquid interface with a combination of surface-active ethyl cellulose nano-particles which are held in place by specific hydrogen bonding with adjacent cellulose nano-rods, providing some structural rigidity and reducing drainage and coalescence within the foam. It is through this synergistic effect that it is expected that highly stable foams could be formed.

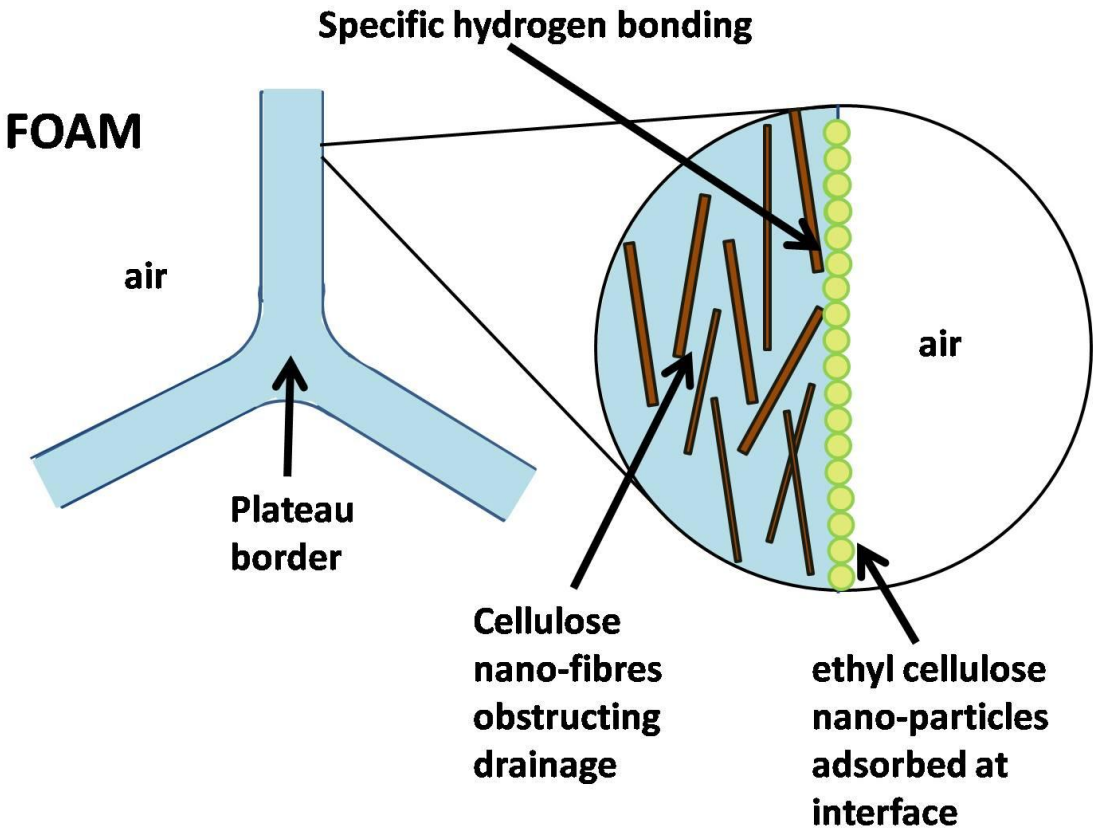


**Figure 3.29. Schematic diagram showing the proposed mechanism of foam stabilisation detailed below.**

It is anticipated that foam scaffolding will work as follows. During air bubble formation the surface-active ethyl cellulose nano-particles migrate to the air-liquid interface, where they adsorb which stabilises the newly-formed air bubbles against immediate coalescence. As drainage takes place in the foam, the air bubbles are drawn closer together and the hydrophilic cellulose nano-rods which remain in the aqueous phase accumulate in the drainage channels within the foam. Held there due to hydrogen bonding with the adsorbed ethyl cellulose nano-particles at the interface, they should delay further gravity-induced drainage through the foam, giving enhanced stability and thereby increasing foam lifetimes. A similar mechanism has been reported for the stabilising effects of certain solid stabilised emulsion systems, where two different morphology particles are used. Abend et al.[26] stabilised paraffin/water emulsions using mixtures of a double hydroxide and clay minerals. Here it is suggested that the double hydroxide particles stabilise the oil droplets whilst the clay particles make a three-dimensional network which helps to prevent droplet coalescence. Whilst similar in

concept to our system, their system uses hetero-coagulation of oppositely-charged clay minerals, while we use only hydrogen bonding.

### 3.6.2. Preparation of cellulose nano-rod/ethyl cellulose-stabilised foams

An aqueous suspension of bacterial cellulose nano-rods was produced as described in chapter 2. Cellulose nano-rods were combined with aqueous suspensions of ethyl cellulose nano-particles which were produced using a solvent change technique that is also described in chapter 2. This resulted in aqueous suspensions with solids content remaining approximately constant at 0.5 wt.%, with changing bacterial cellulose/ethyl cellulose ratios. The ratio of bacterial cellulose-to-ethyl cellulose was varied from 10:1 through 2:1, equal and 1:2 to 1:10, and the foams were produced by hand-shaking (up and down, 20 x) to evaluate the effect of variation of these components on the foamability and foam stability.

### 3.6.3. Effect of varying the ratio between ethyl cellulose nano-particles and cellulose nano-rods on foamability and foam stability

Aqueous suspensions of ethyl cellulose nano-particles and sulphuric acid hydrolysed bacterial cellulose nano-rods were combined at different ratios from 10:1 to 1:10 so that the total solids concentration was 0.5 wt.%. Foams were produced by hand shaking and the foam height over time was monitored.

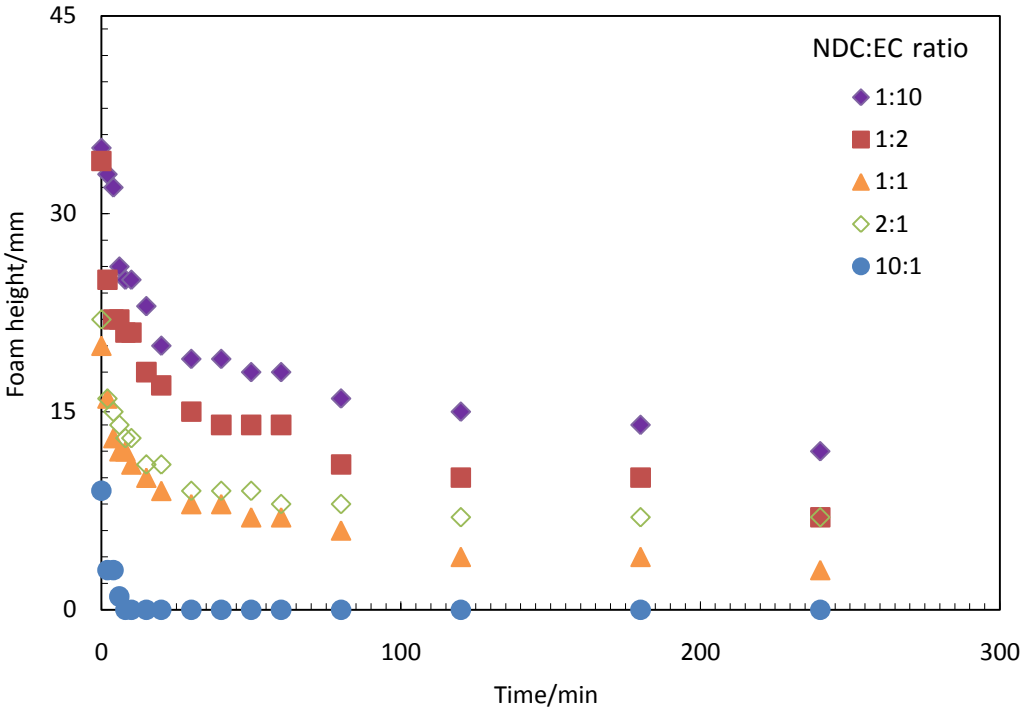


**Figure 3.30. Effect of variation of Nata de Coco: ethyl cellulose ratio on the foamability and stability of aqueous foams stabilised by a 0.5 wt.% mixture of the two materials.**

Foamability of these samples was relatively low when compared with ethyl cellulose-modified bacterial cellulose nano-rods; however, this could be altered by increasing the overall solids concentration in the samples. The foam height reached a plateau, however, the foams eventually collapsed after 1 day at room temperature.

Highest stability and foam volume was observed when the highest concentration of ethyl cellulose was used (1:10, NDC:EC). Stability level steadily increased with increasing concentration of ethyl cellulose in the mixture; the least stable sample was the 10:1 NDC:EC foam which collapsed completely after only 8 minutes. Bubble coarsening was observed in all samples. The factors affecting the success of this method are the size of the ethyl cellulose nano-particles and the method in which the foam is produced. If the size of the nano-particles can be reduced considerably (from above one hundred nanometres to below a hundred nanometres) the scaffolding efficiency could be enhanced. The foamability of the system is quite poor, and it is possible that hand-shaking to produce the foams may not be the most effective method. By using some kind of mechanical mixing a greater foam volume with smaller bubbles could be achieved.

### 3.7. Conclusions

Bacterial cellulose nano-rod suspensions were produced by sulphuric acid hydrolysis of native, gelatinous Nata de Coco and subsequent cleaning and re-dispersion using ultrasound. The cellulose nano-rods were characterised using laser diffraction particle sizing where the size was measured at approximately 400 nm, however, a better estimate of the dimensions of the nano-rods was obtained when images from SEM and TEM were visually assessed. Nano-rods were approximately 1 – 2 μm in length with diameters of around 50 nm. The appearance was similar to that described by other authors. Some nano-rods had a ribbon-like appearance with twists visible along their lengths. These were estimated to have thicknesses around 10 nm and diameters around 50 nm. Modification of the nano-rods via surface coating with waxes and polyelectrolyte did not improve their foamability. When the nano-rods were coated in a layer of ethyl cellulose, foams were formed from aqueous suspensions of the modified nano-rods. Cellulose nano-rods coated in ethyl cellulose gave superior foamability and foam stability than those produced using ethyl cellulose nano-particles alone (or mixtures of the two – see below).

The idea of foam scaffolding was also investigated. Here, ethyl cellulose nano-particles are used to give optimum foamability whilst the accompanying cellulose nano-rods clogging the Gibbs-Plateau channels within the foam could hinder the liquid drainage whilst being held in place by specific hydrogen bonding with the ethyl cellulose nano-particles adsorbed at the gas-liquid interface. Foams stabilised by this technique showed some foamability and stability, with maximal foam volume observed at the highest concentration of ethyl cellulose in the mixture. Ethyl cellulose-modified cellulose nano-rods gave superior foamability.

In the following chapters we explore the possibility of forming micro-rods from shellac and ethyl cellulose and evaluate their foamability.

### 3.8. References


[1] G.R. Stevens, G.H. Heichel. *Biotechnol. & Bioeng. Symp.* 1975, **5,** 27.

[2] M. de Souza Lima, R. Borsali. *Macromol. Rapid Commun.* 2004, **25,** 771.

[3] T. Tsuchida, F. Yoshinaga. *Pure and Applied Chem.* 1997, **69,** 2453.

[4] C.H. Haigler, A.R. White, R. Malcolm Brown Jr, K.M. Cooper. *J. Cell Biol.* 1982, **94,** 64.

[5] G. Ben Hayyim, I. Ohad. *J. Cell Biol.* 1965, **25,** 191.

[6] R. Malcolm Brown Jr, J.H. Martin Willison, C.L. Richardson. *Proc. Natl. Acad. Sci. USA.* 1976, **73,** No. 12, 4565.

[7] J.A. Gascoigne, M.M. Gascoigne. *Biological Degradation of Cellulose.* Butterworths, London. 1960.

[8] A.C. O'Sullivan. *Cellulose.* 1997, **4,** 173.

[9] K. Fleming, D.G Gray, S. Matthews. *Chem. Eur. J.* 2001, **7,** No. 9, 1831.

[10] G. Gahudos, W. Wan, J.L. Hutter. *Langmuir.* 2005, **21,** 6642.

[11] V.L. Finkenstadt, R.P. Millane. *Macromolecules.* 1998, **31,** 7776.

[12] P.S. Belton, S.F. Tanner, N. Cartier, H. Chanzy. *Macromolecules.* 1989, **22,** 1615.

[13] C. Bellman, A. Caspari, V. Albrecht, T.T. Loan Doan, E. Mäder, T. Luxbacher, R. Kohl. *Colloids Surfaces A: Physicochem. Eng. Aspects.* 2005, **267,** 19.

[14] W.J. Orts, J. Shey, S.H. Imam, G.M. Glenn, M.E. Guttman, J.F. Revol. *J. Polym. and the Env.* 2005, **14,** No. 4, 301.

[15] B.G. Rånby. *Discuss. Faraday Soc.* 1951, **11,** 158.

[16] J. Araki, M. Wada, S. Kuga, T. Okano. *Colloids Surfaces A: Physicochem. Eng. Aspects.* 1998, **142,** 75.

[17] X.M. Dong, J.F. Revol, D.G. Gray. *Cellulose.* 1998, **5,** 19.

[18] X.M. Dong, T. Kimura, J.F. Revol, D.G. Gray. *Langmuir.* 1996, **12,** 2076.

[19] J.F. Revol, H. Bradford, J. Giasson, R.H. Marchessault, D.G. Gray. *Int. J. Biol. Macromol.* 1992, **14,** 170.

[20] J. Araki, S. Kuga. *Langmuir.* 2001, **17,** 4493.

[21] W.G. Haigh, H.J. Förster, K. Biemann, N.H. Tattrie, J.R. Colvin. *Biochem. J.* 1973, **135,** 145.

[22] X.M. Dong, D.G. Gray. *Langmuir.* 1997, **13,** 3029.

[23] X.M. Dong, D.G. Gray. *Langmuir.* 1997, **13,** 2404.

[24] J.F. Revol, L. Godbout, D.G. Gray. *J. Pulp and Paper Sci.* 1998, **24,** No. 5, 146.

[25] R. Anton, S. Barlow, D. Boskou, L. Castle, R. Crebelli, W. Dekant, K-H. Engel, S. Forsythe, W. Grunow, J.-C. Larsen, C. Leclercq, W. Mennes, M-R. Milana, I. Rietjens, K. Svensson, P. Tobback, F. Toldra. *Eur. Food Standards Agency J.* 2004, **1.**

[26] S. Abend, N. Bonnke, U. Gutschner, G, Lagaly. *Colloid Polym. Sci.* 1998, **276,** 730.

# CHAPTER 4 – PREPARATION, CHARACTERISATION AND FOAMABILITY OF SHELLAC MICRO-RODS

This chapter is concerned with the preparation and characterisation of micro-rods produced from a natural, food-grade material - shellac. The aim is to produce food-grade micro-rods which would be suitable for stabilising edible foams with applications in the food industry.

It has already been discussed in chapter 1 that since the first use of solid particles as emulsifiers over a hundred years ago[1,2], very stable emulsions and foams have been formed by using such particles.[3-15]

Recently there has been an increased interest into using anisotropic particles as foam stabilisers. Together with the advantages that spherical or spheroidal particles possess, anisotropic (in this case rod-shaped) particles also have greater surface area to volume ratio (and therefore greater interfacial coverage per volume). Disc-shaped particles have been shown to adsorb even more strongly to liquid interfaces than rods or spheres of equivalent volume. High aspect ratio rod-shaped particles can also interweave with neighbouring rods at the interface, giving additional steric stability to the emulsion or foam system being stabilised. These stabilising properties have been observed by Alargova et al.[16-20] In a number of publications, surface-active SU-8 epoxy polymer micro-rods have been produced and shown to produce extremely stable emulsions and foams. The method of production of the micro-rods is highly versatile and allows easy scale-up to much larger volumes. Fig. 4.1 shows a schematic of the main processes involved in the production of polymer micro-rods by using the so-called ‘liquid-liquid dispersion technique’.

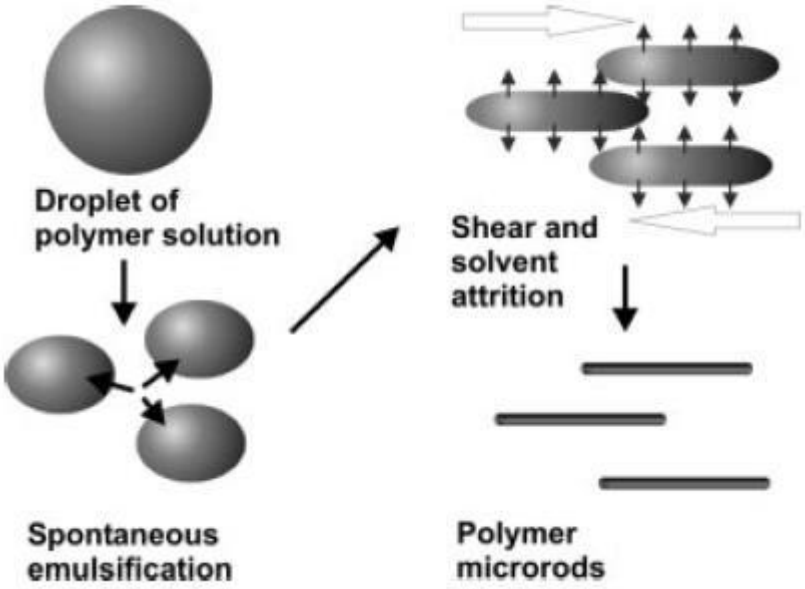


**Figure 4.1. Schematic diagram depicting the main processed involved in the formation of polymer micro-rods by the 'liquid-liquid dispersion technique' pioneered by Alargova et al.[16]**

The method is based on emulsification of a polymer solution under shear, combined with solvent attrition in the surrounding medium. Stopped-flow experiments have shown that the droplets deform and elongate into cylinders, which solidify when the solvent transfers to the continuous phase.

Alargova et al. studied the effect of the shear rate, polymer concentration and the viscosity of the disperse media on the morphology of the produced micro-rods. Increasing the concentration of micro-rod polymer resulted in larger micro-rods being formed, both longer and wider. The rods were also shown to align in an AC electric field. In other studies[19], the rod-shaped particles were found to form stable water-in-oil emulsions, which were used to produce colloidosome capsules that could have a number of potential uses including encapsulation. Further work showed that the SU-8 micro-rods proved to be excellent stabilisers of aqueous foams as well, with good foamability and phenomenal foam lifetimes.[17] The SU-8 polymer micro-rods cover the surfaces of air bubbles densely, and give the appearance of 'hairy bubbles'. It is likely that the inter-weaving of these polymer micro-rods contributes to the steric stability of foams with which they are stabilised. These foams have been branded as 'superstabilised' as a result of their strong, rigid structure.

Although the micro-rods produced by Alargova et al.[17] display a range of remarkable properties, including great foamability and ease of production, they are not food-grade, and therefore not applicable to use in the food industry. Here, we aim to produce food-grade particles with similar or superior properties which pointed us to apply the technique to shellac.

In this chapter we describe shellac micro-rods produced using a liquid-liquid dispersion technique. Micro-rods were produced with lengths ranging from a few tens of to several hundred microns and diameters of a few microns. The effect of varying the preparation conditions of the micro-rods was investigated, and the results are described below. The wettability of shellac was also investigated by examining water drops on a glass slide spin-coated with the material, and by using the gel trapping technique[21-23] to visually analyse individual rods adsorbed at the gas – liquid interface. The foamability and foam stability of shellac micro-rod-stabilised foams was investigated, and it was discovered that the stability of the micro-rod-stabilised foams can be greatly improved by thermal treatment of the micro-rods.

### 4.1. Shellac: chemical structure, origins and uses. Why use shellac?

Shellac is a food grade material and the FDA recognises it as 'Generally Recognised as Safe' (GRAS). Cultivated in the middle- and far-east (India and Thailand), shellac is the refined product of 'lac', a secretion of the lac beetle (fig. 4.2) which feeds on the sap of trees, and leaves the sticky, resin-like lac on the branches where it fed.

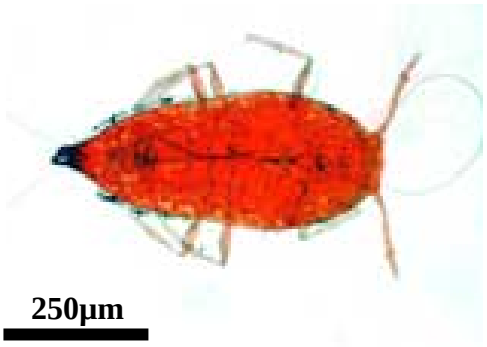


**Figure 4.2. The lac beetle.[24]**

**Figure 4.3. The secreted wax shrouds in which the insects stay until the branches containing the wax are harvested. Many of the insects are replaced in their habitat, so as to ensure a plentiful supply in the future.[25]**

Following a number of washes, and melting, filtration and evaporation processes, a refined product is obtained, although a variety of different grades are recognised, depending on the level of purification.

**Figure 4.4. The appearance of various grades of shellac, a result of different treatment processes.[26]**

Shellac has a complex composition and has not been completely characterised[27-30] but major constituents include aleuritic acid, r-butolic acid, shellolic acid and jalaric acid (fig. 4.5). The molecular weight is around 1000 g $mol^{-1}$, but due to the varying composition the melting point is highly variable, between around 80 – 120 ºC dependent largely on the source of the shellac.[30]

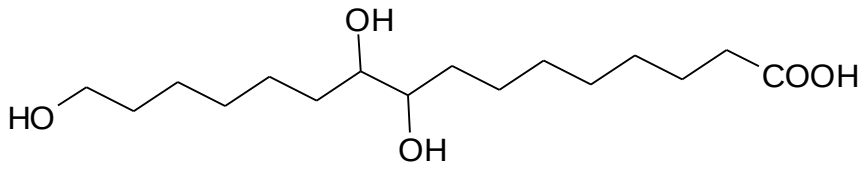


Aleuritic acid

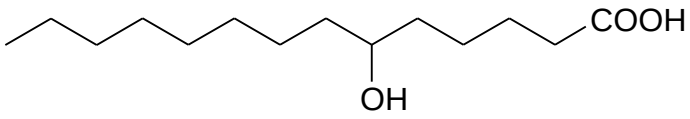


Butolic acid

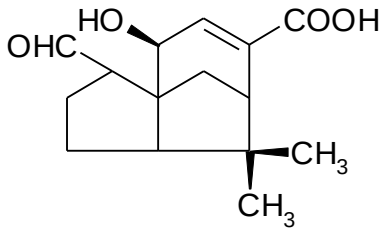


Jalaric acid

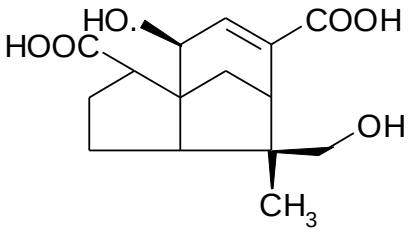


Shellolic acid

**Figure 4.5. Chemical structures of the major components found in shellac wax. Composition of the wax varies considerably depending on where and when the unrefined lac is collected.[30]**

Shellac has been in use for over a hundred years. The primary use of this material is in French polish, but during the early years of music storage and reproduction, shellac was used in the production of records. It has also been used as a tablet coating, and has been used to coat sweets and other products for many years. Shellac is known to many as 'confectioner's glaze'.

Because of its mechanical strength and relatively high melting point together with its food grade status, and hydrophobicity, shellac presents itself as an ideal material to produce food-grade, surface-active micro-rods with good potential to stabilise edible foams.

## 4.2. Technique for the preparation of shellac micro-rods

Although the procedure is described fully in the experimental section, a brief account of the process used for the production of shellac micro-rods is included in this section.

Initially it was necessary to grind down the shellac which facilitated its dissolution into ethanol. This resulted in a viscous solution of shellac in ethanol which was slowly injected into the glycerol/water continuous phase solution in the gap between the rotating mixer head and the inside wall of the beaker – a region of high shear, where drops elongate and undergo solvent attrition at the same time. Once the solvent attrition process was complete, the dispersion of micro-rods was washed to produce an aqueous dispersion. Shellac micro-rods were washed by replacing the supernatant with fresh water. This process was repeated, until an aqueous dispersion was produced.

## 4.3. Investigating the preparation parameters on the properties of the micro-rods produced

### 4.3.1. Effect of disperse phase shellac concentration

It was anticipated that the morphology of the resultant micro-rods would be highly dependent on the ratio of the viscosities of the disperse and continuous phases. To

examine this effect, the viscosities of a range of shellac in ethanol solutions and the continuous phase (aqueous glycerol solution) were measured.

| Shellac concentration (in ethanol) (wt%) | Viscosity/Pa s |
|---|---|
| 50 | 0.0877 |
| 40 | 0.0341 |
| 30 | 0.0136 |
| 20 | 0.0107 |

**Table 4.1. Viscosity of the polymer solutions in the disperse phase measured on a Bohlin CVO120 Hi-Res rheometer at a shear rate of 10.8 $s^{-1}$. A cone (4° slope) and plate geometry was used. For the continuous phase (85% glycerol, 15% Milli-Q water v/v) the viscosity was 0.0294 Pa s.**

Alargova et al. reported that the most successful micro-rod formation occurs when the ratio of viscosities of the disperse and continuous phases is close to unity.[20] Best results in the work here indicate that higher disperse phase viscosities give micro-rods which are increasingly smaller and more uniform in size. However, at a constant shear rate, the viscosity of a 50 wt% solution of shellac in ethanol is still of the same order of magnitude as that of the glycerol/Milli-Q water disperse phase (0.0294 Pa s).

Shellac micro-rods were produced using shellac in ethanol dispersed phases of concentrations ranging from 5 wt% up to 50 wt% shellac in 5% increments. At 5 and 10 wt%, no micro-rods were formed, presumably because the viscosity of the dispersed phase was too low. At 20 – 45 wt%, micro-rods and ribbons were produced, but the overall proportion of particles with rod-shaped geometry in the sample was low, with very high polydispersity in length and diameter of the particles. When 50 wt.% shellac was used, the quality of the micro-rods increased dramatically, with more uniform precipitated particles being produced (figs. 4.7 and 4.8).

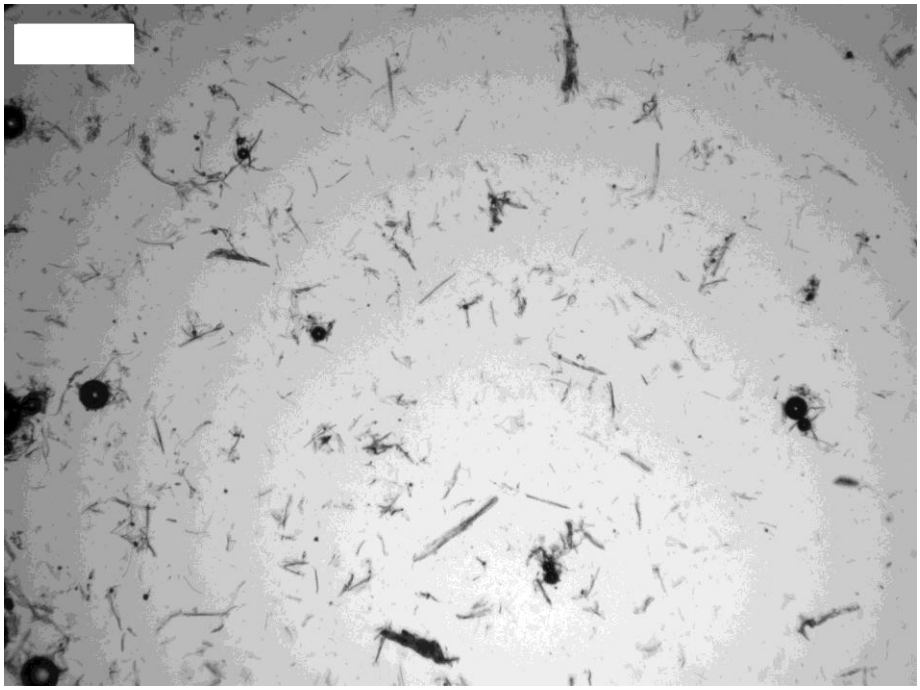

**Figure 4.7. Optical microscopy image of micro-rods produced using a 25 wt% shellac in ethanol solution, continuous phase of 85% glycerol/15% Milli-Q water (v/v) mixture, 1,400 rpm stirring for 10 min. Under these conditions a wide variety of shapes and sizes of precipitates are formed. Scale bar is 250 µm.**

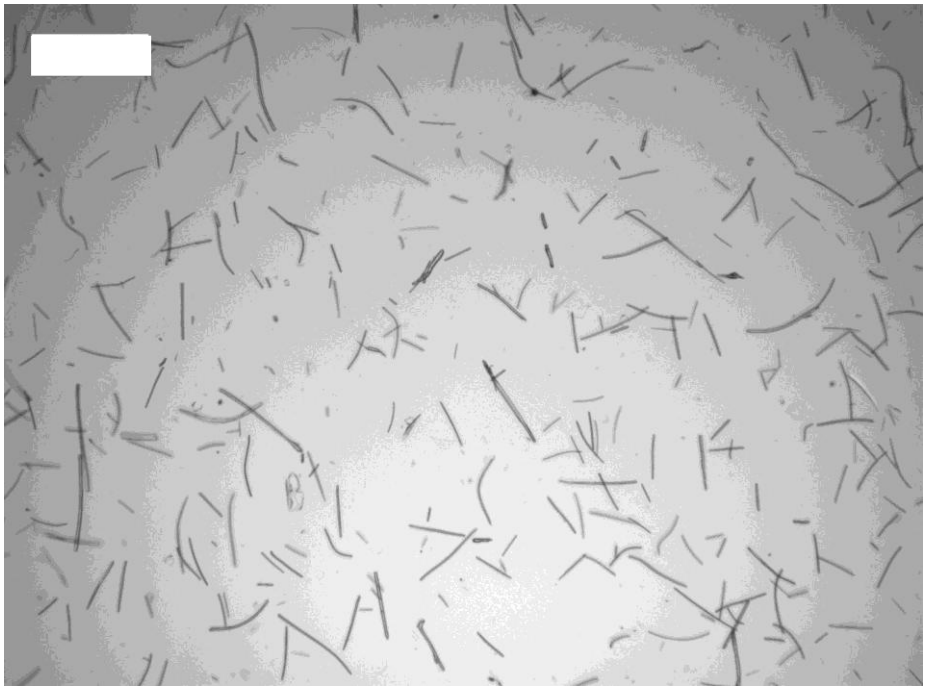

**Figure 4.8. Optical microscopy image of micro-rods produced using a 50 wt% shellac in ethanol solution, identical continuous phase to above, 1,400 rpm stirring for 10 min. Scale bar is 250 µm.**

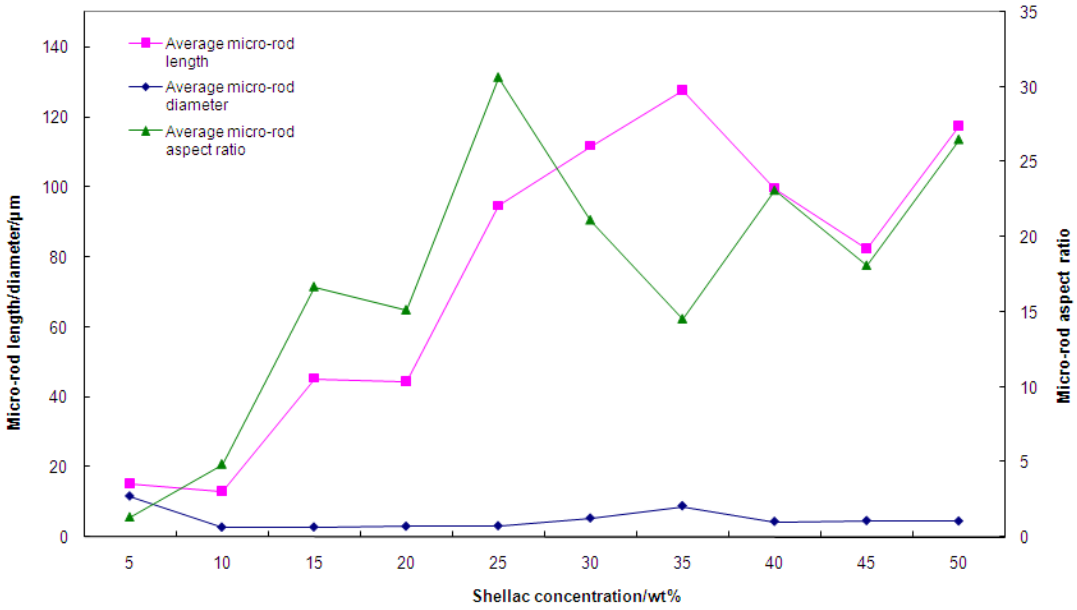


**Figure 4.9. Effect of shellac concentration in ethanol (the disperse phase) on the resulting length, diameter and aspect ratio of micro-rods produced. Stirrer speed was kept constant at 1,400 rpm, and a continuous phase mixture of 85% glycerol and 15% Milli-Q water (v/v) was used.**

Based on these experiments it was decided that 50 wt% was the most suitable concentration to use for the dispersed phase. Together with the remaining conditions described in figure legend 4.9, this was used as the protocol for the production of micro-rods for foaming studies. Higher concentration shellac in ethanol solutions could potentially offer even smaller, more uniform micro-rods (due to increased viscosity and therefore higher shear) but this presents problems in terms of processing. Solutions of such viscosity are difficult to handle, and do not emulsify homogeneously, leading to a low yield of micro-rods. Note that in this work, the term ‘yield’ is a qualitative measure of the relative abundance of high aspect micro-rods observed by optical microscopy. For smaller rods to be produced from such viscous solutions, much higher shear would be a necessity. This is in order to deform and break apart the large and highly viscous drops of disperse phase solution (far higher than the maximum speed of the mixing equipment used by the author).

### 4.3.2. Effect of stirrer speed during micro-rod formation

It has already been established that the shear rate is an important factor in controlling the morphology of the micro-rods formed by the liquid-liquid dispersion technique. One of the ways in which we control the shear rate is to vary the speed of the Cole-Parmer digital reversing mixer. In experiments described below, the disperse phase composition is kept constant, while the shear rate will be varied to investigate the effect on the resultant micro-rods.

The optimal concentration for the injected polymer solution was chosen to be 50 wt.% shellac in ethanol. The continuous phase was an 85% glycerol/15% Milli-Q water (v/v) mixture. The stirring speed of the Cole-Palmer mixer was varied by increments of 100 rpm between 400 and 1,400 rpm using the digital speed control.

Fig. 4.10 shows that the micro-rod length is decreased with increasing stirrer speed which agrees with the work carried out by Alargova et al.[20] where SU-8 epoxy polymer micro-rods were produced using a similar liquid-liquid dispersion technique. This decrease in micro-rod length is caused by the increasingly high shear breaking the elongated polymer-containing drops down into smaller units during the solvent attrition process. A likely explanation is that more intense shearing favours increased levels of secondary rod break-up which occurs after the initial break-up and lengthening of the droplets of polymer solution and creates shorter micro-rods. Such secondary break-up is supported by the work of Alargova et al. where SU-8 polymer micro-rods with flat ends have been produced.[20] Secondary break-up is expected to take place at the end of the solvent attrition process.

We also studied the effect of stirring speed on the micro-rod diameter. There appears to be a downward trend with increasing speed, although not as marked as the changes in the micro-rod length. Using a 50 wt.% shellac in ethanol solution and the highest mixing speed, we calculated a shear rate of ~800 $s^{-1}$.

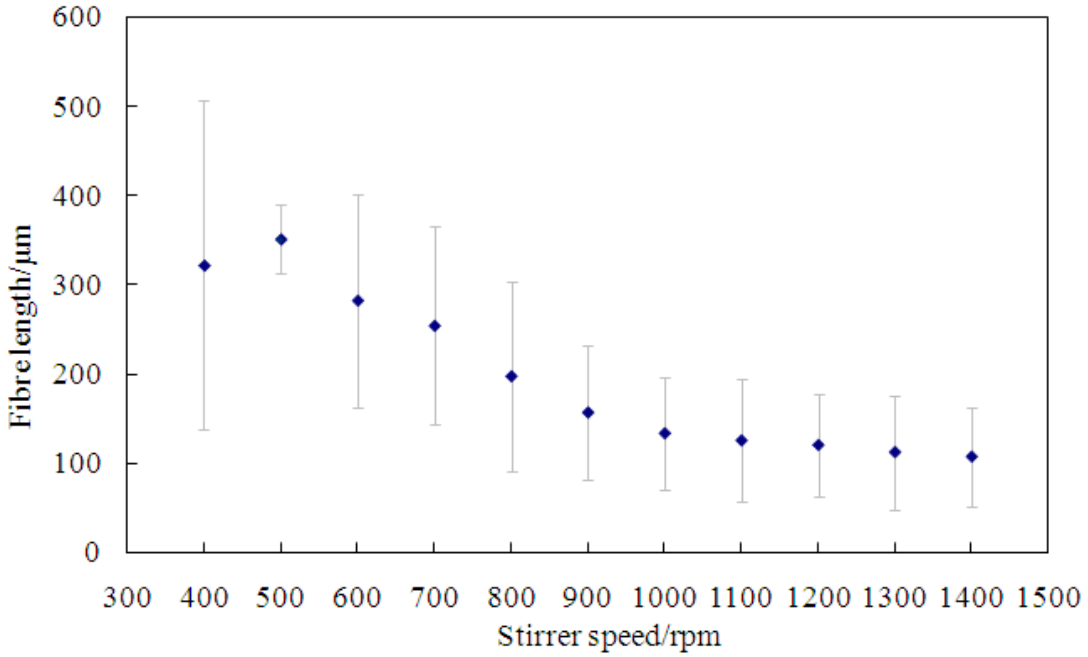


**Figure 4.10. Decrease in shellac micro-rod length with increasing stirring speed from 400 to 1,400 rpm. Error bars are standard deviations from samples of micro-rods measured; optical micrographs with at least 50 micro-rods present were used for measurement purposes.**

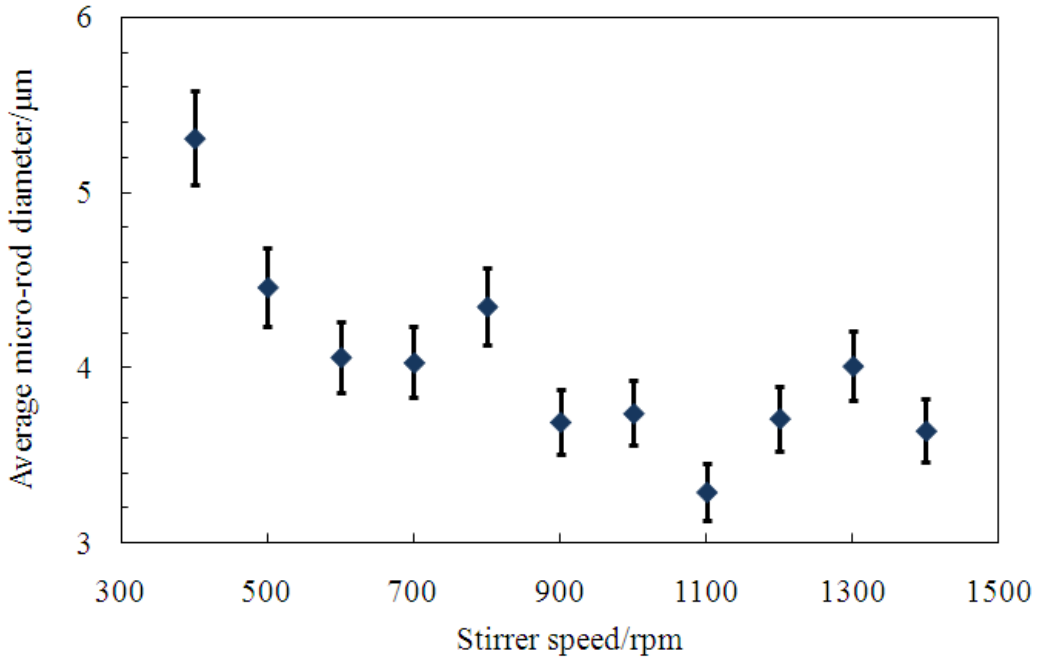


**Figure 4.11. Effect of stirring speed on the diameter of shellac micro-rods. Image overlays containing at least 25 micro-rods present were used for measurement purposes to minimise the uncertainty in the estimation of the equatorial diameters.**

### 4.4. Shellac micro-rod-stabilised foams and foam stability

We discovered that shellac micro-rods are able to stabilise foams well. They provide a steric barrier against bubble coalescence, and form a scaffolding structure within the foam. The micro-rods are also expected to obstruct drainage within the foam structure as they fill the Gibbs-Plateau channels, increasing the lifetime of the foam. When foam height vs. time is plotted for a foam stabilised with shellac micro-rods, all of the above factors lead to a plateauing effect in the shape of the curve. Fig. 4.12 shows a typical time evolution curve of foam height in an enclosed container (protocol described fully in chapter 2). All micro-rods used in the subsequent foamability studies were produced using the optimum protocol described in section 4.3.1.

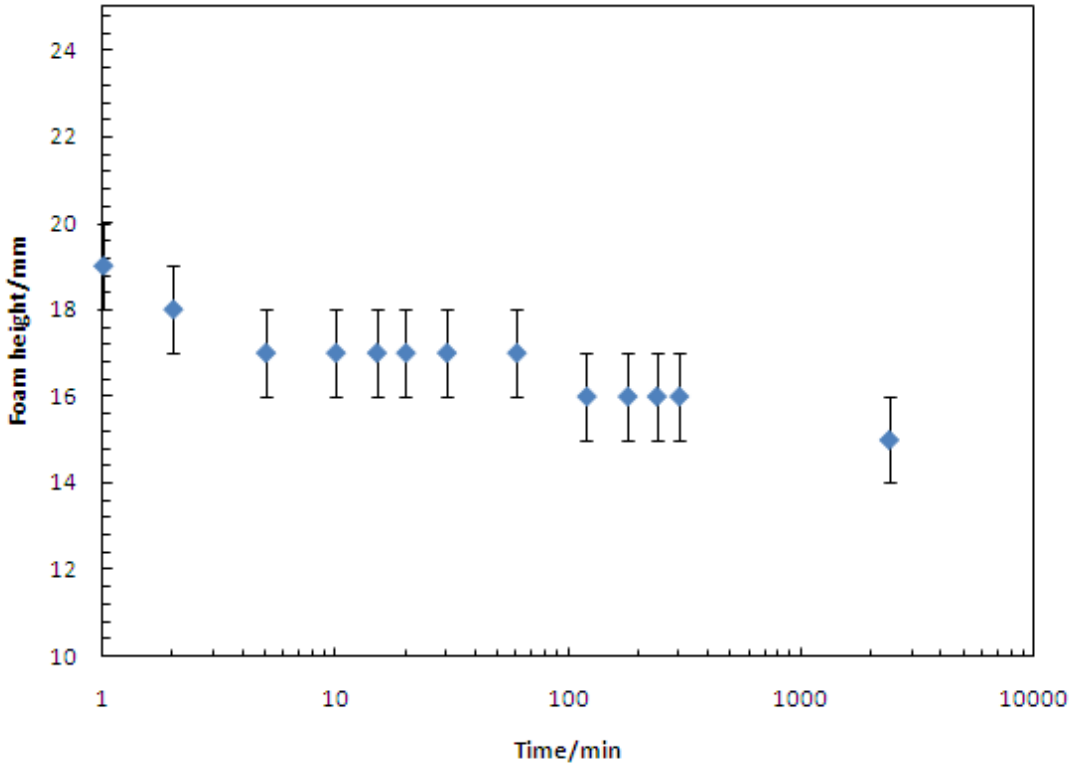


**Figure 4.12. Evolution of foam height over time of a hand-shaken 2 wt.% aqueous suspension of shellac micro-rods. Micro-rods were produced by 'optimum protocol' described in section 4.3.1. The dimensions of the micro-rods are approximately as follows, around 100 µm in length and 4 µm in diameter.**

It is worth mentioning that the formation of shellac micro-rod stabilised foams can be suppressed due to the sticky character of shellac. Whilst the newly-formed shellac

micro-rods are still dispersed in the aqueous glycerol solution, the aggregation process is slow, and the micro-rods remain dispersed for several hours. If the washing and subsequent foam-formation steps are completed quickly enough however, the micro-rods stick together *after* the foam formation and form a scaffold which increases the foam stability. It was found that the problem of micro-rod stickiness could be reduced by mixing shellac with other materials to produce so-called 'hybrid micro-rods'. The maize prolamine zein was used in combination with shellac, and the results from these experiments are discussed in chapter 6.

## 4.5. Optical microscopy of foams stabilised by shellac micro-rods

### 4.5.1. Optical microscopy of shellac micro-rods and foam

Shellac micro-rods were produced using a standard protocol which is described in chapter 2. Fig. 4.13a shows micro-rods which have an inherent curvature. Such curvature should facilitate adsorption to a curved interface, giving greater stability. Fig. 4.13d shows a number of shellac micro-rods adsorbed on the surface of an air bubble. The lengths and diameters of the micro-rods can vary and some rods show significant surface roughness. The reason why some rods appear much smoother than others is not known, but according to the Wenzel equation, increased roughness of a hydrophobic/hydrophilic surface gives increased hydrophobicity/hydrophilicity respectively.[31]

The average dimensions of shellac micro-rods were found to be around 100 μm in length and around 4 μm in diameter for samples produced using a 50 wt.% shellac in ethanol solution (1 mL) added to an 85% glycerol/15% Milli-Q water (v/v) mixture under stirring (1,400 rpm) for 10 min. The conditions are referenced as the optimum production protocol.

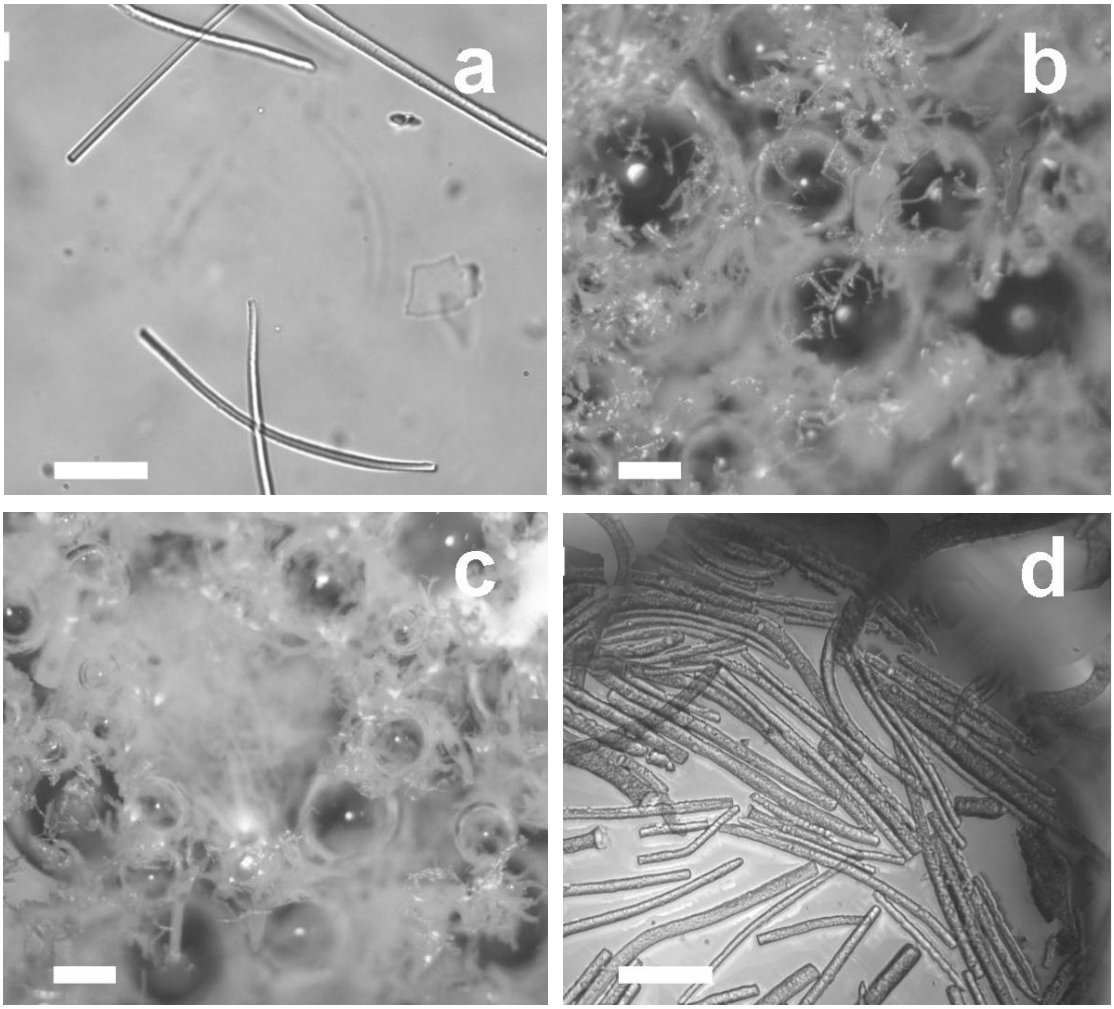


**Figure 4.13. Optical microscopy images of shellac micro-rods produced using the optimum production protocol (a). Micro-rods are shown adsorbing at the gas-liquid interface under reflected light microscopy (b) and (c) and transmitted light (d). Note that the air-liquid interface is only partially covered. Scale bars represent 25 μm ((a) and (d)) and 250 μm ((b) and (c)).**

### 4.5.2. Fluorescence microscopy of shellac micro-rods and foam

In order to ascertain whether or not the micro-rods are hollow or solid, 0.1 wt% Nile Red fluorescent dye was added to the dispersed phase (prior to dispersion in the continuous phase) by stirring in manually. Micro-rods were then produced using a standard procedure (50 wt% Shellac/ethanol solution (dispersed phase), 85% glycerol/15% Milli-Q water (v/v) mixture (continuous phase) stirred at 1,400 rpm for 10 min. The sample morphology was examined using fluorescence microscopy (fig. 14a & b).

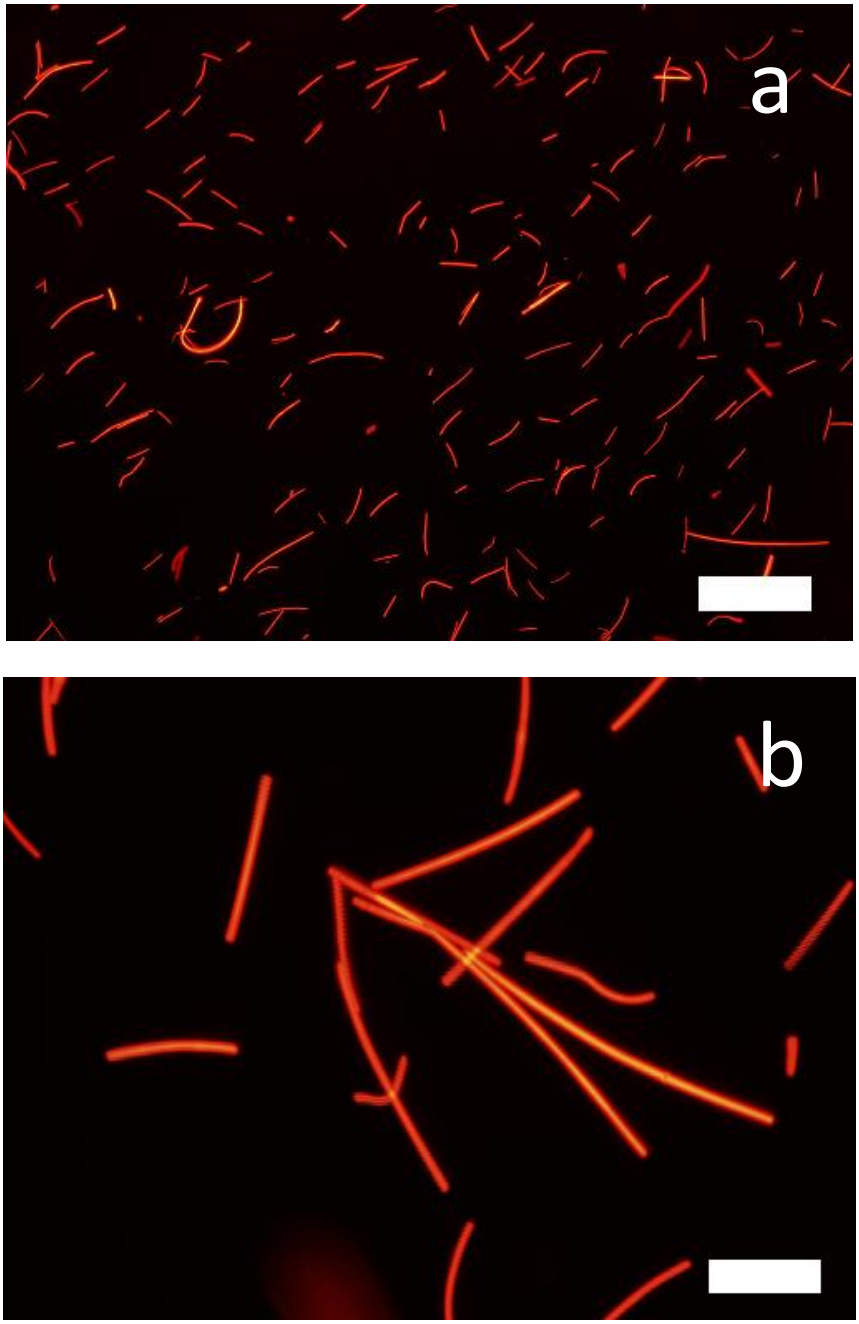


**Figure 4.14. Fluorescence microscopy images of shellac micro-rods doped with Nile Red dye. (a) Shows the dispersion of micro-rods. Scale bar is 250 µm. (b) Shows the increased fluorescence intensity at the centre of the micro-rods, indicating a non-hollow structure. Scale bar is 20 µm.**

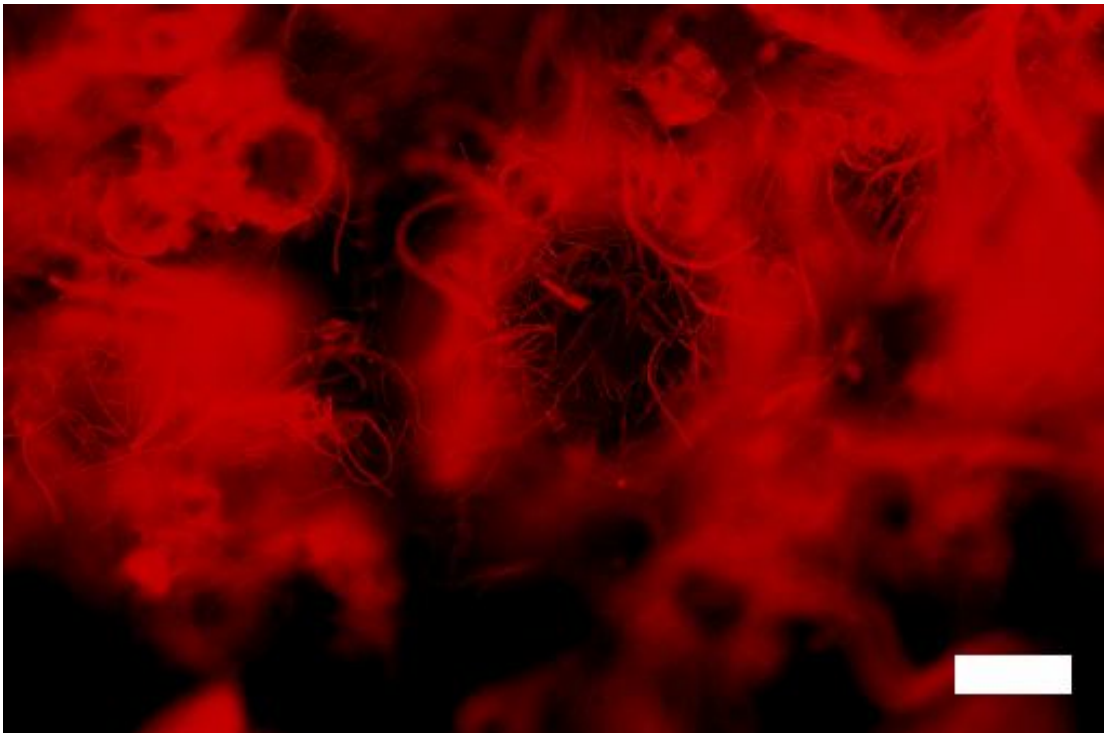

**Figure 4.15. Fluorescence microscopy image of shellac micro-rods doped with a small amount of Nile Red dye, seen looking through a foam. Micro-rods can be seen adsorbing at the air-water interface. Scale bar is 100 µm.**

By doping the shellac micro-rods with Nile Red fluorescent dye it has been shown that it is likely that they are non-hollow in structure. If the opposite were true then one would expect to see more fluorescence intensity at the edges of the micro-rods (see 'Novel ethyl cellulose structures', chapter 5).

### 4.6. Scanning electron microscopy of 'melted' shellac micro-rod-stabilised foam

A foam was produced by hand-shaking of an 2 wt.% aqueous dispersion of shellac micro-rods prepared by the optimal production protocol outlined in section 4.5.1. The height of this foam was monitored over several hours. After an initial steep decrease in foam height due to liquid drainage from the foam, fig. 4.12 shows the reduction in steepness of the foam height vs. time curve, indicating that the foam is stabilised after reaching a certain critical water content. The foam was dried in an ambient atmosphere, and analysed using SEM. We did not observe any visible changes in the foam morphology upon drying. Fig. 4.16 shows the wide variety of shellac micro-rod morphologies in the scaffolding structure left behind after drying.

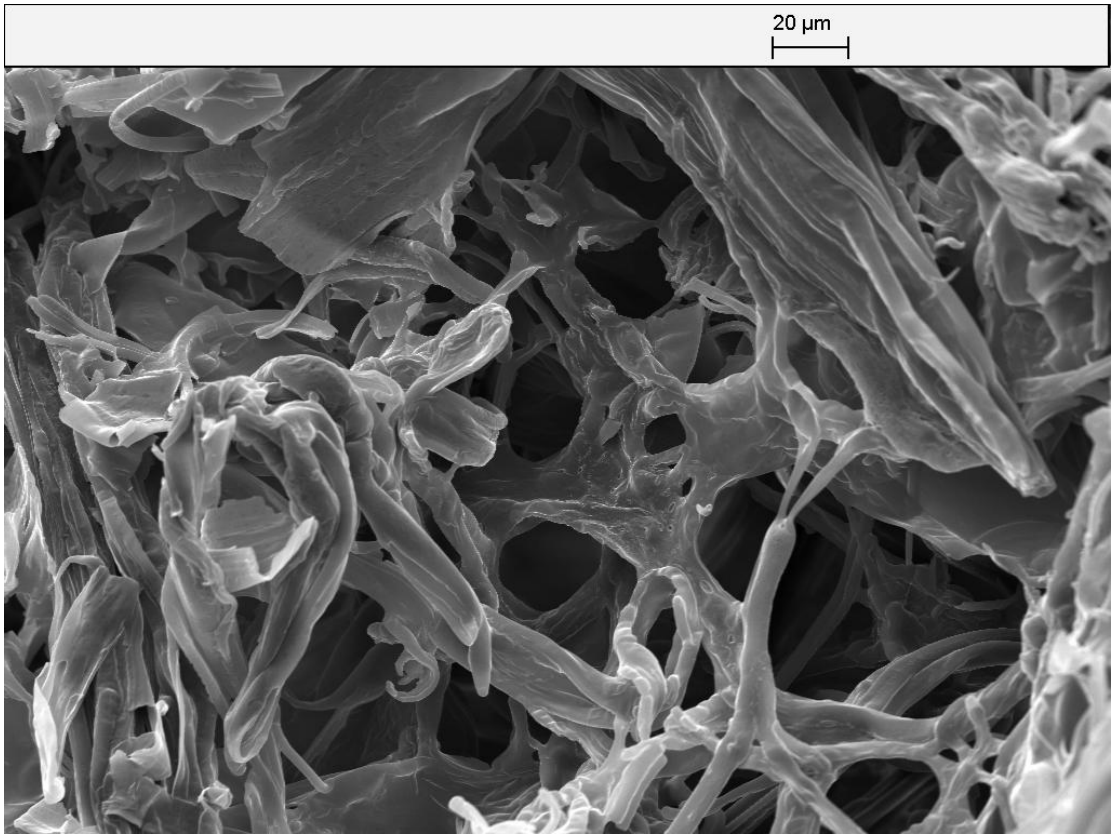


**Figure 4.16. SEM image of the structure of a dried shellac foam. Cavities are visible where air bubbles had been.**

Shellac micro-rods display 'sticky' characteristics when clustered together closely in a suspension. In order to prevent this, a suspension of micro-rods was heated to toughen them (similar to annealing), thereby increasing their hardness and thus increasing the structural integrity of the foam. However, when the micro-rods were heated up to 90 ºC, they congealed to form a single mass of molten shellac. This problem was resolved by producing a shellac micro-rod-stabilised foam prior to heating in a soda glass vial. Fig. 4.17 shows how the micro-rods have fused to each other and formed a harder, more resilient structure.

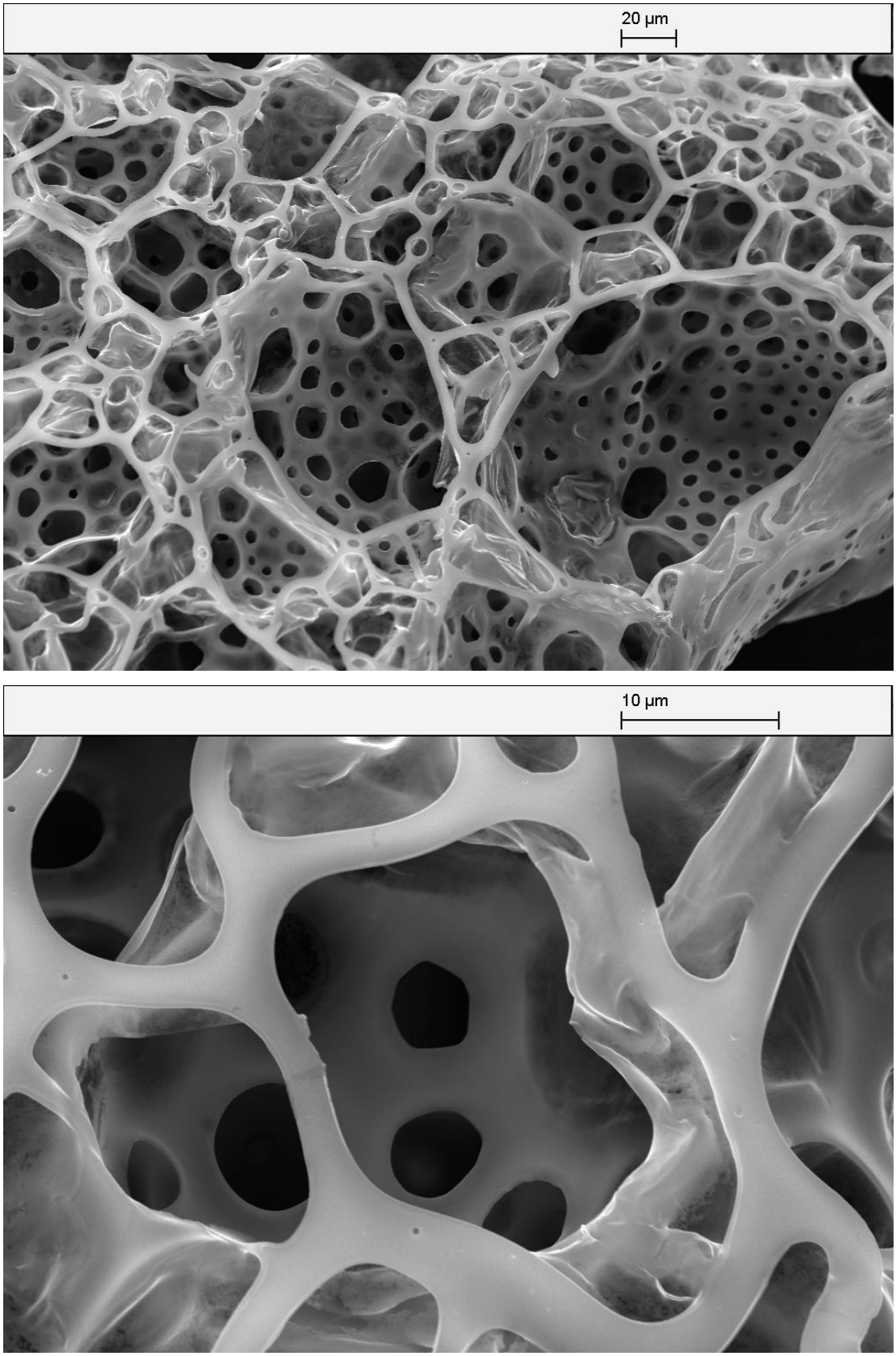


**Figure 4.17. (Top) shows an SEM image of the structure produced by heat treating shellac micro-rods which were previously trapped in a foam. The bottom image shows a close-up of the same area.**

In order to better understand the structure within the foam, fluorescent doping of the separate components could be carried out enabling one to locate the aqueous films and micro-rod layers.

### 4.7. Study of the adsorption of shellac micro-rods at liquid surfaces by using the 'Gel Trapping Technique'

Shellac micro-rods were produced using an identical protocol to that described in section 4.5.1 in preparation for use with the so-called 'gel trapping technique' developed by Paunov.[21-23] This method was devised to facilitate the measurement of contact angles of small particles at interfaces, where optical microscopy cannot offer fine enough resolution. The technique involves two steps. The gelling and trapping of micro-particles at the liquid interface and the replication of the adsorbed micro-particles at the interface using polydimethylsiloxane (PDMS). This cured, solid PDMS layer can subsequently be peeled off and analysed by scanning electron microscopy, where the three phase contact angle of sub-micron particles can be estimated. Fig. 4.18 illustrates the main steps involved in the GTT.

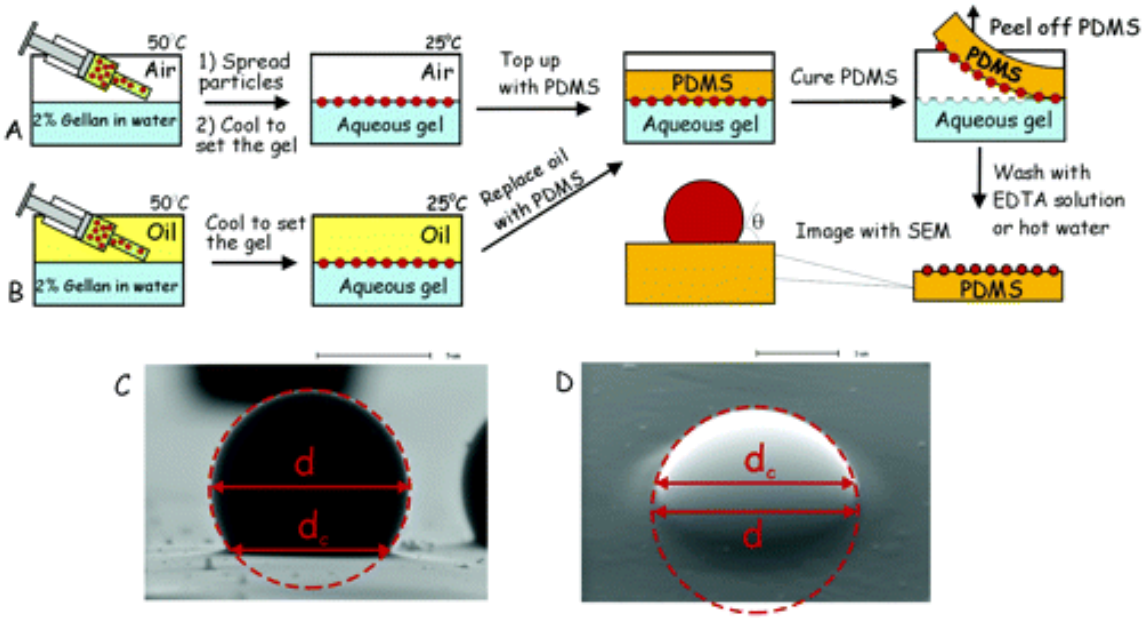


**Figure 4.18. Main processes involved in the gel trapping technique for particles adsorbed at the air-water (A) and oil-water (B) interface. Scanning electron microscope images (C) & (D) display typical visual results from which contact angles may be estimated.[21]**

Initially, the aqueous solution of Gellan must be filtered (see experimental section) to remove surface-active impurities. Care must be taken to ensure that during filtration the Gellan does not set and block the column. To this effect the column is heated using hairdryers/heatguns to prevent clogging and the filtrate collected in a glass flask on a hotplate. Once filtered, the solution of Gellan is poured into Petri dishes for the introduction of the micro-rods that are to be trapped at the air-water interface. In the standard GTT procedure[21], particles are 'spread' at the interface using a suitable spreading solvent. However, due to the solubility of shellac wax in typical spreading solvents such as isopropanol, n-propanol and ethanol, the shellac micro-rods were added as a dispersion in water. Once added, the gel is set by cooling below the gelling temperature. A mixture of PDMS and a curing agent is then poured on top. When set, the solid, rubbery PDMS layer is peeled off, picking up the shellac micro-rods from the gel layer. This is washed in Milli-Q water at pH 9, then at standard pH, and covered, to prevent airborne contaminants attaching to the sticky PDMS surface before imaging by SEM. Figs. 4.18c & d demonstrate a method for calculation of the contact angle of adsorbed spherical particles using this technique. The contact angle θ is found as follows:

$$\sin \theta = d_c/d$$

where $d_c$ and $d$ are the particle contact line diameter and equatorial particle diameter respectively.[21] The SEM images revealed micro-rods with a variety of morphologies, adsorbing at the interface at what seem to be a variety of contact angles, although it is very difficult to estimate these angles due to the irregular morphology of the micro-rods. The fact that the rods seem to lie mainly out of the PDMS indicates that they resided mainly in the aqueous phase prior to being lifted away with the polymer. This could mean that the shellac micro-rods adsorb with a relatively small contact angle, and are exposed mainly to the aqueous phase.

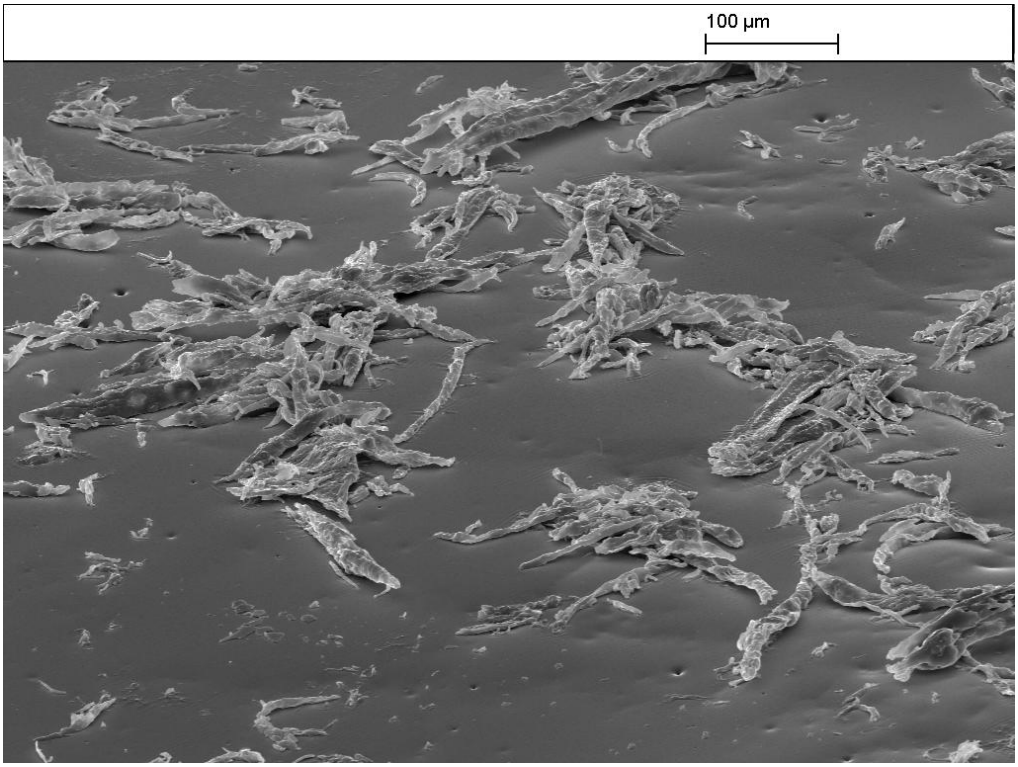


**Figure 4.19. Wide field view using scanning electron microscopy of shellac micro-rods partially embedded in the surface of the PDMS layer following the GTT. The embedded parts of the micro-rods previously resided in the air phase, whereas the visible parts previously resided in the water phase.**

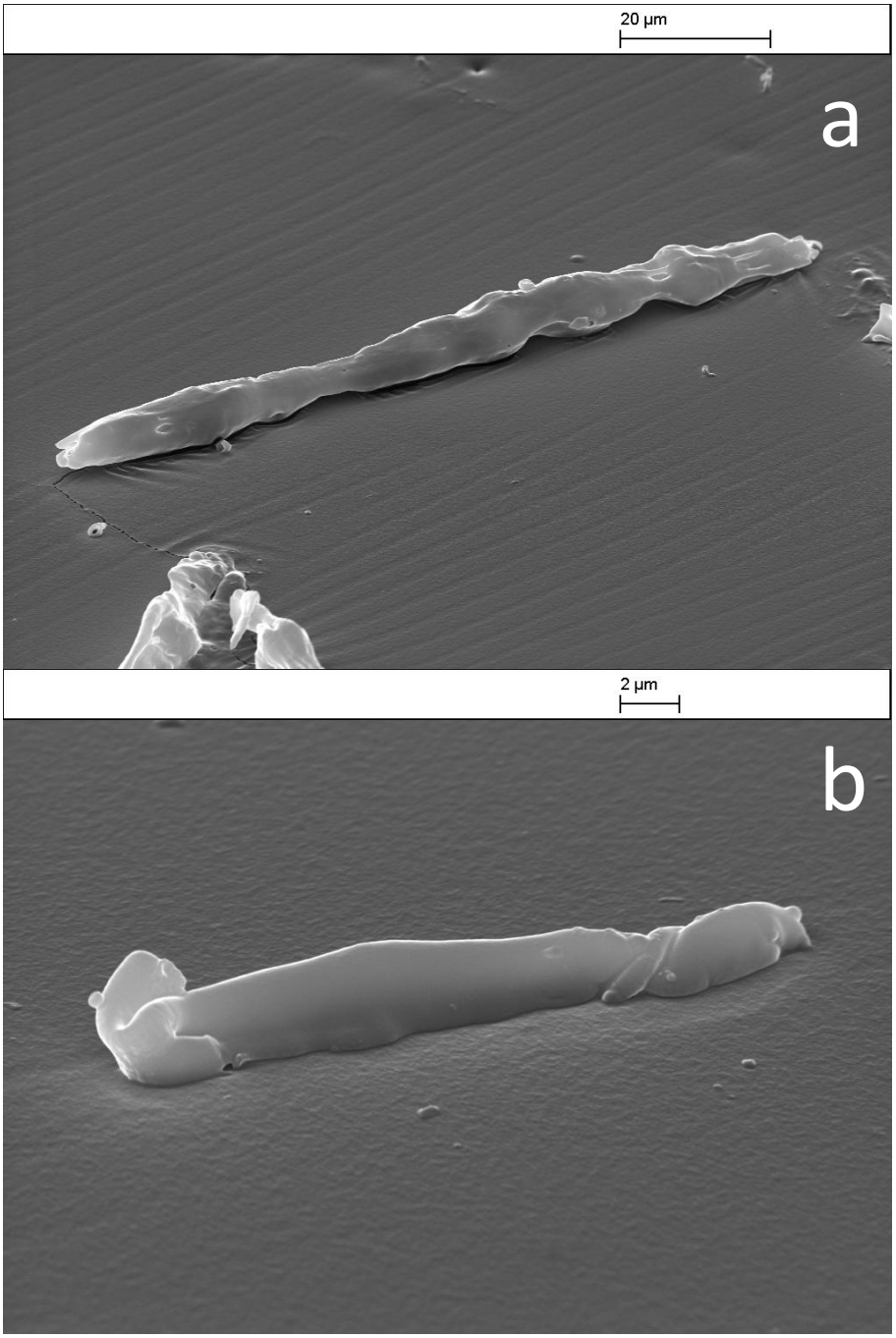


**Figure 4.20. SEM images of large (A) and smaller (B) shellac micro-rods embedded to different degrees into the PDMS layer following the GTT. It is difficult to ascertain the extent to which these micro-rods are embedded within the PDMS.**

4.7.1. Estimation of the contact angle of sessile water drops on shellac

In order to estimate the hydrophobicity of the shellac surface, the contact angles of sessile water drops on glass slides which had been previously spin-coated with shellac (using 50 µL of a low-viscosity 5 wt% solution of shellac in ethanol) were measured using a Krüss Drop Shape Analyser 10 (DSA) apparatus.

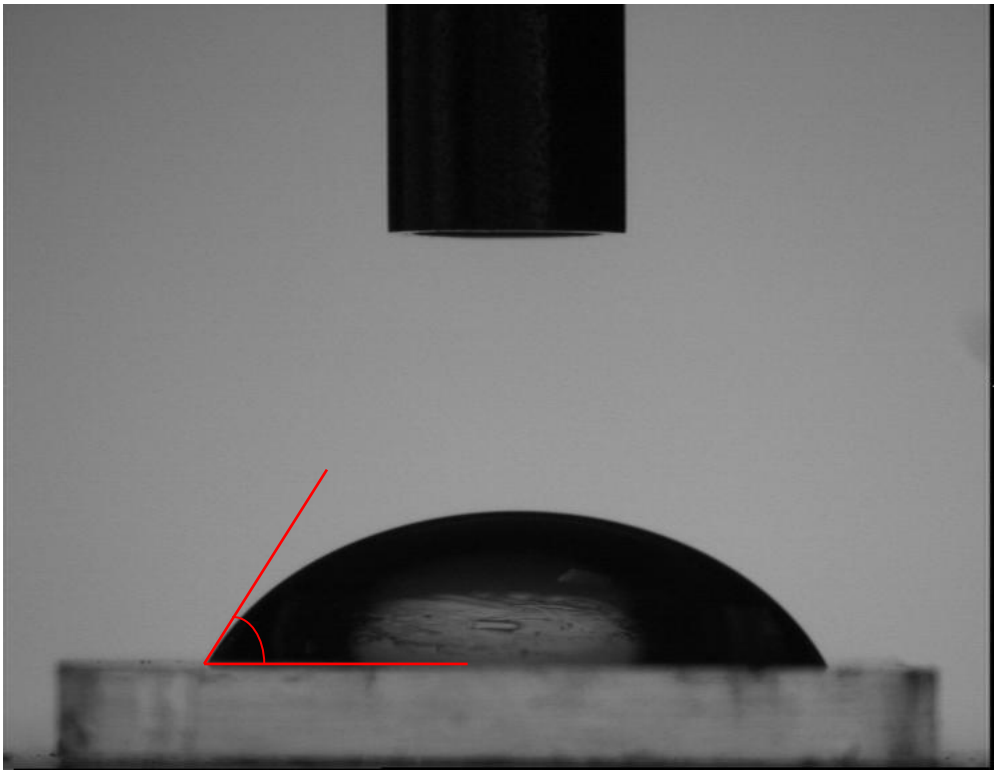

**Figure 4.21. Approximate contact angle (in air) of a sessile drop of Milli-Q water resting on a glass slide (cleaned with ethanol and dried with compressed air) spin-coated with shellac. The shellac film contact angle was estimated to be 58±0.5º.**

The contact angle was estimated to be approximately 58º which shows a moderate hydrophilicity of this material and explains why shellac micro-rods were shown to reside predominantly in the aqueous phase in SEM images (figs. 4.19 and 4.20). When the spin-coated shellac, ethyl cellulose and zein films (see following chapters) were checked using SEM it was found that their surfaces were not completely smooth, but instead possessed a number of small holes where gas may have escaped. Degassing the polymer solvents prior to spin-coating may reduce this effect.

## 4.8. Conclusions

In this chapter, we describe for the first time the production of food-grade shellac micro-rods using an in-shear-flow dispersion and solvent attrition technique'. We were able to control the morphologies of the resultant micro-rods. It was found that an increase in stirrer speed led to the formation of shorter micro-rods, with a more uniform size distribution. The use of shellac in ethanol solutions of higher concentrations (up to 50 wt.%) resulted in the production of particles of improved micro-rod morphology compared with those produced using lower concentrations of shellac. Shellac solutions of low concentration (up to 10 wt.%) generally gave particles of amorphous morphology.

Shellac micro-rods were characterised by optical, fluorescence and scanning electron microscopy which allowed us to measure the length and the diameter distributions of the micro-rods. It was found that using an optimised production protocol (50 wt.% shellac in ethanol solution, 10 min stirring in an 85% glycerol, 15% Milli-Q water (v/v) mixture at 1,400 rpm) the average micro-rod length was approximately 100 µm and diameter was around 4 µm. Fluorescent microscopy showed that the micro-rods are almost certainly non-hollow in structure, due to the greater fluorescence intensity being observed in the centre of the micro-rods. Scanning electron microscopy (along with optical microscopy) showed the highly variable surface morphology of the shellac micro-rods. It is apparent that while some of the micro-rods possess highly smooth surfaces, many are quite rough and irregular. With the use of the 'gel trapping technique', scanning electron microscopy showed the attachment position of the micro-rods at the water-air interface.

Shellac micro-rods showed good surface activity, and stabilisation of air bubbles in aqueous foams. The aqueous foams stabilised by shellac micro-rods had lifetimes exceeding several weeks, as the shellac formed a solid matrix around the foam bubbles, so that the structure could not collapse. Some disadvantages of using shellac micro-rods as foam stabilisers were observed however. Due to the stickiness of the micro-rods of this material, they readily aggregate once washed of the glycerol in which they were suspended during their formation. For this reason it is believed that the use of a less-sticky material for the production of micro-rods for foam stabilisation purposes would

be highly advantageous. We found that ethyl cellulose could be a potentially more promising material and we present our results with it in the next chapter.

### 4.9. References


[1] W. Ramsden. *Proc. Roy. Soc.*, 1903, **72,** 156.

[2] S.U. Pickering. *J. Chem, Soc.*, 1907, **91,** 2001.

[3] R. Aveyard, B.P. Binks, J.H. Clint. *Adv. Colloid Interface Sci.*, 2003, **100 – 102**, 503.

[4] B.S. Murray, R. Ettelaie. *Curr. Opin. Colloid Interface Sci.,* 2004, **9,** 314.

[5] A.B. Subramaniam, M. Abkarian, L. Mahadevan, H.A. Stone. *Nature,* 2005, **438,** 930.

[6] U.T. Gonzenbach, A.R. Studart, E. Tervoort, L.J. Gauckler. *Angew. Chem. Int. Ed.,* 2006, **45,** 3526.

[7] E. Dickinson, R. Ettelaie, T. Kostakis, B.S. Murray. *Langmuir,* 2004, **20,** 8517.

[8] B.P. Binks, J.A. Rodrigues. *Angew. Chem., Int. Ed.,* 2005, **44,** 441.

[9] K. Golemanov, S. Tcholakova, P.A. Kralchevsky, K.P. Ananthapadmanabhan, A. Lips. *Langmuir,* 2006, **22,** 4968.

[10] B.P. Binks, R. Murakami. *Nature Mater.,* 2006, **5,** 865.

[11] T. Kostakis, R. Ettelaie, B.S. Murray. *Langmuir*, 2006, **22,** 1273.

[12] B.P. Binks, T.S. Horozov. *Angew. Chem., Int. Ed.,* 2005, **44,** 3722.

[13] B.P. Binks, B. Duncumb, R. Murakami. *Langmuir,* 2007, **23,** 9143.

[14] B.P. Binks, R. Murakami, S.P. Armes, S. Fujii, A. Schmid. *Langmuir*, 2007, **23,** 8691.

[15] S.L. Kettlewell, A. Schmid, S. Fujii, D. Dupin, S.P. Armes. *Langmuir,* 2007, **23,** 11381.

[16] R.G. Alargova, D.S. Warhadpande, V.N. Paunov, O.D. Velev. *Langmuir,* 2004, **20,** 10371.

[17] R.G. Alargova, K.H. Bhatt, V.N. Paunov, O.D.Velev, *Adv. Mater.,* 2004, **16,** 1653.

[18] V.N. Paunov, P.F. Noble, O.J. Cayre, R.G. Alargova, O.D.Velev. MRS Proceedings Fall 2004, volume 845, AA5.18.1-5.

[19] P.F. Noble, O.J. Cayre, R.G. Alargova, O.D.Velev, V.N. Paunov. *J. Am. Chem. Soc.,* 2004, **126,** 8092.

[20] R.G. Alargova, V.N. Paunov, O.D.Velev, *Langmuir,* 2006, **22,** 765.

[21] V.N. Paunov. *Langmuir,* 2003, **19,** 7970.

[22] O.J. Cayre, V.N. Paunov. *Langmuir,* 2004, **20,** 9594.

[23] O.J. Cayre, V.N. Paunov. *J. Mater. Chem.*, 2004, **14,** 3300.

[24] www.sos-arsenic.net

[25] **www.wisdomfurniture.com/images/lacbeetle.jpg**

[26] www.nurbei.de

[27] B.B.Shaeffer, H.Weinberger, W.M.Howlett Gardner. *Ind. Eng. Chem.* 1938, **4,** 451

[28] C.E.Barnes, *Ind. Eng. Chem.* 1938, **4,** 449

[29] H.Weinberger, W.M.Howlett Gardner. *Ind. Eng. Chem.* 1938, **4,** 454

[30] S.K. Sharma, S.K. Shukla, D.N. Vaid. *Def. Sci. J.* (India), 1983, **33,** No.3, 261.

[31] R.N. Wenzel. *Ind. Eng. Chem.* 1936, **28,** No. 8, 988.

# CHAPTER 5 – MICRO-RODS MADE FROM ETHYL CELLULOSE FOR FOAM STABILISATION: PREPARATION AND CHARACTERISATION

This chapter is concerned with the production of anisotropic micro-particles from the food-grade[1] material ethyl cellulose using similar protocols as for shellac micro-rods.

Particle wettability (characterised by the three-phase contact angle made by the particle at the gas-liquid or liquid-liquid interface) is a key parameter determining the particle adsorption and how strongly the particle will attach to the liquid interface. Furthermore it has been shown by several collaborating workers[2-6] that hydrophobic polymer micro-rods are able to stabilise emulsion and foam systems to a very high degree. Using the same technique as employed here, aqueous foams have been produced which had a shelf life exceeding several weeks and were deemed to be 'superstabilised'. Anisotropic particles are able to give more efficient stabilisation of interfaces due to their greater surface area to volume ratios.[2] This will be exploited in this work, by producing high aspect ratio micro-rods which are able to interweave and lock together at the interface, providing additional steric stability.

Due to its food-grade specification, and hydrophobic characteristics, it was expected that micro-rods of ethyl cellulose would provide good foamability and foam stabilisation, with great potential for inclusion as a stabiliser in food formulations.

This chapter goes on to introduce ethyl cellulose together with reasons for its use in this work. The effect of using different solvent chemistries in the production of ethyl cellulose micro-rods was investigated, and once the optimal conditions for preparation of ethyl cellulose micro-rods were found, the effect of additives such as electrolyte, methyl cellulose, urea and acid and base (to alter pH) were examined. Interesting structures formed from the addition of dilute ethyl cellulose solutions to regular continuous phase mixtures under high shear are presented. We have examined the aspect ratio of the micro-rods and their efficacy in stabilisation of food foams. The ethyl-cellulose micro-rods were also used as emulsifiers to test their efficacy. Scanning electron microscopy, fluorescence and optical microscopy were all employed to examine the micro-rods produced. Finally, conclusions are drawn from all of the findings of the chapter.

### 5.1. Structure, properties and uses of ethyl cellulose

Ethyl cellulose (EC) is an ethyl ether of cellulose. The production of this hydrophobic polymer was patented well over 50 years ago, and there have been a number of refinements in the process.[8,9] EC is normally produced by grafting ethyl groups to two opposite oxygen atoms on each ring of the cellulose chain from the corresponding ethyl halide (ethyl chloride[10]), in the presence of a base. It has been used for many years as a food coating[11] (due to its non-toxic nature and resistance to moisture) and also in pharmaceuticals as a tablet excipient.[12]

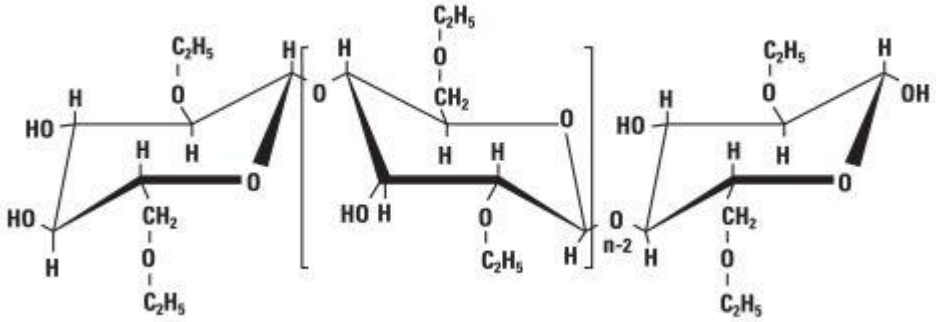

**Figure 5.1. Molecular structure of ethyl cellulose (Ethocel$^{TM}$).[13]**

Previously, long fibres of EC have been produced by a process called electrospinning.[14] Electrospinning was invented over one hundred years ago and involves the formation of a charged jet of polymer solution by a strong electric field and yields fibres of very fine and controllable diameter. Different polymers and production conditions can give a variety of fibres morphologies and sizes.[15] In this study however, micro-rods with smaller aspect ratios than long fibres are required, and these may be produced using the 'in-shear-flow liquid-liquid dispersion and solvent attrition technique'.[2]

### 5.2. Effect of the polymer solvent on the properties of ethyl cellulose micro-rods produced

Solvent chemistry for the dispersed phase polymer solution was investigated. Tetrahydrofuran, acetone and ethanol were chosen, as all of them dissolve EC, and all are miscible with the aqueous glycerol continuous phase. The use of these different

solvents gave rise to the production of micro-rods with very different morphologies, which are described below.

### 5.2.1. Ethyl cellulose micro-rods produced using tetrahydrofuran

In order to investigate the effect of the concentration of EC in the disperse phase, solutions of EC in tetrahydrofuran from 5 to 15 wt.% (in 2.5% increments) were produced, and these were introduced to a disperse phase solution added to 50 mL of 85% glycerol/15% Milli-Q water (v/v) mixture under stirring from Cole Parmer Digital Reversing Mixer (10 min)). In this instance, stirrer speed was kept constant at 350 rpm.

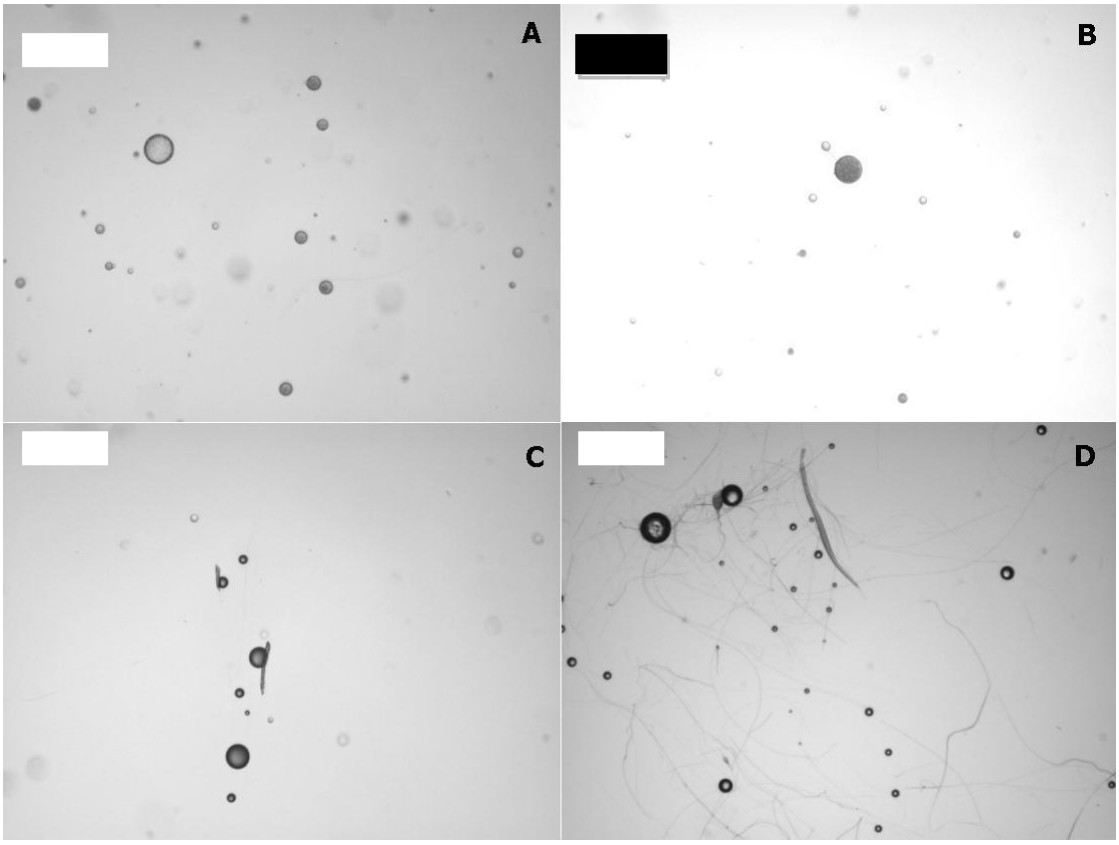


**Figure 5.2. Optical microscopy images showing the effect of variation of ethyl cellulose concentration in dispersed phase from 5% (A) to 7.5% (B), 10% (C) and 15% (D) at 350 rpm in 85% (aq) glycerol. Micro-rods are only produced at the highest weight percentage. Scale bars are 100 μm.**

Below 10 wt.% EC in THF, no micro-rods were formed. This is because the viscosity of the dispersed phase is too low. Average micro-rod length increased from 116 μm to 415

μm when the concentration of EC was increased from 10 wt.% to 15 wt.%. The increased EC concentration and the increased shear due to the higher viscosity give rise to longer micro-rods. Fig. 5.2.A - D shows the results of using polymer solutions of low viscosity when performing the liquid-liquid dispersion technique to produce micro-rods. Only when the polymer concentration was increased above 15 wt.% were micro-rods of less extreme (<20) aspect ratios formed. This experiment also served to highlight that a higher stirring speed is necessary to produce micro-rods with useful aspect ratios.

The effect of increasing the speed of stirring was also examined. The continuous phase was 50 mL of 85% glycerol/15% Milli-Q water (v/v) mixture (hereinafter referred to as the 'optimal continuous phase'). The concentration of EC in THF (dispersed phase) was 10 wt.%. Stirring speeds of 350, 700 and 900 rpm were chosen.

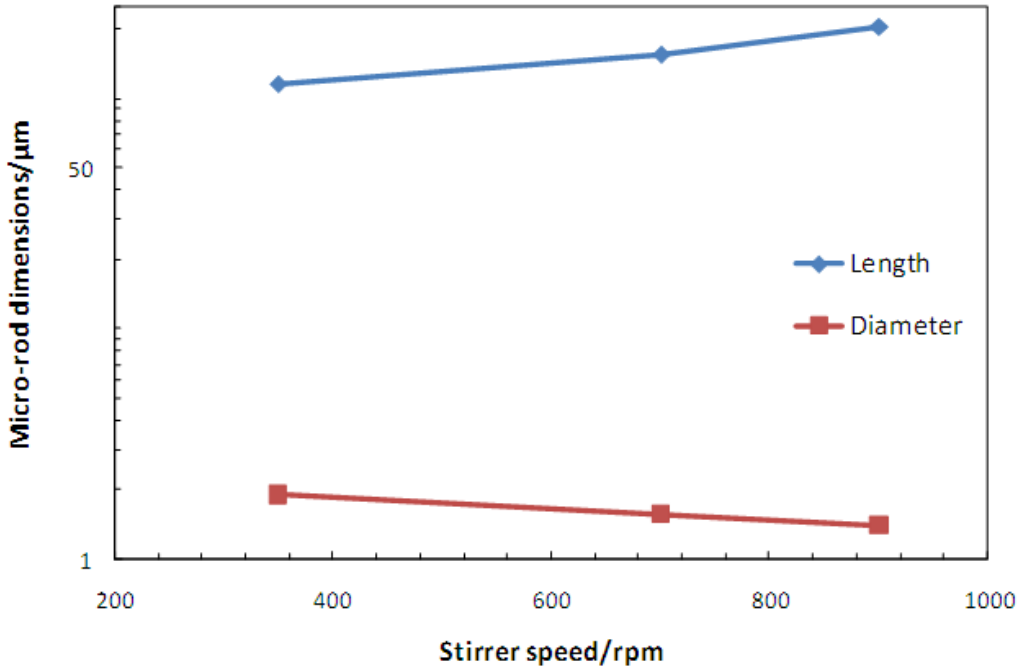


**Figure 5.3. Effect of stirrer speed on the formation of ethyl cellulose micro-rods produced from a 10 wt.% solution in THF. As stirrer speed is increased, the average micro-rod length increases, and the diameter shows a slight decrease. Micro-rod dimensions were measured from optical micrographs (3D reconstruction images) containing at least 30 micro-rods.**

As the stirring speed increases, there is a steady increase in length of the micro-rods. This suggests that the polymer solution displays plastic behaviour, and as the shear rate increases, the droplets of polymer solution stretch more, rather than breaking into shorter micro-rods during the solvent attrition stage of the process like shellac micro-

rods described in chapter 4. This effect has been observed in studies by Alargova et al.[6] where polystyrene fibres were produced using a similar technique; very long micro-rods were produced and the sample had a morphology like that of a ball of wool. Fig. 5.4 shows the polystyrene fibres produced by Alargova et al., while as a comparison, figs. 5.5 & 5.6 illustrate the excessive length of the EC micro-rods produced in this work.

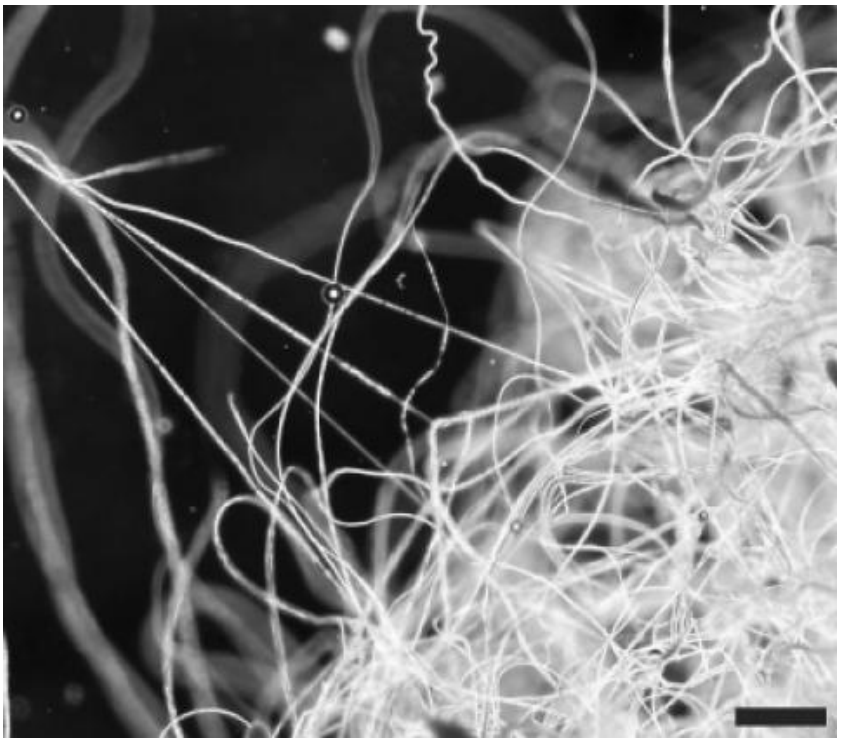

**Figure 5.4. Polystyrene fibres produced by Alargova et al. using the liquid-liquid dispersion technique.[6] Scale bar is 200 µm**.

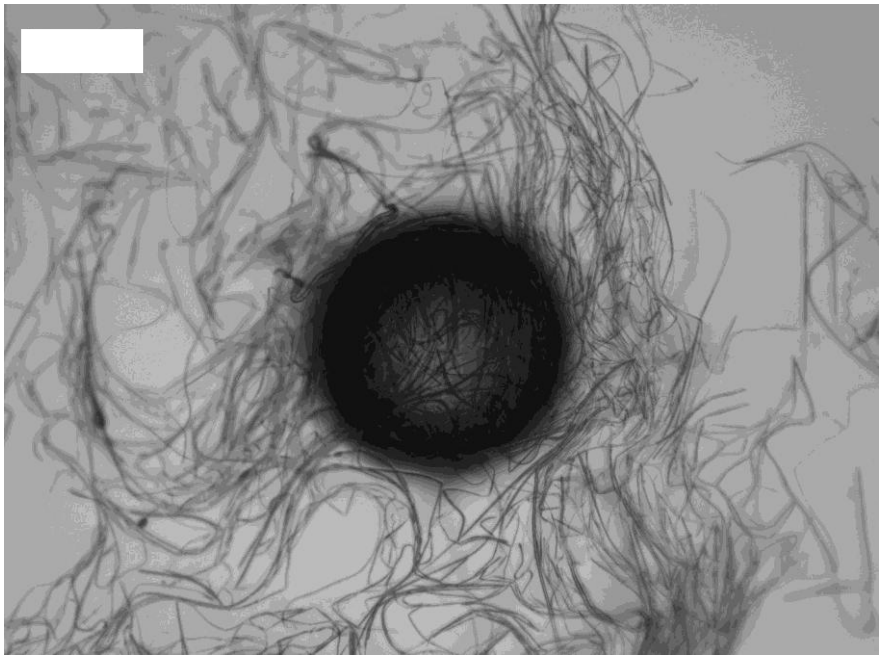

**Figure 5.5. Optical microscopy image of ethyl cellulose micro-rods produced from the addition of a 15 wt.% solution of ethyl cellulose in THF to an optimal continuous phase at 700 rpm for 10 min. Fibres are adsorbing at the air-water interface of this air bubble. Scale bar is 100 µm.**

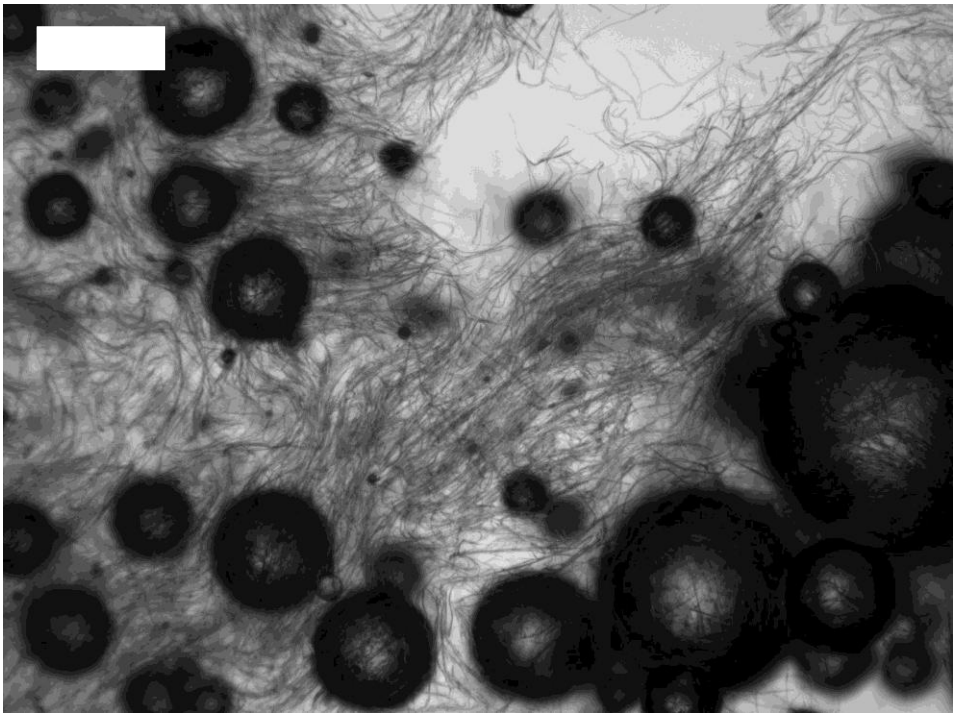

**Figure 5.6. Optical microscopy image of a collection of air bubbles in water stabilised by a dispersion of ethyl cellulose fibres of extreme aspect ratio, produced from a tetrahydrofuran solution. Scale bar is 250 µm.**

The EC micro-rods/fibres produced by the method above were able to stabilise air bubbles for several days, the dense covering of EC micro-rods offering enhanced steric stability and thereby preventing close approach and contact of neighbouring air bubbles. Foamability using these micro-rods was relatively poor though, and this is most likely due to their excessive length preventing their efficient attachment on the surface of bubbles.

From these results it is apparent that shorter micro-rods must be investigated to try to improve their foamability. This is investigated in section 5.3.1, where a dispersion of micro-rods is subjected to high speed shear from an impeller.

The effect of altering the continuous phase water concentration was also investigated. Pure glycerol, 95 vol.% glycerol with 5 vol.% Milli-Q water and 85 vol.% glycerol with 15 vol.% Milli-Q water were used. Micro-rods were produced using a fixed protocol (1 mL of 15 wt.% EC in THF disperse phase solution was added to 50 mL of continuous phase under stirring from a Cole Parmer Digital Reversing Mixer (750 rpm, 10 min)).

| **Water content in continuous phase/vol.%** | **Average micro-rod length/μm** | **Average micro-rod diameter/μm** |
|---|---|---|
| 15 | 199 | 1.7 |
| 5 | 72 | 1.6 |
| 0 | 159 | 3.3 |

**Table 5.1. Average length and diameter of micro-rods produced in a continuous phase comprising glycerol combined with 15 vol.%, 5 vol.% or no added Milli-Q water. No obvious pattern in the size or morphology of the resultant micro-rods is apparent.**

The effect, however, is not easily quantifiable. No obvious trends were seen in the morphology or dimensions of the micro-rods produced. This could be because factors other than viscosity of the continuous phase alone may be responsible. One problem could be the changing solubility of THF in the continuous phase as water is eliminated. Generally, the shortest micro-rods with aspect ratios between 50 and 100 are produced when the water concentration in the continuous phase increases without significantly reducing the viscosity of the continuous phase.

### 5.2.2. Ethyl cellulose micro-rods produced using ethanol solvent

Solutions of EC in ethanol were produced by heating (~60 °C, hotplate stirrer) and stirring. Solutions from 5 wt.% EC up to 30 wt.% (in 5% increments) were made. Using a standard production protocol (1 mL of disperse phase added to 50 mL of the optimal continuous phase) under shear (2,000 rpm, 10 min)), it was found that micro-rods were only produced when the higher viscosity disperse phase solutions (25 and 30 wt.%) were used. When low viscosity solutions were injected into the continuous phase under high speed shear only irregular, small precipitates were formed. Micro-rods were produced by using 30 wt.% EC in ethanol solution as dispersed phase which gave large, wide, ribbon-shaped micro-rods.

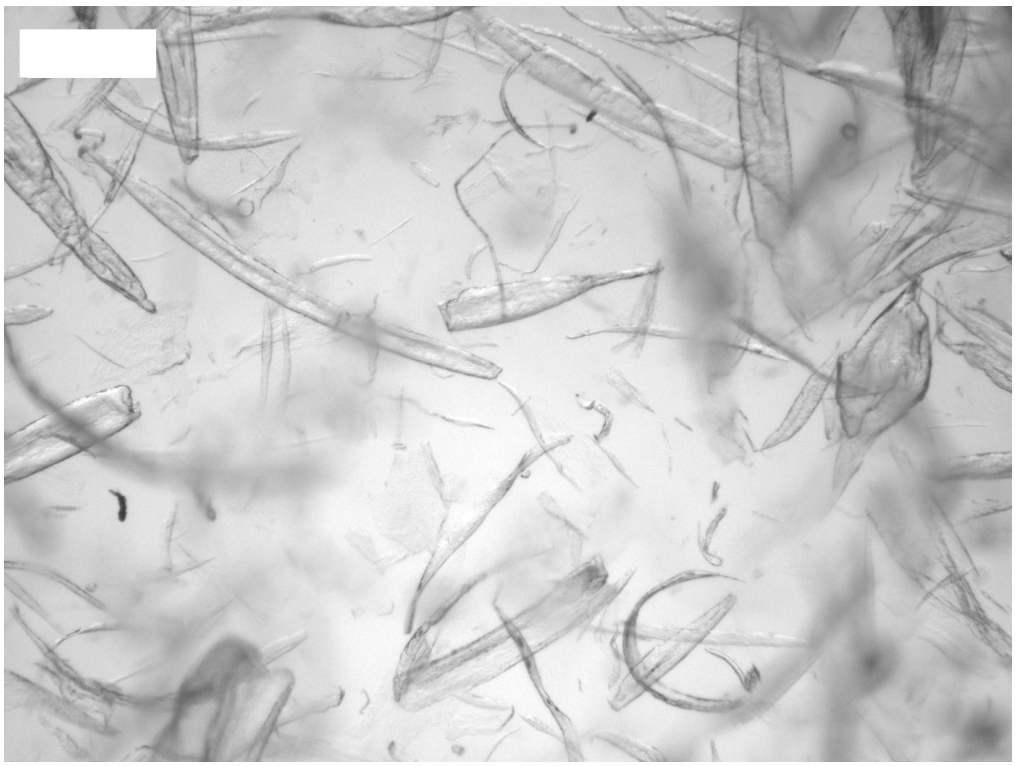

**Figure 5.7. Optical microscopy image showing the morphology of ethyl cellulose 'ribbons' produced using a 30 wt.% ethyl cellulose/ethanol solution with an optimal continuous phase being stirred at 2,000 rpm for 10 min. Scale bar is 250 µm.**

These particles were several hundreds of microns in length and up to a hundred microns in diameter making them much too large for stabilising small foam bubbles. Fig. 5.7 shows the appearance of EC micro-rods produced using this dispersed phase chemistry. Variation of the water content in the continuous phase (0 – 25 wt.%) did not allow

production of micro-rods with better morphology/dimensions (fig. 5.8). Another solvent must be investigated in order to produce micro-rods which would be better suited for foam stabilisation.

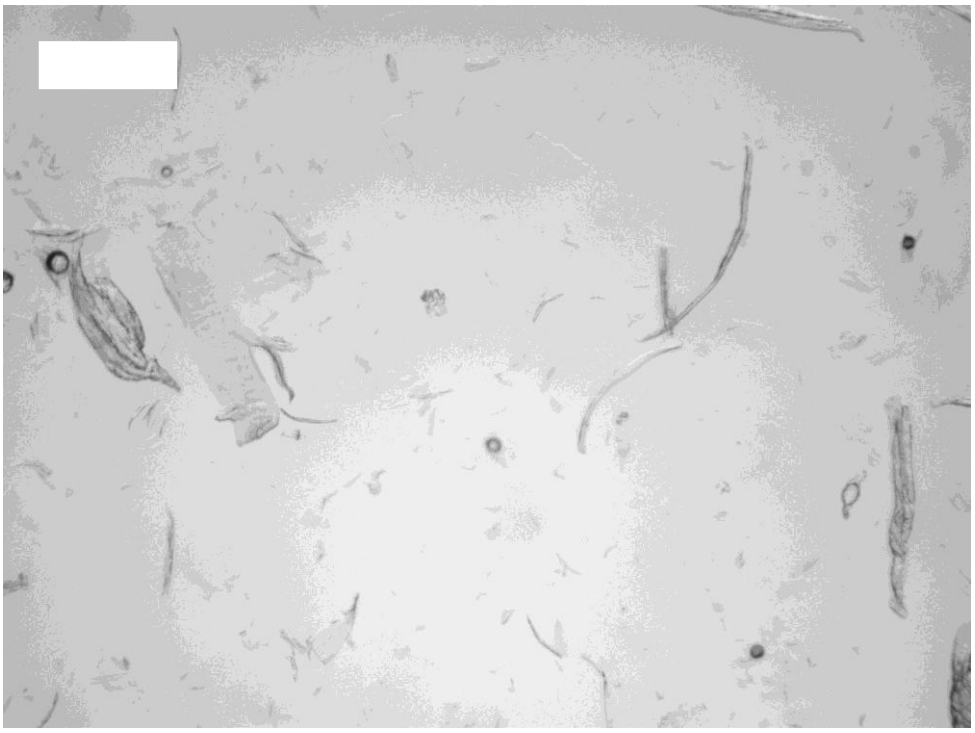

**Figure 5.8. Optical microscopy image of ethyl cellulose particles produced by injecting a 30 wt.% solution of ethyl cellulose in ethanol into a continuous phase of 95% glycerol 5% Milli-Q water (v/v) mixture under 2,000 rpm mixing for 10 min. Scale bar is 250 µm.**

### 5.2.3. Ethyl cellulose micro-rods produced using acetone

When the previous procedure was repeated using a 30 wt.% EC in acetone solution, fairly straight micro-rods of average length 76 µm and high aspect ratios between 50 and 100 were produced (figs. 5.9 and 5.10). Reducing the percentage of EC in the dispersed phase caused a reduction in uniformity of the resultant micro-rods, together with an increase in the proportion of amorphous precipitated formations, as observed with shellac micro-rods (see chapter 4). Micro-rods produced also appear to have a rough surface. Surface roughness can amplify the surface wettability of a material[16] and EC is already hydrophobic, therefore surface roughness may improve the surface activity of the micro-rods. This procedure for micro-rod preparation was used in the

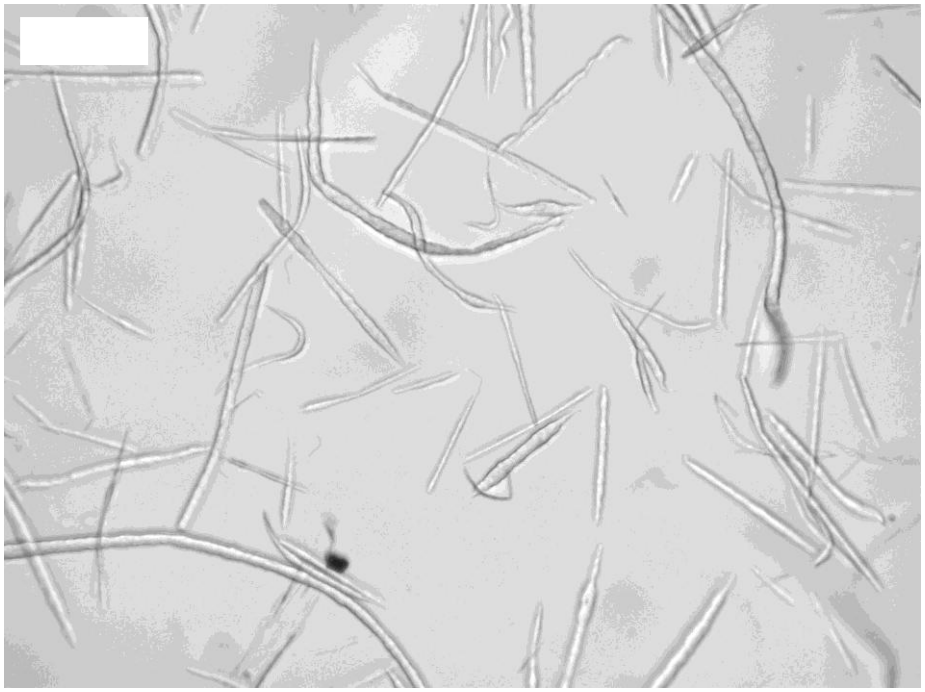

**Figure 5.9. Optical microscopy image showing the morphology of ethyl cellulose micro-rods produced using a 30 wt.% ethyl cellulose/acetone solution injected into 50 mL of optimal continuous phase being stirred at 2,000 rpm for 10 min. Scale bar is 25 µm.**

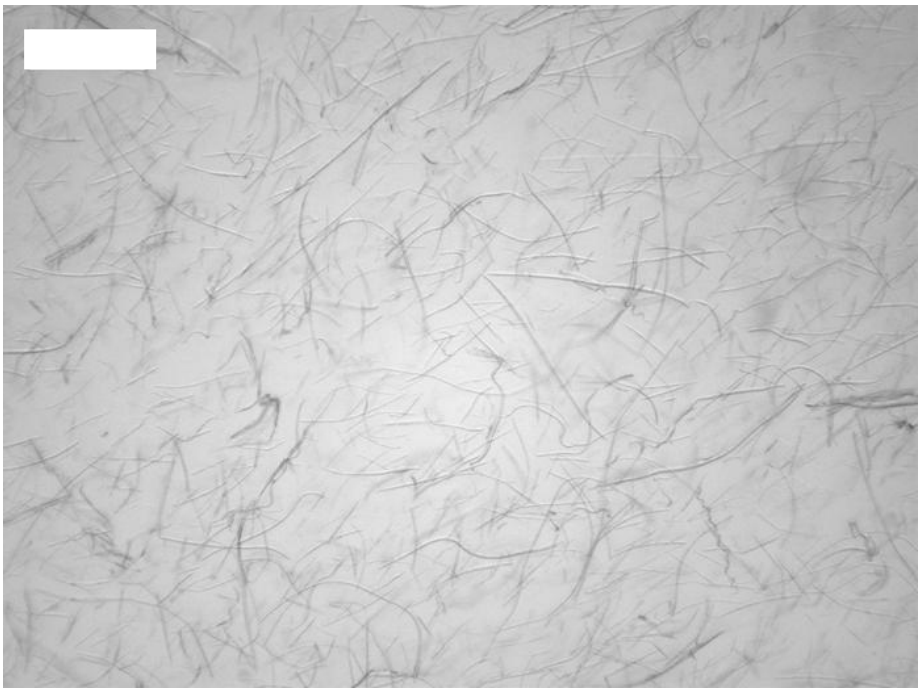

**Figure 5.10. Wider field view of the above sample, illustrating the micro-rod dimensions and the transparency of the micro-rods compared with shellac micro-rods (chapter 4). Scale bar is 100 µm.**

fabrication of so-called ‘lumpy micro-rods’ and ‘ballooned micro-rods’ which are described in chapter 7.

#### 5.2.3.1. Effect of the stirrer speed on the formation of micro-rods

In order to investigate the effect of increased stirrer speed on the size and morphology of resultant EC micro-rods, a batch of micro-rods were produced, using identical conditions except for varying the stirrer speed. The disperse phase solution (1 mL) was added to the continuous phase (50 mL of 85% glycerol/15% Milli-Q water (v/v) mixture) under shear for 10 min. Stirrer speed was varied between 400 and 2,000 rpm in 200 rpm increments. The resulting micro-rods were examined by optical microscopy. This technique was not successful however. At stirrer speeds below 2,000 rpm, long fibres of EC were formed, and it proved difficult to determine their dimensions accurately (see fig. 5.11).

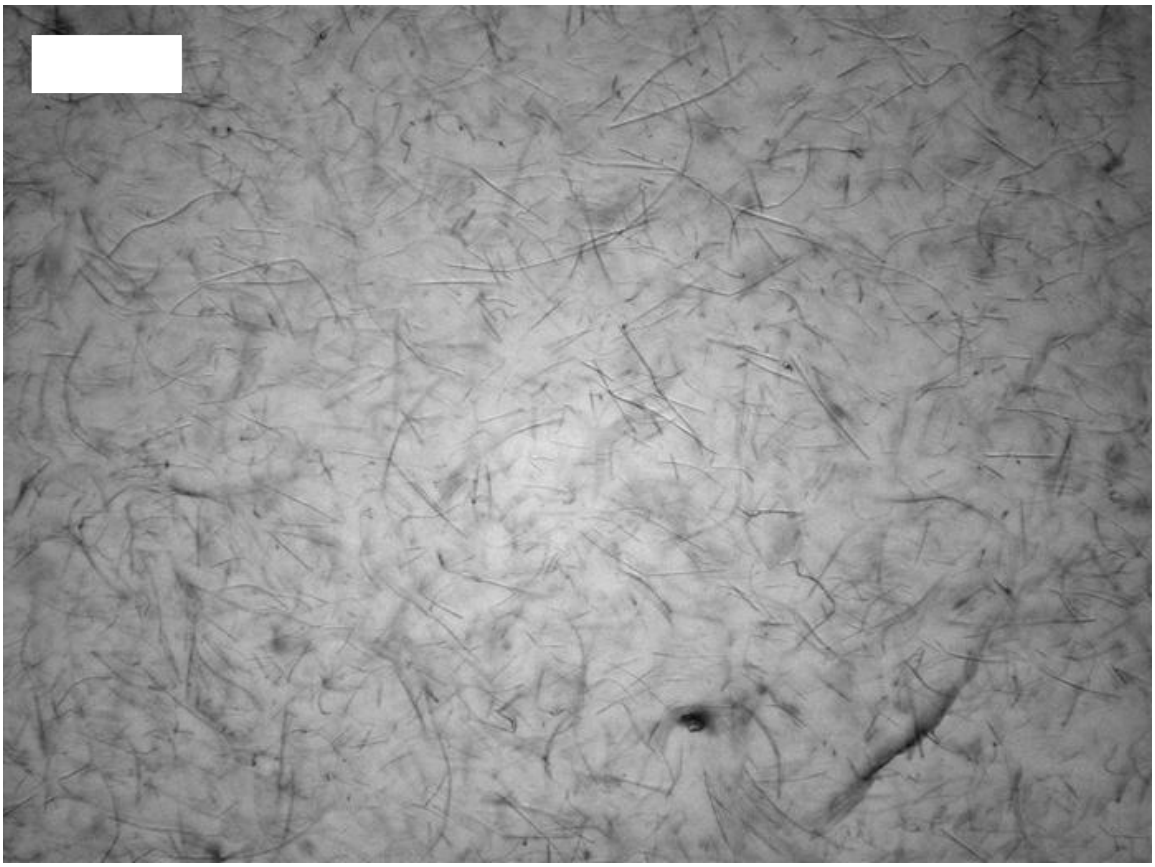

**Figure 5.11. Optical microscopy image of ethyl cellulose micro-rods produced from a solution in acetone with stirring at 1,800 rpm, the lengths of which proved difficult to measure. Scale bar is 100 µm.**

### 5.3. Effect of high shear mixing – cutting the fibres down to size

Due to the difficulties found in reducing the length of EC micro-rods by increasing the shear rate which has been shown to be effective in previous studies using shellac and SU-8 epoxy resin[6], it was decided to try to mechanically shorten the EC micro-rods. By shearing suspensions of micro-rods at high speed using an Ultra Turrax (IKA Werke, Ultra Turrax T25 Basic) and sampling the micro-rods at various time intervals of mixing, it was aimed to decrease the micro-rod length with increased time of high speed shearing. The EC micro-rods were sheared at 0.5 wt.% in aqueous suspension at 8,000 rpm from 30 sec. to 20 min.

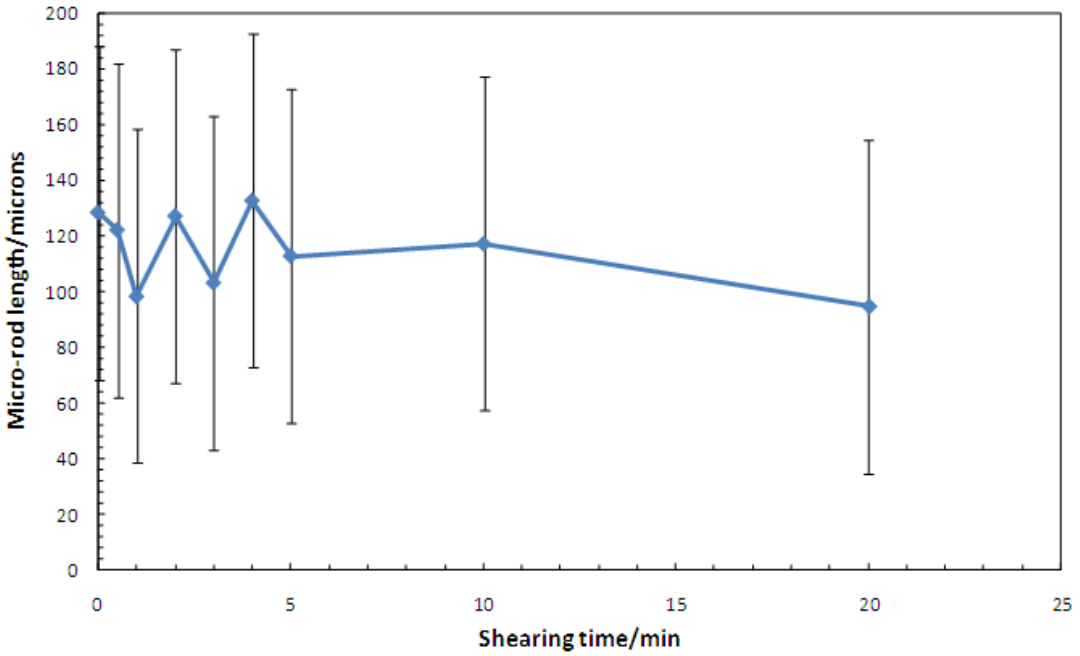


**Figure 5.12. Effect of high speed shearing (8,000 rpm) on the length and standard deviation in length of the resultant ethyl cellulose micro-rods. Error bars are 1 standard deviation in micro-rod length either side of each point.**

It was found that the use of high shear in this way did not noticeably alter the size of the micro-rods, or improve the polydispersity of the suspension, therefore the EC micro-rods cannot be significantly shortened by this process. Further work in this area could investigate the effect of elevated shearing speed up to the maximum speed of the mixer, 24,000 rpm.

## 5.4. Foamability of ethyl cellulose micro-rods

The purpose of the work investigating the production of EC micro-rods is to use the resultant micro-rods for foam stabilisation. All micro-rods used in the foamability studies were produced by injecting a 30 wt.% ethyl cellulose in acetone solution into a dispersed phase comprising 85% glycerol and 15% Milli-Q water (v/v) under shear at 2,000 rpm for 10 min. On their own, EC micro-rods produced from an acetone disperse phase (used here) show relatively poor foamability, therefore it is necessary to reduce the repulsive forces present in the system by addition of electrolyte and/or changing the system pH. These factors are investigated below.

### 5.4.1. Effect of added electrolyte

Initially, the effect of added NaCl on the foamability of the micro-rods was investigated. NaCl was added at 0.01, 0.1, 0.5 and 2.0 M concentrations to the aqueous phase (Milli-Q water, 10 mL). Foams were produced by hand shaking (20 times) and pH was not altered from that of the Milli-Q water (pH 6.5). Fig. 5.13 shows that only when the electrolyte concentration is raised up to 2 M is foam stability increased to a superior level. Initial foamability of the 0.5 M sample is as high as the 2 M sample, but stability is poor in comparison. After initial drainage the foams are quite stable, shown by the flattening out of the foam height vs. time curves.

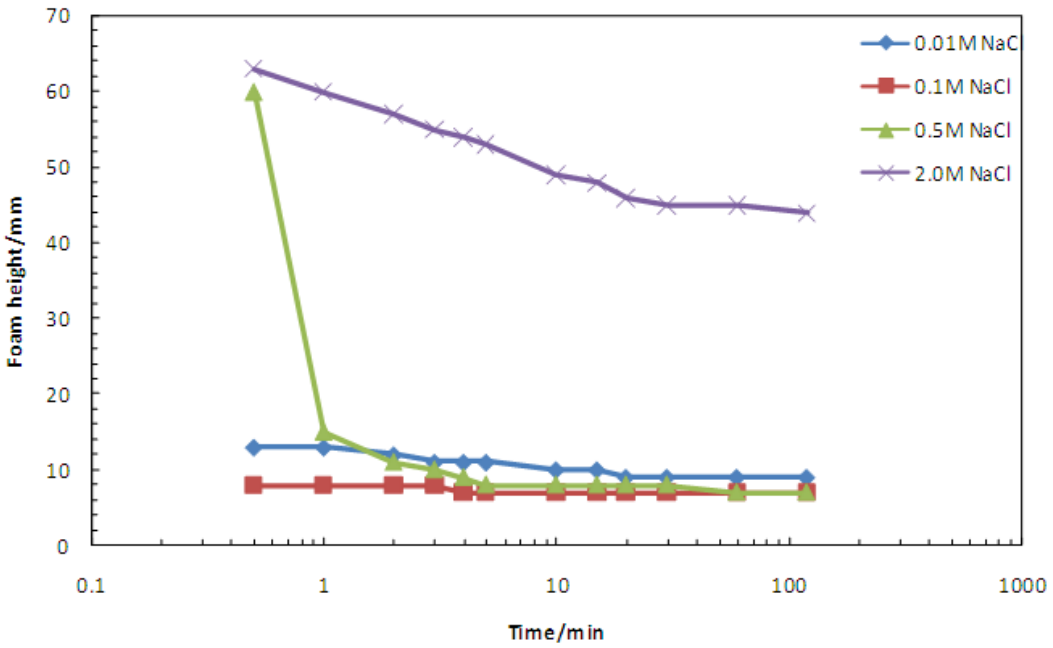


**Figure 5.13. Effect of added NaCl on the foamability/foam stability of a 2.4 wt.% aqueous dispersion of ethyl cellulose micro-rods. Uncertainty in the measurement of the recorded foam heights is considered to be ±2 mm. This is half the diameter of the maximum bubble size, which is recorded at the end of the experiment, after bubble coarsening has occurred.**

### 5.4.2. Effect of changing pH

The pH of the aqueous part of the foams was varied from pH 3 to 5, 7 and 10 by addition of either dilute HCl or KOH and subsequent checking of pH using a Fisher Scientific pH probe and meter. No electrolyte was added to the foams. Fig. 5.14 shows the evolution of foam height with time. Maximum foamability and foam stability was observed at lower pH (3 and 5) due to reduction of negative charge on the surfaces of the ethyl cellulose micro-rods lowering the electrostatic repulsion between the micro-rods and the air-liquid interface.

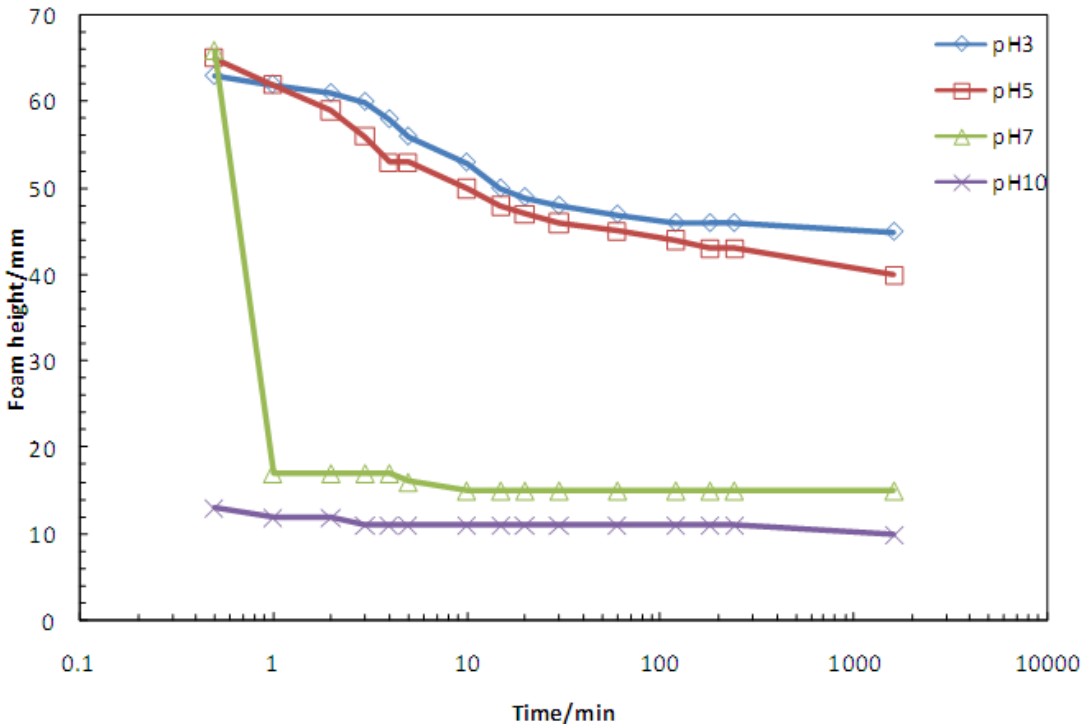


**Figure 5.14. Effect of changing pH on the foamability and stability of 2.4 wt.% ethyl cellulose micro-rod-stabilised aqueous foams.**

5.4.3. Effect of altering electrolyte concentration with fixed pH

Having found that optimum foamability of ethyl cellulose micro-rods used in this study occurred around pH 3, the effect of varied salt concentration at pH 3 was investigated. Foams were produced with 2.4 wt.% EC micro-rods and NaCl incorporated at concentrations of 1, 2, 3 and 4 M in 10 mL samples. All of the electrolyte concentrations used show a similar effect on the foamability and stability of the pH 3 system. After the initial drainage the foams reach a plateauing effect where they are "scaffolded" by the remaining network of EC micro-rods. Fig. 5.15 shows a plot of foam height vs. time to resolve the behaviour of the foams in the first moments after formation.

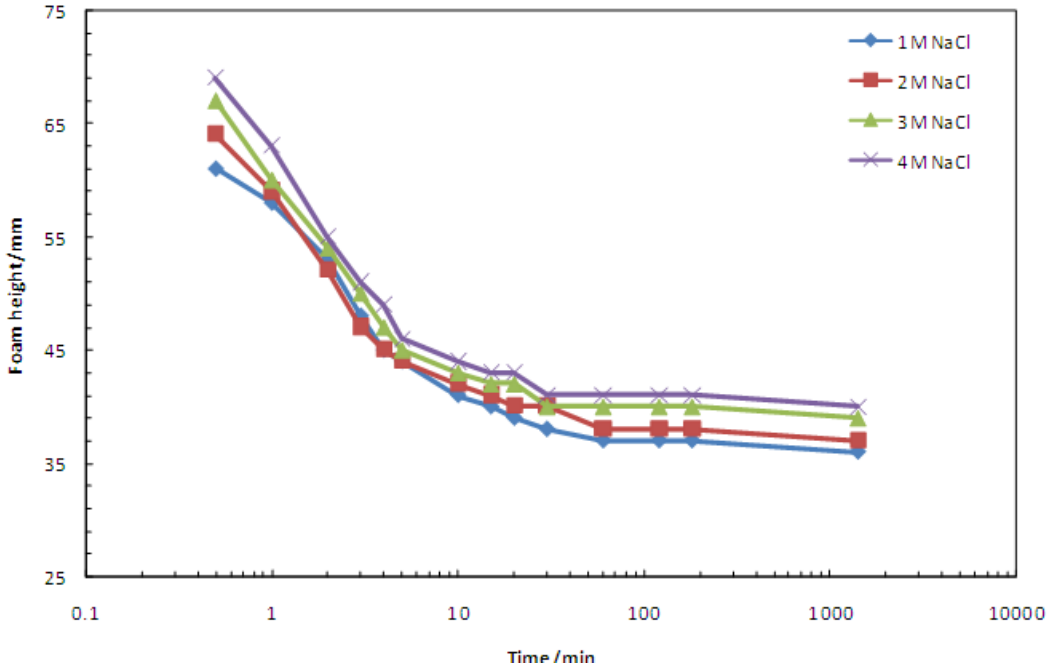


**Figure 5.15. Effect of varied salt concentration at fixed pH (3) on the foamability/foam stability of aqueous foams stabilised by 2.4 wt.% ethyl cellulose micro-rods.**

In summary, when an optimal pH for foam formation is used, the effect of addition of NaCl between 1 M and 4 M shows no clear benefit for the foamability and the foam stability.

### 5.4.4. Effect of altering pH at fixed electrolyte concentration

In a further experiment, the effect of varied pH in the presence of a fixed concentration of electrolyte (NaCl) was investigated. Section 5.4.1 described the effect of addition of 2 M NaCl which enhanced stability and foamability over foams with low or zero NaCl concentration. Therefore, in this experiment 2 M NaCl was used in conjunction with pH of 2.7, 4.5, 7.1 and 10.25. Fig. 5.16 illustrates the effects observed.

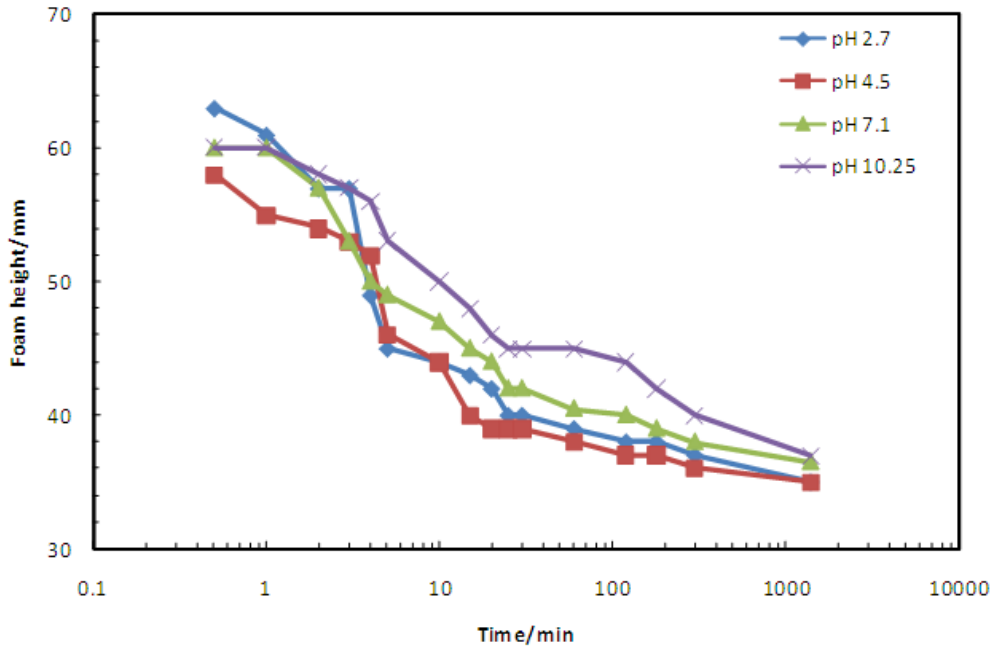


**Figure 5.16. Height and stability of aqueous foams stabilised by 2.4 wt.% ethyl cellulose micro-rods in the presence of 2 M NaCl and varied pH. Uncertainty in the measurement of the recorded foam heights is considered to be ±2 mm. This is half the diameter of the maximum bubble size, which is recorded at the end of the experiment, after bubble coarsening has occurred.**

From the measurements made, it seems that the increase in pH at fixed NaCl concentration slightly increases both the foamability and the long-term stability of the foams.

### 5.4.5. Effect of added urea

At elevated concentrations (6-8 M) urea can behave as a chaotropic agent, where it disrupts hydrogen bonding and the hydrophobic interactions. This may affect the EC micro-rods hydrophobic interactions with neighbouring micro-rods and their adsorption at the interface. To examine this, aqueous dispersions of the micro-rods were produced as before (2.4 wt.%) and to both samples urea was added forming 2 solutions, one 2 M and one 8 M. The pH was unchanged and no electrolyte was added. Figure 5.17. shows the foam height vs. time for both samples.

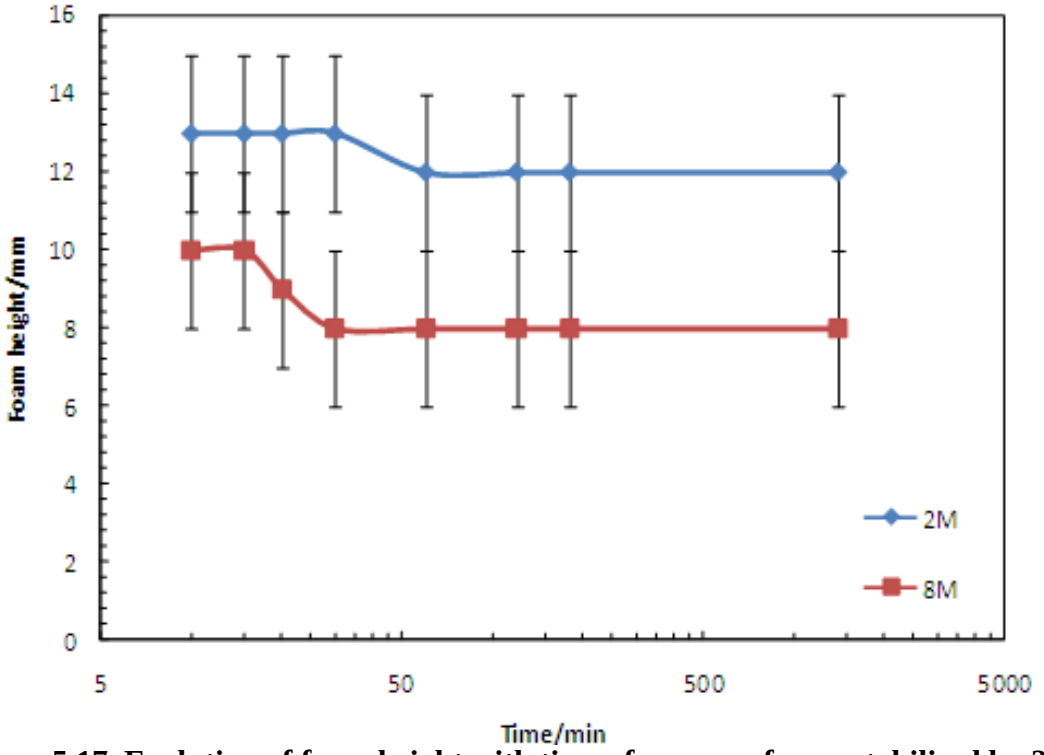


**Figure 5.17. Evolution of foam height with time of aqueous foams stabilised by 2.4 wt.% ethyl cellulose micro-rods in the presence of 2 and 8 M urea. Errors calculated from standard deviation of three repeats.**

It can be seen that in this example the addition of urea gave decreased foamability to the EC suspensions. When 8 M urea was used, the greatest decrease in foaming was observed, possibly a reflection that at this high concentration, the hydrophobic attractive forces which facilitate scaffolding of the EC micro-rods are being decreased by the urea.

### 5.5. Ethyl cellulose – methyl cellulose micro-rod-stabilised foams

In order to further investigate ways to improve the foamability of EC micro-rods, it was decided to fabricate rods in the presence of a surface-active additive, methyl cellulose. Methyl cellulose (Methocel™, Dow Inc.) is a food grade, hydrophilic methyl ether of cellulose which, unlike ethyl cellulose, is water soluble. By combining solutions of both ethyl- and methylcellulose (in tetrahydrofuran and water respectively) in the correct proportions it is hoped that micro-rods with enhanced foamability could be produced. This could occur due to the hydrophilic polymer being trapped within the EC bulk during micro-rod formation, but dissolving out during the washing process, giving extra porosity, increasing surface roughness.

The disperse phase for the rods was produced as follows: into a mixture (90:10) of THF and Milli-Q water, EC and methyl cellulose were added at 15 and 1 wt.%, 15 and 2 wt.% and 15 and 4 wt.% respectively, to produce 3 different phases with 15:1, 7.5:1 and 3.75:1 ratios (approximately) of EC to methyl cellulose. These disperse phase mixtures were added to an 85% glycerol, 15% Milli-Q water mixture (v/v) continuous phase (50 mL) under shear (1,300 and 2,000 rpm in separate experiments, Cole Parmer Digital Reversing Mixer, Servodyne) for ten minutes each to produce the micro-rods. Fig. 5.18 shows the morphology of the micro-rods.

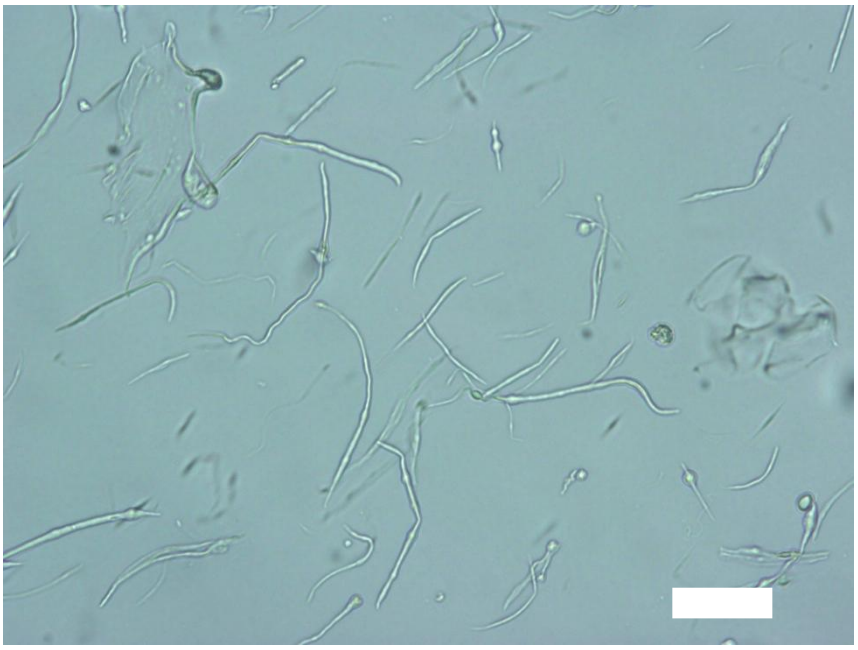

**Figure 5.18. Optical microscopy image of ethyl cellulose micro-rods containing methocel (initial ratio before washing 7.5:1 EC:MC). Some micro-rods appear to contain lumps which could be encapsulated methocel. Scale bar is 25 μm.**

After washing with Milli-Q water, to remove glycerol and free methocel, the EC micro-rods were added to graduated cylinders containing approximately 10 mL of Milli-Q water resulting in suspensions of rods of approximately 2 wt.%. Foams were produced by hand-shaking (20 times up and down), and the foam height against time was monitored over several hours. Fig. 5.19 shows the foam stability of all polymer ratios at 1,300 rpm (top) and 2,000 rpm (bottom).

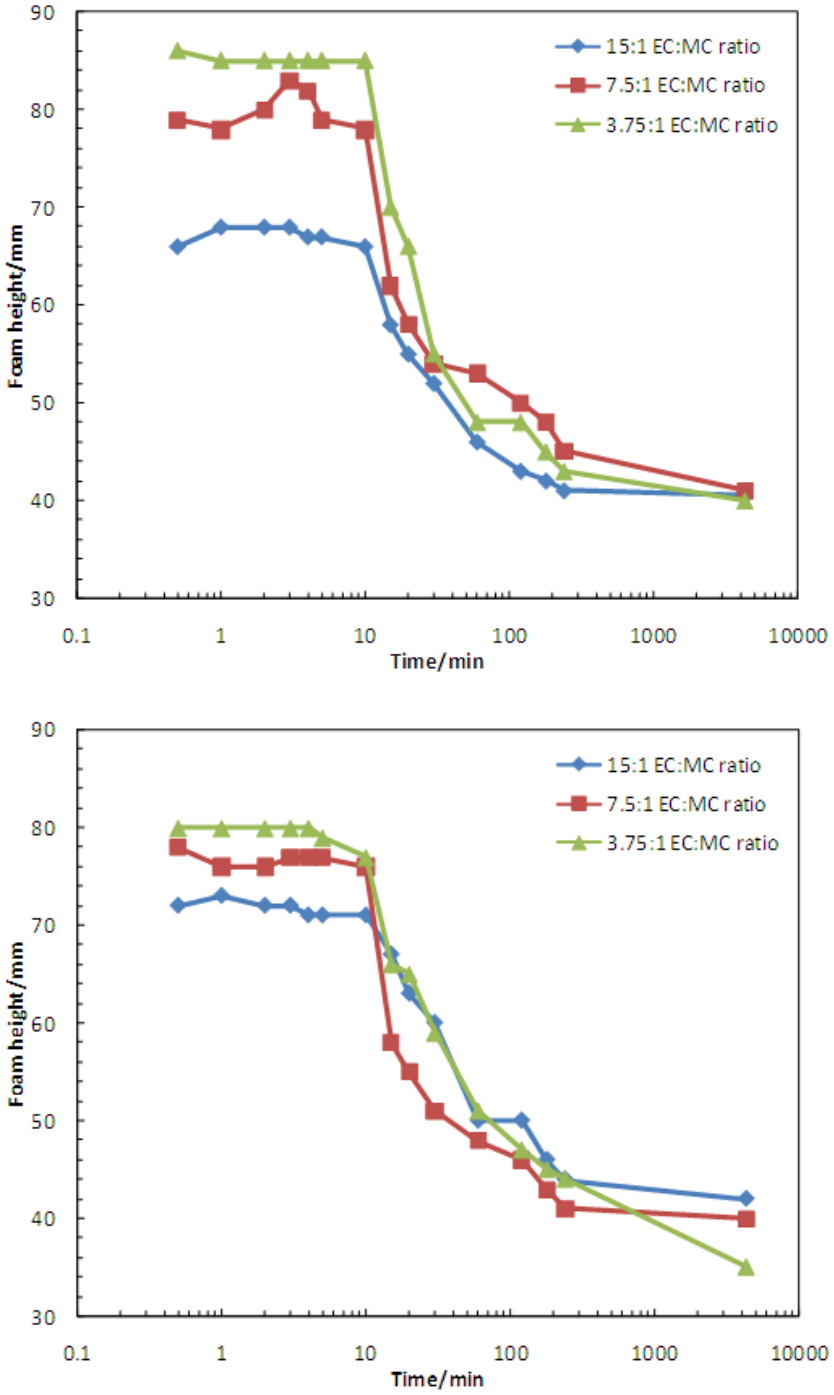


**Figure 5.19. Height and stability of aqueous foams stabilised by ethyl cellulose micro-rods produced in the presence of varying concentrations of methyl cellulose at stirrer speeds of 1,300 rpm (top) and 2,000 rpm (bottom). Uncertainty in the measurement of the recorded foam heights is considered to be ±2 mm. This is half the diameter of the maximum bubble size, which is recorded at the end of the experiment, after bubble coarsening has occurred.**

A further observation of EC micro-rods produced from a THF disperse phase containing Milli-Q water and methocel is the dramatically reduced length in the rods compared with rods produced using a pure EC/THF disperse phase, which were found to have extreme aspect ratios and be fibre-like. This reduction may be due to the presence of methocel creating 'break points' along the micro-rods, giving them brittle character and encouraging micro-rod break-up. The resultant shorter micro-rods could give enhanced foamability compared with the long micro-rods produced previously with EC only. Fig 5.20 demonstrates the micro-rod length with changing EC/MC ratio and stirrer speed. Average micro-rod length is around 40 μm compared with several hundred microns for pure micro-rods of EC from THF (section 5.2.1.).

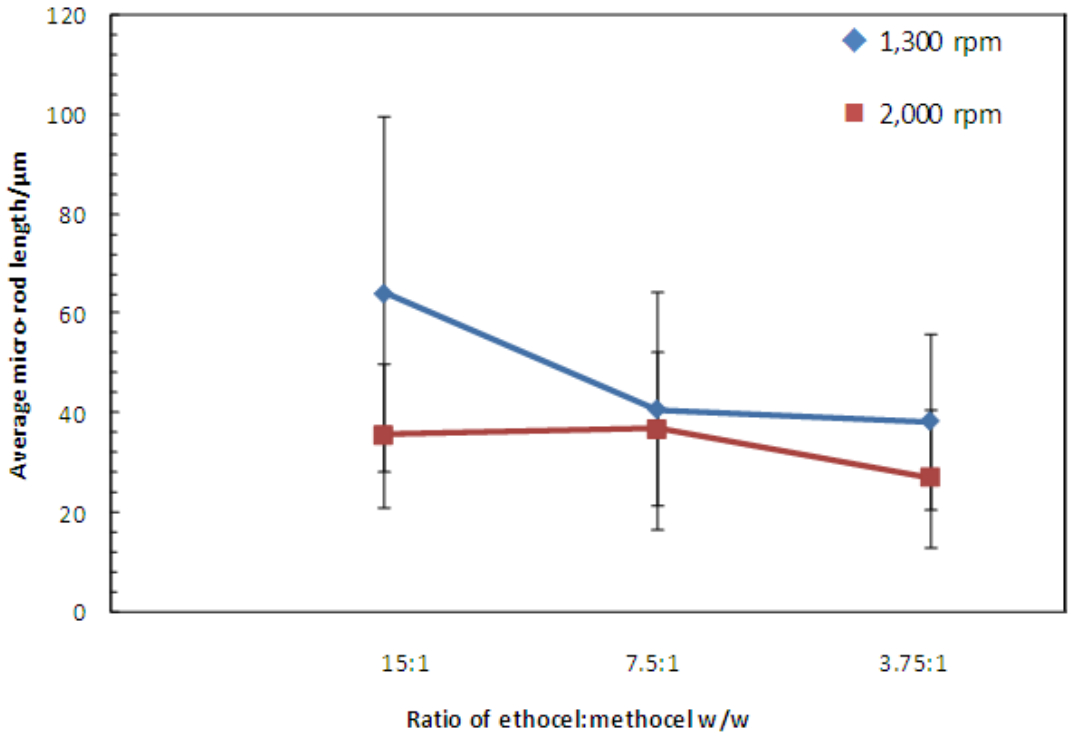


**Figure 5.20. Average length of ethyl cellulose micro-rods produced using different ratios of ethyl cellulose to methocel and stirrer speeds during micro-rod fabrication of 1,300 and 2,000 rpm.**

In conclusion, micro-rods formed from a combination of EC and methyl cellulose showed reasonable foamability and good stability over several days. It is not clear how much methocel has remained from the micro-rod production process or the washing/isolation procedure afterwards, but the two foams containing the highest concentrations of methocel gave the best initial foamability, indicating that some free methocel may remain, as it foams well in aqueous solution. It may also be of interest to

examine such composite polymer micro-rods by SEM to check for any change in texture that may have been caused by the methocel.

### 5.6. Effect of high shear mixing on the morphology of the particles produced

When solutions of very low concentration (0.1% w/w for example) of EC in acetone solution were injected (in several small volume aliquots, e.g. 1 μL) into 50 mL of optimal continuous phase under high shear mixing (IKA Ultra Turrax T25 Basic, 8,000 rpm, 8 mm diameter impeller attachment) unusual structures were observed. The micro-rod particles formed were in relatively low yield compared with other amorphous EC precipitates. They possessed a multi-limbed structure as shown in figures 5.21A – C and it was thought that structures such as this may be able to occupy the nodal areas and Plateau borders within foams, delaying drainage and thus increasing the foam stability. It was possible to deduce whether or not the structures were hollow or solid by staining with fluorescent Nile Red dye. Figures 5.21A - D show the hollow nature of these structures. However, due to the low yield of these particles, it was not possible to gain a quantity sufficient for foam stabilisation studies.

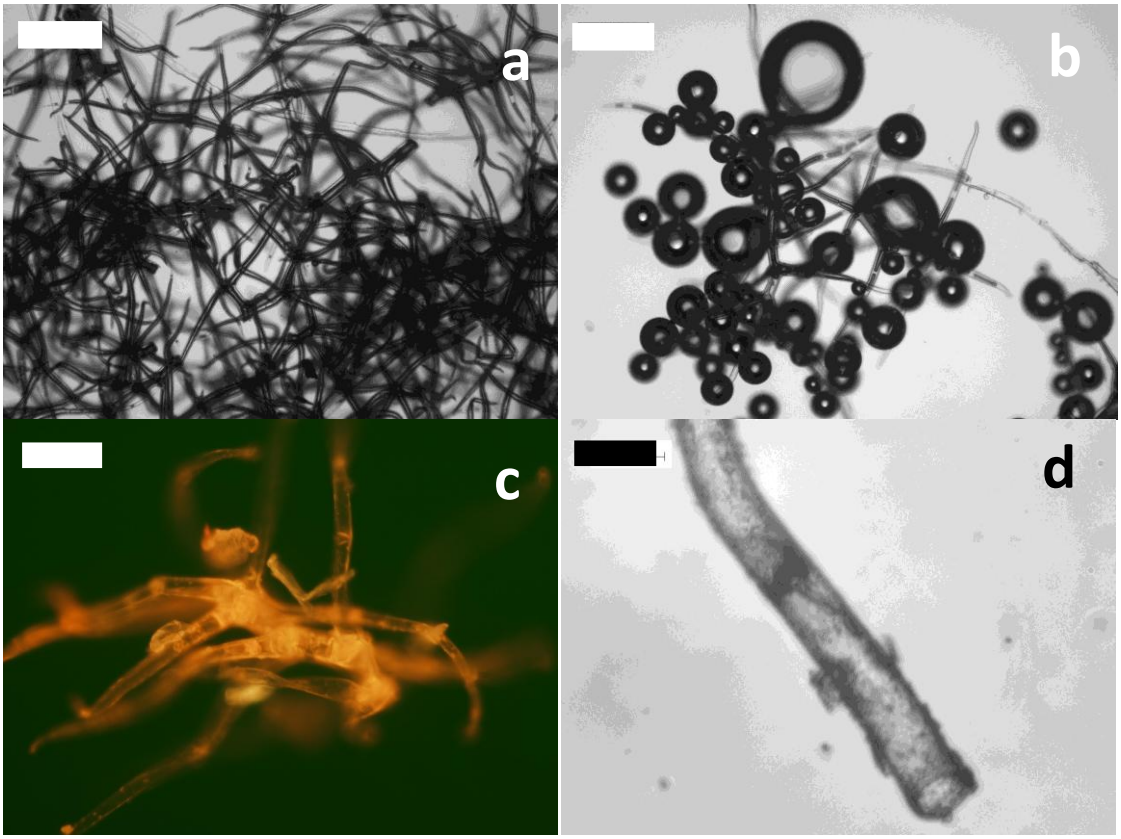


**Figure 5.21. Optical microscopy images of A) a cluster of the star-like tubular structures produced by adding 0.1 wt.% ethyl cellulose in acetone to a 50 mL of 85% glycerol/15% Milli-Q water (v/v) continuous phase under 8,000 rpm shear (IKA Ultra Turrax). B) Air bubbles entwined in the limbs of the surface-active ethyl cellulose structure. C) Structure stained with Nile Red dye and observed using fluorescence microscopy. A hollow structure is evident, as fluorescence intensity is greater near the edges of the limbs. D) A separate limb displaying an open, tubular morphology. Scale bars are 100 µm (A&B) and 25 µm (C&D).**

### 5.7. Emulsions stabilised by ethyl cellulose micro-rods

Further to the work carried out on the foam stabilising properties of EC micro-rods, a study on the efficacy of the rods as emulsifiers was undertaken. Previous studies have shown the efficacy of SU-8 epoxy micro-rods as emulsifiers[5] during the formation of so-called 'hairy colloidosomes' where water-in-oil emulsions were produced as a result of emulsifying an aqueous hydrocolloid solution into a tricaprylin oil phase using the micro-rods as stabilisers. The emulsion was gelled by cooling, and the micro-rod covering on the resultant gelled 'hairy colloidosomes' remained intact after washing,

showing the stability gained by interweaving of the adsorbed rods. It was anticipated that the same effect would be observed with the use of EC rods produced using an acetone disperse phase. Previous work in the author's group (E.L. Sharp and V.N. Paunov – unpublished results) using the gel trapping technique[17,18] to 'arrest' the positions of the micro-rods at the interface shows that rods adsorbed at the oil-water interface possessed rough surfaces together with a degree of hydrophobicity. The parts of the micro-rods which are buried in the PDMS matrix would have resided initially in the oil phase.

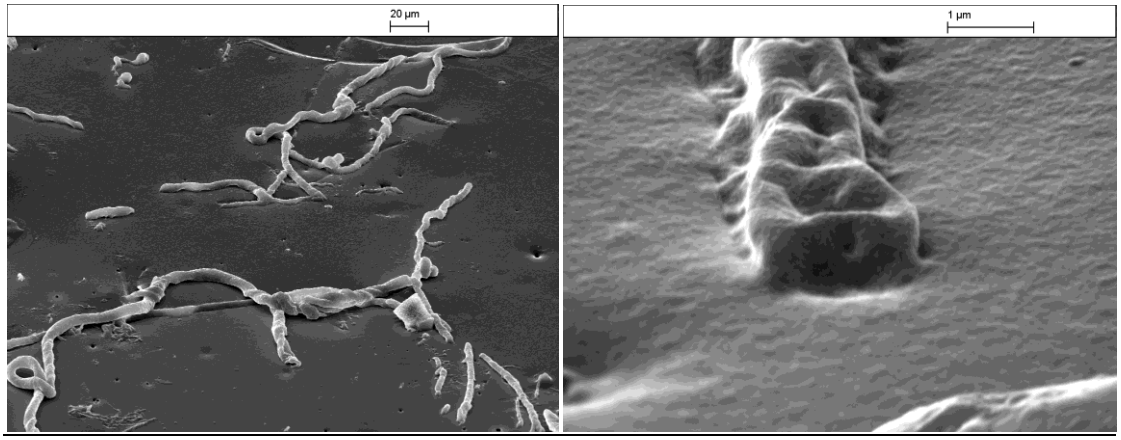


**Figure 5.22. SEM images of ethyl cellulose micro-rods trapped in PDMS after the gel trapping technique[17] has been applied. The wider angle view (left) highlights the twists and bends in the long fibres while the right hand image shows the roughness of the ethyl cellulose. As the cross section of the micro-rod is not cylindrical, unlike for simple spheres, for which the calculation is shown in previous chapter, the contact angle that the micro-rod makes at the oil-water interface is hard to estimate from the SEM images.**

Due to the relatively large size of the EC micro-rods used for this work it is expected that if an emulsion is formed, the drop size will be very large. Generally, large drops are affected by gravity and cream rapidly, causing subsequent flocculation and leading to drop coalescence. It was expected that this situation will be counteracted by the steric stability barrier created by a layer of adsorbed micro-rods.

In this study, aqueous suspensions of EC micro-rods were produced from a 33 wt.% solution in acetone 1 mL of which was added under shear (2,000 rpm, 10 min) to 50 mL of 85% glycerol/15% Milli-Q water (v/v) continuous phase. The samples were

dried in an oven, and weighed out as a dry powder for use as an emulsifier. Initially, a 30% heptane, 70% Milli-Q water (v/v) system with 1.3 wt.% EC micro-rods was used. The materials were added in the following order: water, EC, oil. The mixture was sheared by Ultra Turrax at 11,000 rpm for 2 min and the resulting opaque emulsion was subjected to a drop test and conductivity measurement. Conductivity was found to be 0.28 μS $cm^{-1}$, which together with the drop test result indicated a water-in-oil emulsion. Fig. 5.23 shows an optical micrograph of the resulting emulsion.

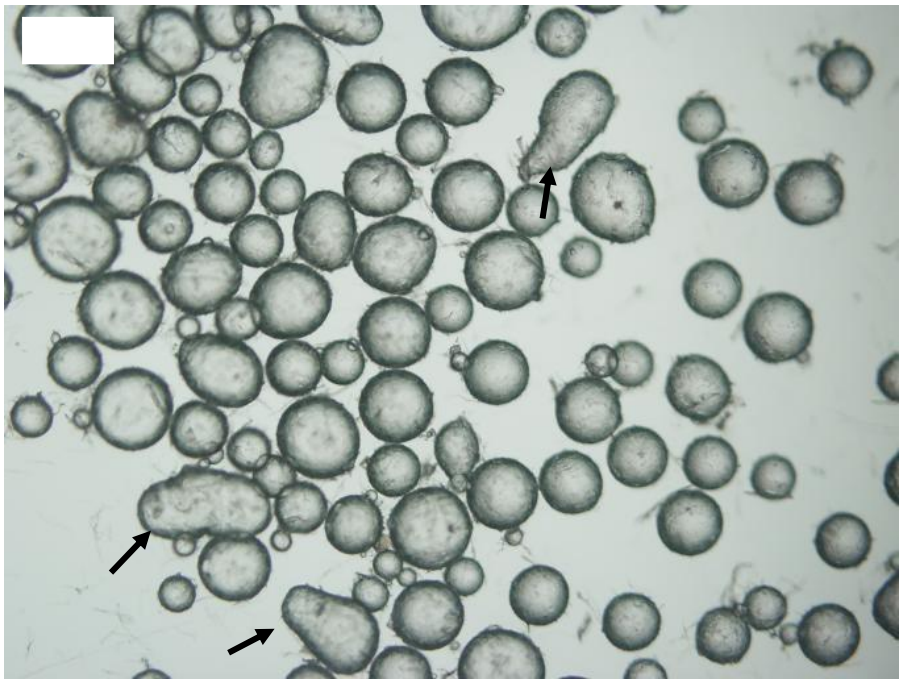

**Figure 5.23. Optical microscopy image of water in heptane emulsion stabilised by 1.3 wt.% ethyl cellulose micro-rods. Large drops are produced, due to the size of the micro-rods. Evidence of partial coalescence[19] is observed (black arrows), the process being halted by the layer of adsorbed micro-rods resisting interfacial shrinkage. Scale bar is 250 μm.**

As expected, large water-in-heptane drops around 200 – 300 μm in diameter were observed as a consequence of the EC micro-rods having lengths around 100 μm. Evidence of partial coalescence was also observed, with irregularly-shaped drops produced as a result of the resistance of the layer of intertwined EC micro-rods to rearrange in accordance with the reduced surface area associated with the coalescence. This shows that the adsorbed layer of EC micro-rods is not always dense enough to

prevent the droplet coalescence. Fig. 5.24 shows the extent of the coverage of the EC micro-rods. Longer rods appear to simply project off the end of the curved drop surface.


**Figure 5.24. Optical microscopy image (several images overlaid to give extended depth of field) of water drops in heptane coated in a layer of adsorbed ethyl cellulose micro-rods (1.3 wt.%) showing the intertwined arrangement of micro-rods.**

The EC micro-rod coated water drop size was easily visible to the naked eye. They had the behaviour of tiny glass beads, and were able to roll over one another, remaining intact due to the protective barrier created by the adsorbed EC micro-rods.

A further observation of the emulsion through optical microscopy was the rapid evaporation of the continuous phase (heptane) due to the heat of the microscope light bulb. This process produced a cellular structure (fig. 5.25A) which strongly resembled an aqueous foam, but which was in fact a collection of discrete polyhedral water droplets separated by the adsorbed EC micro-rods in a heptane layer. This structure survived the drying process for several minutes, and when the structure was punctured using a sharp glass edge, water was released from within (fig. 5.25B).

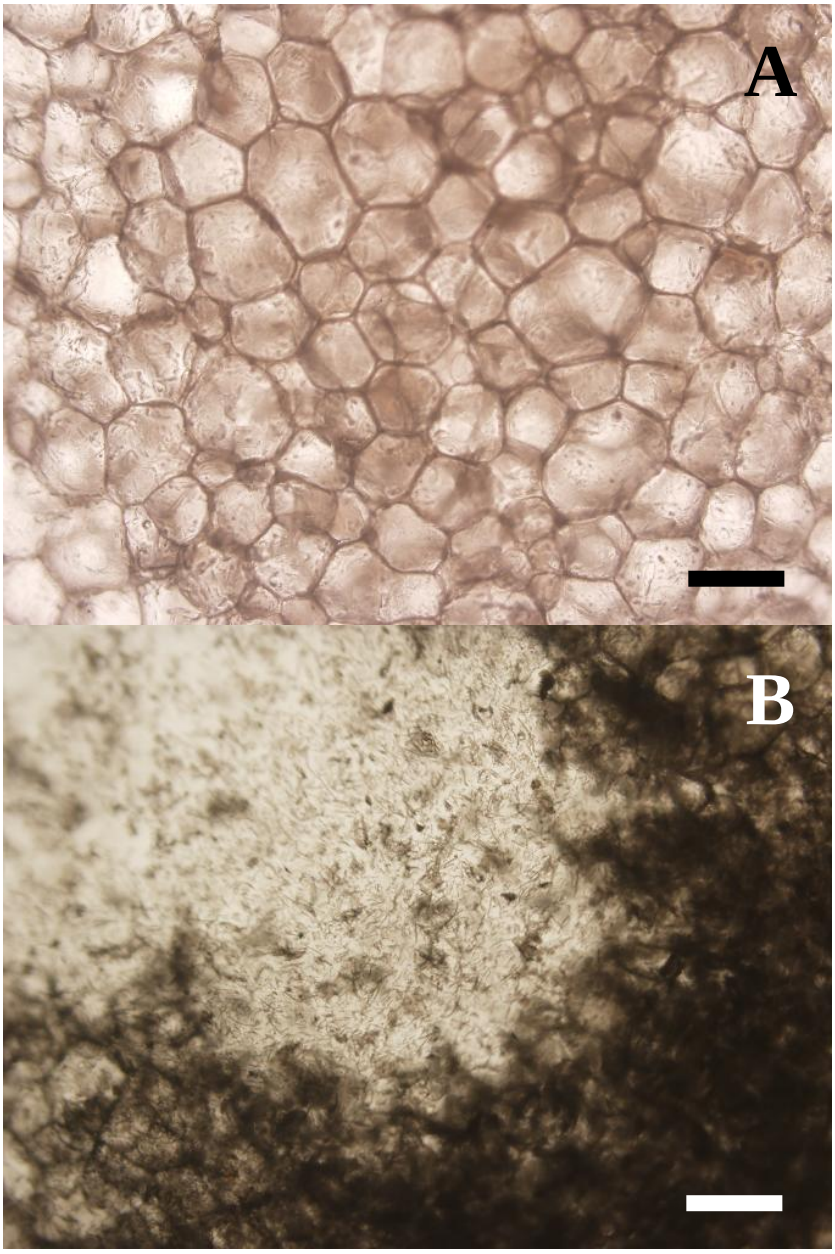


**Figure 5.25. Optical microscopy images of (A) closely-packed polyhedral water drops stabilised by an adsorbed layer of ethyl cellulose micro-rods. (B) Piercing of the bulk structure leading to the release of water and free EC micro-rods. Scale bars are 250 µm.**

Further investigation by optical microscopy (figs. 5.26A & B) showed the incomplete interfacial coverage given by the EC micro-rods, even close to the points of intersection with other neighbouring drops.

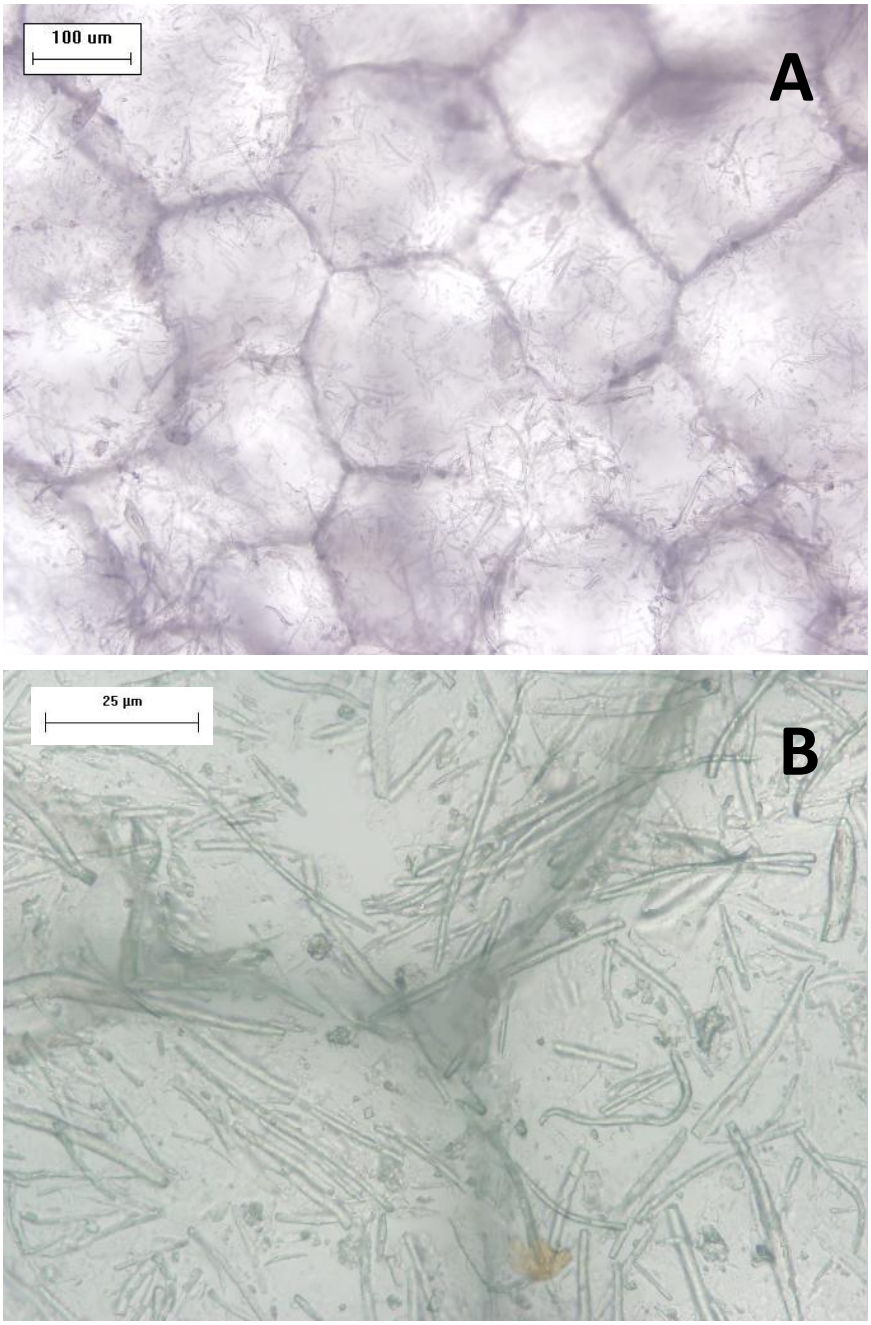


**Figure 5.26. 3D reconstruction optical microscopy images of (A) the polyhedral structure of the water drops in heptane, stabilised by ethyl cellulose micro-rods and (B) the intersection of three polyhedral water drops, showing the partial interfacial coverage given by the adsorbed EC micro-rods.**

### 5.7.1. Effect of ethyl cellulose micro-rod concentration on emulsion drop size

It is expected that by increasing concentrations of the emulsifier the average droplet size decreases due to the additional interfacial area created by the adsorption of the

emulsifier at the interface. In this experiment, the concentration of EC micro-rods added to the oil and water was varied to see if the same effect is observed in this system. In order to reduce problems associated with evaporation caused by the volatile heptane continuous phase used previously, undecane was used in this work. EC micro-rod concentrations of 2.6, 1.95, 1.3, 0.65 and 0.33 wt.% were used, together with undecane (7 mL) and Milli-Q water (3 mL) and all emulsions were produced by shearing with Ultra Turrax at 11,000 rpm for 2 min.

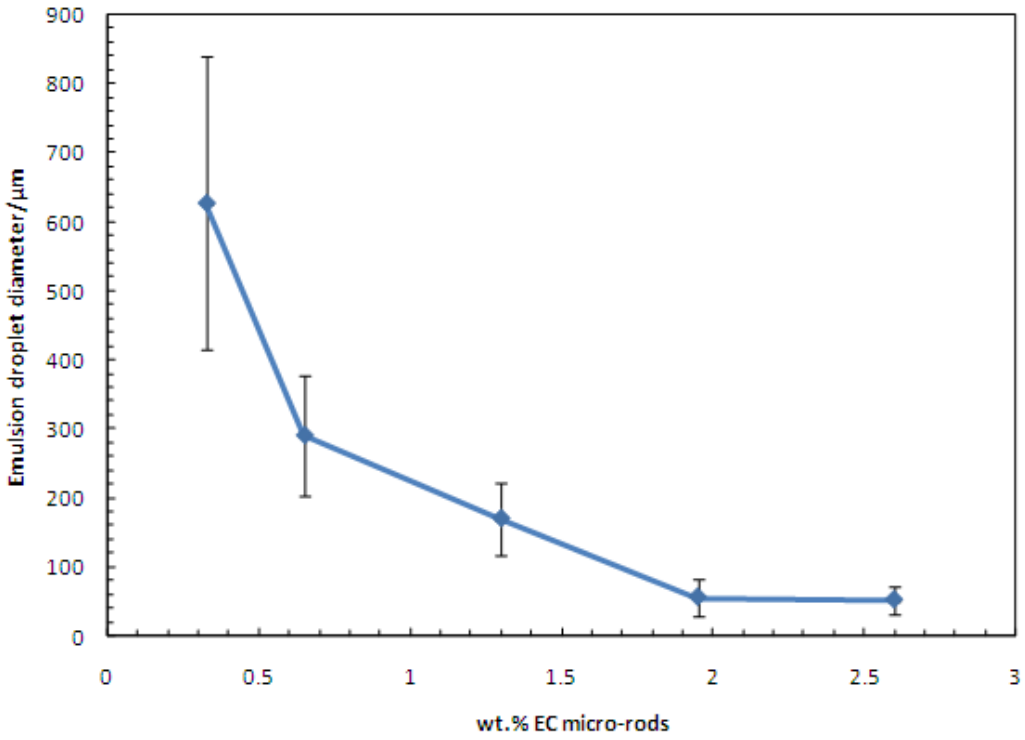


**Figure 5.27. Change in average drop size of water in heptane emulsions stabilised by various concentrations of ethyl cellulose micro-rods. Error bars represent one standard deviation each side of the mean droplet diameter. Measurements taken from optical micrographs containing at least 50 drops.**

Fig. 5.27 shows a clear reduction in drop size with increasing EC micro-rod concentration in agreement with expected trends. There is a plateauing in the decrease in drop size however, and this could be countered by using increased shearing energy. Fig. 5.28 shows the emulsion drops achieved using the different micro-rod concentrations.

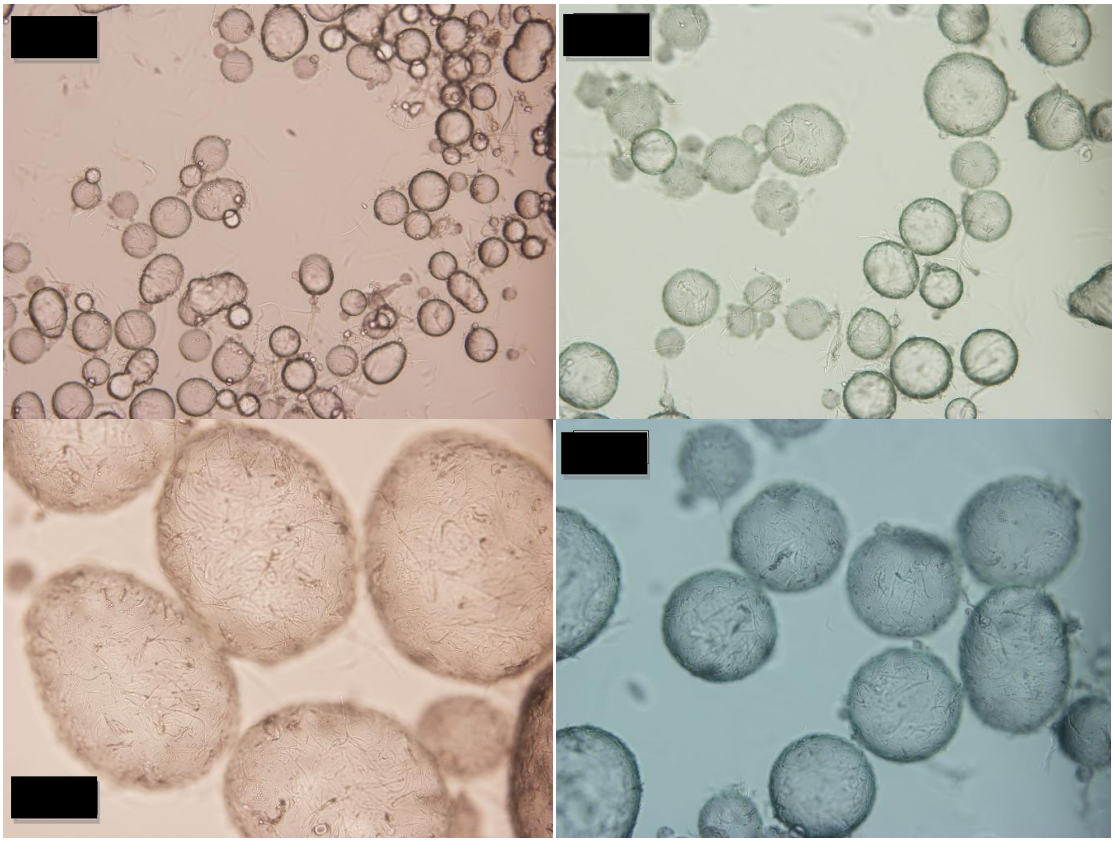

**Figure 5.28. Optical microscopy images showing the effect of ethyl cellulose micro-rod concentration on water-in-undecane emulsion droplet size. Weight percentages of micro-rods used were (clockwise from top left) 2.6, 1.3, 0.65 and 0.33. All scale bars are 100 μm.**

Future investigations on the use of EC micro-rods as emulsifiers could include the effect of added electrolyte and varied pH, together with a comparison with EC micro-rods produced from a THF disperse phase. This study, however, goes outside the scope of this thesis.

### 5.7.2. Production of ethyl cellulose 'cages' by drying the emulsion

To investigate the integrity of the layer of adsorbed EC micro-rods on the surfaces of emulsion drops, and test their degree of entanglement, the emulsions which had previously been produced were dried, to see if hollow EC micro-rod 'cages' could be formed. Noble et al. used cross linking with glutaraldehyde to stabilise the outer shells of colloidosomes[5] produced from anisotropic micro-rods, but in our case, only the steric entanglement and hydrogen-bonding of the adjacent EC micro-rods hold the structure in

place. Emulsions produced from 3 mL Milli-Q water, 7 mL undecane and 0.195 g EC micro-rods were sheared for 2 min at 11,000 rpm and dried in open air on a glass slide. A lower proportion of disperse phase (water) was used in order for as many drops as possible to remain discrete, retaining their integrity. Figs. 5.29A & B show the dried structures which remained at lower and higher magnification respectively.

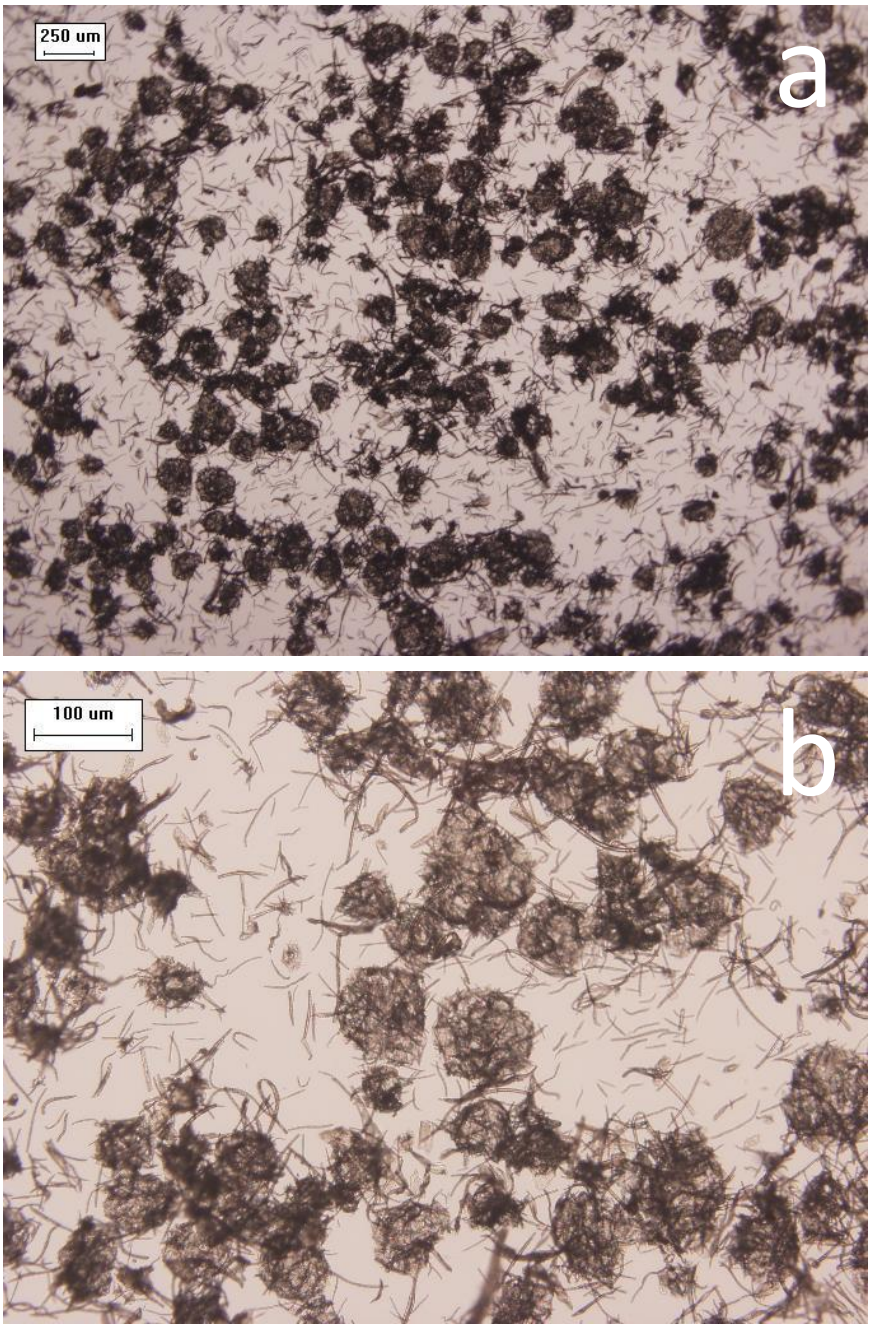


**Figure 5.29. Optical microscopy images of ethyl cellulose micro-rod structures formed as a result of drying water-in-undecane emulsion drops which were stabilised by the micro-rods.**

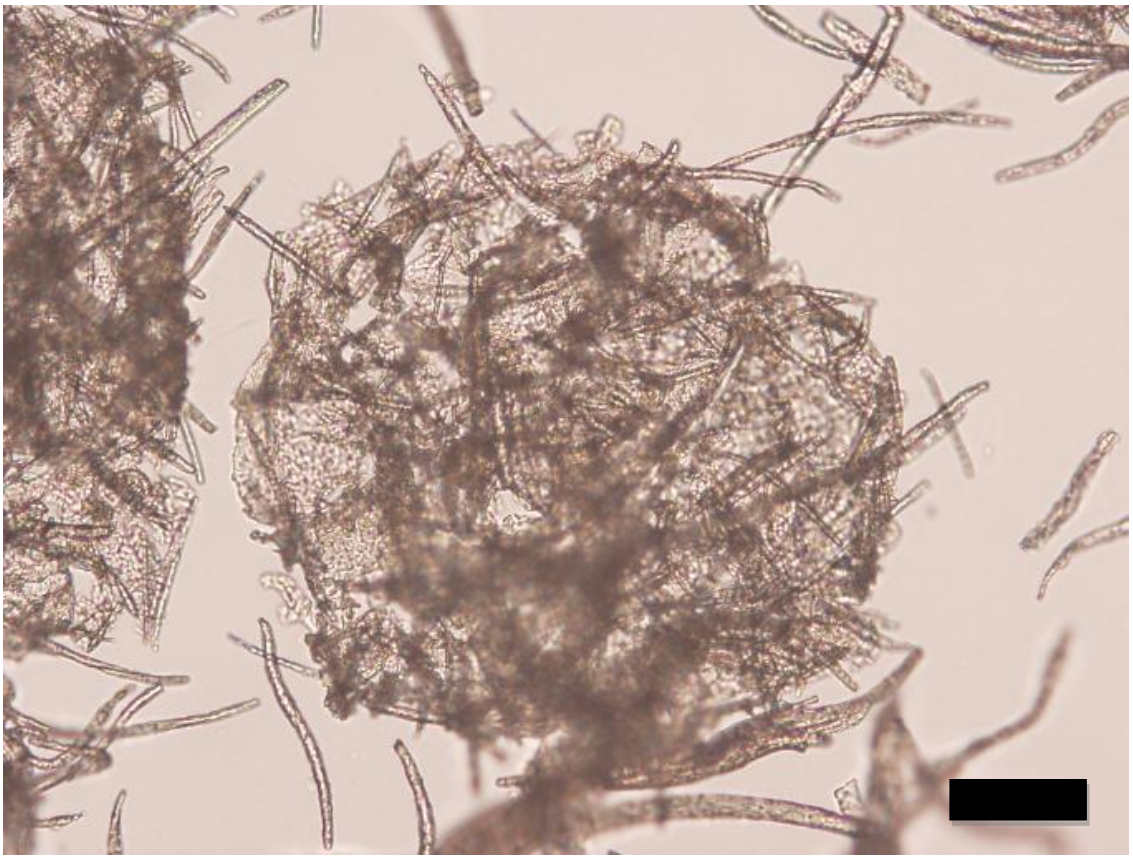

**Figure 5.30. Optical microscopy image of an ethyl cellulose micro-rod structure formed as a result of drying water-in-undecane emulsion drops which were stabilised by the micro-rods. Scale bar is 25 μm.**

5.7.2.1. Scanning electron microscopy of the ethyl cellulose micro-rod structures

Glass slides coated with portions of the dried EC micro-rod-stabilised emulsion were analysed by SEM to reveal whether or not the 3-dimensional structure (so-called 'cages') had remained after the evaporation. Previous viewing by optical microscopy had not been conclusive; however, when the samples were viewed at angles of up to 80º from vertical by SEM, it became immediately apparent that the structures were in fact 'flat as pancakes' in most cases. The following images (figs. 5.31. and 5.32) illustrate this.

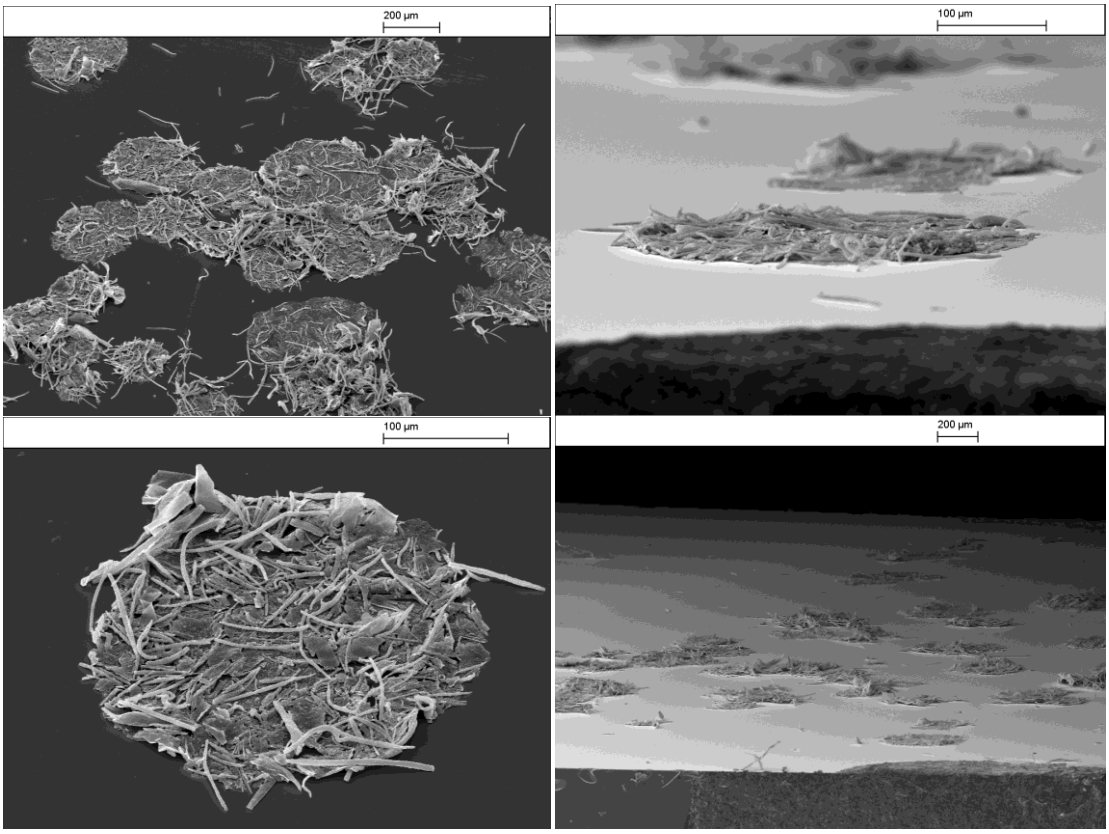


**Figure 5.31. (From top left, clockwise) SEM images of a group of structures which were previously a flocc of water drops in undecane stabilised by ethyl cellulose micro-rods prior to total drying. The flat structures view at 80º from vertical. A wider field view of the same. Viewed at 40º from vertical, a single disc of intertwined ethyl cellulose rods is seen.**

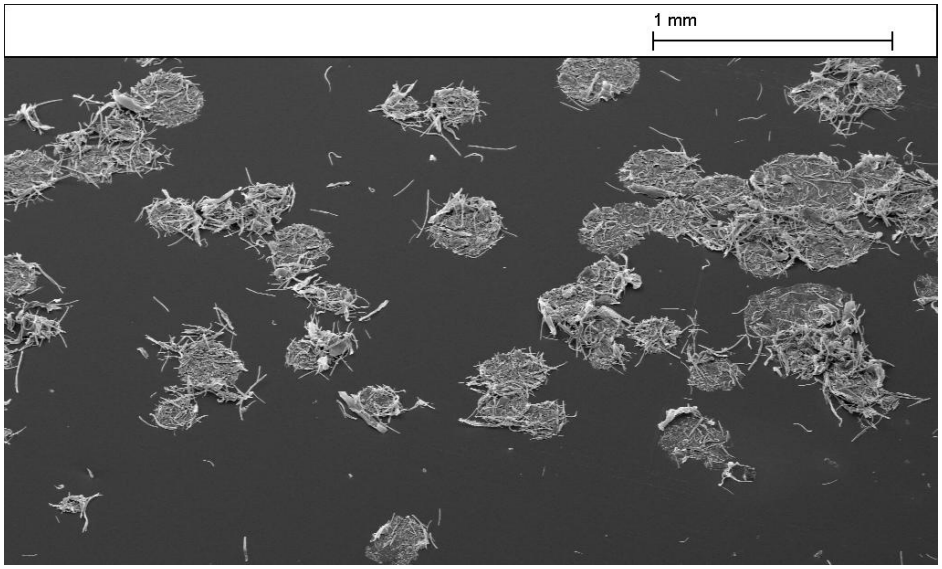


**Figure 5.32. SEM image of a group of structures which were previously water drops in undecane stabilised by ethyl cellulose micro-rods prior to total drying. Viewed at 40º from vertical.**

### 5.7.3. Rehydration of the dried emulsion

The dried EC cages were rehydrated to see if the structures could withstand this treatment. Fig. 5.33 shows that despite the inundation, a number of pockets of air coated with EC micro-rods were observed. Whether these formed during the process of rehydration, or whether they are previously-formed cages which were strong enough to withstand the rehydration of the slide is not clear. Figs. 5.33 (C) and (D) demonstrate that the structures are quite fragile; this micro-rod-stabilised air bubble remained for only 2 minutes.

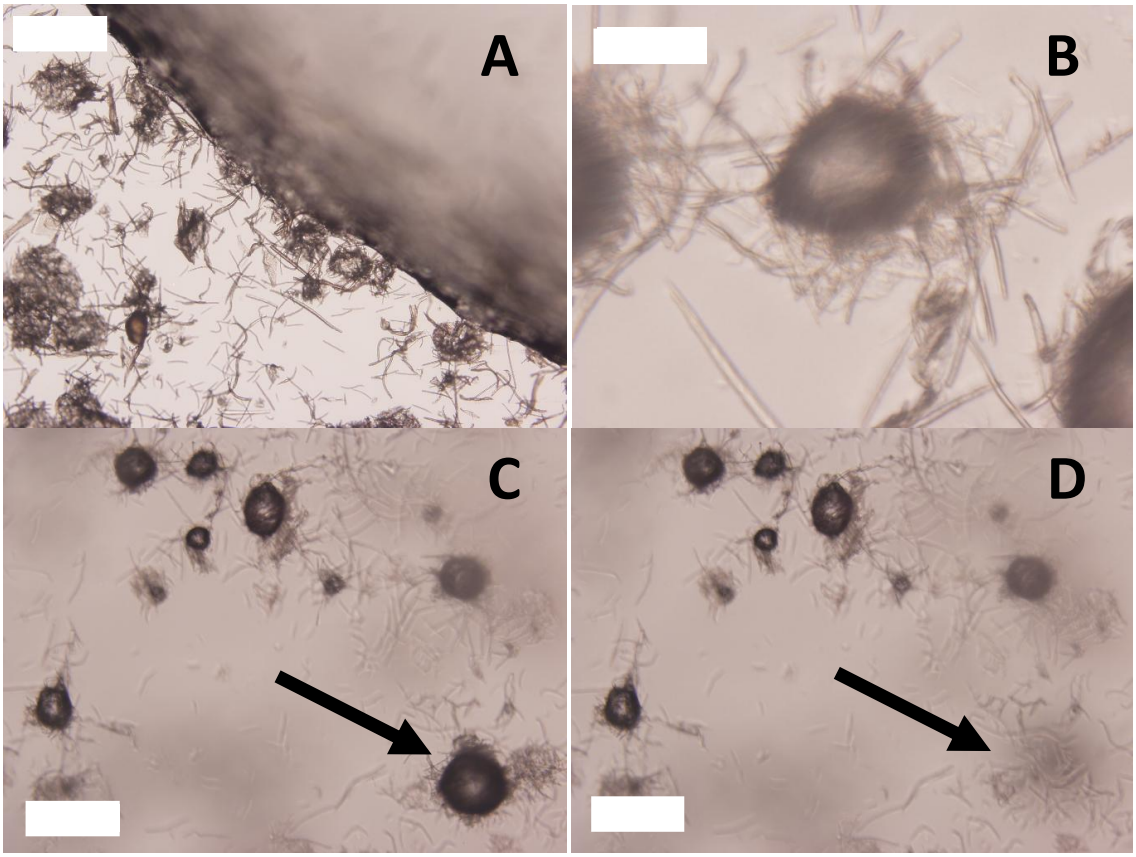


**Figure 5.33. Optical microscopy images of dried ethyl cellulose micro-rod-stabilised water-in-undecane emulsion (A) during rehydration. (B) shows what appears to be an air bubble which is being stabilised by the micro-rods. Images (C) & (D) respectively show the same sample area before and after an air bubble covered in a layer of ethyl cellulose micro-rods bursts a few minutes after rehydration. Scale bars are 100 μm (A, C & D) and 25 μm (B).**

5.7.4. Estimation of the contact angle of sessile water drops on ethyl cellulose

In order to estimate the hydrophobicity of the ethyl cellulose surface, the contact angles of sessile water drops on glass slides which had been previously spin-coated with EC (using 50 µL of a low-viscosity 5 wt% solution of EC in acetone) were measured using a Krüss Drop Shape Analyser 10 (DSA) apparatus. Details of this apparatus are shown in experimental chapter 2.

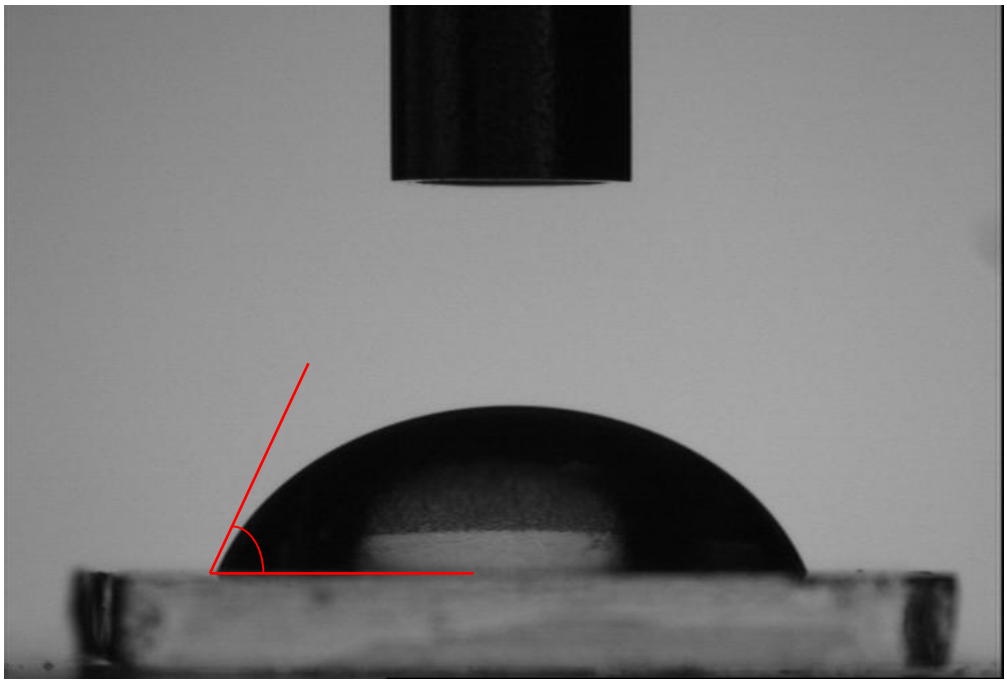

**Figure 4.24. Approximate contact angle (in air) of a sessile drop of Milli-Q water resting on a glass slide spin-coated with ethyl cellulose (from a 5 wt.% solution in acetone). The contact angle (measured from 3 separate images) was estimated to be 64 ± 0.7º.**

The three phase contact angle of a sessile water drop in air on an ethyl cellulose surface was estimated to be approximately 64 ± 0.7º which shows a moderate hydrophilicity of this material although less than shellac, on which water drops in air had a three phase contact angle of 58 ± 0.5º.

## 5.8. Conclusions

In this chapter, food grade micro-rods made from EC have been produced. By varying the fabrication parameters and the type of solvent used in the process, a degree of control over the resultant morphology of the EC micro-rods produced has been gained. By using tetrahydrofuran as a disperse phase solvent, long thin fibres of EC were produced. The use of ethanol lead to the formation of large flat ribbons, whereas when acetone was used as disperse phase solvent, EC micro-rods with lengths under 100 μm and diameters less than 5 μm were produced which demonstrated good foamability. The foamability of the micro-rods, together with the stability of the hand-shaken aqueous foams was evaluated, and foamability was enhanced with the addition of NaCl and separately, with lowered pH. It was found that once initial liquid drainage had taken place, foams could remain stable in a closed container for several weeks. The effect of added urea was also investigated, which showed that urea can destabilise the EC micro-rod stabilised foams.

Attempts were made to reduce the length of excessively long micro-rods by high shear mixing, but this was not successful. When another polymer was added to the disperse phase however (methyl cellulose), the micro-rod length was cut dramatically, indicating that this encourages micro-rod break-up during formation caused by methocel 'break-points' along the micro-rods, making them more brittle.

Another observation was the formation of EC structures of unusual morphology by introducing small aliquots of disperse phase solution at very low concentration to the continuous phase under high shear mixing, rather than under paddle stirring. These structures possessed hollow, limb-like extremities which it seemed would have been ideally suited to clogging the Gibbs-Plateau borders in foams, but unfortunately this could not be tested because of the low yields in which these particles were produced.

Finally the EC micro-rods were used as emulsion stabilisers and it was found that water-in-oil emulsions with large drops were formed, and that stability was better than would be expected for systems with such large drops. Emulsions were stable to coalescence for a number of days. Increasing the concentration of EC micro-rods used to stabilise the emulsions lead to a decrease in average drop diameter as should be expected. When a volatile oil (such as heptane) was used as the continuous phase in the emulsions, an interesting structure was formed upon evaporation of the oil, very much

like an aqueous foam in appearance. The polyhedral water drops remained separate for some time before complete evaporation of the water disperse phase, during which time the water could be liberated from the bulk structure by piercing using a fine edge. Emulsion drops displayed evidence of partial coalescence too, caused by the inability of the interface to reduce its surface area and also rearrange in shape (to spherical) because of the adsorbed layer of EC micro-rods. This is caused because the micro-rods are practically irreversibly adsorbed.

The emulsion drops were also dried in an attempt to produce hollow 'cages' formed from EC micro-rods. When analysed by scanning electron microscopy it was found that the cages were not able to withstand the drying and are with a flat appearance.

### 5.9. References


[1] R. Anton, S. Barlow, D. Boskou, L. Castle, R. Crebelli, W. Dekant, K-H. Engel, S. Forsythe, W. Grunow, J.-C. Larsen, C. Leclercq, W. Mennes, M-R. Milana, I. Rietjens, K. Svensson, P. Tobback, F. Toldra. *Eur. Food Standards Agency J.* 2004, **1.**

[2] R.G. Alargova, D.S. Warhadpande, V.N. Paunov, O.D. Velev. *Langmuir,* 2004, **20,** 10371.

[3] R.G. Alargova, K.H. Bhatt, V.N. Paunov, O.D.Velev, *Adv. Mater.,* 2004, **16,** 1653.

[4] V.N. Paunov, P.F. Noble, O.J. Cayre, R.G. Alargova, O.D.Velev. MRS Proceedings Fall 2004, volume 845, AA5.18.1-5.

[5] P.F. Noble, O.J. Cayre, R.G. Alargova, O.D.Velev, V.N. Paunov. *J. Am. Chem. Soc.,* 2004, **126,** 8092.

[6] R.G. Alargova, V.N. Paunov, O.D.Velev, *Langmuir,* 2006, **22,** 765.

[7] B.P. Binks, T.S. Horozov. In *Colloidal Particles at Liquid Interfaces,* Chapter 1, Cambridge University Press, 2006.

[8] US 002 381 972 14/08/1945.

[9] US 017 929 2A1 2/08/2007.

[10] In *Reigel's Handbook of Industrial Chemistry,* 10th Ed. Kluwer Academic/Plenum Publishers, New York, 2003.

[11] M.I. Beck, I. Tomka, E. Waysek. *Int. J. Pharm.,* 1996, **141,** 137.

[12] S. Indiran Pather, I. Russell, J.A. Syce, S.H. Neau. *Int. J. Pharm.,* 1998, **164,** 1.

[13] http://www.dow.com/dowexcipients/images/EthylcelluloseStructure

[14] X. Wu, L. Wang, H. Yu, Y. Huang. *J. Appl. Poly. Sci.* 2005, **97,** 1292.

[15] J. Doshi, D.H. Reneker. *J. Electrostat.*, 1995, **35,** 151.

[16] R.N. Wenzel. *Ind. Eng. Chem.*, 1936, ***28,*** 988.

[17] V.N. Paunov. *Langmuir*, 2003, **19,** 7970.

[18] O.J.Cayre, V.N. Paunov. *Langmuir*, 2004, **20,** 9594.

[19] S. Arditty, C.P. Whitby, B.P. Binks, V. Schmitt, F. Leal-Calderon. *Eur. Phys. J. E.*, 2003, **11,** 273.

# CHAPTER 6 – PROTEIN-BASED MICRO-RODS: PREPARATION, PROPERTIES AND CHARACTERISATION

This chapter considers zein as a potentially promising material for the production of edible micro-rods for food-grade foam formulations. Applying the same techniques of micro-rod production employed in this thesis, the effect of production conditions on the resultant micro-rods is discussed. The effect of application of ultrasound on the already formed micro-rods is presented. Studies on the foamability of zein are then carried out, and the effect of added electrolyte, urea and pH are investigated. Hybrid micro-rods containing both zein and shellac wax in different proportions are also produced, and their foamability assessed. We discuss the suitability of zein for micro-rod stabilised food foams and point out some suggestions for future directions.

## 6.1. History, structure, properties and uses of zein

Zein is a maize storage protein (or prolamine) and has been studied since the early nineteenth century. The first US patent for the extraction of zein was granted later on, in 1891 (Osborne), however this method, using 95% aqueous ethanol for extraction and gaining up to just 40% yield – a large improvement over previous laboratory methods which could yield around 5%, was not used in industry. Many other patents were granted in the following years but commercial extraction did not begin until well into the twentieth century. Zein production continued on a relatively large scale (>15 million pounds/yr over ten times the current amount) but demand dropped around the middle of the 20$^{th}$ century due to the significantly lower cost of synthetic polymers.[1] It is believed that one cause of this high cost was in fact the lack of demand and it is hoped that current renewed interest in the material may help to increase the demand and hence lower production costs to a more reasonable level.

Classified as ‘Generally Recognised As Safe’ (GRAS) by the FDA (like shellac), zein is commonly referred to as ‘confectioners glaze’, as it has been used to coat food products for a number of years. As such, a large number of studies have therefore been conducted on the properties of zein films[2-5] and on films formed from mixtures of zein and other materials such as starch[6] and ethyl cellulose.[7] Zein has also been used in the encapsulation of essential oils[8] and in the production of recycled paper.[9] Zein is a complex material. The structure of zein (alpha-zein, the most

predominant form) is considered to be formed from a collection of helical sections of amino acid residues forming an overall rod shape, with approximate aspect ratio 6-7:1 and molecular mass 19 or 22 kDa. This information is accompanied by a detailed analysis performed by Momany et al.[10] A further detailed study is presented by Cabra et al.[11]

Interest in zein has greatly increased in recent times due to the necessity for more environmentally-friendly materials. Zein could be used as a replacement for certain plastics due to its biodegradability. Previously, the principle factor holding zein production back was the relatively high processing cost, but in the modern economic climate with hydrocarbon-based products costing increasingly more, the merits of this protein-based material are being revisited with increasing frequency. Zein however does not provide a totally effective barrier to moisture, which limits its use as a film coating material for foods (unless they are to be dry-stored) but it may be improved by cross-linking with other materials.[12,13] For example Budi Santosa et al.[12] suggest that the water absorption of zein may be reduced by plasticizing with oleic acid. These shortfalls have also been addressed by coating of zein[14,15] and it is hoped that this could be further improved in the future.

### 6.2. Effect of solvent chemistry on the morphology of zein micro-rods

Due to the different surface groups present in zein molecules, they solubilise best in a mixed solvent comprising both hydrophilic and hydrophobic character. We found that zein dissolved well in a mixture of 10% water and 90% propan-1-ol (v/v). When this ratio was altered to 5 and 95 wt.% respectively, the zein could not be dissolved completely. To investigate the effect of water content on the properties of the micro-rods produced using the same technique employed in previous chapters, a series of solutions of zein in water/propan-1-ol were made, with the percentage of water varied from 10 to 50 wt.% and the concentration of zein at 28.6 wt.%. Micro-rods were produced by addition of the disperse phase (1 mL) to a continuous phase comprising glycerol (85%) and Milli-Q water (15%) by volume (50 mL, in a 250 mL beaker) under stirring from a Cole Parmer Digital Reversing Mixer (2,000 rpm, 10 min). The resulting suspension was washed with Milli-Q water by filtration (Whatman No. 1 filter paper,

large, pore size 11 µm). The micro-rods were examined by optical microscopy, to look for trends in size and/or morphology.

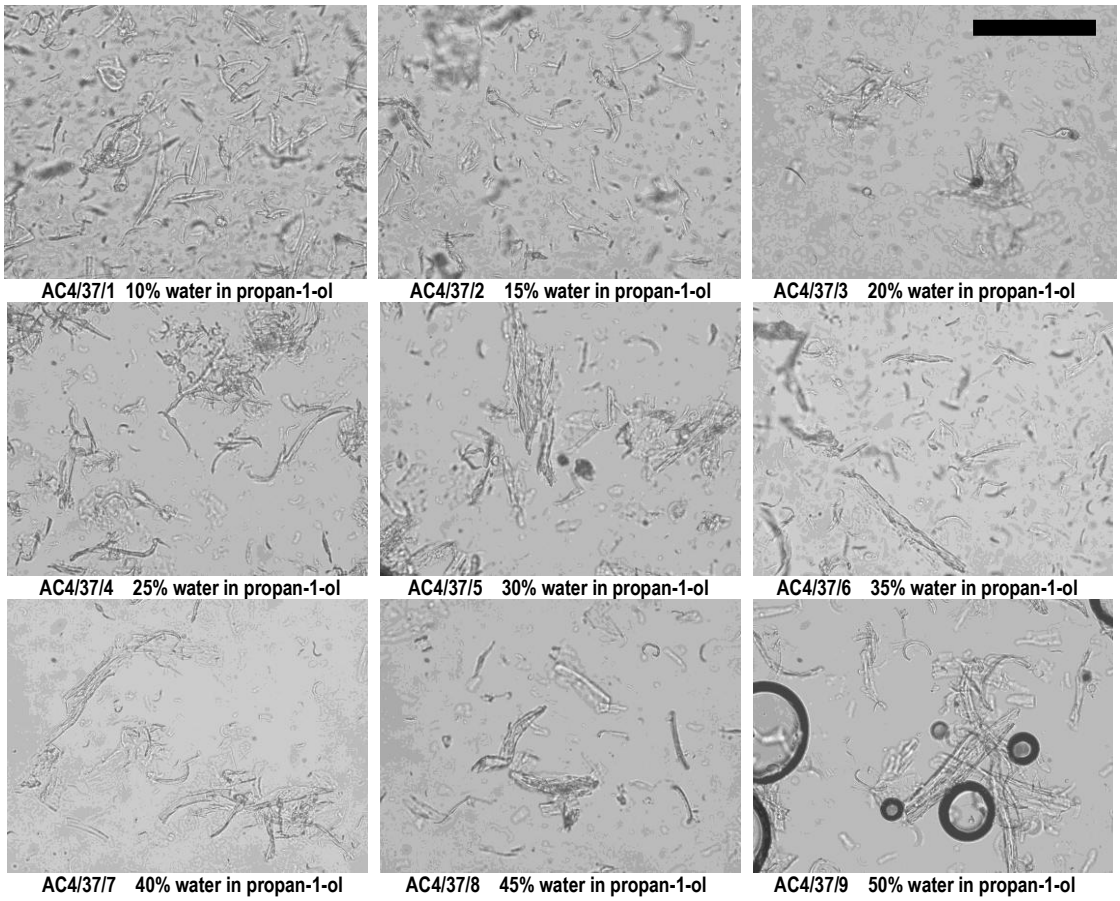


**Figure 6.1. Optical microscope images illustrating the effect of disperse phase water concentration on the morphology of the resultant zein micro-rods. Elevated water levels reduce the quality of the rods in the sample, with larger, less-uniform precipitated structures observed. Scale bar is 250 µm.**

Fig. 6.1 shows that the smallest and most rod-like zein particles are formed when the lowest concentration of water in the zein solution is used. In this case, 10% was found to be sufficient. As the concentration of water is increased towards 50%, the micro-rods become larger, and lose their rod-like shape. The reason for this is not fully understood.

### 6.3. Effect of stirrer speed on micro-rod properties

In previous chapters using shellac and ethyl cellulose we looked at the effect of the stirrer speed on the morphology of the resultant micro-rods. For shellac, a clear trend showing decreased micro-rod length with increased shear rate was observed, and this agreed with previous work (refer to chapter 4). A similar experiment was carried out using solutions of zein in propan-1-ol/water mixtures (10% vol. water) to produce zein micro-rods at different stirrer speeds. Zein concentration was 28.6 wt.%. Portions of disperse phase of 1 mL were added to the continuous phase (85% glycerol, 15% Milli-Q water (v/v) 50 mL) under stirring (500, 1,000, 1,500 and 2,000 rpm) for 10 min (Cole Parmer Digital Reversing Mixer) and the resultant micro-rods were washed with Milli-Q water by filtration before analysis by optical microscopy, and measurement of average micro-rod length. At least 50 micro-rods per optical micrograph were analysed to determine dimensions. Fig. 6.2 illustrates the result.

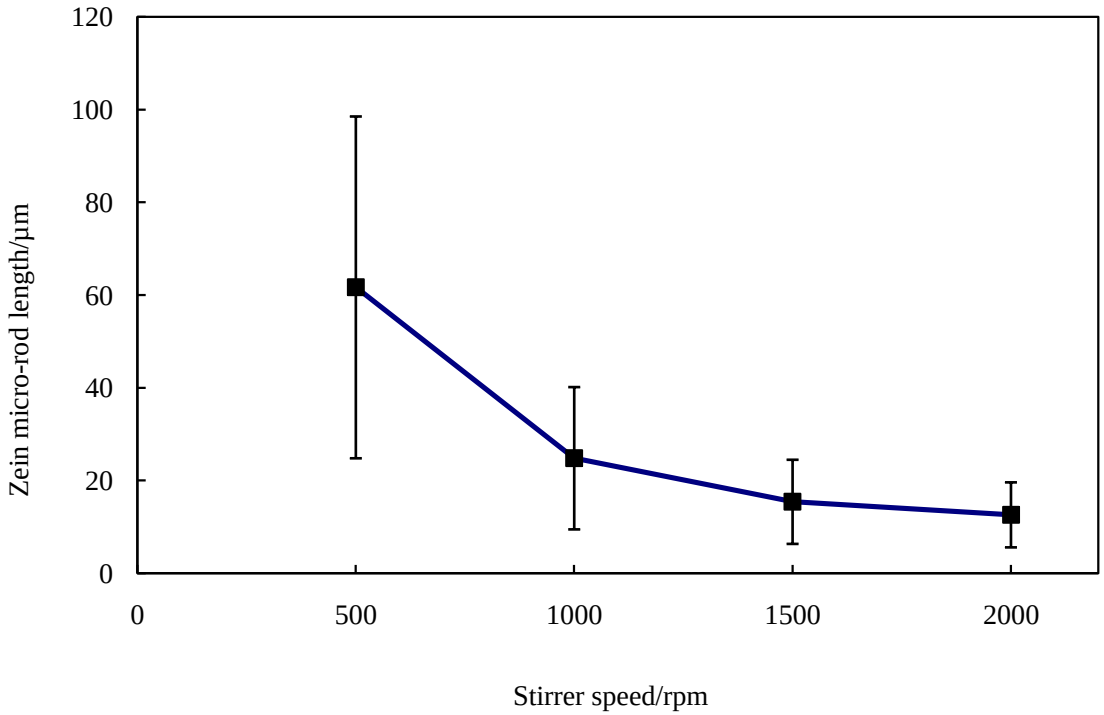


**Figure 6.2. Effect of stirrer speed on the length of zein micro-rods produced from 28.6 wt.% solutions in propan-1-ol/water (90:10). A clear negative trend in micro-rod length is observed with increased shear rate.**

In agreement with results obtained with similar micro-rods produced by a similar protocol made from shellac, a clear downward trend in the micro-rod length with increased stirrer speed (and hence shear) was observed, with some levelling off after 1,500 rpm stirring.

### 6.4. Effect of zein concentration in the disperse phase on the properties of zein micro-rods

Zein was found to be soluble up to at least 50 wt.% in 90% propan-1-ol/10% water (v/v) mixture, therefore a range of zein micro-rods were produced, made using solutions ranging from 2.5 wt.% up to approximately 50 wt.%, in order to investigate the effect of this parameter on micro-rod morphology. Zein micro-rods were produced as follows. The zein solutions were added in 1 mL aliquots to the continuous phase (85% glycerol/15% Milli-Q water mixture (v/v), 50 mL in 250 mL beaker) under stirring (2,000 rpm, 10 min) using a Cole Parmer Digital Reversing Mixer. Resultant micro-rods were washed in Milli-Q water by filtration to produce an aqueous suspension. Micro-rods were analysed using optical microscopy to observe qualitative effects of the varied disperse phase concentration. When low concentration zein disperse phases (2.5 – 20 wt.%) were used, the resultant micro-rod morphologies were poor. Large plate-like fibres were formed; similar to those produced from ethyl cellulose using an ethanol based disperse phase. Much of the resultant suspension contained particles of amorphous morphology. This agrees with results observed using shellac micro-rods, where amorphous particles were produced using lower concentration disperse phase solutions and appears to be due to the low viscosity of the solutions. Table 6.1 shows the effect of disperse phase zein concentration on the viscosity of the solution.

| [Zein]/wt.% | Viscosity/Pa s |
|---|---|
| 20 | 0.02 |
| 30 | 2.5 |
| 40 | 8.8 |
| 50 | 21 |

**Table 6.1. Viscosity of zein solutions at a range of concentrations in 90% propan-1-ol/10% Milli-Q water (v/v) at a constant shear rate of 12.7 $s^{-1}$. Viscosity of the continuous phase at the same shear rate was 0.029 Pa s.**

Theory of the liquid-liquid dispersion technique[16] states that the ratio of viscosities between the disperse and continuous phases is of key importance, and this is no different with zein solutions. 25 wt.% zein in a 90 % propan-1-ol/10% Milli-Q water (v/v) mixture gave improved morphology and uniformity in the resultant rods compared with those produced with lower wt.% zein solutions. Figs. 6.3a and b illustrate this.

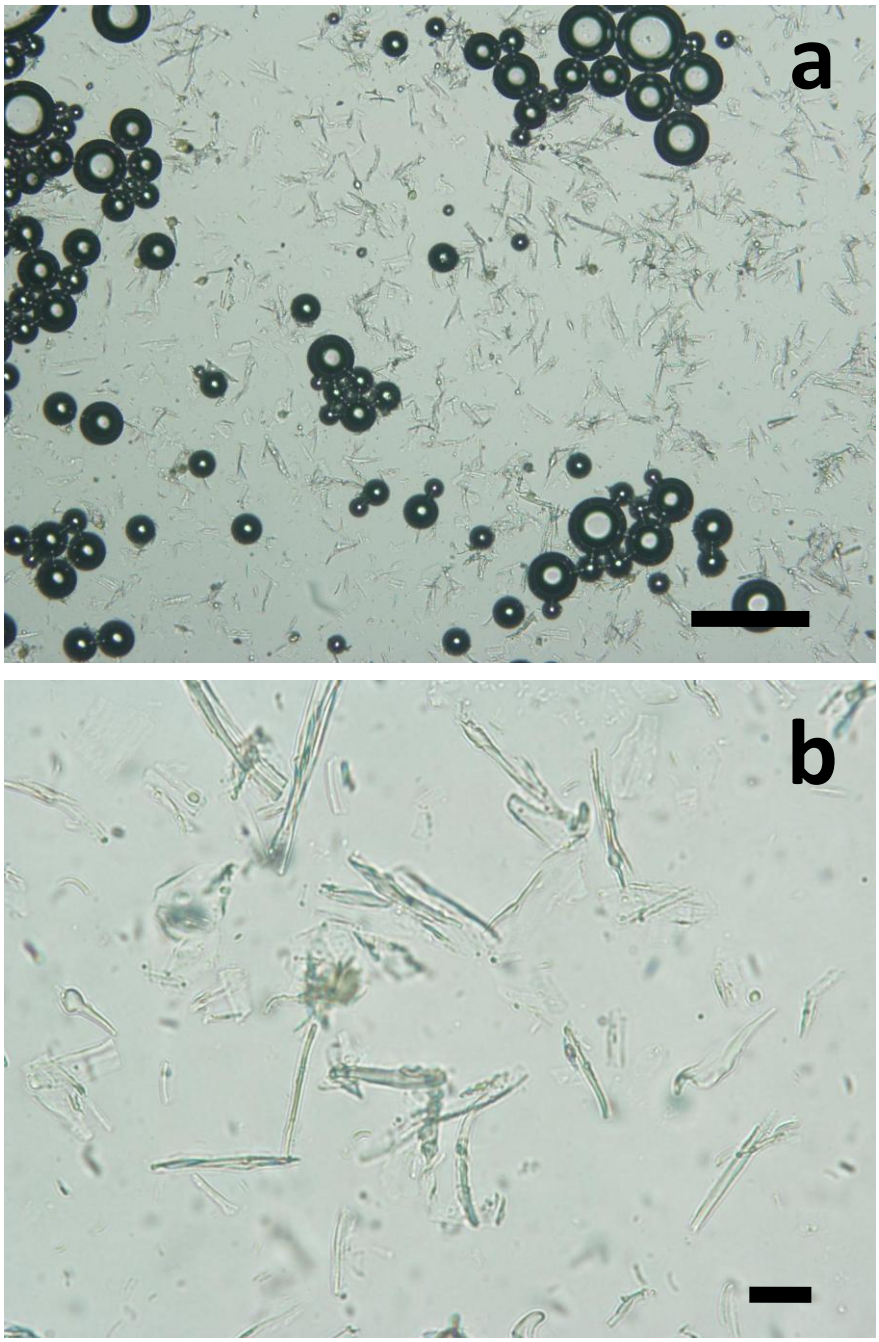


**Figure 6.3a & b. Optical microscopy images of zein micro-rods produced using solutions in water/propan-1-ol mixtures of intermediate viscosity, showing some improved morphology. Scale bars in a & b are 100 µm and 20 µm respectively.**

Figs. 6.3a & b illustrate that while resultant micro-particles have mainly micro-rod morphology using this zein solutions of intermediate viscosity although some particles still exhibit large, flat, ribbon-like morphology, and so higher viscosity solutions were employed. When 42 and 50 wt.% solutions of zein in 90% propan-1-ol/10% Milli-Q water mixtures (v/v) were used, improved results were obtained, despite the large disparity between the viscosities of the dispersed and continuous phases (figs.6.4a & b).

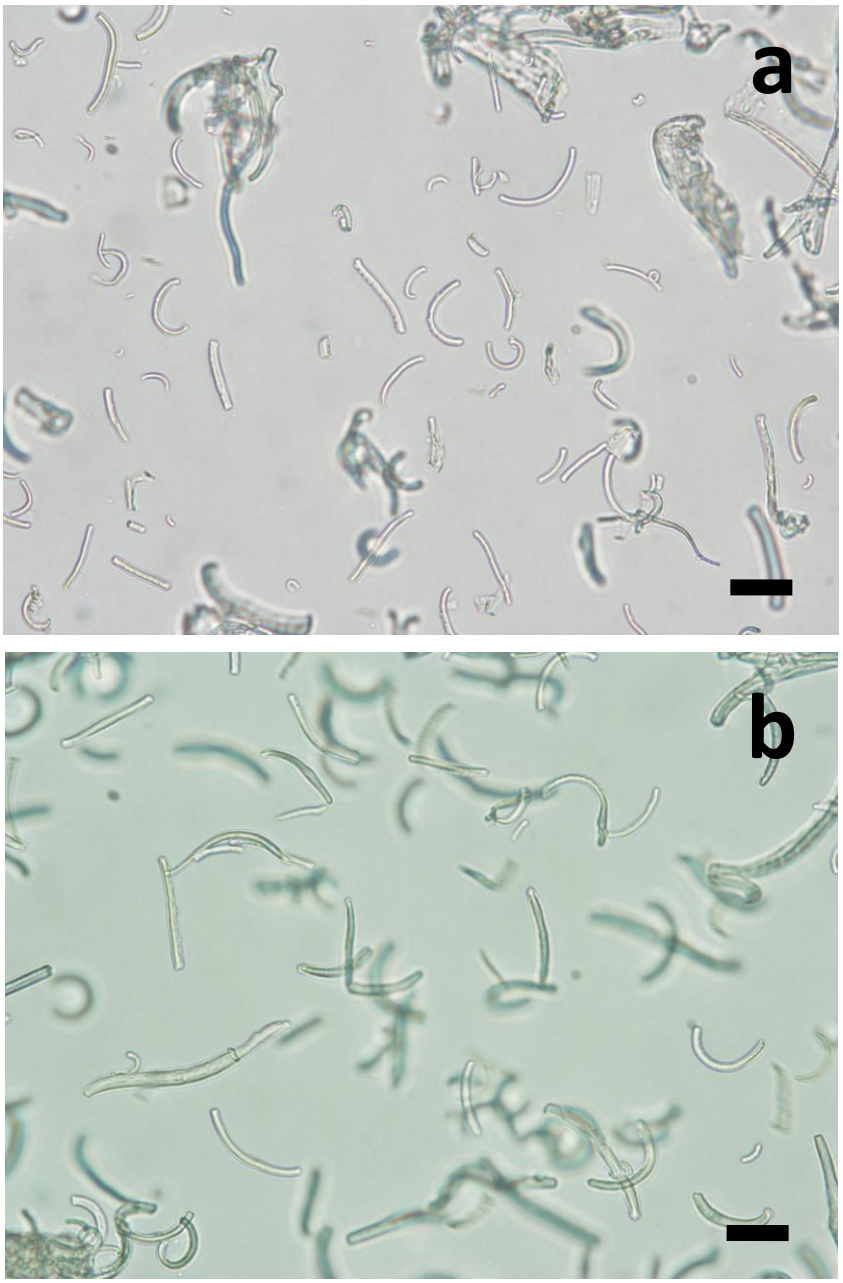


**Figure 6.4a & b. Optical microscopy images of zein micro-rods produced using 42 wt.% (a) and 50 wt.% (b) solutions in 90% propan-1-ol/10% Milli-Q water (v/v) mixtures. When the lower concentration solution is used, more amorphous material is produced (a). Scale bars are both 20 μm.**

Micro-rods appeared more cylindrical and regular, with fewer irregularly-shaped particles being produced. Even fewer amorphous, irregularly-shaped particles were observed using a 50 wt.% zein disperse phase as shown above. However, excessive zein loadings lead to solutions of high viscosity which are difficult to inject into the continuous phase.

### 6.5. Effect of ultrasound on zein micro-rods

Ultrasonic treatment is commonly used to disperse particles in suspension which display a tendency to aggregate due to attractive surface-to-surface interactions. In the case of zein and shellac wax, the particles which contact one another have a tendency to aggregate possibly due to formation of hydrogen bonds. For the suspensions of zein micro-rods, the effect of ultrasound on their integrity was investigated. A Branson Digital Sonifier 450 (400 W maximum output power) was used to apply the ultrasonic energy to suspensions of zein micro-rods. An aqueous suspension of zein micro-rods was produced from a 29 wt.% solution of zein in a 90% propan-1-ol/10% Milli-Q water (v/v) mixture. The suspension was divided into four equal samples, each placed in soda glass vials, and subjected to ultrasonic treatment for 90 seconds at 0% (control) 5, 10 and 15% intensity. No ice jacket was used as the intensity of ultrasound used did not heat the sample above 40 ºC. Fig. 6.5a-d illustrates the effects observed. The images above show that the modest levels of ultrasound used here were easily enough to destroy the morphology of the micro-rods.

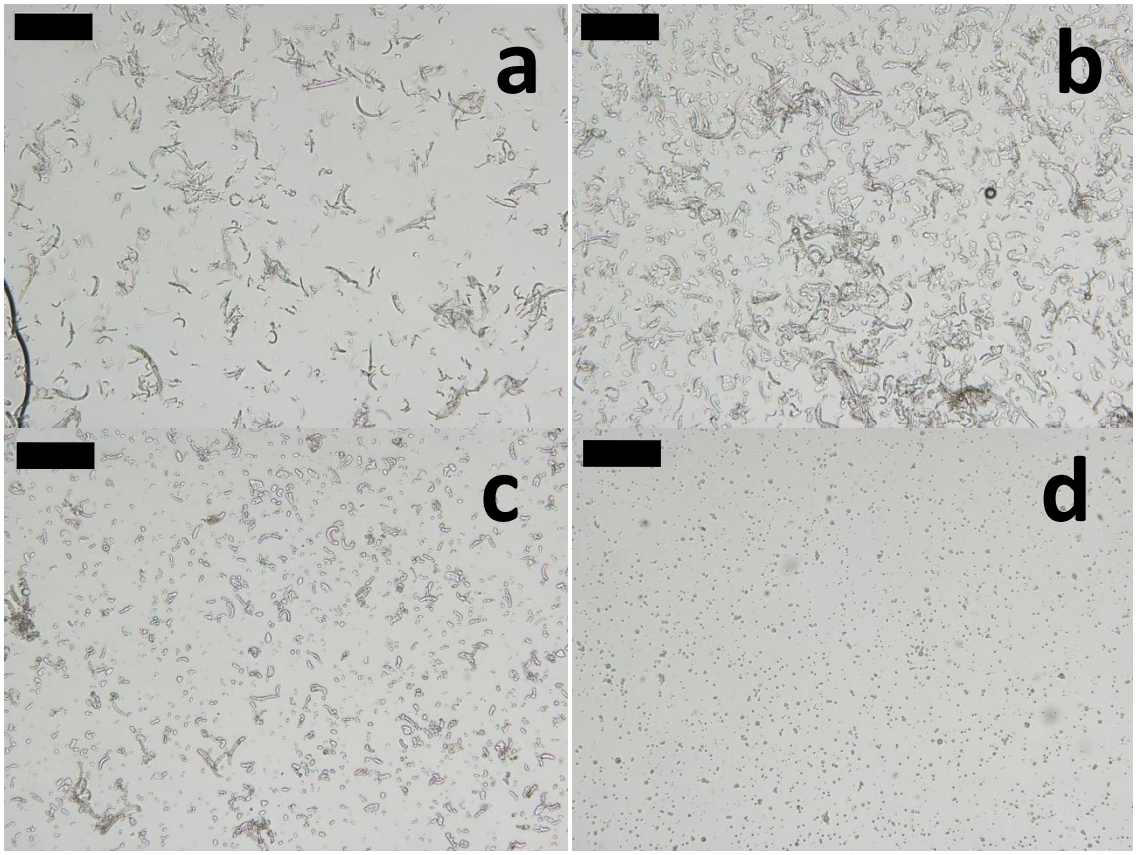


**Figure 6.5. Optical microscopy images to illustrate the effect of ultrasonic treatment on zein micro-rods. (a) shows the particles prior to the treatment, while the remaining images show the resulting particles after 90 seconds of exposure at 5% (b), 10% (c) and 15% intensity (d). The micro-rods are gradually reduced into smaller particles of much lower aspect ratio indicating that even ultrasonic treatment of relatively low power is extremely detrimental to the integrity of zein micro-rods. Scale bars are 50 µm.**

### 6.6. Foaming of zein micro-rods

The aim of this work is to ascertain the efficacy of these food-grade anisotropic micro-particles as foam stabilisers. Approximately 2 wt.% aqueous suspensions of zein micro-rods were used in foaming experiments. The protocol and conditions used in the foaming experiments are described in full in experimental chapter 2. Fig. 6.6 shows the foam height versus time for an aqueous foam stabilised by 1.95 wt.% zein micro-rods alone. It can be seen that in a similar manner to aqueous foams stabilised by shellac micro-rods, a reduction in the steepness of the foam height versus time curve is observed after initial liquid drainage from the foam has occurred. The following sections will describe the effects of additives on the foamability and foam stability of zein micro-rod-stabilised foams in more detail.

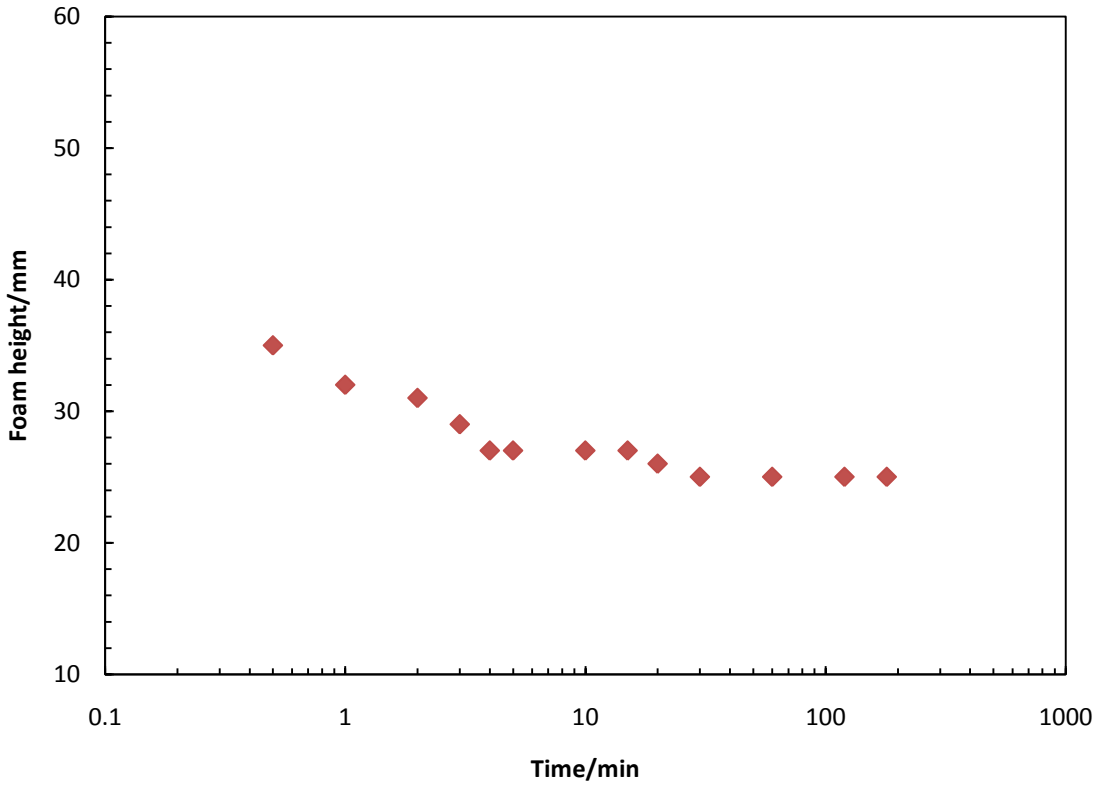


**Figure 6.6. Time evolution of foam height of aqueous foam stabilised by 1.95 wt.% zein micro-rods. The plateauing of the line indicates a reasonably stable foam being obtained once initial liquid drainage has occurred.**

### 6.6.1. Effect of added electrolyte

The effect of electrolyte on the foamability and foam stability of zein micro-rod-stabilised aqueous foams was investigated using sodium chloride as the background electrolyte. Foams were produced using 1.95 wt.% zein micro-rods suspended in Milli-Q water. The micro-rods used were produced from a 28.6 wt.% solution of zein in aqueous propan-1-ol (10% Milli-Q water) added to a continuous phase comprising 85% glycerol and 15% (by volume) Milli-Q water under stirring provided by a Cole Parmer Digital reversing mixer (2,000 rpm, 10 min) before being washed with Milli-Q water by filtration (Whatman No. 1 papers, pore size approximately 11 μm) several times to remove glycerol. NaCl was added to the aqueous suspension of zein micro-rods (10 mL in volume) at 0, 1, 2 and 3 M concentrations and foams were all produced by hand-shaking, with foam height being monitored over several hours. Fig. 6.7 shows that the presence of background electrolyte had no observable effect on foaming of zein micro-rod suspensions.

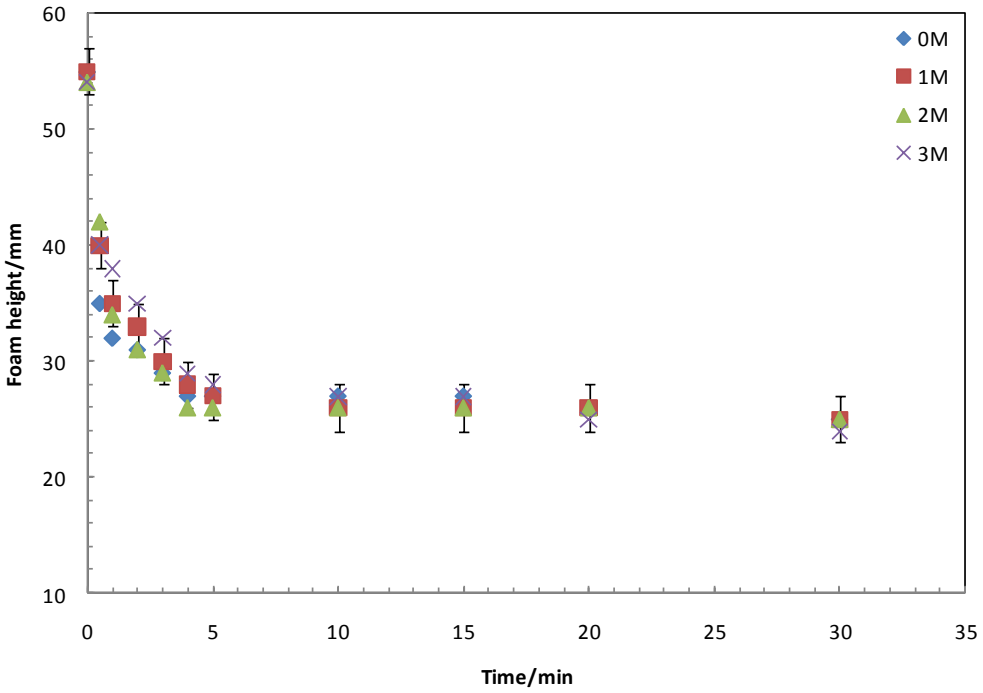


**Figure 6.7. Effect of concentration of NaCl on the foamability of zein micro-rod stabilised (1.95 wt.%) aqueous foams. It can be seen that after liquid drainage the decrease in foam height levels out. Error bars on the remaining sets of points have been omitted for clarity.**

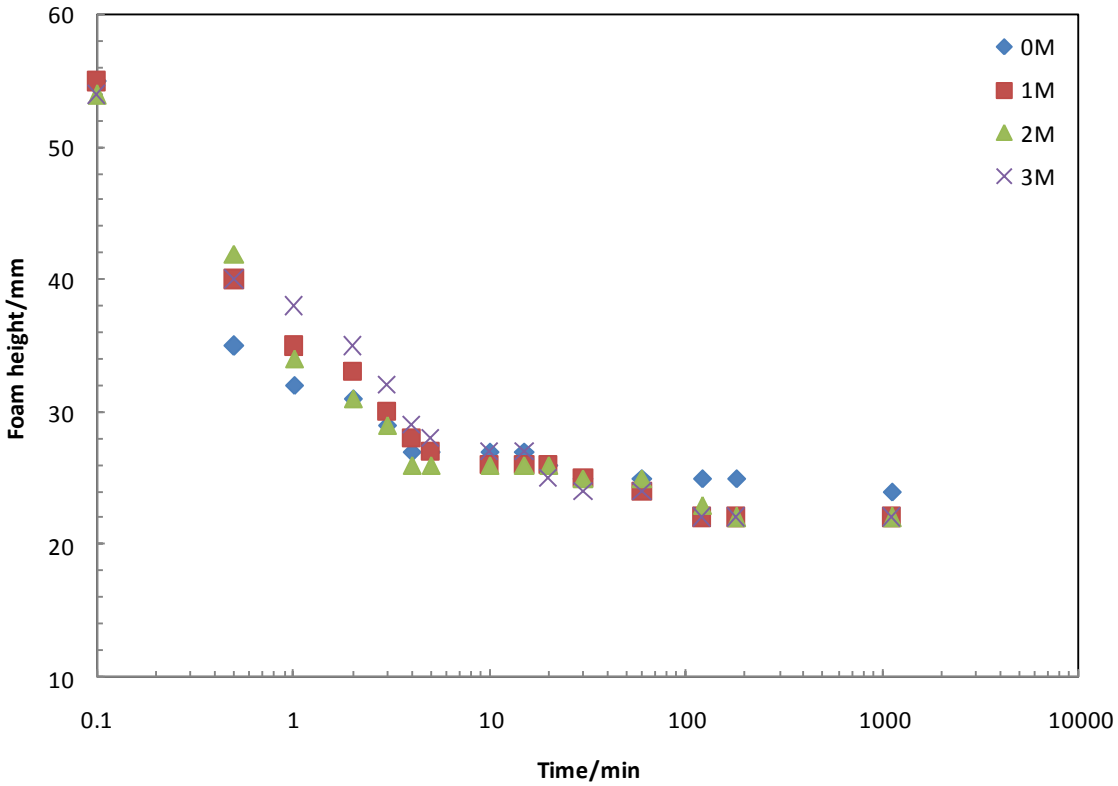


**Figure 6.8. Plot of foam height against time showing the effect of concentration of NaCl on the foamability of zein micro-rod stabilised (1.95 wt.%) aqueous foams. Expanding the initial few minutes of measurements shows that foamability in the first few minutes was improved marginally when NaCl was present.**

The change in foam height initially appears slightly slower for the foams containing greater amounts of NaCl, but all foams show levelling out behaviour, suggesting that once initial drainage has taken place, the foams are reasonably stable to bubble coalescence for several days.

The presence of sodium chloride in zein micro-rod-stabilised aqueous foams does not appear to give any noticeable improvement in foamability as it does with ethyl cellulose micro-rod-stabilised aqueous foams (previous chapter). Both materials are known to be partially hydrophilic (in the case of zein the author refers to the most prevalent form, α-zein, which is what commercial zein is considered to be), with three phase contact angles of sessile water drops on the surfaces of EC and zein of 64° and 58° respectively.

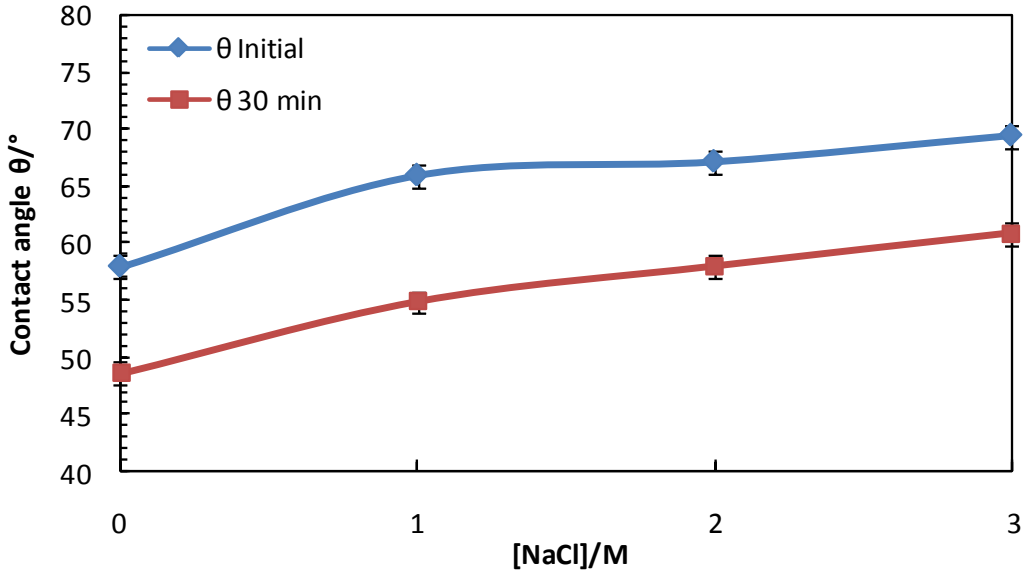


**Figure 6.9. Effect of NaCl molarity on the contact angle of sessile water drops on zein coated glass substrates initially and after 30 min.**

The effect of electrolyte concentration on the contact angle of NaCl containing sessile water drops on zein coated glass substrates was also investigated (fig. 6.9). It was found that higher salt concentrations gave rise to higher apparent contact angles.

In order to further improve the foamability of this system, the influence of pH was investigated.

6.6.1.1. Effect of added electrolyte with fixed pH

The concentration of NaCl in the aqueous phase was varied between 0 and 3 M and the pH was fixed at 7 (fig. 6.10) and then at 9 (fig. 6.11 in a separate experiment. When the pH was fixed at 7, a subtle increase in foamability and stability was observed with the inclusion of NaCl at 1 & 2 M. At a fixed pH of 9, the opposite was observed where optimum foamability and stability was recorded in the absence of electrolyte together with a steady decrease in foamability and stability with increasing NaCl concentration.

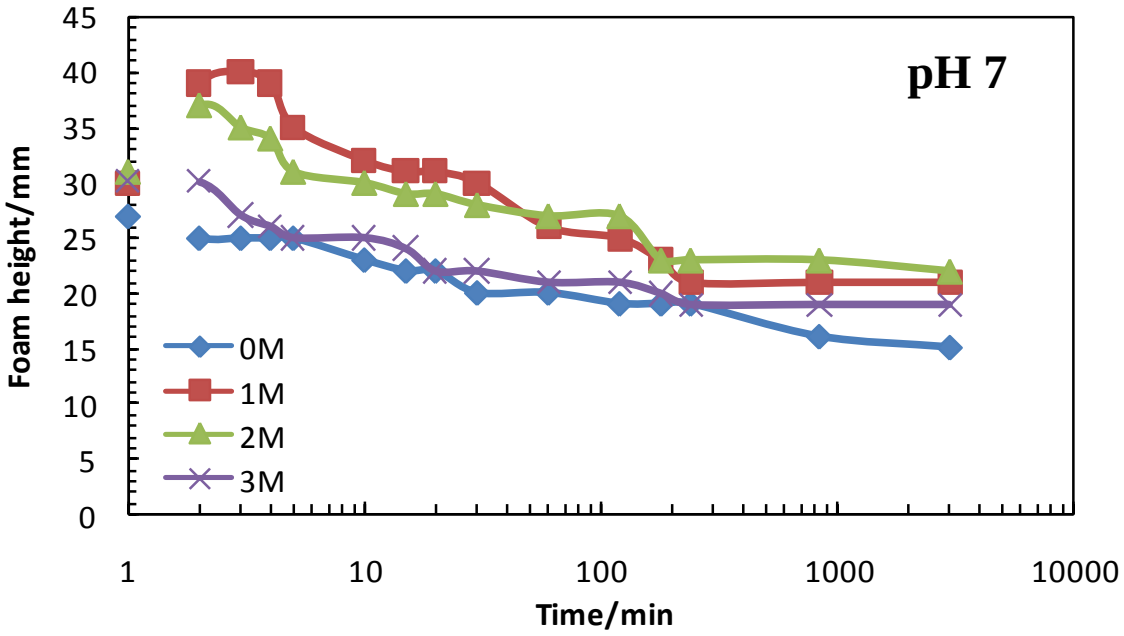


**Figure 6.10. Effect of NaCl concentration at a fixed pH of 7 on the foamability and stability of a 2 wt.% aqueous suspension of zein micro-rods.**

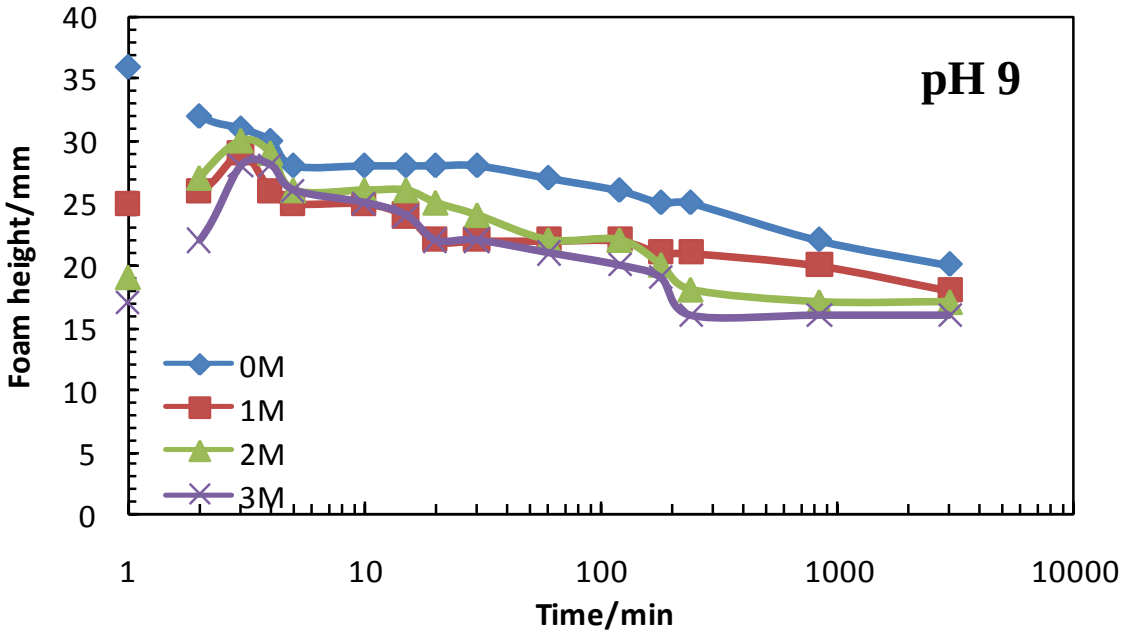


**Figure 6.11. Effect of NaCl concentration at a fixed pH of 9 on the foamability and stability of a 2 wt.% aqueous suspension of zein micro-rods.**

6.6.2. Effect of altered pH

The pH of the aqueous part of the foams was varied from pH 7 to 8.1 and 9.5 by addition of dilute KOH and subsequent checking of pH using a Fisherbrand Hydrus 400 pH probe and meter. No electrolyte was added to the foams. Fig. 6.12 shows a short term foam stability curve whilst fig. 6.13 shows a graph of foam height against time (longer term) giving an expanded view of the first stages of drainage allowing easier comparison to be made between the different samples. The isoelectric point of zein is around 6.8 and it can be seen that increasing the pH of the aqueous phase of the foams above this value led to a severe drop off in foam stability. Above the isoelectric point the surface groups of the constituent proteins will be quite negatively charged, and this is likely to have impeded micro-rod adsorption at the air-liquid interface. In this example, elevated pH gave a slight increase in foamability, but reduced stability.

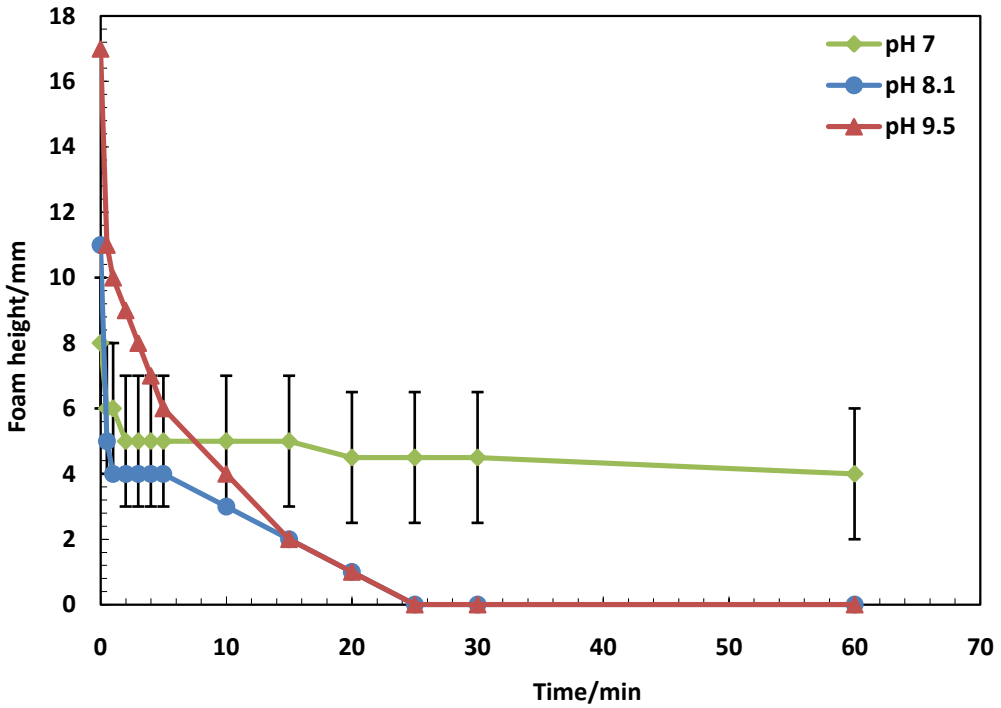


**Figure 6.12. Effect of pH of the aqueous phase on the foamability of zein micro-rod-stabilised (1.95 wt.%) aqueous foams. In this example, elevated pH gives a slight increase in foamability, but reduced stability. Error bars represent the uncertainty in estimating the diameter of a bubble of maximum size which has coarsened over time. Error bars on the remaining sets of points have been omitted for clarity.**

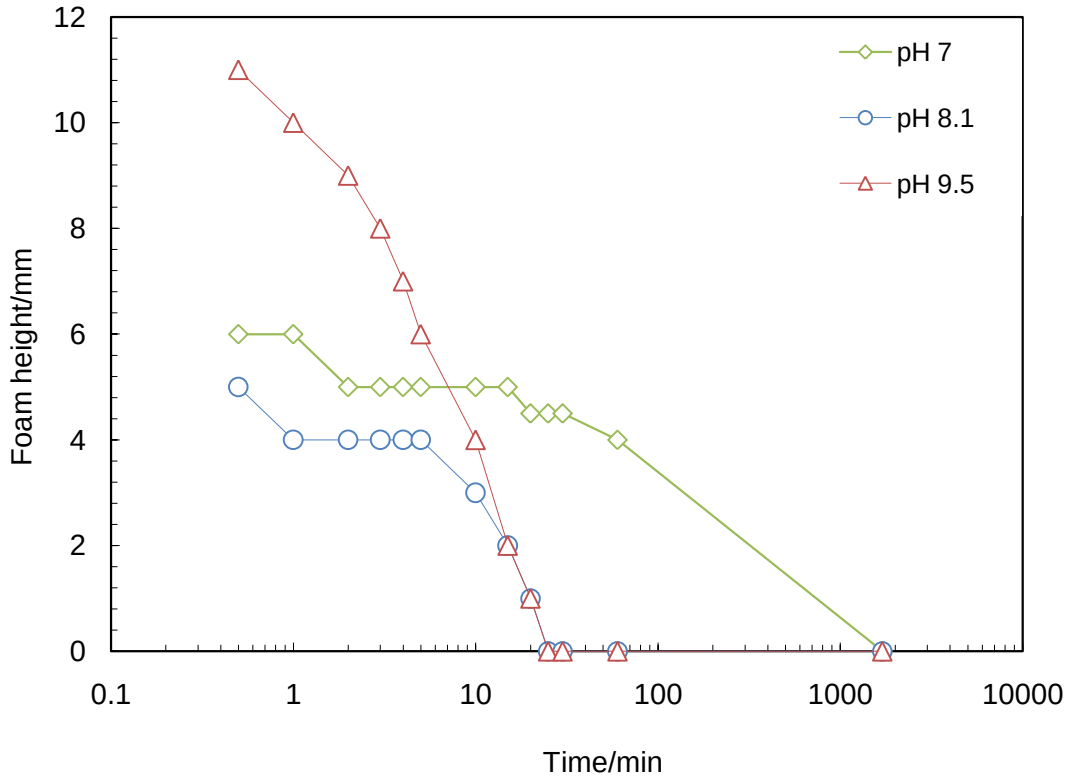


**Figure 6.13. Plot of foam height against time showing the effect of varied pH on the foamability of zein micro-rod stabilised (1.95 wt.%) aqueous foams. Expanding the initial few minutes of measurements shows the increased foamability of the higher pH samples, and also the rapid reduction in foam height due to their poor stability. Around the pH of the isoelectric point of zein, the pH 7 sample gave the greatest stability.**

The stability of these aqueous foams is relatively poor, suggesting the necessity for further investigation into improvement of the performance of these food-grade hydrophobic micro-rods. The effect of pH on the contact angle of sessile water drops on zein coated glass substrates was also investigated. It was found that slightly higher apparent contact angles were observed at pH 7 and 9 than at lower pH, as shown in fig. 6.14, however, the differences are marginal.

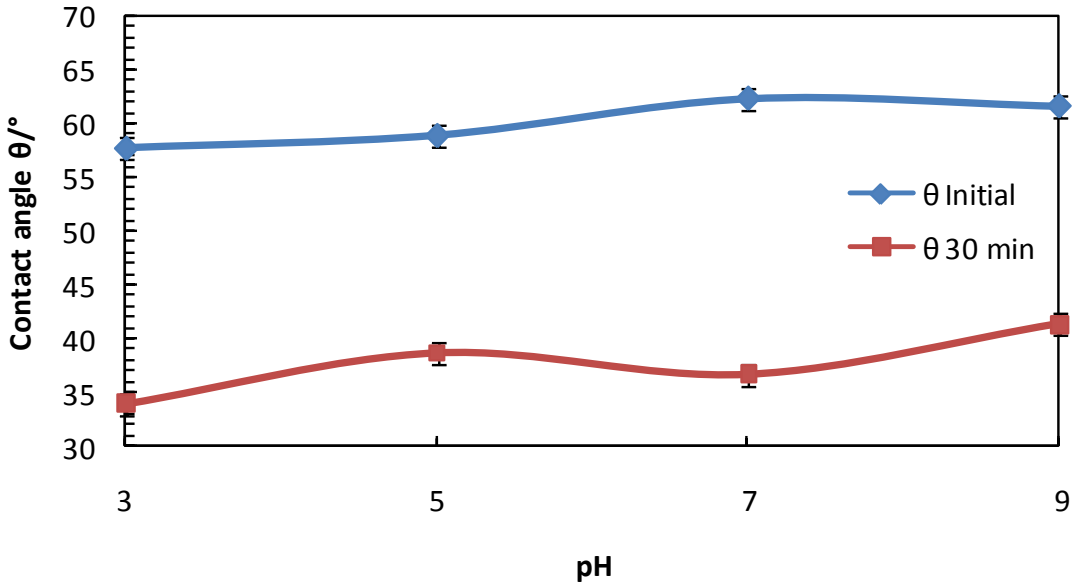


**Figure 6.14. Effect of pH on the contact angle of sessile water drops on zein coated glass substrates initially and after 30 min.**

6.6.3. Effect of added urea

Urea is a so-called chaotropic agent, expected to disrupt hydrogen bonding present in the zein proteins; possibly causing destruction of the micro-rods formed, but more likely reducing the level of micro-rod inter-weaving at the interface where hydrogen bonds may contribute to steric stabilisation of the foam. This may depend on the concentration of urea used. The urea is also likely to disrupt the hydrogen bonding which occurs in the structured water region around the interface of the water and the hydrophobic surface of the zein micro-rods. Micro-rods and foams were produced using the same protocols used before (2 wt.% zein micro-rods), with two foams being produced by hand-shaking, one with 2 M urea in the aqueous portion and the other with 8 M urea. The foam height with time of the two samples was monitored over several hours and this is shown in fig. 6.15. At the highest concentration of urea, the foam exhibited superior initial foamability, but poorer long-term stability. Microscopic observation revealed that the size of the micro-rods had been reduced, leaving much smaller fragments of zein behind, which did not give good foam stability over time periods greater than 1 hour. It appears that the high concentration of urea caused the zein micro-rods to be broken down (urea displays chaotropic behaviour at high concentrations, > 6 – 8 M). The

resultant smaller particles would have given the increased initial foamability together with the poorer long term stability (compared with zein *micro-rod*-stabilised foams).

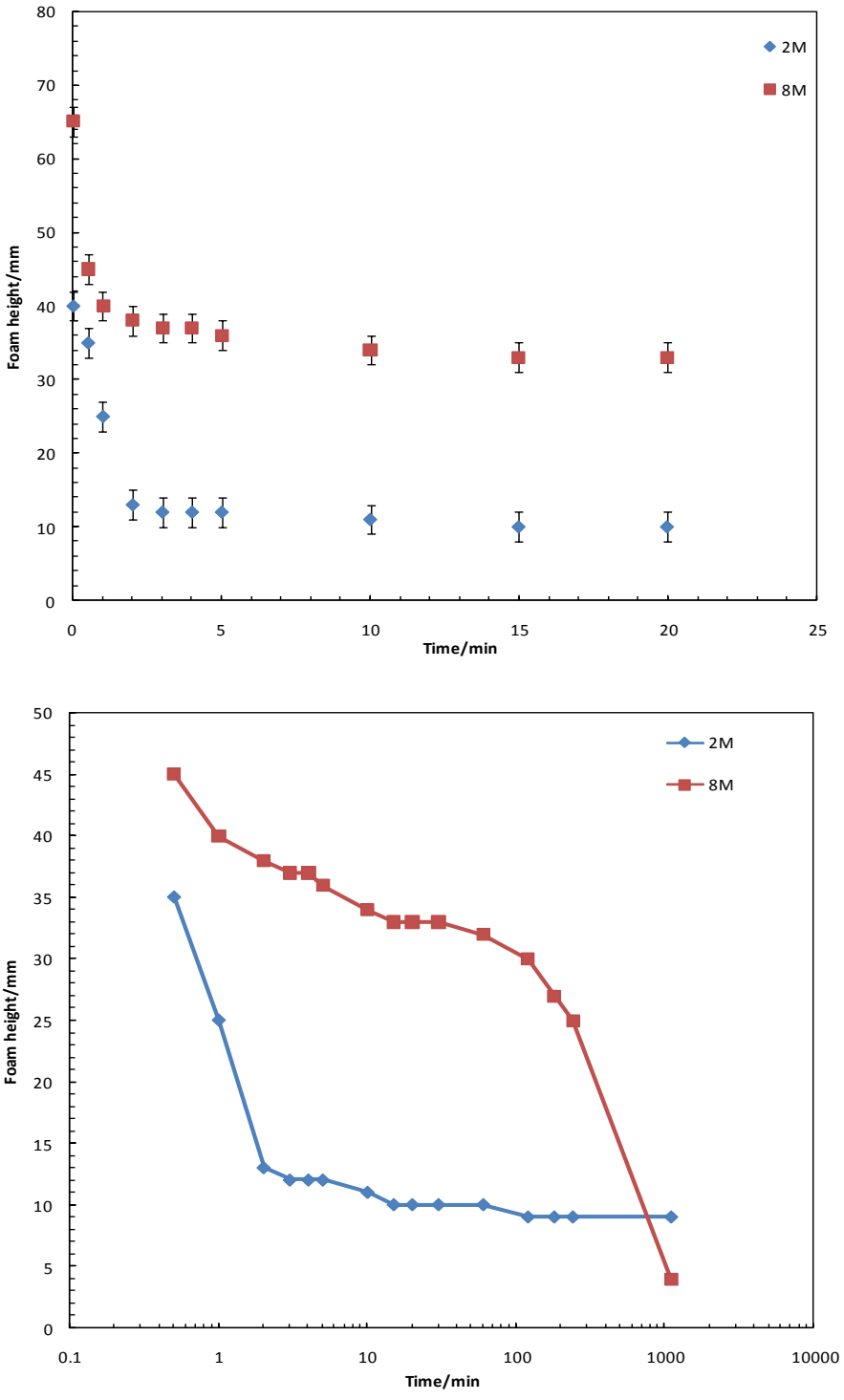


**Figure 6.15. Effect of added urea on the foamability and stability of aqueous foams stabilised by 2 wt.% zein micro-rods. Despite initial improved foamability, the foam containing 8 M urea is destabilised.**

### 6.7. Hybrid zein-shellac micro-rods

In order to improve the foamability of zein micro-rods, it was decided to combine the zein with another material, shellac wax to form a hybrid micro-rod formulation. Previously investigated, shellac wax was found to exhibit surface active properties, together with better foam stability than zein micro-rods. The disadvantage of using shellac however is the aggregation of the resultant micro-rods. During the purifying process before the foam formation, micro-rod aggregation is pronounced, and can lead to the adsorption of large aggregates, rather than individual micro-rods. It is anticipated that combination of the two materials may improve the foamability and stabilising performance of zein micro-rods without producing aggregating micro-rods.

Hybrid zein-shellac micro-rods were produced by injecting mixed disperse phases into the continuous phase under high speed shearing. The disperse phases (typically 50 wt.% shellac in ethanol and 28.6 wt.% zein in 90:10 propan-1-ol/water) were mixed in small quantities directly before addition to the continuous phase to ensure homogeneous mixture. The remaining preparation conditions were identical to those used in the production of pure zein micro-rods.

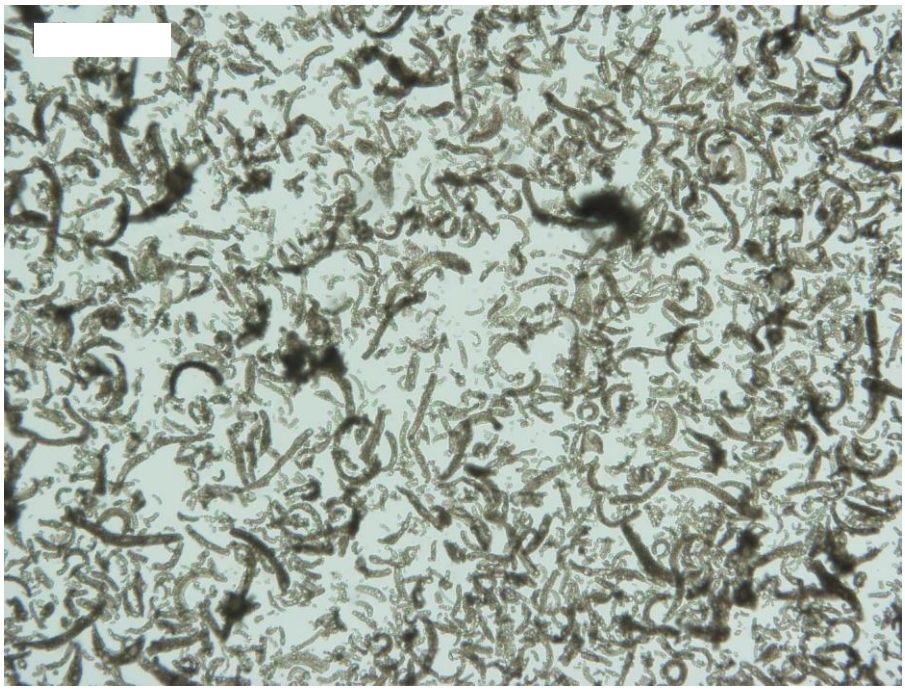

**Figure 6.16. Optical microscopy image of hybrid zein shellac micro-rods. The aspect ratios of these micro-rods are smaller than those composed of either pure shellac or pure zein. Scale bar is 200 µm.**

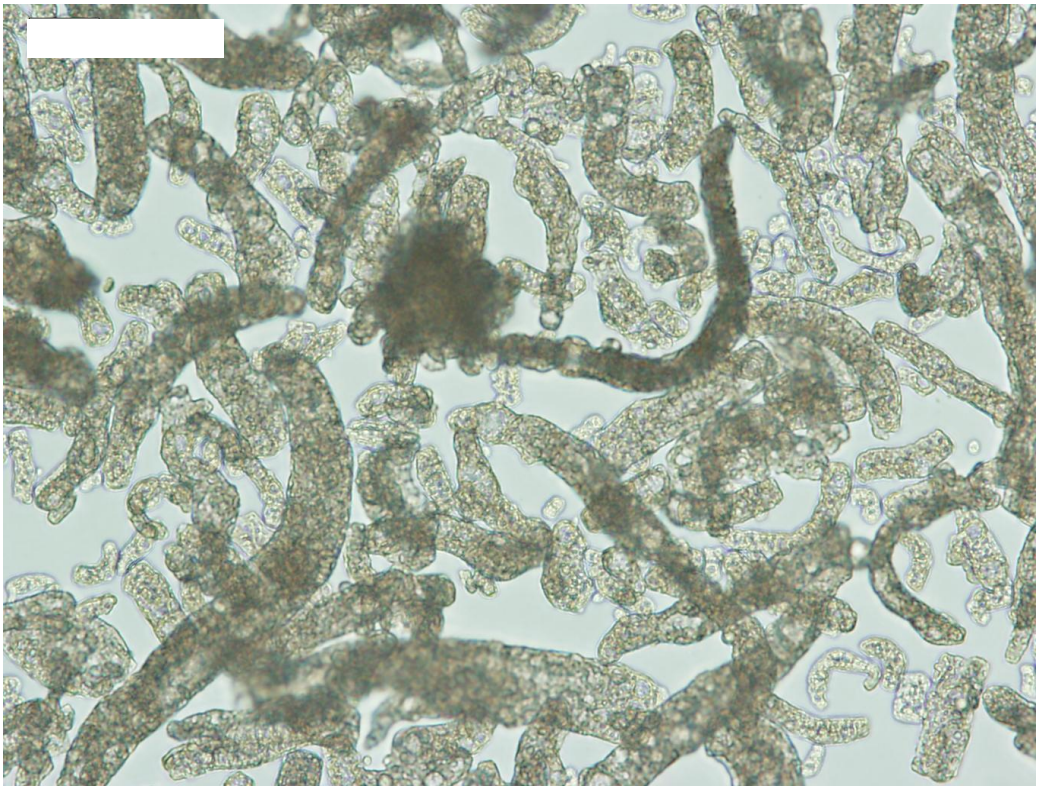

**Figure 6.17. Optical microscopy image of hybrid zein shellac micro-rods. It is apparent that the micro-rods are quite broad (up to 20 µm) in diameter and irregular in shape. Scale bar is 50 µm.**

### 6.7.1. Effect of pH and polymer ratio on foamability of hybrid micro-rods

The effect of pH has been shown to make noticeable changes to the foaming performance of zein micro-rod-stabilised aqueous foams and so this is investigated below, in conjunction with the effect of altering the ratio of the two polymers present. In order to assess the effects of the full range of ratios of the two materials, it was hoped to produce mixtures of shellac and zein ranging from 10:90 to 90:10 (proportions by weight), however, for most of these combinations, the micro-rods produced aggregated too much, and could not be re-dispersed once purified in Milli-Q water. The two most viable mixtures were the 80% and 90% zein (20% and 10% shellac respectively) (w/w) samples. Hybrid micro-rods were produced using these mixtures and the resultant micro-rods tested at a range of pH values to examine the effect of this on foamability. Figs. 6.18 and 6.19 illustrate the foam height vs. time at low, intermediate and high pH of 90% zein and 80% zein (w/w) micro-rods respectively.

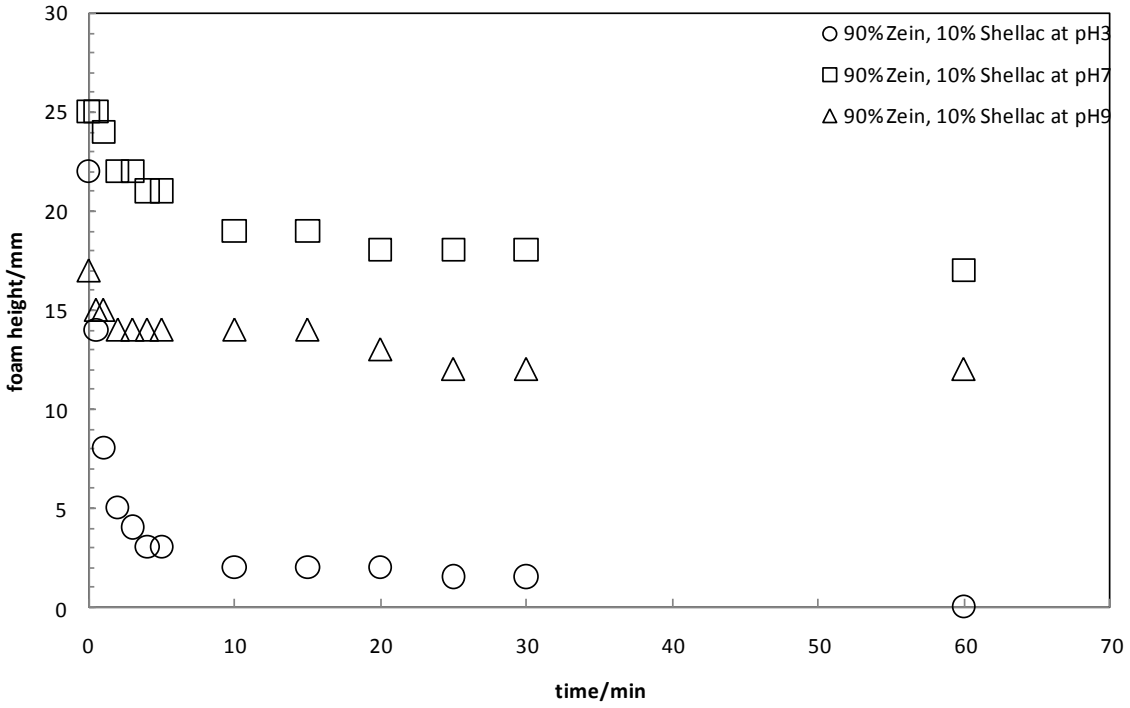


**Figure 6.18. Foam height of hybrid micro-rods containing 90% zein and 10% shellac (w/w) measured over 1 hour at low, intermediate and high pH.**

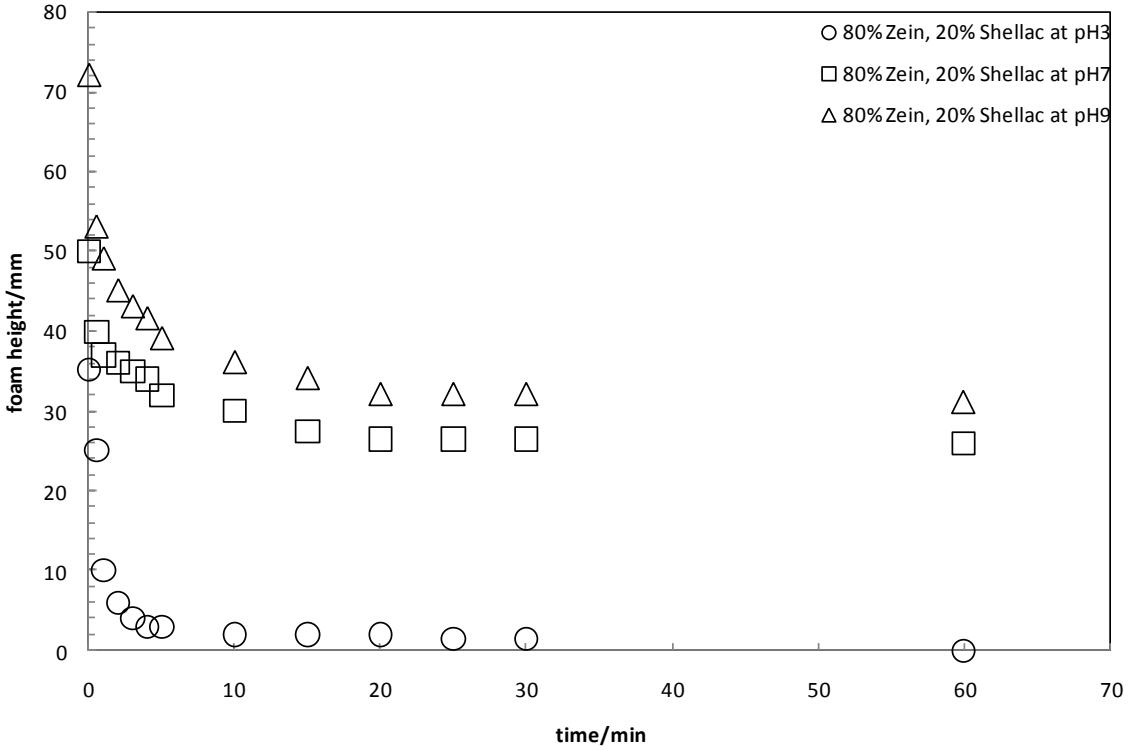


**Figure 6.19. Foam height of hybrid micro-rods containing 80% zein and 20% shellac (w/w) measured over 1 hour at low, intermediate and high pH.**

Fig. 6.20 combines the two different polymer ratios displaying the comparative performance of all samples. It clarifies that foamability and foam stability were both poor at pH 3, and it also shows that hybrid micro-rods containing a higher shellac concentration gave superior foaming performance than those with the lowest shellac content.

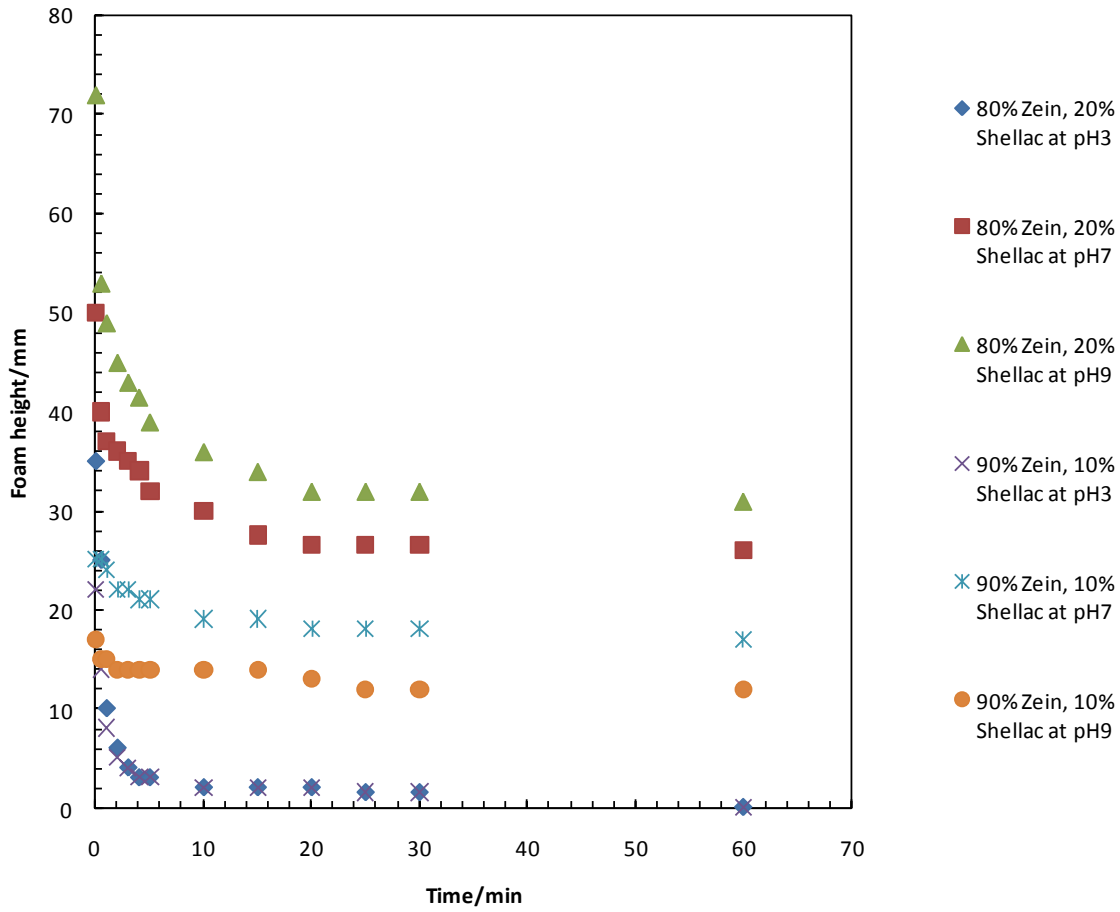


**Figure 6.20. Foam height of hybrid micro-rods containing 80% and 90% zein and 20% and 10% shellac (w/w) respectively measured over 1 hour at low, intermediate and high pH.**

The greatest zein-shellac synergy was observed at pH 7 and 9 at 80 wt.% zein. Here, both the foamability and foam stability is increased. However, if the cylinders containing the foams were disturbed, it was noted that zein micro-rods fell from the bottom of the foams, to the base of the tube, indicating that they do not adhere to one another as strongly as shellac micro-rods, but also that they do not display as much buoyancy either.

## 6.8. Zein micro-rods captured at the air-water interface by the gel trapping technique

We attempted to estimate the contact angles of zein micro-rods at the air-water interface using the gel trapping technique.[17] The process is described in more detail in chapter 4, together with schematic diagrams. Here, zein micro-rods were trapped at the air-water interface by spreading (as an aqueous suspension) with a pipette. The aqueous phase (containing 2 wt.% gellan, a gelling hydrocolloid) was then gelled by cooling to room temperature. The PDMS/curing agent mixture was then poured on top of the gelled aqueous phase, and this layer was also allowed to set. Once solid, the PDMS layer was peeled off, washed in high pH Milli-Q water (pH raised to 9 using KOH) and examined by SEM taking care not to expose the samples to dust, as the PDMS resin is very sticky, and can trap many airborne contaminants, affecting microscopic viewing. Figs. 6.21 to 6.23 show the adsorbed zein micro-rods which appear to have significant surface roughness. The solid PDMS base represents what would have previously been the air phase, and considering that the rods seem predominantly to rest out of the PDMS, this seems to suggest that they are relatively hydrophilic in character. This may however (as in the case of shellac micro-rods which were treated in an identical manner) be partly due to the spreading media used to disperse the rods at the interface. In the literature, particles studied by the GTT are spread using a so-called ‘spreading solvent’ such as isopropanol. As the food grade micro-rods produced in this work show partial solubility in solvents such as these however, it was chosen to spread the micro-rods using water. This may have affected the success of the spreading of the micro-rods at the interface.

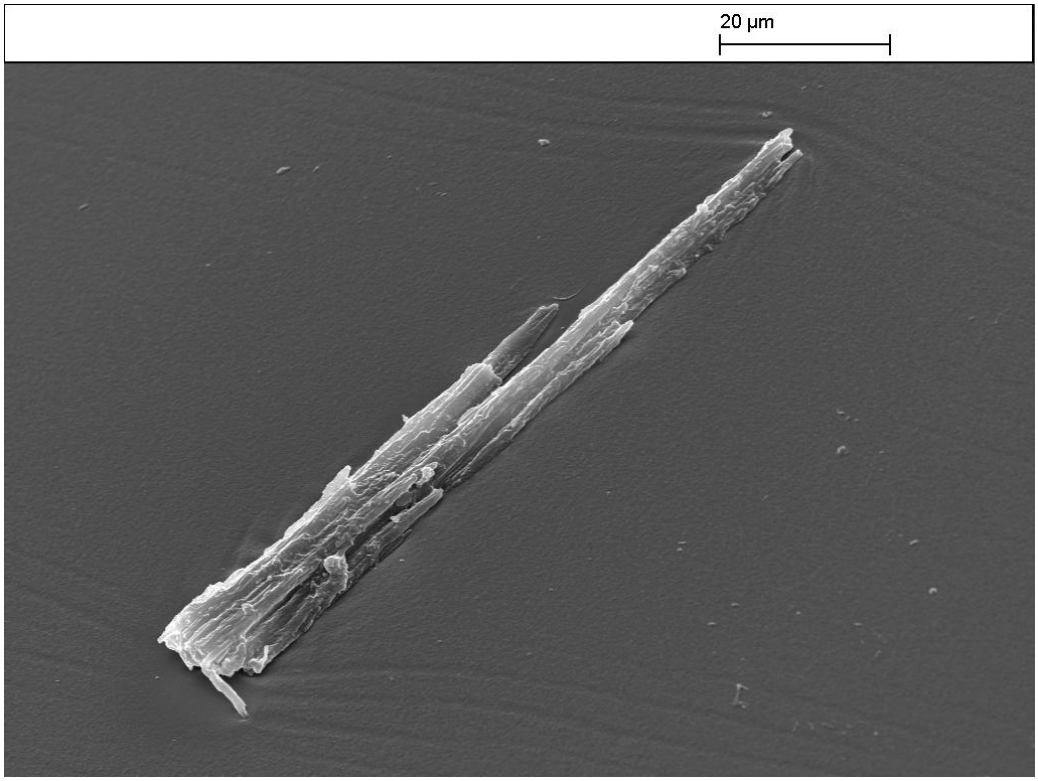


**Figure 6.21. SEM image of a zein micro-rod captured at the air-liquid interface by the GTT. The appearance of this micro-rod suggests that it may be formed from smaller and narrower aggregated micro-rods.**

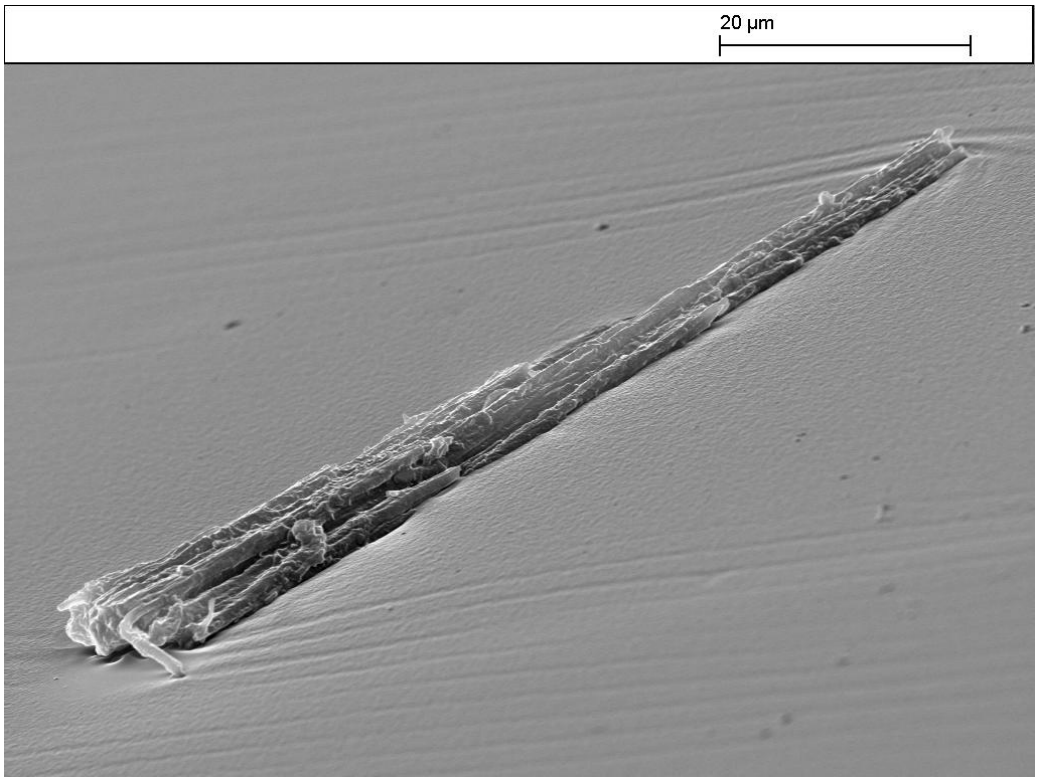


**Figure 6.22. SEM image of a zein micro-rod captured at the air-liquid interface by the GTT. The micro-rod is captured from a shallower viewing angle in this image.**

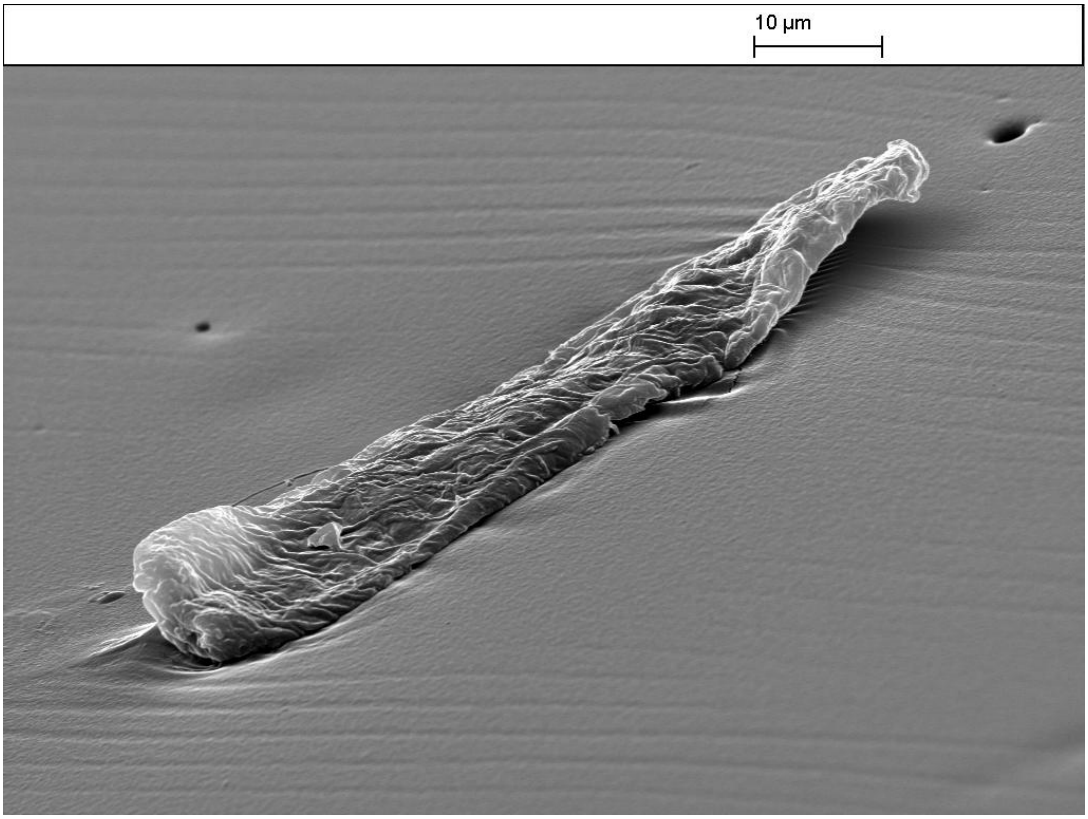


**Figure 6.23. SEM image of a zein micro-rod embedded in the PDMS surface. Notice the surface texture of zein micro-rods compared to the relatively smooth shellac micro-rods described in chapter 4.**

## 6.9. Conclusions

In this chapter, the technology used so far in the production of food-grade anisotropic micro particles has been extended to produce micro-rods from the maize prolamine zein. The effects of the production parameters were investigated, and an optimized protocol was developed, using a similar continuous phase to that used previously, but with different disperse phase composition. It was found that zein dissolved well in aqueous mixtures of ethanol, propan-1-ol and isopropanol (all containing 10% by volume Milli-Q water). Following the production of viscous solutions of zein, the resultant micro-rods were examined, and it was found that micro-rods with the most uniform shape and size were formed when 90% propan-1-ol/10% Milli-Q water (v/v) mixture was used as the disperse phase solvent. As with ethyl cellulose and especially shellac, poorer micro-rods were obtained when disperse phase solutions of lower zein content (and therefore lower viscosity) were employed. The effect of the water

concentration in the disperse phase was also investigated. It was found that increasing the water concentration further above the minimum required for adequate zein solubility led to the formation of particles of amorphous morphology, increased size and increased polydispersity. Since all of these characteristics are not desirable, it was decided to maintain the lowest water content in the disperse phase for production of zein micro-rods.

Increased shearing speed (and hence shear rate) during micro-rod formation decreased the micro-rod lengths and their polydispersity. The foamability of zein micro-rods was also assessed, in the presence of additives such as electrolyte, urea and HCl/KOH/NaOH (to alter pH). Pure zein micro-rods (in a pH-neutral aqueous suspension at 1.95 wt.%) gave reasonably poor foamability, and foams collapsed after only 10 min in closed containers on the bench. Foamability and foam stability was not affected noticeably by the addition of NaCl up to 3 M in concentration. Increasing the pH of the aqueous phase lead to increased initial foamability of zein micro-rods but with reduced stability compared with pH 7 foams (around the isoelectric point of zein). When NaCl concentration was varied with fixed pH at 7 and then 9, at pH 7, a subtle increase in foamability and stability was observed with the inclusion of NaCl while at pH 9, the opposite was observed where optimum foamability and stability was recorded in the absence of electrolyte.

The effect of added urea at a concentration of 2 M did not improve foam stability or foamability of 2 wt.% aqueous suspensions of zein micro-rods. When 8 M urea was added, this led to improved initial foamability but reduced stability. This was caused by the chaotropic action of urea at high concentration breaking down the zein micro-rods into smaller particles. The smaller zein particles gave enhanced short-term foamability but poor long-term foam stability.

Foamability of zein micro-rods was improved by incorporation of an additional food grade material – shellac. Hybrid micro-rods were produced which contained up to 20 wt.% shellac to increase their surface-activity without increasing their aggregation and foamability was improved above that shown by pure zein micro-rods. It was found that the best foamability was exhibited by the rods with the highest shellac concentration (constrained to 20 wt.% due to problems with aggregation – discussed) and at higher pH values (9).

The effects of pH and NaCl concentration on the three phase contact angles of sessile water drops on zein-coated glass substrates was also investigated. It was found

that the presence of electrolyte increased the apparent contact angle, while for varied pH the highest contact angles were also achieved at higher pH (7 and 9).

Zein micro-rods were also trapped at the air-liquid interface by the gel trapping technique, and analyzed by scanning electron microscopy. Their surfaces were shown to be considerably rougher than shellac micro-rods (chapter 4).

Overall, we have shown that zein micro-rods of controllable size may be produced using an in-shear-flow dispersion solvent attrition technique, which could have the potential to be used as food grade additives for foam formulations, whether pure, or with shellac wax in the case of hybrid fibres with further improved foaming performance.

## 6.10. References


[1] J.W. Lawton, *Cereal Chem.*, 2002, **79,** 1.

[2] M.A. Del Nobile, A. Conte, A.L. Incoronato, A. Panza, *J. Food Eng.*, 2008, **89,** 57.

[3] Y. Wang, G.W. Padua, *J. Agric. Food Chem.*, 2004, **52,** 3100.

[4] N. Parris, D.R. Coffin, *J. Agric. Food Chem.*, 1997, **45,** 1596.

[5] H.J. Park, M.S. Chinnan, *J. Food Eng.*, 1995, **25,** 497.

[6] N. Parris, L.C. Dickey, M.J. Kurantz, R.O. Moten, J.C. Craig, *J. Food Eng.*, 1997, **32,** 199.

[7] C.A. Romero-Bastida, E. Flores-Huicochea, M.O. Martin-Polo, G. Velazquez, J. Antonio-Torres, *J. Agric. Food Chem.*, 2004, **52,** 2230.

[8] N. Parris, P.H. Cooke, K.B. Hicks, *J. Agric. Food Chem.*, 2005, **53,** 4788.

[9] N. Parris, M. Sykes, L.C. Dickey, J.L. Wiles, T.J. Urbanik, P.H. Cooke. *Progress in Paper Recycling*, 2002, **11,** (3), 24.

[10] F.A. Momany, D.J. Sessa, J.W. Lawton, G.W. Selling, S.A.H. Hamaker, and J.L. Willett., *J. Agric. Food Chem.*, 2006, **54**, (2), 543.

[11] V. Cabra, R. Arreguin, A. Galvez, M. Quirasco, R. Vazquez-Duhalt, A. Farres, *J. Agric. Food Chem.*, 2005, **53,** 725.

[12] F.X. Budi Santosa, G.W. Padua, *J. Agric. Food Chem.*, 1999, **47** (5), 2070.

[13] D.J. Sessa, A. Mohamed, J.A. Byars, *J. Agric. Food Chem.*, 2008, **56,** 7067.

[14] Q. Wang, G.W. Padua, *J. Agric. Food Chem.*, 2005, **53,** 3444.

[15] A.M. Rakotonirainy, G.W. Padua, *J. Agric. Food Chem.*, 2001, **49,** 2860.

[16] R.G. Alargova, V.N. Paunov, O.D.Velev, *Langmuir*, 2006, **22,** 765.

[17] V.N. Paunov. *Langmuir*, 2003, **19,** 7970.

# CHAPTER 7 – MICRO-RODS CONTAINING PARTICULATE INCLUSIONS: PREPARATION, PROPERTIES AND CHARACTERISATION

This chapter discusses the fabrication and characterisation of new micro-rods with particle additives which lead to new functionality. The formation of micro-rods with particulate inclusions is based on a modification of the standard technique previously applied to the production of micro-rods. We report the fabrication of micro-rods which incorporate magnetic micro-particles for potential targeted delivery and functional rods which attain their modified shaped by input of thermal energy and microwave radiation. We discuss the role of the particulate additives on the foamability and foam stability of the produced foams stabilised by these new micro-rods.

## 7.1. Micro-rods containing 'lumps': principles and materials

Functional micro-rods can possess interesting properties and so can the structures formed from their suspensions. We have produced lumpy micro-rods in a simple, one-step process where the micro-particles used as lumps in the micro-rods are entrapped inside the micro-rods. Other methods have been used to produce micro-rods or fibres with entrapped or attached micro- or nano-particles with useful or novel properties. Chen et al. report the production of cotton fibre/silver nano-particle composites which displayed antibacterial activity.[1] By grafting a chelating monomer onto the cotton fibres, the authors were able to adsorb silver ions onto the composite structures, resulting in cotton fibres with attached silver nano-particles which showed antibacterial activity. These fibres could form the basis of textiles with antibacterial properties which could have great potential in medical or clothing industries. The combination of metals with other substrate fibres was investigated by Lysenko et al.[2] Here, bactericidal activity against different types of cell was observed depending on the kind of fibre used as substrate and on the quantity and shape of adsorbed silver nano-particles. Pinto et al.[3] described the growth of gold nano-particles on various forms of cellulose fibres (including bacterial cellulose and wood cellulose) via the use of layer by layer (LbL) attachment with polyelectrolyte. The optical properties of the final composite materials were varied by the addition of silica 'shells' around the gold nano-particles, which were then deposited by heterocoagulation (with polyelectrolyte) in a similar way. Such

cellulose-based materials could have great utility in the production of paper with security features for identification and banknotes. The same group have also reported novel nano-composites comprising just silica and cellulose fibres, which could have potential uses in high-tech industries such as biotechnology, pharmaceuticals or photonics.[4] Yu et al.[5] report the production of polymer optical fibres which have been doped with quantum dots and also fluorescently-doped silica nano-particles. Their novel method of incorporation of the dopants into the fibres allows materials which are not very compatible with the fibres to be added. The method involved dispersal of the nano-particles desired for encapsulation in a solution of the fibre polymer, before total drying of the mixture. This was achieved by grinding of the solid to a powder to increase surface area and then thorough oven-drying and formation of a large, precursor fibre using a pre-form. The optical polymer fibre was then produced by drawing a much narrower fibre, about 400 μm in exterior diameter into lengths of several centimetres. The doping of optical fibres in this way affords great control over the properties of the resultant optical fibres, which have potential utility in the optics industry. Novel fibres have also been used to form a controlled delivery system for use with drugs. Polacco et al.[6] describe the production of hollow, biodegradable fibres with encapsulated drug-loaded nano-particles. The fibres, formed from a copolymer blend of poly(lactic acid) and ε-caprolactone were produced by either wet or dry spinning. Drug-loaded nano-particles were added to water to form an aqueous suspension that was syringed along with the copolymer solution (during the spinning process) giving polymer fibres with cavities which contained the nano-particles. Such fibres are bio- and haemocompatible, so they have great potential utility as drug delivery agents, and the potential for simultaneous release of different agents was facilitated by the entrapment of nano-particles loaded with different drugs within the hollow fibres. Controlled release of drugs from the fibres has also been reported.

We used a variation of the method described in the previous chapters to produce ‘lumpy’ micro-rods by the suspension of micro-particles within the disperse phase prior to its injection into the continuous phase under shear. During micro-rod formation, as the droplets of disperse phase with suspended micro-particles elongate into cylindrical forms and the solvent is transferred to the continuous phase (in which it is soluble) the micro-particles can become trapped within the solid micro-rod structures, displaying ‘lumpy’ morphology. Fig. 7.1 shows a schematic representation of the main processes involved. Particles chosen for the ‘lumps’ in the micro-rods included sporopollenin,

porous silica particles, yeast cells and pollen grains. It is expected that such novel, functional micro-rods could have unique properties giving the potential for enhanced foam stabilising, or be useful as building blocks for novel materials on a larger scale. Lumpy micro-rods could give enhanced foam stability by way of the lumps anchoring in the nodal regions and Plateau borders within the foam structure and retarding drainage as well as potentially giving increased steric stability.

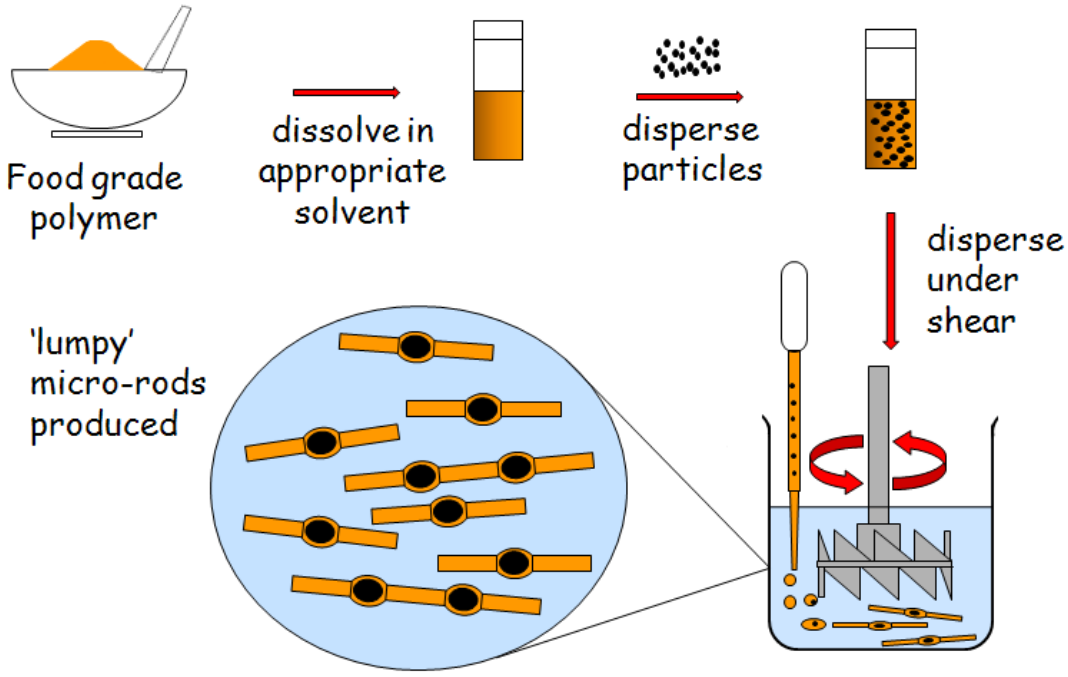


**Figure 7.1. Schematic diagram of the main processes involved in the formation of so-called 'lumpy' micro-rods.**

### 7.2. Micro-rods containing sporopollenin micro-particles

The protective outer portion (or 'exine') of pollen grains is comprised largely of a material called sporopollenin, one of nature's most resistant polymers. Sporopollenin particles from *Lycopodium Clavatum* (a type of moss) may possess great utility as vehicles for drug delivery due to their hollow structure, size (around 28 μm in diameter) and excellent chemical resistance (they can resist attack from both strong acids and bases). We produced micro-rods which have lumps that are relatively large in respect to the diameter of the rods themselves by using sporopollenin micro-particles. These lumps may then permit anchoring of the micro-rods within the drainage channels of the

foams in which they lie. Work in which sporopollenin micro-particles are encapsulated into shellac and ethyl cellulose micro-rods respectively is described below.

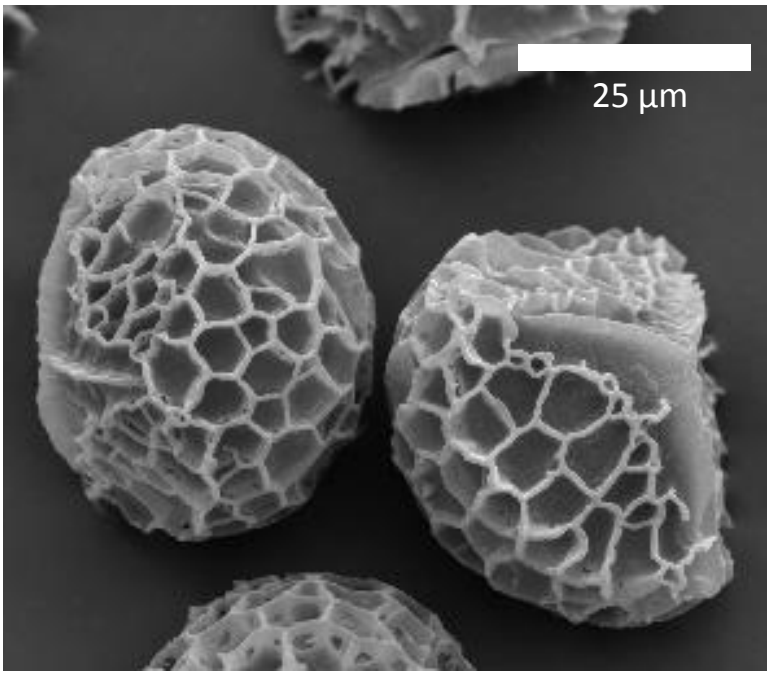


**Figure 7.2. SEM image of sporopollenin from *Lycopodium Clavatum*. The sporopollenin particles of a particular species are monodisperse and are very similar in appearance. The approximate diameter of these particles is 28 µm.[7]**

### 7.2.1. Shellac micro-rods containing sporopollenin micro-particles

In order to produce lumpy shellac micro-rods with sporopollenin micro-particles, sporopollenin (1 wt.% with respect to shellac) was suspended in a viscous 50 wt.% shellac in ethanol solution by sonication (90 sec, 35% power intensity, 1 sec pulse on, 0.5 sec pulse off, Branson Digital Sonicator 450) to form the disperse phase for lumpy micro-rod production. The disperse phase (1 mL) was added to the continuous phase (50 mL 85% glycerol/15% Milli-Q water (v/v) mixture) under stirring (2,000 rpm, 10 min) from a Cole Parmer Digital Reversing Mixer. The resultant lumpy micro-rods were washed by filtration (Whatman No. 1 filter paper) 4 times to remove excess glycerol before microscopic observation. Figs. 7.3 to 7.7 show the resultant micro-rods.

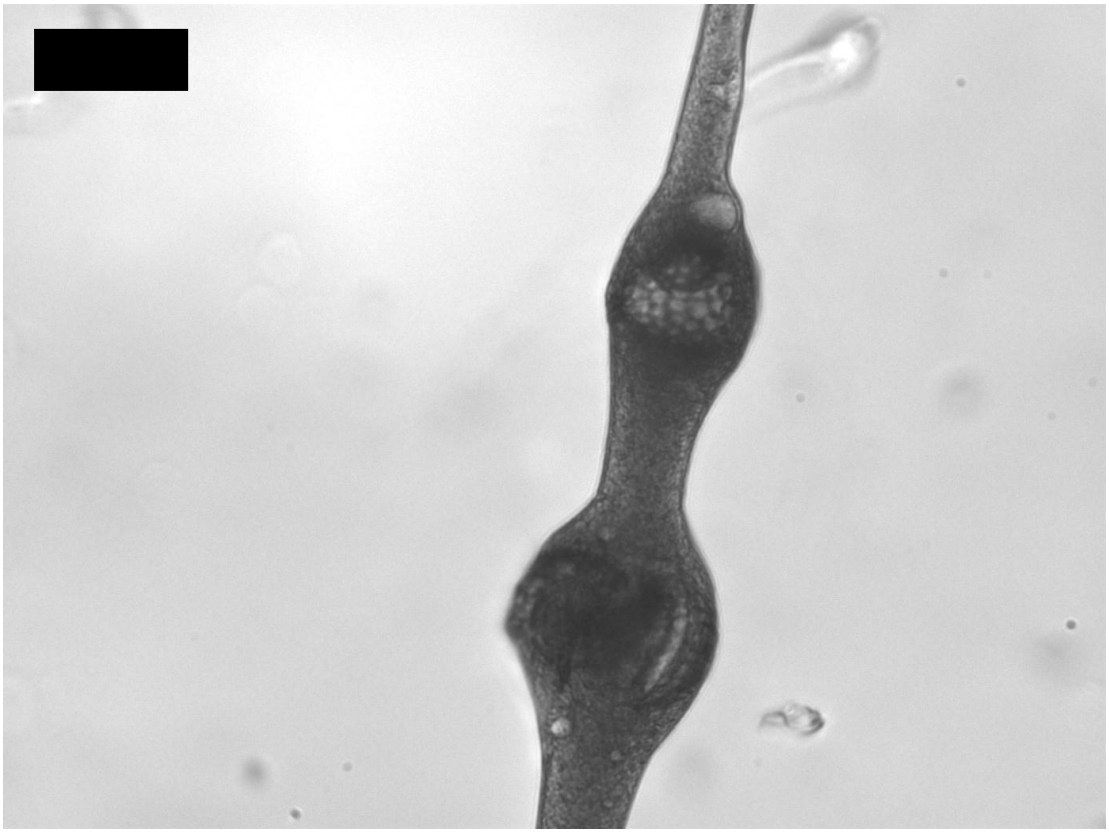

**Figure 7.3. Optical microscopy image of a large lumpy shellac micro-rod containing 2 entrapped sporopollenin particles. The intricate structure of the sporopollenin particle at the top can be seen clearly. Scale bar is 25 µm.**

**Figure 7.4. A wider field optical microscopy image showing a range of resultant shellac micro-rods, including those which have single entrapped sporopollenin particles, and well as those with multiple particles entrapped. Micro-rods with no particles are also seen, together with some extremely large and wide micro-rods with many trapped particles. Scale bar is 100 µm.**

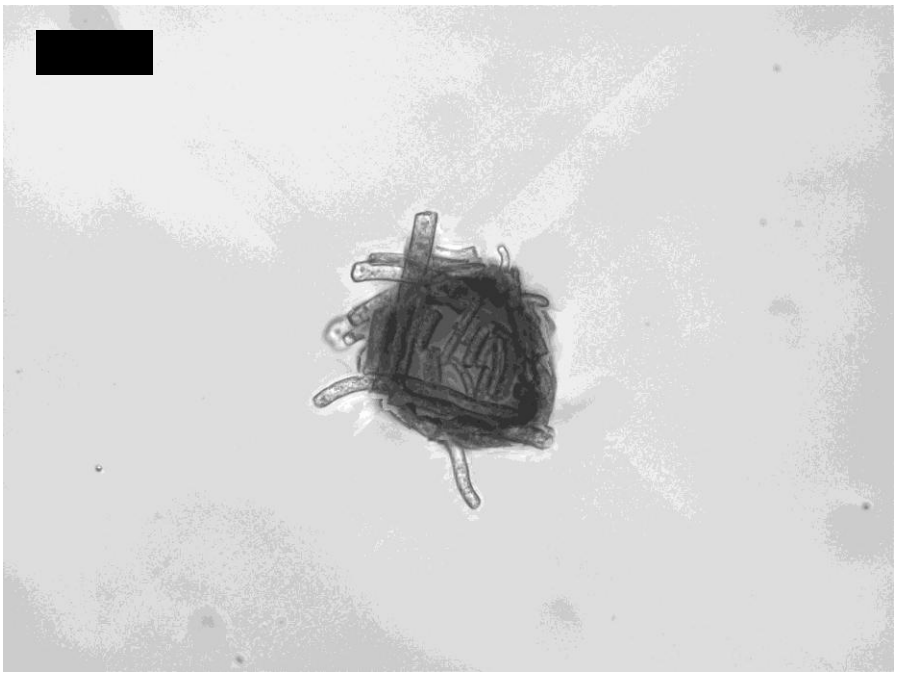

**Figure 7.5. Optical microscopy image of a small air bubble stabilised by adsorbed shellac micro-rods which have no entrapped sporopollenin particles, this having led to their narrower diameter and reduced length. Scale bar is 25 µm.**

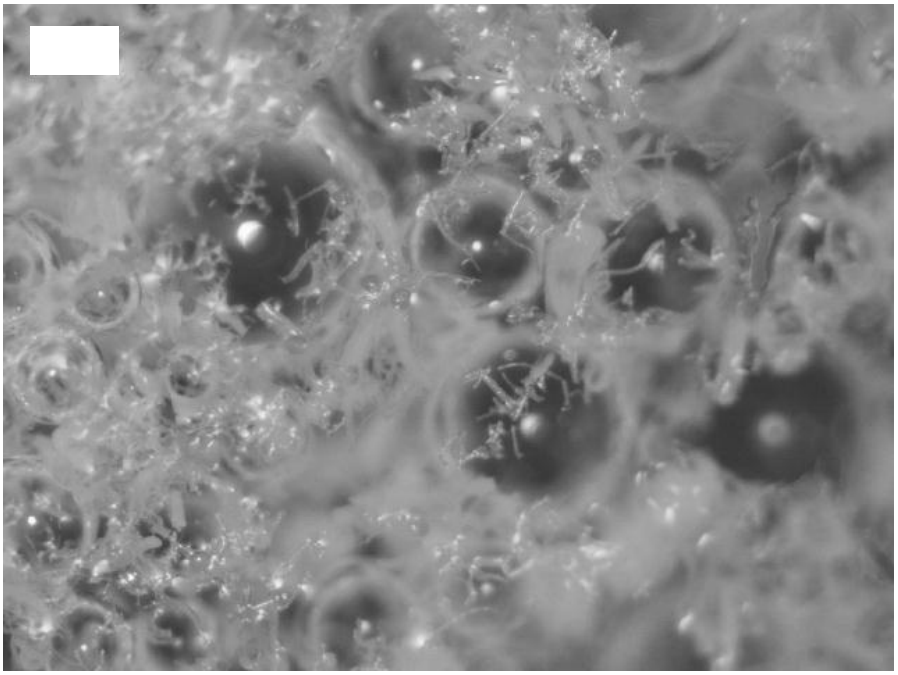

**Figure 7.6. Reflected light micrograph of air bubbles stabilised by lumpy micro-rods. Some bubbles display very sparse coverage of the interface. Scale bar is 250 µm.**

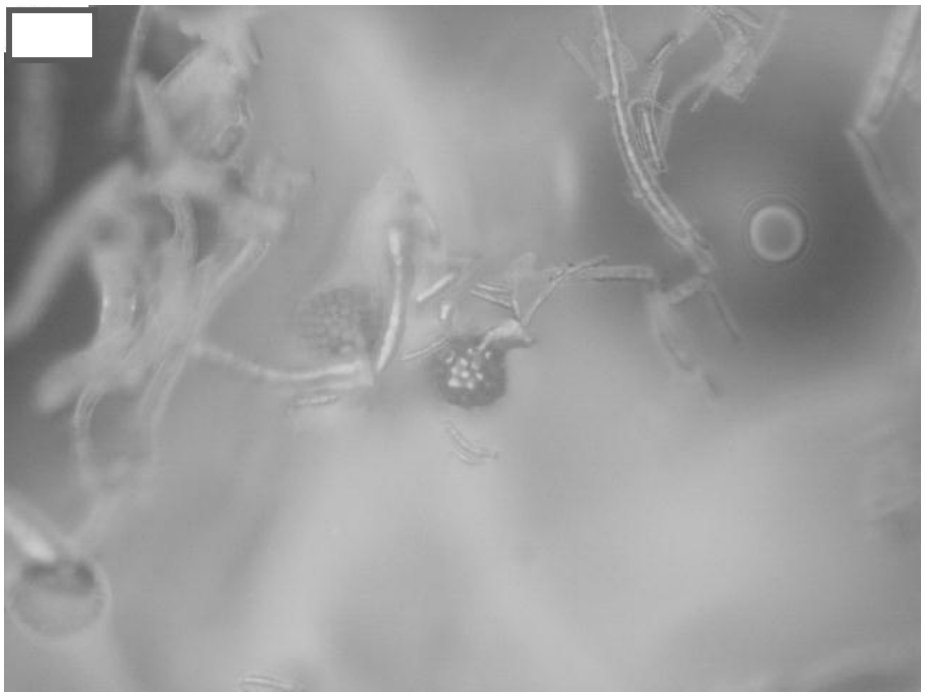

**Figure 7.7. Reflected light micrograph of sporopollenin micro-particles present in the above foam, seen at higher magnification. Scale bar is 50 µm.**

This initial work on shellac micro-rods containing large sporopollenin lumps has produced micro-rods which display modest foamability, although a detailed study has

not yet been conducted. Micro-rods were produced with single entrapped sporopollenin particles; however it has been observed that during micro-rod formation aggregates of sporopollenin particles are produced in the bulk of the polymer, leading to the formation of larger rods with fairly large diameters (fig. 7.4). It is unclear how this could be avoided. The use of lower particle concentrations would lead to a smaller percentage of micro-rods with encapsulated sporopollenin and increased sonication of the disperse phase would lead to evaporation of the solvent, creating a viscous, unusable gel. Further work on fine-tuning of the disperse phase viscosity could potentially improve the problem.

### 7.2.2. Ethyl cellulose micro-rods containing sporopollenin micro-particles

#### 7.2.2.1. Micro-rods produced using acetone as disperse phase solvent

Here we use the same procedure as described in section 7.2.1, except with a 30 wt.% ethyl cellulose in acetone solution containing 1.6 wt.% sporopollenin micro-particles as disperse phase. Ethyl cellulose micro-rods containing sporopollenin lumps were produced, which have a morphology which is displayed in figs. 7.8 to 7.10.

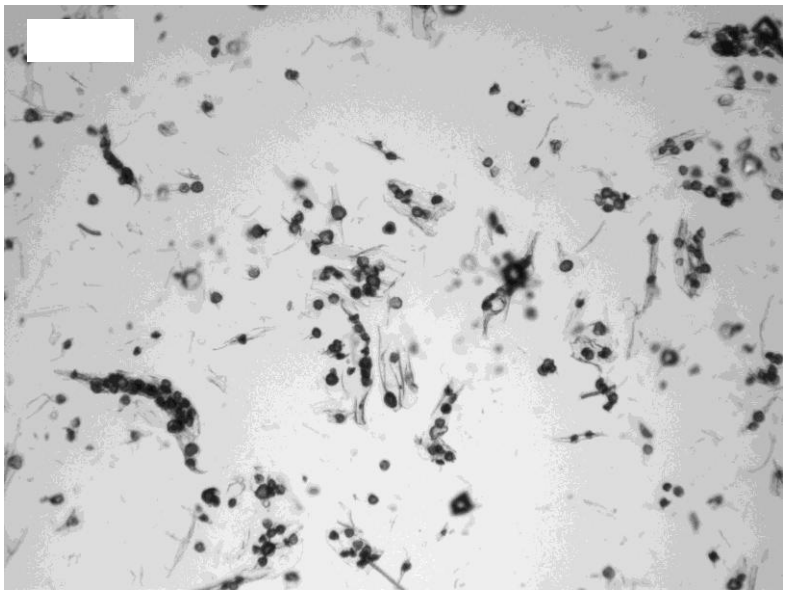

**Figure 7.8. A wide field optical microscopy image showing a number of resultant ethyl cellulose micro-rods, including those which have single encapsulated sporopollenin particles, and well as those with multiple particles entrapped. Scale bar is 250 µm.**

The encapsulation of sporopollenin within ethyl cellulose micro-rods typically leads to the formation of micro-rods containing large lumps (as desired) but also micro-rods with no encapsulated particles at all, and some very large micro-rods with too many sporopollenin particles within. This is a similar result to that observed with shellac micro-rods; the yield of rods with desired appearance is too small, and this may be due to the relatively large size of the encapsulated particles (with respect to the diameter of the micro-rods which would normally be produced as a result of this procedure). The likely reason for this is that they are disrupting the liquid flow during the micro-rod formation process leading to the production of too many micro-rods of large diameter (equal or greater than the diameter of the particles).

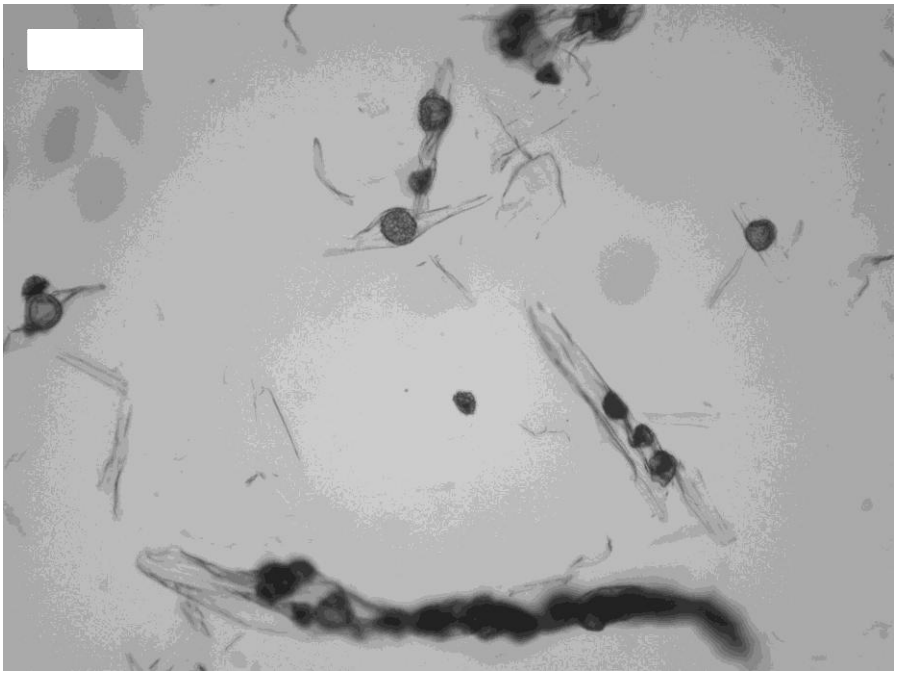

**Figure 7.9. Optical microscopy image of sporopollenin particles entrapped within ethyl cellulose micro-rods. The micro-rods appear quite transparent. A similar behaviour is seen here as with the shellac micro-rods where over-size rods are observed in which many sporopollenin particles have been entrapped. Scale bar is 100 μm.**

**Figure 7.10. Optical microscopy image of entrapped sporopollenin micro-particles within ethyl cellulose micro-rods. The structure of the sporopollenin is clearly visible. Scale bar is 25 µm.**

#### 7.2.2.2. Micro-rods produced using tetrahydrofuran as disperse phase solvent

These micro-rods were produced using the same procedure as in section 7.2.1, except with a 15 wt.% ethyl cellulose in tetrahydrofuran solution containing 3.2 wt.% sporopollenin micro-particles as disperse phase. All other conditions were the same. In this case, the concentration of sporopollenin micro-particles is clearly too high and has led to the formation of amorphously-shaped precipitates with large numbers of the micro-particles trapped inside (figs. 7.11 & 7.12).

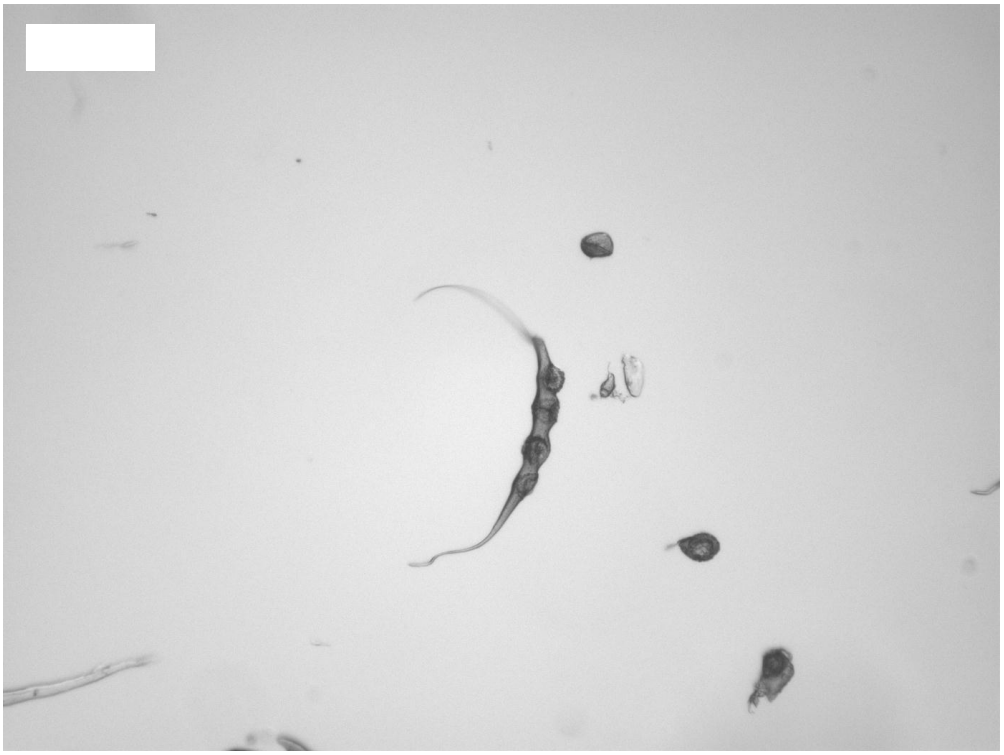

**Figure 7.11. Optical microscopy image of ethyl cellulose micro-rods shaped precipitate containing a number of entrapped sporopollenin micro-particles together with some free particles. Scale bar is 100 µm.**

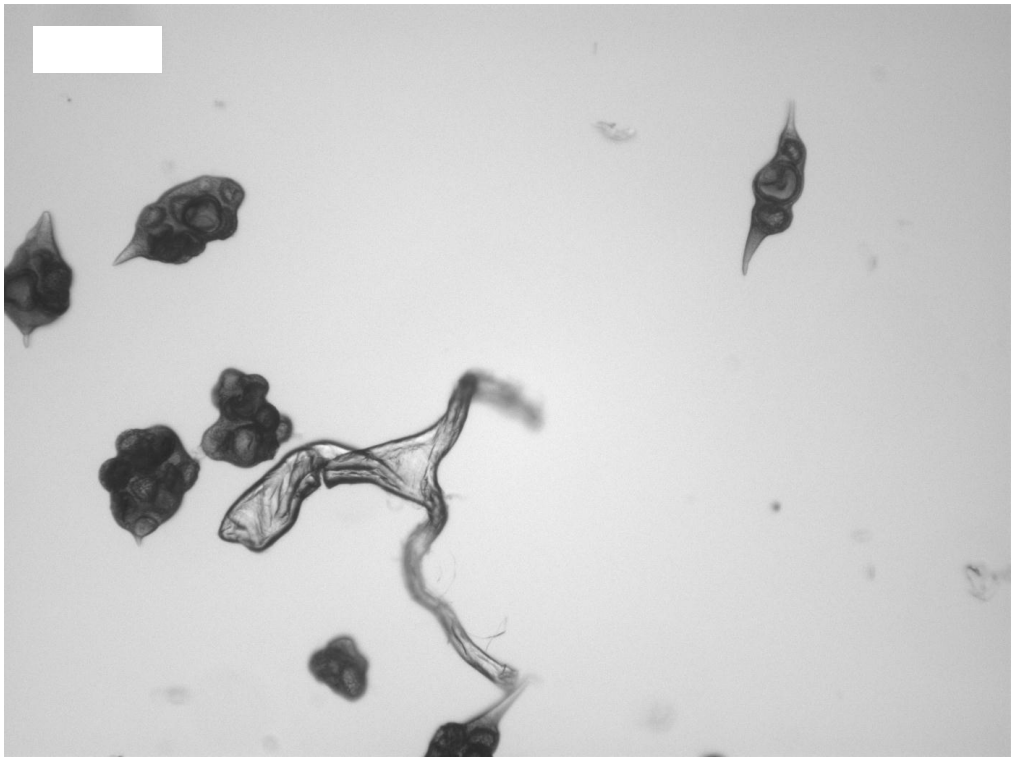

**Figure 7.12. Optical microscopy image of ethyl cellulose precipitates containing a large number of encapsulated sporopollenin micro-particles. Scale bar is 100 µm.**

## 7.3. Micro-rods containing pollen micro-particles

### 7.3.1. Shellac micro-rods containing pollen micro-particles

Pollen from *Lycopodium Clavatum* was incorporated in shellac micro-rods in addition to the work carried out with sporopollenin. The spores are of a similar size to the sporopollenin. Initially pollen spores (1 wt.% with respect to shellac) were suspended in a viscous 50 wt.% shellac in ethanol solution by sonication (90 sec, 35% intensity, 1 sec pulse on, 0.5 sec pulse off, Branson Digital Sonicator 450) to form the disperse phase for lumpy micro-rod production. However, very few encapsulated pollen spores were observed in the micro-rods produced, so the concentration of pollen was increased to 10 wt.% with respect to shellac in order to improve the yield of lumpy micro-rods. Figs. 7.13.a – d illustrate the range of results.

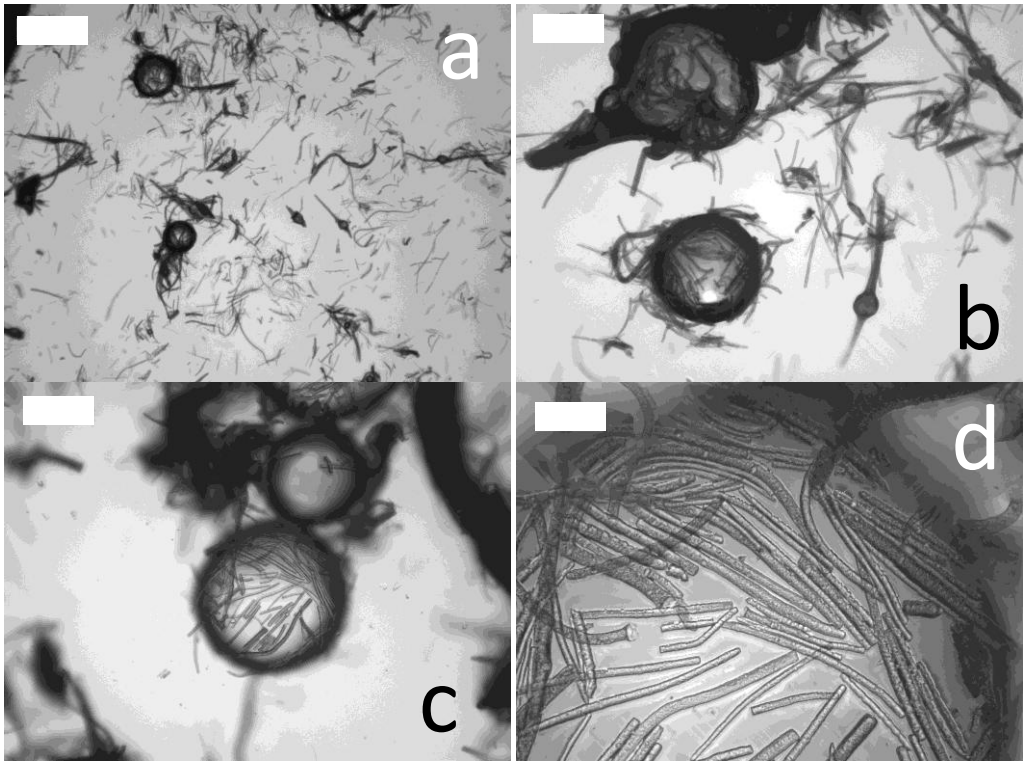


**Figure 7.13. Optical microscopy images of shellac micro-rods with entrapped pollen. Only a small fraction of the micro-rods have entrapped pollen spores present (a) but those with particles entrapped have narrow diameters either side of the spore (b). The micro-rods with no particles trapped adsorb at the air-liquid interface (c). Alignment is seen at the interface (d, a 3D reconstruction composed of 25 images). Scale bars are 250 μm (a), 100 μm (b & c) and 25 μm (d).**

In summary, even when the concentration of pollen spores was increased ten-fold, the proportion of rods with encapsulated particles was very low. This may be due to the large diameter of the pollen particles compared with the diameter of the EC micro-rods produced in these conditions.

## 7.4. Micro-rods containing porous silica micro-particles

### 7.4.1. Shellac micro-rods containing hydrophobic Aeroperl™ silica micro-particles

Aeroperl R806/30 porous silica micro-particles (Degussa, 2 wt.% with respect to shellac weight) were dispersed in a 50 wt.% shellac in ethanol solution by sonication (90 sec, 35% intensity, 1 sec pulse on, 0.5 sec pulse off, Branson Digital Sonicator 450) to form the disperse phase for lumpy micro-rod production. The remainder of the procedure was the same as that described in section 7.2.1. The particles are polydisperse (diameters range from between ~ 5 and 30 µm) and this can be seen well in fig. 7.14a where large shellac micro-rods containing silica micro-particles are aggregating together. Fig. 7.14b shows a single micro-rod with an entrapped porous silica particle.

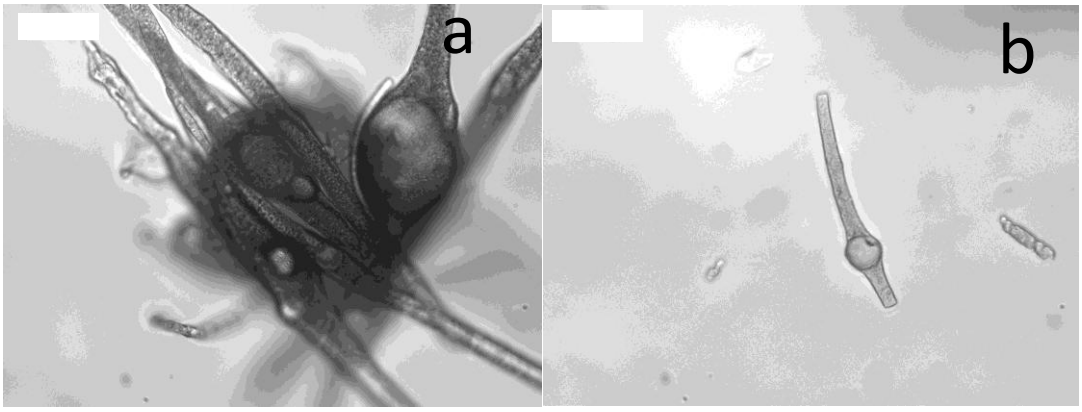


**Figure 7.14. Optical microscopy images of large shellac micro-rods containing encapsulated silica micro-particles (a) and a smaller micro-rod with a single entrapped particle (b). Scale bars are 25 µm.**

### 7.4.2. Ethyl cellulose micro-rods containing hydrophobic Aeroperl™ silica micro-particles

Aeroperl R806/30 porous silica micro-particles (Degussa, 3.3 wt.% with respect to ethyl cellulose weight) were dispersed in a 30 wt.% ethyl cellulose in acetone solution by sonication (90 sec, 35% intensity, 1 sec pulse on, 0.5 sec pulse off, Branson Digital Sonicator 450) to form the disperse phase for lumpy micro-rod production. The remainder of the procedure was the same as that described in section 7.2.1. The resultant micro-rods are shown below.

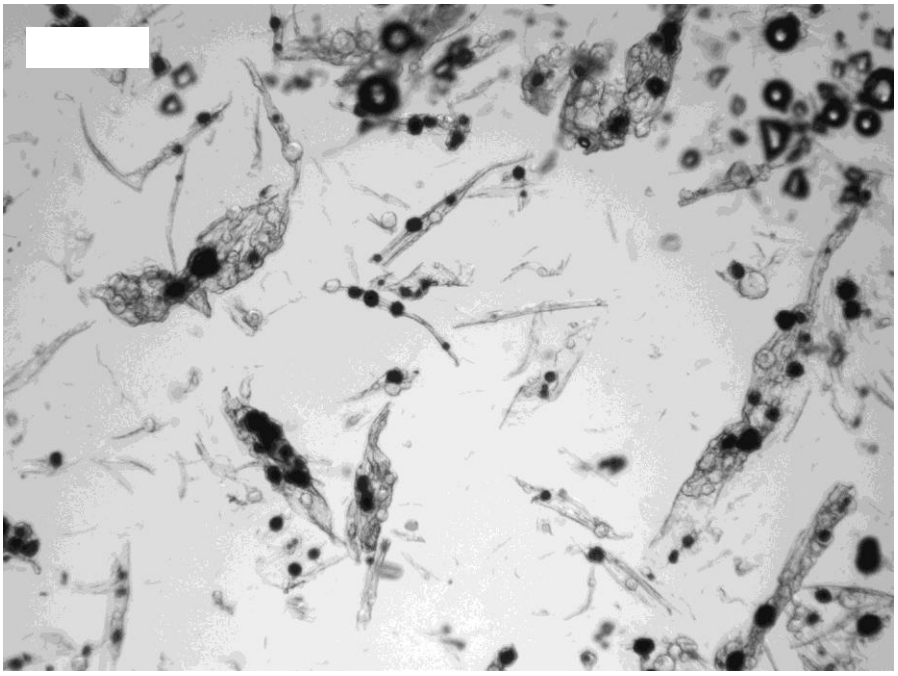

**Figure 7.15. Optical microscopy image of ethyl cellulose micro-rods produced from an acetone dispersed phase solution containing Aeroperl$^{TM}$ R806/30 porous silica micro-particles. Scale bar is 250 µm.**

The resultant micro-rods are large compared with rods containing no encapsulated particles, and the uniformity of the micro-rods within the sample is quite poor. A large proportion of the porous silica particles appear to have been entrapped though, in stark contrast to the shellac micro-rods with pollen grains. Some of the entrapped particles appear dark whereas most transmit light (fig. 7.16) which indicates that there is still air entrapped in the porous particles. Some of the rods have also taken the form of twisted ribbons (as shown in fig. 7.17).

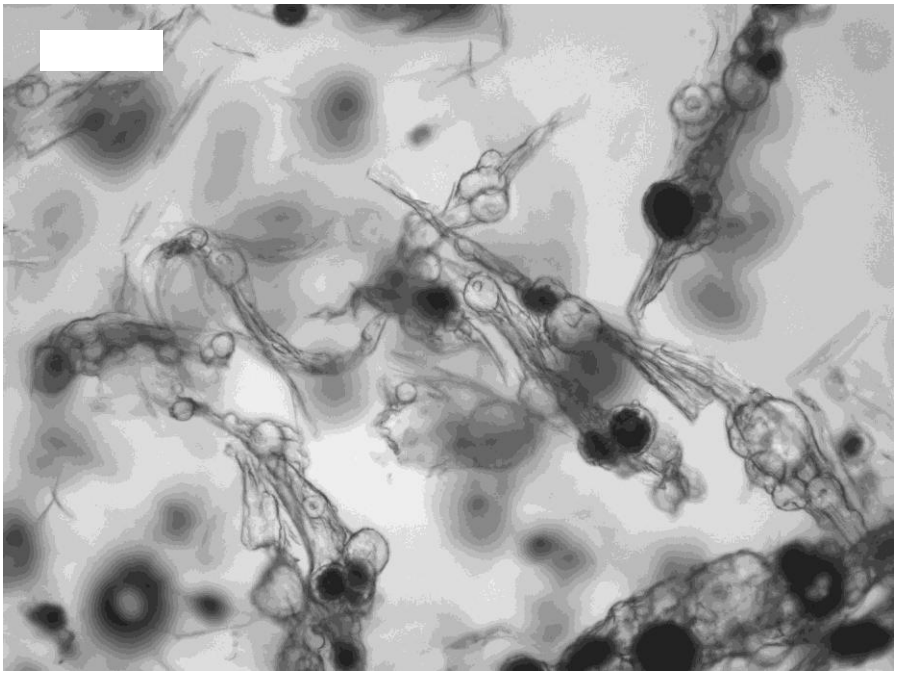

**Figure 7.16. Optical microscopy image of ethyl cellulose micro-rods produced from an acetone dispersed phase solution containing Aeroperl™ R806/30 porous silica micro-particles. Scale bar is 100 µm.**

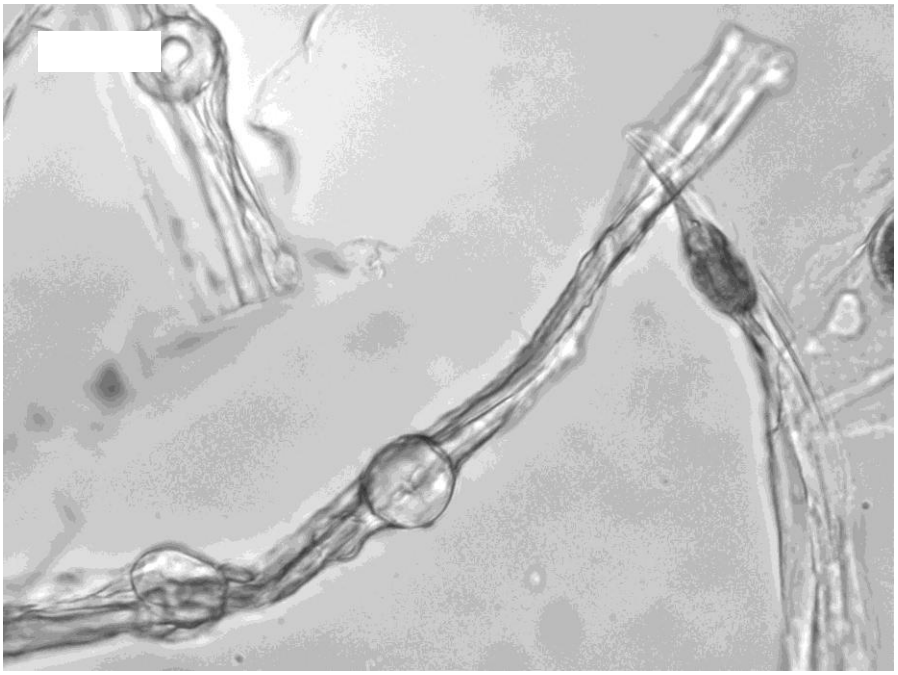

**Figure 7.17. Optical microscopy image of ethyl cellulose micro-rods produced from an acetone dispersed phase solution containing Aeroperl™ R806/30 porous silica micro-particles. Some of the micro-rods have taken the form of twisted ribbons. Scale bar is 25 µm.**

We also tried the same technique with a different solvent. Aeroperl R806/30 porous silica micro-particles (Degussa, 3.3 wt.% with respect to ethyl cellulose weight) were dispersed in a 15 wt.% ethyl cellulose in tetrahydrofuran solution by sonication (90 sec, 35% intensity, 1 sec pulse on, 0.5 sec pulse off, Branson Digital Sonicator 450) to form the disperse phase for lumpy micro-rod production. The remainder of the procedure was the same as that described in section 7.2.1 and the resultant micro-rods are shown below.

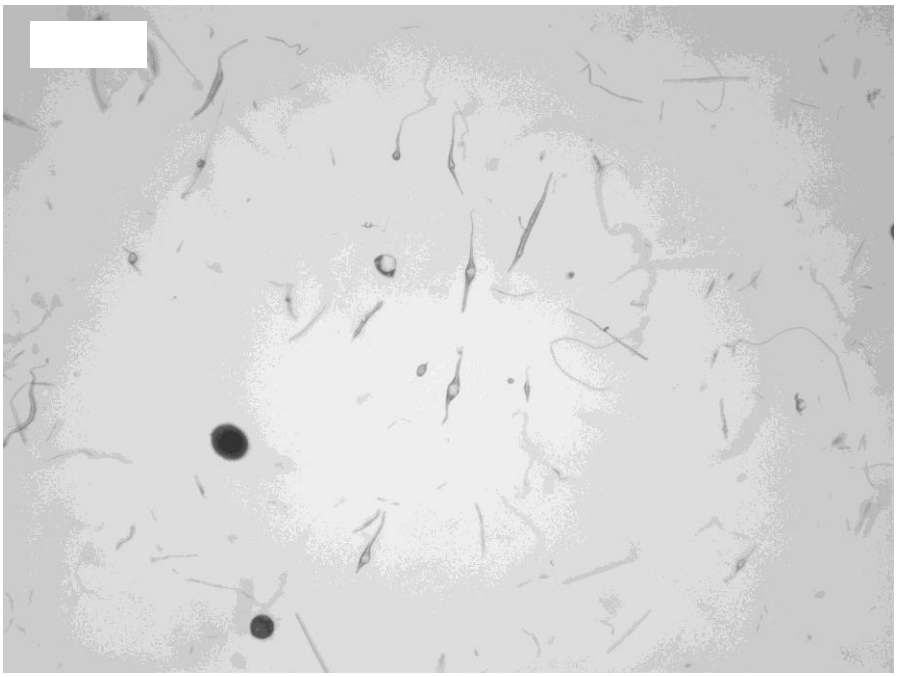

**Figure 7.18. Optical microscopy image of ethyl cellulose micro-rods produced from a tetrahydrofuran dispersed phase solution containing Aeroperl™ R806/30 porous silica micro-particles. The yield of lumpy micro-rods was low but the micro-rods had high aspect ratios. Scale bar is 100 µm.**

The resultant micro-rods were longer, with narrower diameters as observed with ethyl cellulose micro-rods produced from a tetrahydrofuran dispersed phase with no entrapped particles. However, the yield of micro-rods with entrapped particles was too low. A further observation with this particle-polymer-solvent combination though is the lack of impact of the relatively large particle size on the diameter of the micro-rods produced (fig. 7.19).

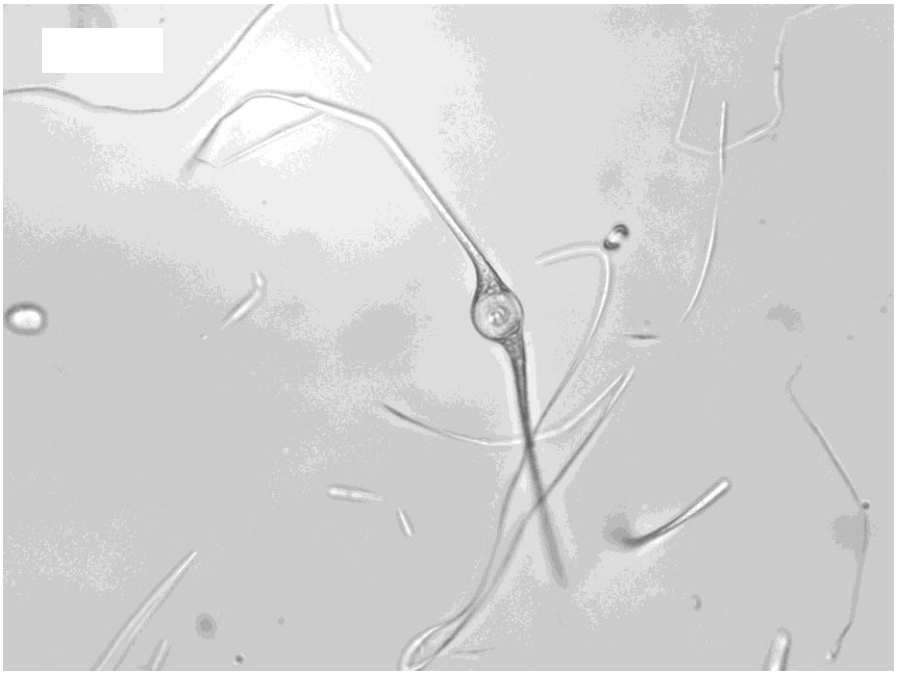

**Figure 7.19. Optical microscopy image of ethyl cellulose micro-rods produced from a tetrahydrofuran dispersion of Aeroperl$^{TM}$ R806/30 porous silica micro-particles. Micro-rod diameter is very narrow compared with the size of the entrapped silica particle, unlike lumpy micro-rods formed from shellac and ethyl cellulose from an acetone dispersed phase. Scale bar is 25 μm.**

## 7.5. Micro-rods containing yeast cells – 'lumpy micro-rods'

### 7.5.1. Shellac micro-rods containing yeast cells

It was decided to produce shellac micro-rods containing smaller lumps and so yeast cells were chosen, given their diameters around 7 μm. 10 wt.% hydrated yeast cells were added to a shellac-in-ethanol solution of 50 wt.% concentration. The cells were hydrated to facilitate their dispersion in the solvents used. The images indicate that the micro-rods with single cell inclusions were not significantly thicker than the unmodified shellac micro-rods (fig. 7.20).

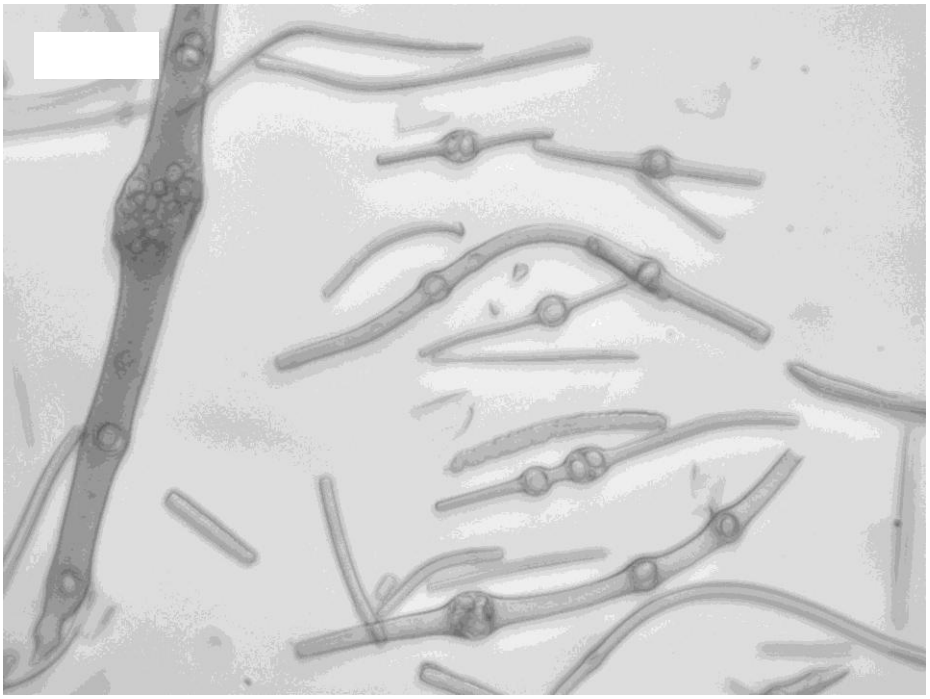

**Figure 7.20. Optical microscopy image of shellac micro-rods containing hydrated yeast cells (10 wt.%). A few larger micro-rods containing yeast cell aggregates were observed but mainly single cells have been encapsulated. Scale bar is 25 µm.**

### 7.5.2. Effect of micro-rod 'lumpiness' on stability of foams

Shellac in ethanol (50 wt.%) dispersed phase solutions (1 mL each) were treated with 0, 16 wt.%, 28.5 wt.% and 37.5 wt.% of added (hydrated) yeast (dry weight; added as slurries in ethanol). Micro-rods were produced with each dispersed phase, 1 mL disperse added to a 85% glycerol/15% Milli-Q water (v/v) mixture continuous phase under stirring, 2,000 rpm for 10 minutes, Cole Parmer Digital Reversing Mixer. The resulting micro-rods were washed in Milli-Q water by filtration to remove glycerol and foams were made by hand shaking using each set of micro-rods. The foam height with time for each sample was monitored to investigate any effect of the amount of yeast cells 'lumps' in each fibre. The control experiment was done with unmodified shellac micro-rods as foam stabilisers. As can be seen in fig. 7.21, in the first few minutes after shaking, drainage of water from the foam occurs rapidly. After this, the foam remains stable for over 2,000 minutes. When yeast cell lumps are incorporated in the micro-rods, there is a steady decrease in the drainage speed (i.e. rate of decrease in initial foam

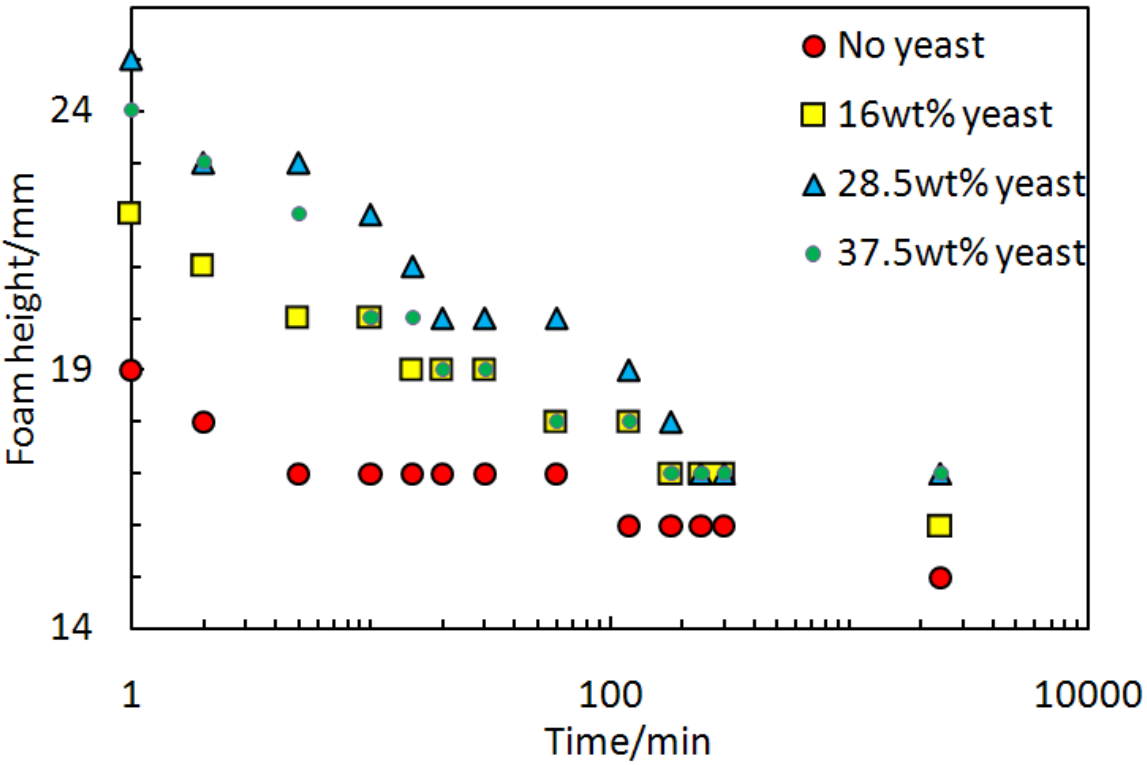


**Figure 7.21. Change in foam height over time of foams stabilised by ~2 wt.% shellac micro-rods containing increasing concentration of yeast cell 'lumps'. Liquid drainage appears to be retarded by the presence of the cells.**

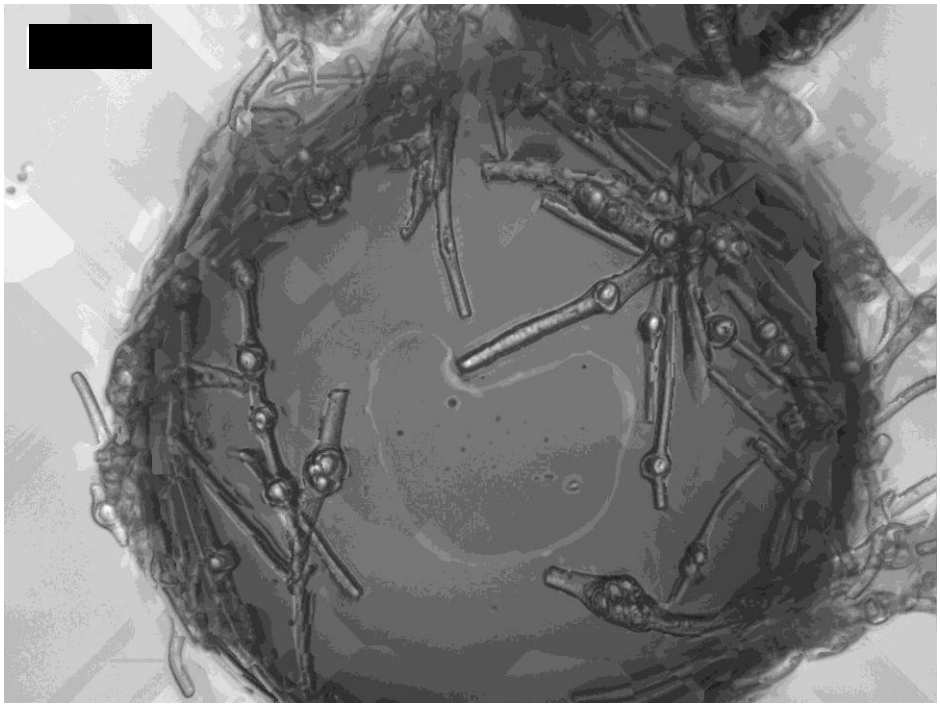

**Figure 7.22. Extended depth of field image of 'lumpy' shellac micro-rods containing 28.5 wt.% added yeast cells adsorbed around an air bubble approximately 150 µm in diameter. Scale bar is 25 µm.**

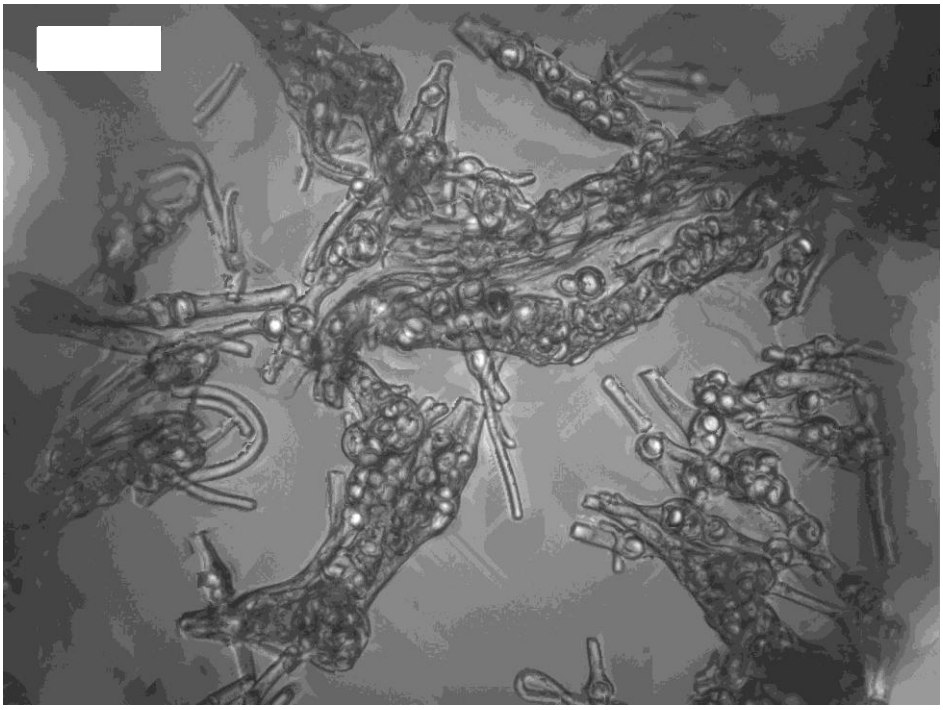

**Figure 7.23. Extended depth of field image of 'lumpy' shellac micro-rods containing 37.5 wt.% incorporated yeast cells. At this concentration of added cells, the diameter of some micro-rods has been increased. Scale bar is 25 µm.**

height) when the amount of yeast included is increased from 0 to 16 wt.%, and from 16 wt.% to 28.5 wt.%. This suggests that lumpy shellac micro-rods are providing enhanced levels of foam stabilisation, possibly due to their accumulation in the Gibbs-Plateau borders of the foam, hindering drainage of water from the foam films. There is no further increase in this effect as the amount of yeast is increased further and this may be because a critical concentration of yeast cells in the micro-rods has been reached. Fig. 7.23 shows that micro-rods containing this extra amount of yeast cells are longer and wider than those produced from the 28.5 wt.% added yeast sample (fig. 7.22).

### 7.5.3. Ethyl cellulose micro-rods containing yeast cells

It was also decided to use smaller particles to create the lumps in ethyl cellulose micro-rods. Hydrated yeast cells were added to 12.5 wt.% ethyl cellulose in tetrahydrofuran solutions at 10 wt.% and dispersed using sonication. Micro-rods were then produced using a similar technique as before.

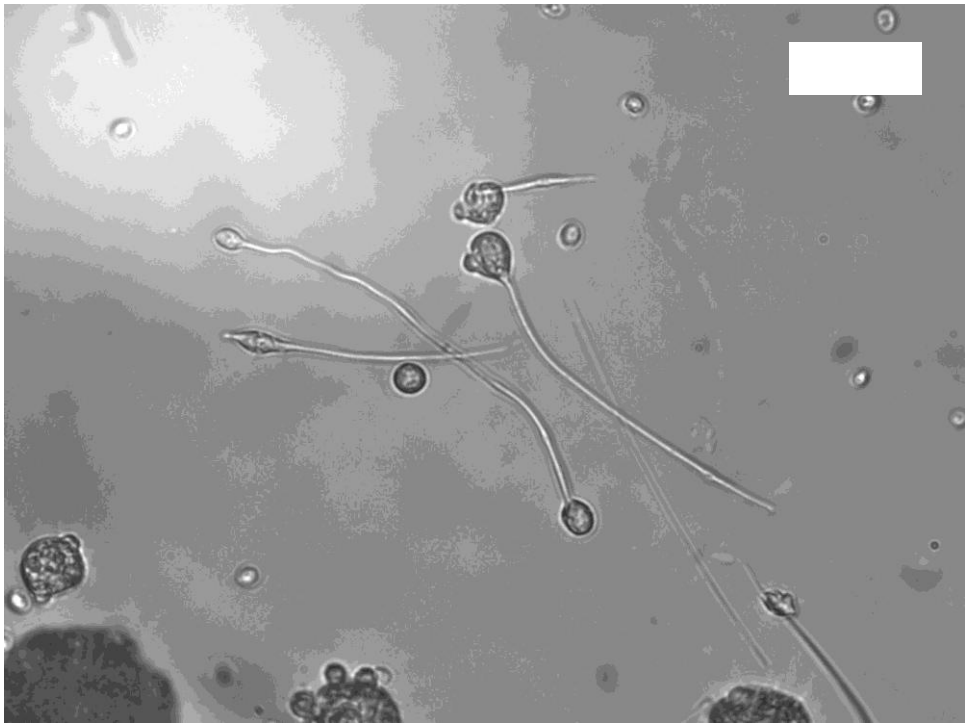

**Figure 7.24. Optical microscopy image of ethyl cellulose micro-rods produced from 12.5 wt.% ethyl cellulose in THF solution containing 10 wt.% yeast cells which have formed aggregates during the micro-rod formation process. Scale bar is 25 µm.**

It was found that although the yeast cells had been successfully encapsulated within the micro-rods, a large proportion of the cells had been incorporated as aggregates. Further experiments with more intensive ultrasonic treatment and more thorough stirring to homogenize the dispersed phase were carried out, but it was not possible to produce lumpy ethyl cellulose micro-rods with single yeast cell lumps. Fig. 7.24 (above) shows the ethyl cellulose micro-rods containing yeast cell aggregates.

## 7.6. Ethyl cellulose ‘ballooned’ micro-rods

### 7.6.1. Preparation of ‘ballooned’ micro-rods by thermal degradation of sodium bicarbonate

Sodium bicarbonate crystals were ground down to a size of approximately 5 μm by using a pestle and mortar and incorporated in ethyl cellulose micro-rods produced using acetone as the dispersed phase solvent. Briefly, in order to produce ballooned micro-rods, the micro-rods containing sodium bicarbonate were heated to thermally degrade the bicarbonate, releasing carbon dioxide and hence blowing bubbles of gas inside the micro-rods. The heating was performed in the original continuous media, which was a glycerol/glycol mixture, which permitted heating to temperatures exceeding 170 ºC.

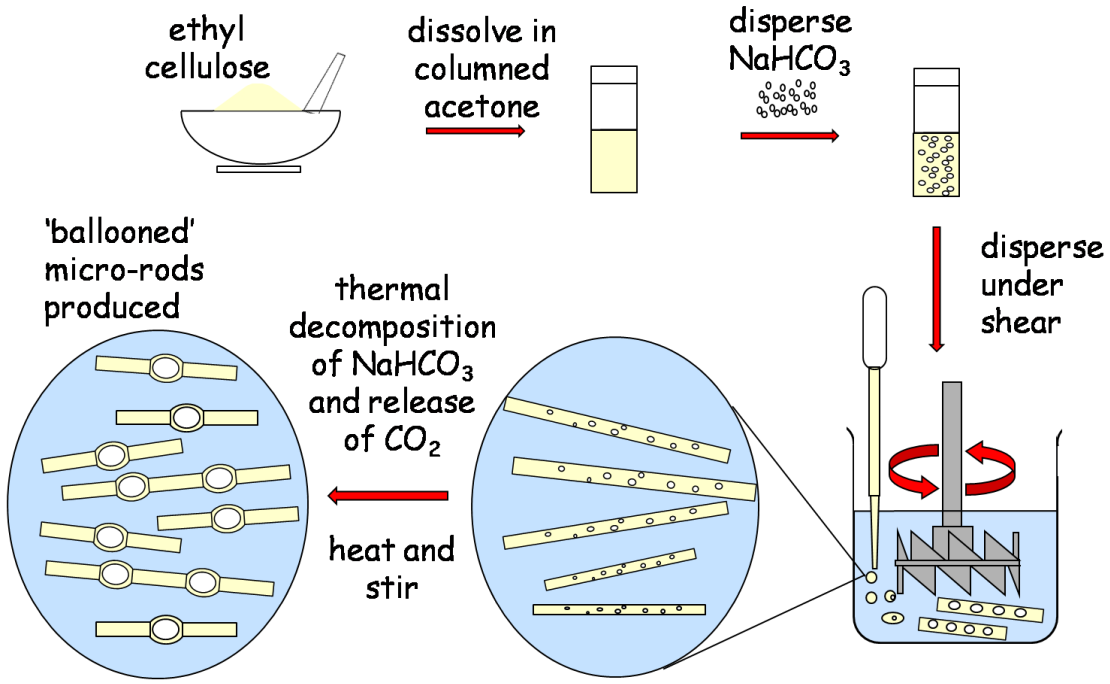


**Figure 7.25. Schematic diagram showing the main processes involved in the formation of so-called ‘ballooned’ micro-rods from the thermal degradation of sodium bicarbonate. The presence of water was found to be an important factor determining whether or not this technique was successful (see section 7.6.2.).**

Initially, ethyl cellulose micro-rods containing ground sodium bicarbonate crystals were produced by adding 30 wt.% ethyl cellulose in acetone solution containing

0.2 g crushed $NaHCO_3$ crystals to a continuous phase comprising a 85% glycerol/15% Milli-Q water (v/v) mixture and stirring for 10 min at 2,000 rpm. The micro-rods were heated to 170 °C for 30 min with magnetic stirring at 300 rpm and then isolated and washed with Milli-Q water by filtration.

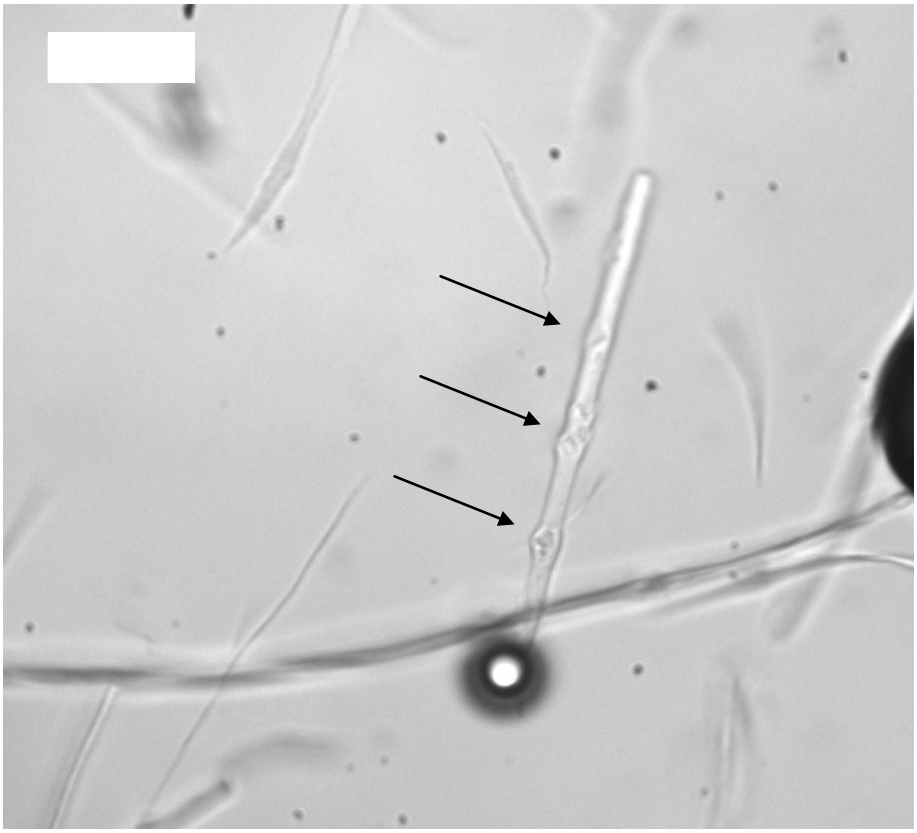

**Figure 7.26. Optical microscopy image of ethyl cellulose micro-rods containing sodium bicarbonate crystals (arrowed) pre-heat treatment. Scale bar is 25 µm.**

### 7.6.2. Effect of the presence of water on the formation of 'ballooned micro-rods'

Following the production of ethyl cellulose micro-rods which contained $NaHCO_3$ micro-crystals using a continuous phase comprising 85% glycerol and 15% Milli-Q water (v/v), the suspension was not diluted any further before being placed on a stirrer hotplate and a magnetic stirrer bar was added. The suspension was heated with stirring to 170 ºC and this temperature was maintained with stirring for 30 min. After this period the suspension of micro-rods was cooled to room temperature and examined using optical microscopy.

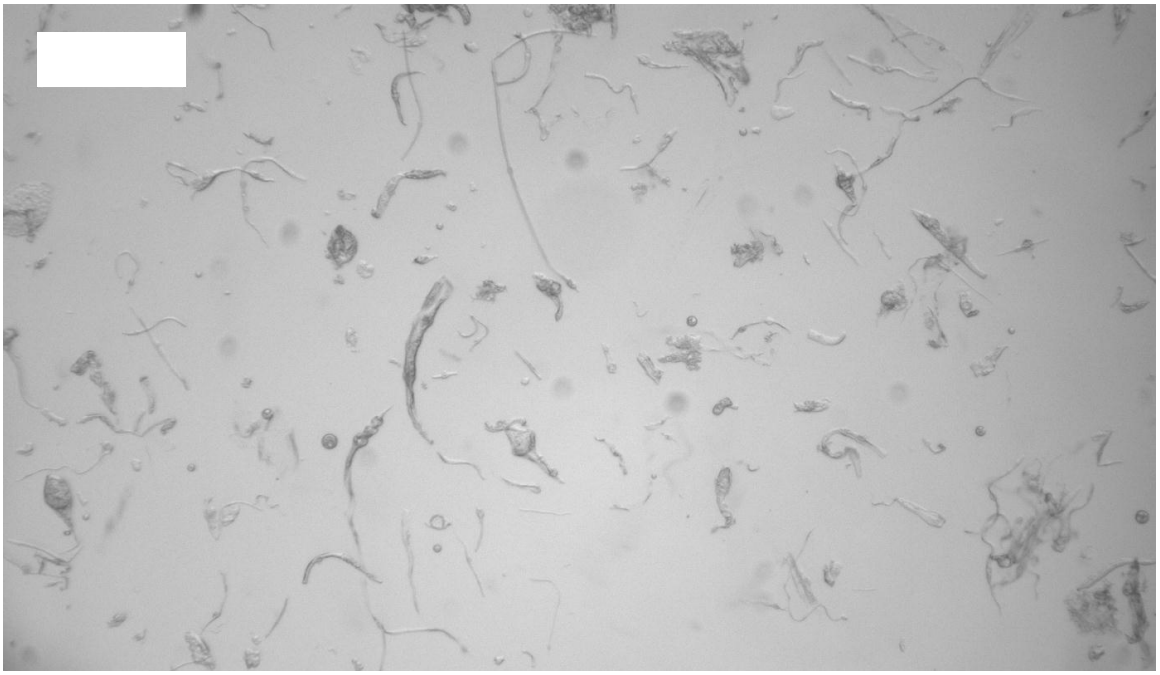

**Figure 7.27. Optical microscopy image of EC micro-rods containing sodium bicarbonate after heat treatment produced using aqueous media. No 'ballooned' micro-rods were observed. Scale bar is 100 µm.**

The result was that no ballooned micro-rods were formed. The process was repeated with the removal of water to investigate the effect this might have. The acetone used in production of the dispersed phase was columned in alumina twice to dry it, and the standard, aqueous continuous phase (85% glycerol/15% Milli-Q water (v/v) mixture) was replaced with one comprising 75% glycerol and 25% ethylene glycol (v/v). Upon the heating and subsequent cooling process (same as previous) using the modified procedure, ballooned micro-rods were successfully produced due to the thermal degradation of sodium bicarbonate producing $CO_2$ gas within the micro-rods. Micro-rods clearly have large lumps, and the majority of micro-rods have been affected. It seems that removing water facilitates the successful encapsulation of sodium bicarbonate micro-crystals into the EC micro-rods.

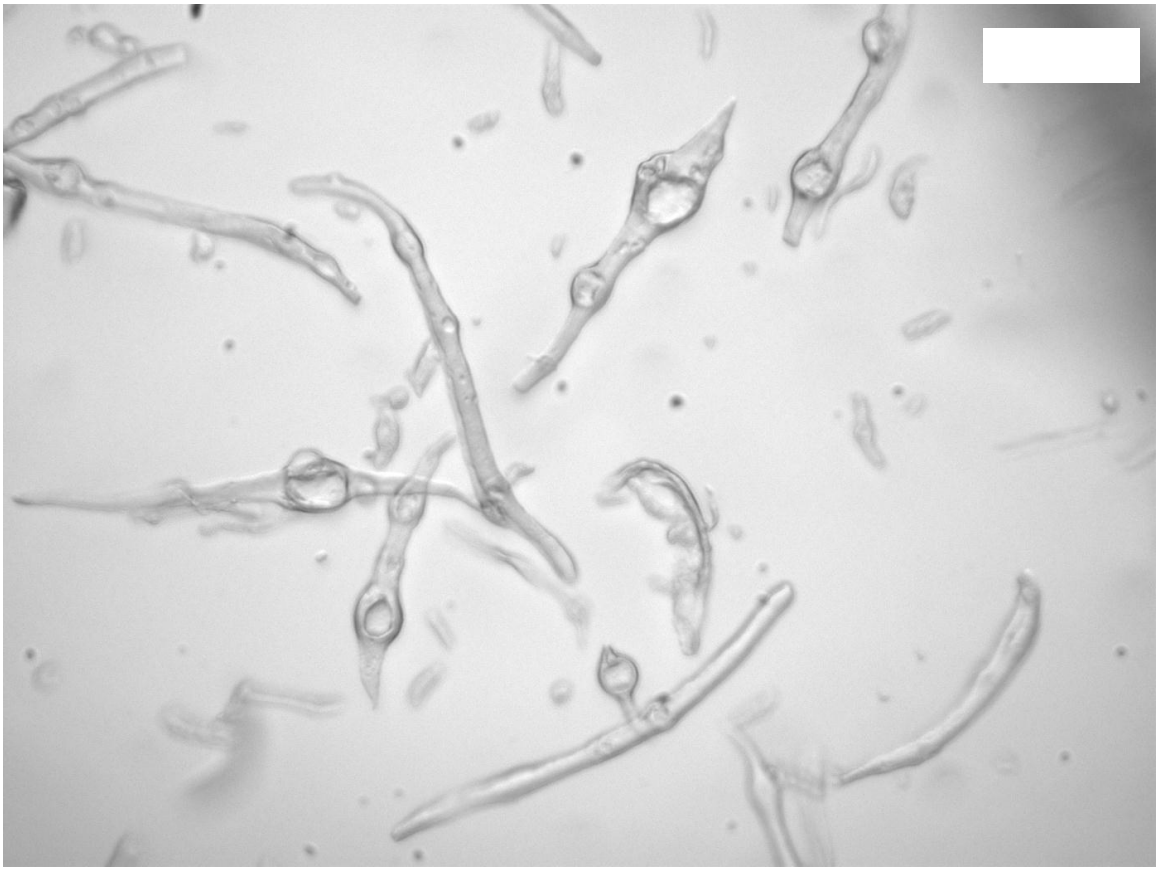

**Figure 7.28. Optical microscopy image of EC micro-rods containing entrapped sodium bicarbonate micro-particles after heat treatment in a non-aqueous continuous phase (75% glycerol, 25% ethylene glycol, v/v). Scale bar is 25 µm.**

In order to determine the morphology of the micro-rods, the EC was fluorescently doped using 0.001% w/w Nile Red dye in the disperse phase. Fig. 7.29 shows that the 'bubbles' in the micro-rods appear to be hollow, with extra fluorescence intensity being seen towards the edges of the inflated areas.

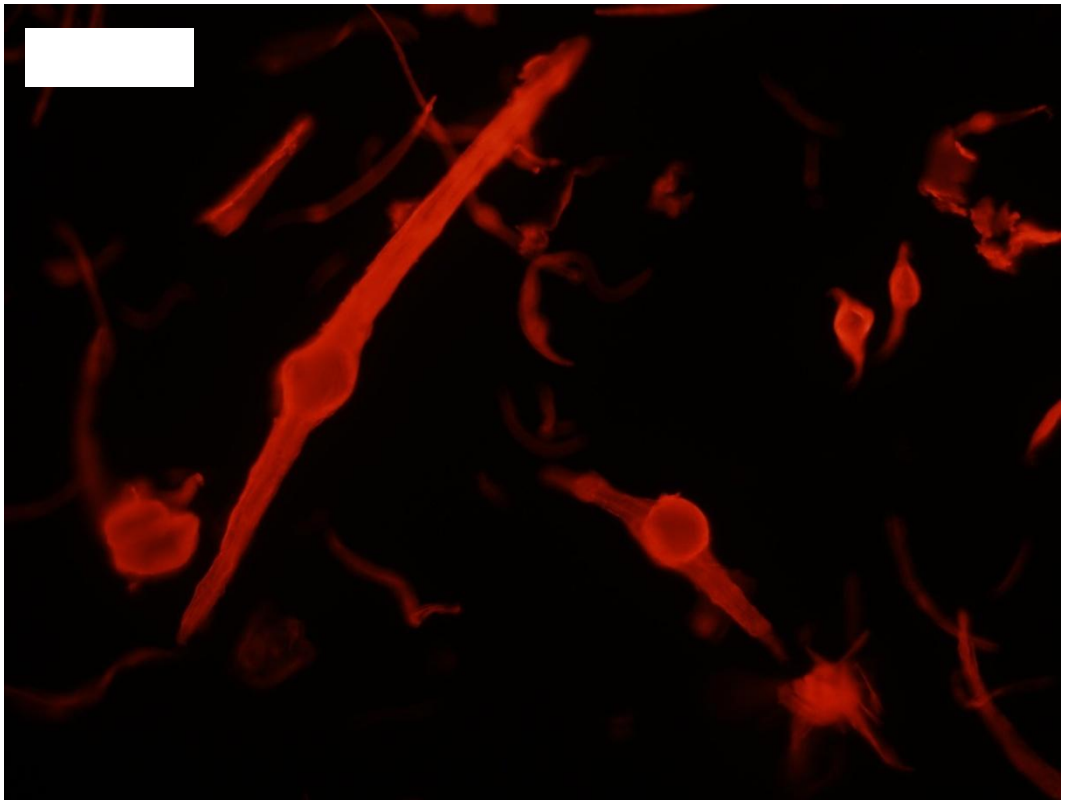

**Figure 7.29. Fluorescence microscopy image of ethyl cellulose 'ballooned' micro-rods where the lumps are hollow; a result of the thermal decomposition of sodium bicarbonate encapsulated within the micro-rods. The micro-rods were stained with a small amount of Nile Red dye. Scale bar is 25 μm.**

## 7.7. Ethyl cellulose micro-rods containing copper micro-particles: effect of treatment with microwave radiation

Copper micro-particles (<10 μm in diameter) were added to a 30% ethyl cellulose in acetone solution and the dispersion was homogenised by ultrasonic treatment, before adding to a continuous phase which was a 85% glycerol/15% Milli-Q water (v/v) mixture and stirring for 10 min at 2,000 rpm. Ethyl cellulose micro-rods with encapsulated copper particles were produced using a protocol described in section 2.3.7.3 and are shown in fig. 7.30. Aqueous fibre suspensions were then exposed to microwave radiation from a 650 W domestic microwave oven and then imaged by optical microscopy (fig. 7.31)

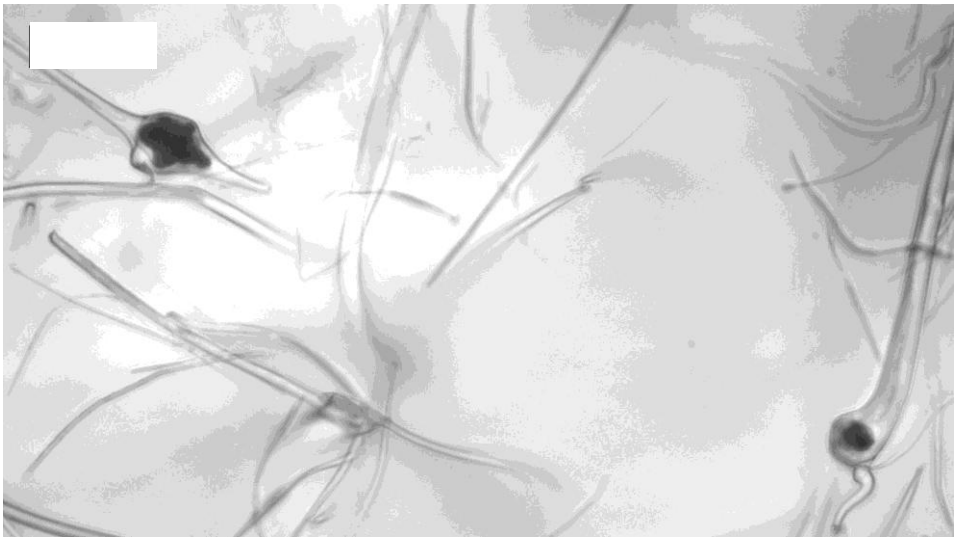

**Figure 7.30. Optical microscopy image of ethyl cellulose micro-rods containing copper micro-particles pre-microwave treatment. Scale bar is 25 µm.**

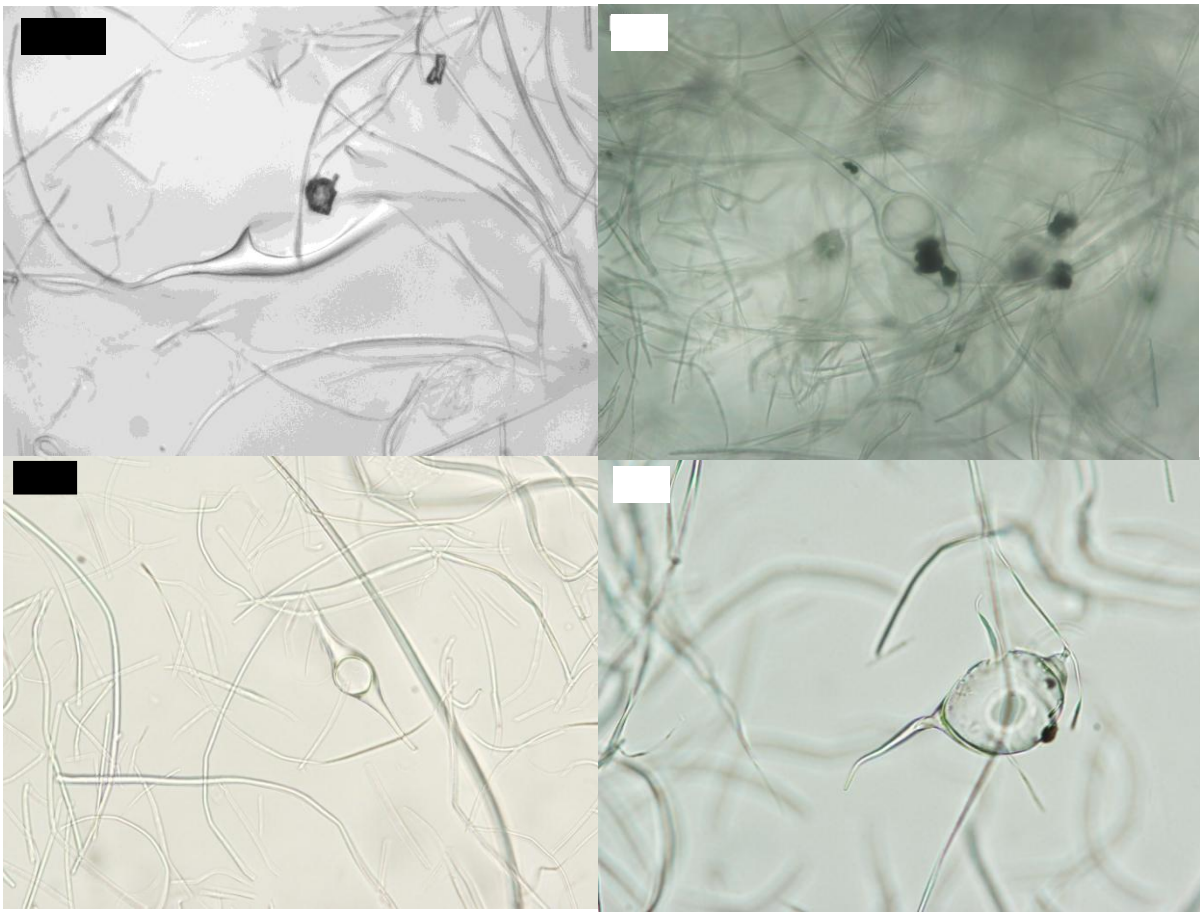

**Figure 7.31. Characteristic blown-up 'ballooned'-type micro-rods observed after microwave treatment of copper-containing micro-rods. Scale bars are 25 µm.**

A number of different treatment times at different microwave power levels were tried systematically, however unfortunately it was not possible to produce a good yield of ‘ballooned’ micro-rods. A future direction could be to experiment with a non-aqueous continuous phase as for sodium bicarbonate ‘ballooned’ micro-rods.

### 7.8. Magnetic micro-rods of shellac and ethyl cellulose

Shellac and ethyl cellulose micro-rods containing iron oxide nano-particles were made to investigate any effect this might have on the properties and utility of the micro-rods produced. The magnetic nano-particles were fabricated by chemical co-precipitation in air of iron (II) and (III) chlorides using ammonium hydroxide.[8]

Concentrations of magnetic nano-particles in micro-rods of 1, 3 and 15 wt.% (w.r.t. shellac weight) were used. We found that micro-rods containing 1 wt.% iron oxide nano-particles did not respond to application of an external magnetic field provided by a neodymium magnet. When 3 wt.% was used (see fig. 7.32) the micro-rods could be moved easily by the magnet, and they clearly show alignment in the magnetic field.

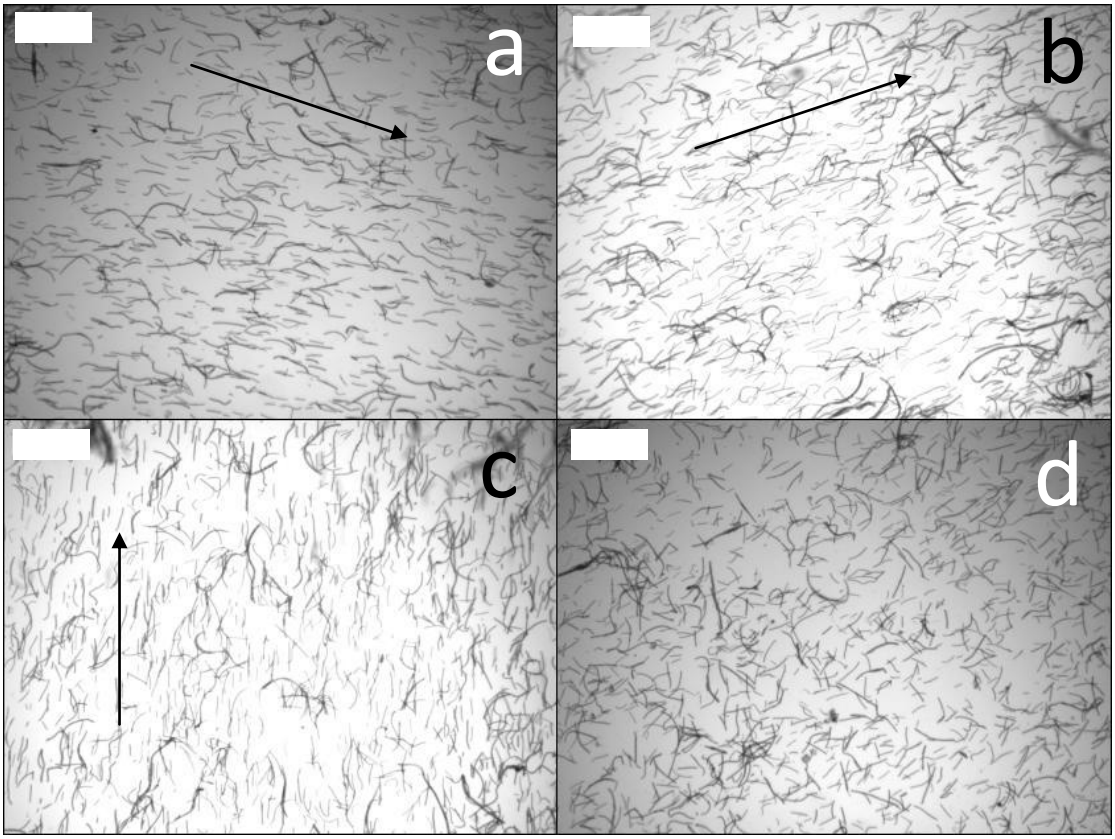


**Figure 7.32. Optical microscopy images of magnetic Shellac micro-rods, (a) to (c) aligning under the influence of a magnet positioned in 3 different directions and (d) in a random orientation with no magnetic field applied. Scale bars are all 250 µm.**

However, the incorporation of higher concentrations of magnetic nano-particles into the micro-rods had a negative impact on the uniformity of the micro-rods. When 15 wt.% of magnetic nano-particles was introduced, a high number of very large and non-uniform micro-rods were seen.

Ethyl cellulose magnetic micro-rods were produced by adding 5 wt.% iron oxide nano-particles to a solution of 12.5 wt.% ethyl cellulose in tetrahydrofuran. This dispersion was added to 85% glycerol/15% Milli-Q (v/v) mixture under shear for 10 min at 1,100 rpm. Micro-rods produced from an ethyl cellulose/tetrahydrofuran solution were not as uniform as those made with shellac, but also respond to an external magnetic field (fig. 7.33).

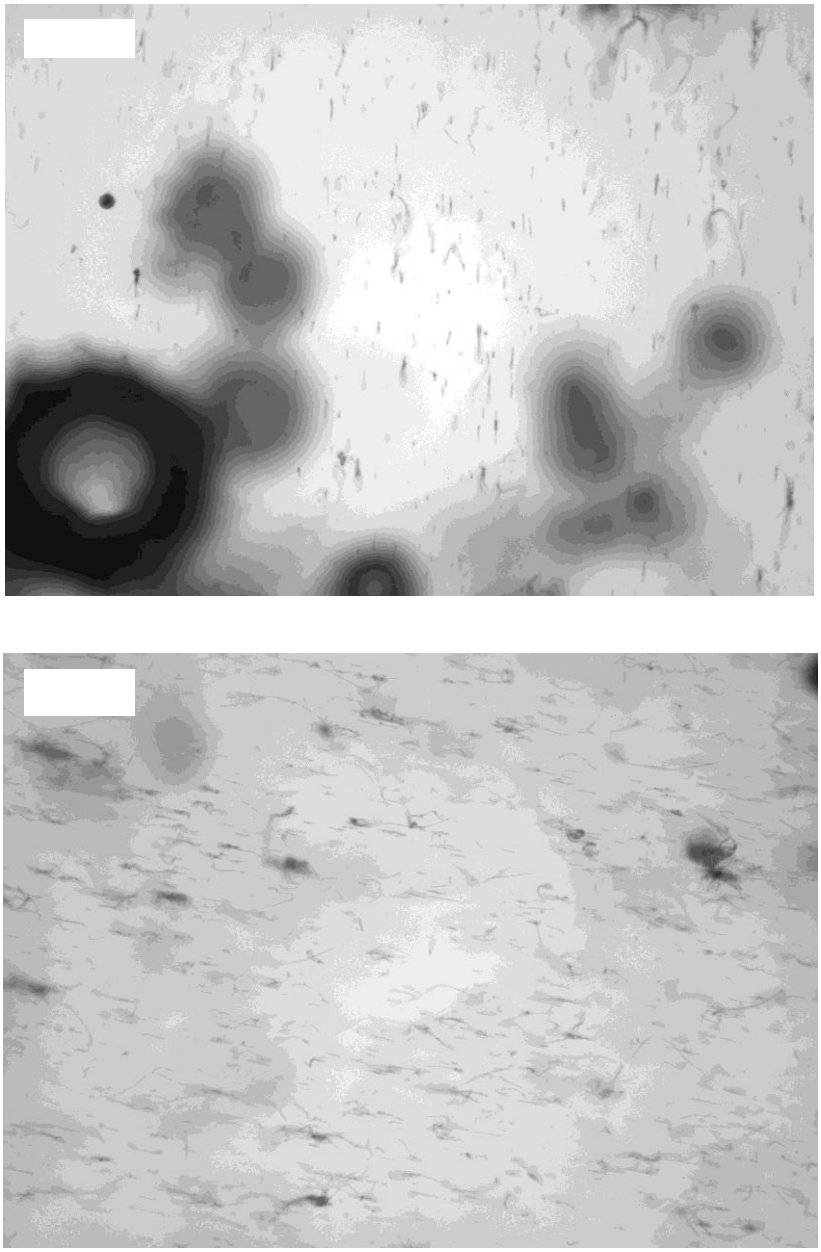

**Figure 7.33. Optical microscopy images of ethyl cellulose magnetic micro-rods oriented in different directions due to the influence of an external magnetic field provided by a neodymium magnet. Scale bars are 100 μm.**

We expected that an aqueous foam stabilised by magnetic micro-rods would be formed and could be subsequently destroyed in a triggered manner by the application of a strong, external magnetic field. Magnetic shellac micro-rods containing 3 wt.% magnetic particles showed modest foamability, and portions of foam could be pulled to

the bottom of a glass vial using a neodymium magnet, indicating that a degree of manipulation of the foam was possible. This may be useful for future applications. However, we were not successful in breaking the magnetic foams by using an external magnetic field due to the enhanced stability of the shellac scaffolding structure.

## 7.9. Conclusions

In this chapter we demonstrate that solid micro- and nano-particles can be successfully incorporated within micro-rods formed through an in-shear-flow solvent attrition dispersion technique. The produced functional polymer micro-rods have great potential as foam or emulsion stabilisers with enhanced foam stabilising ability. The incorporation of particles much larger than the diameters of the micro-rods in which they are to be encapsulated gave non-uniform micro-rods. The most common observation when using large particles was the production of rods which had diameters similar to those of the entrapped particles, as though the particles are disrupting the shear flow processes which occur during micro-rod formation. Interestingly, however, ethyl cellulose micro-rods produced from a tetrahydrofuran dispersed phase containing entrapped Aeroperl$^{TM}$ porous silica micro-particles displayed small, high aspect ratio rods with the large, roughly spherical particles near the centre.

Lumpy yeast-shellac micro-rods have also been presented which have shown that with the correct morphology, lumpy micro-rods may be able to retard liquid drainage in aqueous foams. These rods are food-grade, and have great potential as additives in the food industry.

Other types of interesting rods investigated include magnetic micro-rods with entrapped magnetic particles allowing the rods to be manipulated in an external magnetic field. Clear alignment of both shellac and ethyl cellulose magnetic micro-rods was observed. ‘Ballooned’ micro-rods have also been produced. These may be produced in two different ways. Thermal degradation of sodium bicarbonate to produce ballooned ethyl cellulose micro-rods, and microwave radiation-induced localised heating of copper micro-particles which are trapped within ethyl cellulose rods giving inflated ‘bubbles’ in them.

Further work on individual types of novel lumpy or ballooned micro-rods may yield superior micro-rods for foam stabilisation use, or form the building blocks of functional materials on a macroscopic scale.

## 7.10. References


[1] C-Y. Chen, C-L. Chiang. *Mater. Lett.,* 2008, **62,** 3607.

[2] A.A. Lysenko, O.V. Astashkina, N.I. Sverdlova, A.P. Zinov'ev, N.G. Medvedeva, I.L. Kuzyakova. *Fibre Chem.*, 2007, (2), **39,** 144.

[3] R.J.B. Pinto, P.A.A.P. Marques, M.A. Martins, C.P. Neto, T. Trindade. *J. Colloid Interface Sci.* 2007, **312,** 506.

[4] R.J.B. Pinto, P.A.A.P. Marques, A.M. Barros-Timmons, T. Trindade, C.P. Neto. *Compos. Sci. Technol.,* 2008, **68,** 1088.

[5] H.C.Y. Yu, A. Argyros, G. Barton, M.A. van Eijkelenborg, C. Barbe, K. Finnie, L. Kong, F. Ladouceur, S. McNiven. *Opt. Express,* 2007, (16), **15,** 9989.

[6] G. Polacco, M.G. Cascone, L. Lazzeri, S. Ferrara, P. Giusti. *Polym. Int.,* 2002, **51,** 1464.

[7] V.N. Paunov, G. Mackenzie, S.D. Stoyanov. *J. Mater. Chem.,* 2007, **17,** 609.

[8] D. Maity, D.C. Agrawal. *J. Magn. Magn. Mater.*, 2007, **46,** 308.

# CHAPTER 8 – MICRO-ROD CAPSULES: A NOVEL METHOD FOR ENCAPSULATION OF LIQUID ADDITIVES INTO MICRO-AMPULES: PREPARATION AND CHARACTERISATION

This chapter introduces a further embodiment of the in-shear-flow dispersion solvent attrition technique used to produce novel food-grade micro-rods where here we describe novel functional rod-shaped micro-capsules in which oil additives are encapsulated in a single step process. Firstly, the technique of preparation is described and the effect of varying the production parameters on the properties of the resultant micro-rod capsules is discussed. Finally, an overview of the main achievements is presented and summarised.

Micro-encapsulation is defined as 'entrapment of a compound or a system inside a dispersed material for its immobilisation, protection, controlled release, structuration and functionalisation'.[1] Encapsulation of oils may improve their handling properties in formulations with added protection from oxidation, enzymes and adverse conditions such as low and high pH media.[2] Other advantages include the ability to mask unpleasant tastes[3] and odours, and increased stability and shelf-life.

Capsules can be fabricated in a variety of shapes, and range in size from large hollow molecules (e.g. cyclodextrin) to nano-capsules[4], micro-capsules up to macro-capsules, which, at several hundred microns to a few millimetres in size are visible to the naked eye. Furthermore, capsules can be fabricated with multiple walls or multiple cores. In matrix type capsules, the encapsulated additive is distributed throughout the structure of the capsule, rather than the conventional structure of a capsule wall and a liquid centre.

The contents of microcapsules may be released into the external media in a variety of ways. Mechanical agitation, for example in chewing gum[2], is where chewing releases encapsulated sweeteners and/or flavourings. Release may also be triggered by a change in pH or temperature, depending on the capsule wall material, and the environment in which release is to be achieved. Temperature triggered release can be achieved for capsules the walls of which are fabricated from easily melt-able materials e.g. fat crystals.

Existing methods for the production of micro-capsules include spray drying, spray cooling, fluidized bed coating and liposome entrapment. Spray drying is a widely-used, economical process.[5] Capsules are formed when a mixture of the payload and the

capsule wall material (usually as a homogeneous aqueous suspension) are atomised at a nozzle and blasted by hot air which rapidly dehydrates and dries the dispersed droplets. The dried micro-capsules are collected at the base of the spray drying apparatus. Spray chilling involves the same principle except that the atomised mixture of payload and capsule wall material is chilled to solidify the wall (usually vegetable oil) and capsules produced using this technique can release their payloads by melting. One disadvantage of the spray drying/freezing techniques however is the low percentage of payload incorporated within the capsules produced. Normally only 20 – 30% of the capsule material is payload, with the rest being wall material.[6] Fluidised bed encapsulation involves the coating of solid particles which are suspended in a chamber of fast moving, hot air, by finely dispersed wall material. If the capsule wall material has been dissolved in a volatile solvent then it can then be solidified by further heating. If the material is a hot melt, it can be solidified by cooling.[7] Micro-capsules produced by the fluidised bed method are commonly used in dried foods, and the capsule payloads may be released by heating or by hydration. Liposome entrapment involves the capture of a liquid active ingredient by either single or multiple lipid bi-layers and this may be achieved by emulsification, as lipids can behave as surface-active agents. Lipids such as lecithin, which is derived from egg-yolk, also have the advantage of being food grade materials. The permeability of the liposomes can be varied according to the number of lipid bilayers and the type of lipids chosen. This gives great flexibility over the encapsulation and release characteristics of liposomes.[2] The disadvantage of using liposomes for encapsulation is their limited shelf-life.

Micro-encapsulation technology is an ever-advancing field of great interest, and new methods to increase efficiency and lower costs are being presented all the time. Here we present a novel method to produce anisotropic micro-capsules in a single step process from inexpensive, food-grade materials. Such capsules could have great potential utility in the food industry due to food-grade properties and also have the additional function of foam stabilising agents. Further investigation into capsule properties such as permeability and release profiles could yield viable micro-capsules with dual functionality.

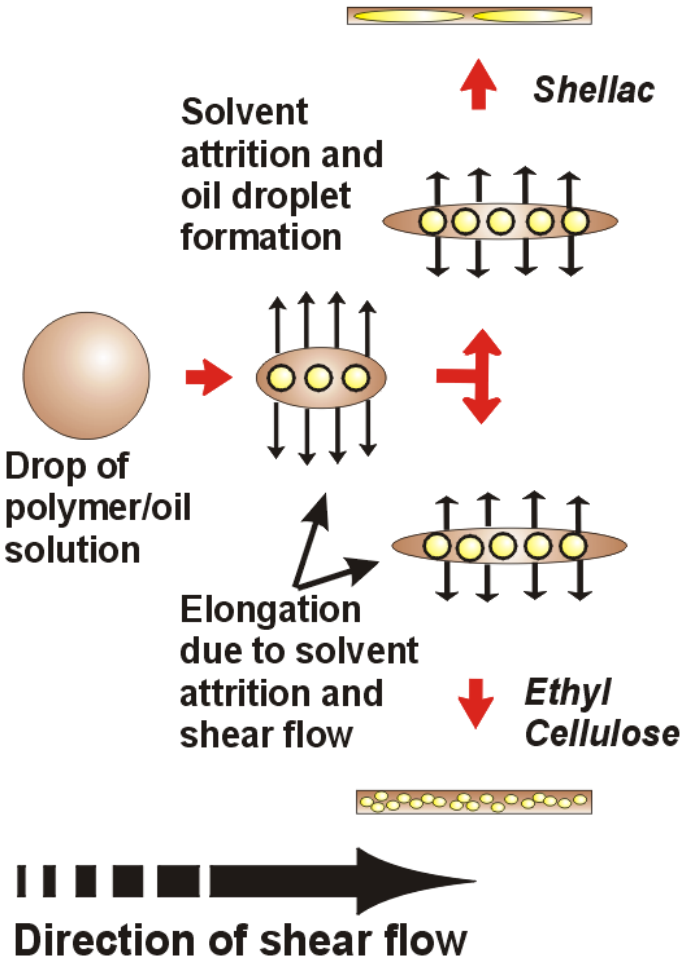


**Figure 8.1. Schematic diagram showing the main processes involved in micro-ampule formation. Large drops of polymer/oil solution in ethanol break-up on addition to the viscous glycerol-water mixture continuous phase under shear. The droplets are elongated in the direction of the shear flow, and (micro-rod polymer) solvent is transferred from the drops into the continuous phase. As the solvent concentration lowers, drops of the oil which is insoluble and immiscible with the continuous phase become trapped within the elongating and solidifying polymer rods leading to the formation of micro-rod ampules containing compartments of oil.**

### 8.1. Micro-rod capsules – method of preparation

The procedure for the production of micro-rod capsules is simple and has only one step in addition to the protocol required to produce polymer micro-rods.[8,9,10] Once a solution of the polymer in the appropriate solvent has been made, the required volume of oil is added to the mixture which is injected into the continuous phase under shear.[11] The drops of the encapsulated oil become trapped within the micro-rods as the polymer solvent transfers to the continuous phase by a solvent attrition process. This leads to the formation of micro-rod capsules, with large compartments of encapsulated oil or smaller pockets throughout the structure of the rod, like a matrix or multi-core-style capsule.[2] The reason for these differences depends on the affinity between the encapsulated oil and the micro-rod polymer. The system minimises the interfacial area between the two phases if they have a poor affinity for each other, i.e. higher interfacial tension. A schematic diagram showing the main processed involved on the production of micro-rod capsules is shown below.

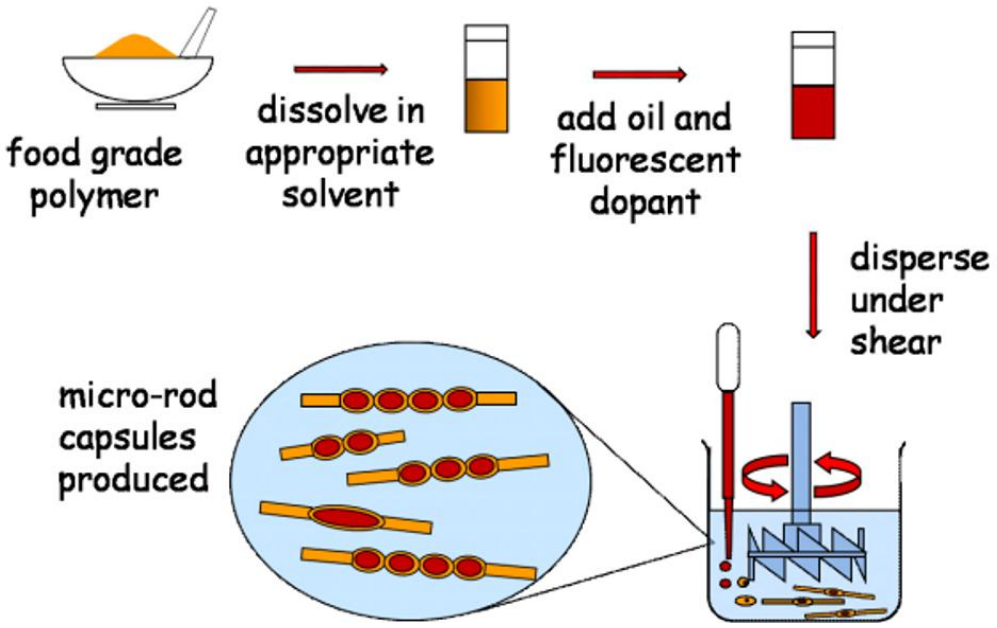


**Figure 8.2. Schematic diagram depicting the main processes involved in the formation of micro-rod capsules. The oil to be encapsulated is manually mixed with the dispersed phase, and becomes trapped within the micro-rods as they form as a result of the in-shear-flow dispersion solvent attrition technique used.**

## 8.2. Effect of oil type on success of encapsulation

In these experiments a number of oils types with differing molecular weights and hydrophobicities where investigated to provide potential models of oils which could be used in food formulations.

### 8.2.1. Encapsulation of model oils - squalane

Squalane, a branched hydrocarbon was incorporated in shellac micro-rods at 17 wt.% using the protocol outlined above (50 wt.% shellac in ethanol dispersed phase solution used). Fig. 8.3 shows lumpy areas in the micro-rods where relatively large pockets of the oil have been trapped.

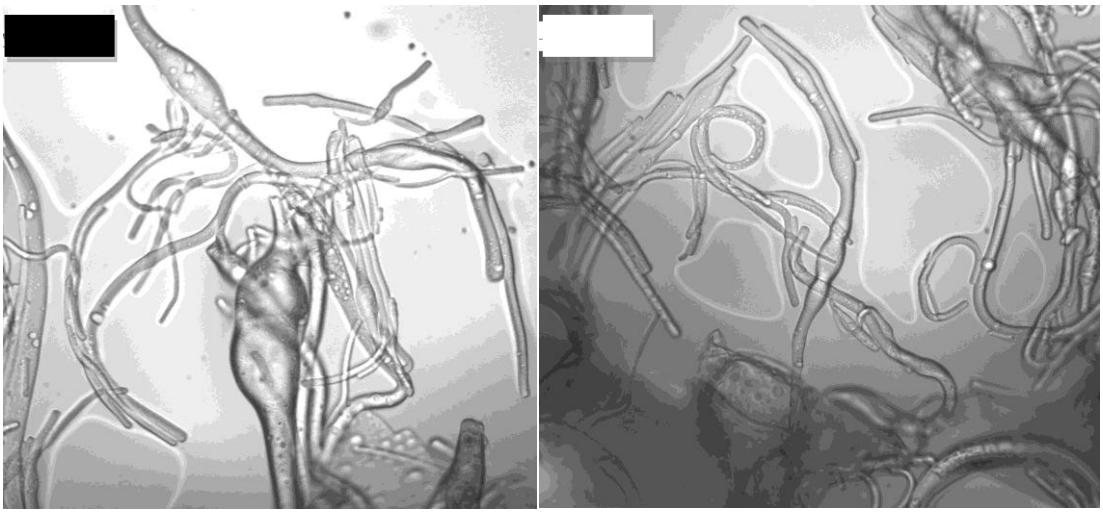

**Figure 8.3. Optical microscopy images of shellac micro-ampules containing 17 wt.% encapsulated squalane. The oil appears to be trapped in long compartments along the length of the micro-rods. Scale bars are 25 µm.**

### 8.2.2. Undecane

Undecane (Aldrich) was added to a 30 wt.% ethyl cellulose in acetone dispersed phase solution to produce micro-rods with 50 wt.% encapsulated undecane. Fig. 8.4 shows that micro-rod morphology has not been altered noticeably, but that the oil seems to have been incorporated within the micro-rods as much smaller droplets, spread

throughout the structure, in contrast to the situation observed in 8.2.1 with shellac/squalane micro-rod micro-capsules. The lower figure shows that these micro-rods with encapsulated oil adsorb well at the gas-liquid interface, stabilising air bubbles.

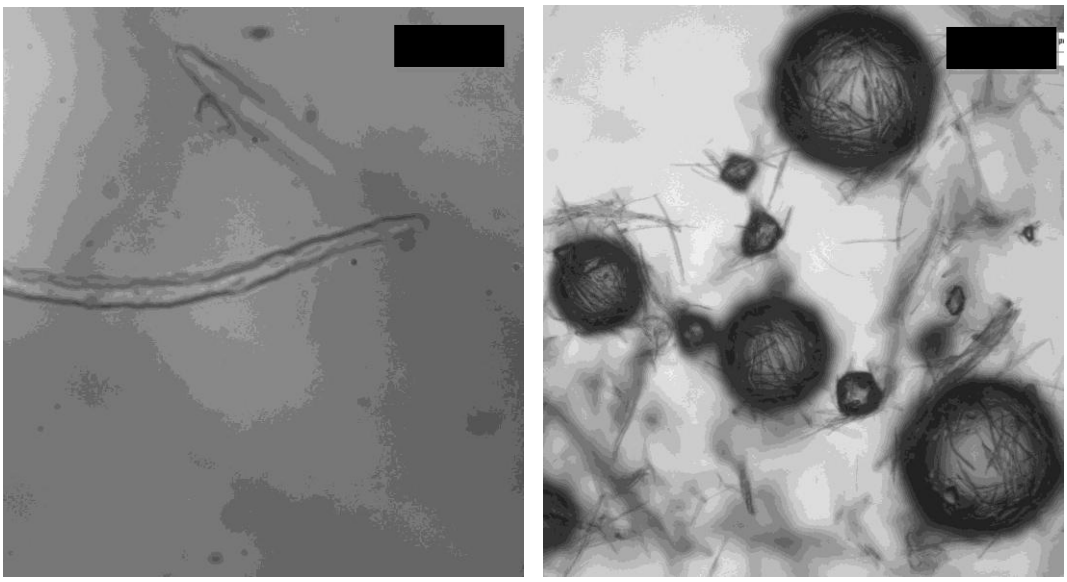

**Figure 8.4. Optical microscopy images of ethyl cellulose micro-rods containing 50 wt.% entrapped undecane. The morphology of the micro-rods remains almost unaffected despite the addition of oil and they appear to adsorb at the gas-liquid interface. Scale bars for left and right hand images are 10 μm and 100 μm respectively.**

### 8.2.3. Tricaprylin

Tricaprylin was incorporated in shellac to produce micro-rods with 40 wt.% tricaprylin content. The swollen appearance of a number of the micro-rods suggests that much of the tricaprylin has been entrapped within the shellac; however, it is also apparent that this oil has affected the micro-rod formation process acting as a co-solvent for shellac (along with ethanol). The result of this is the production of amorphous micro-rods, with larger sizes and polydispersity.

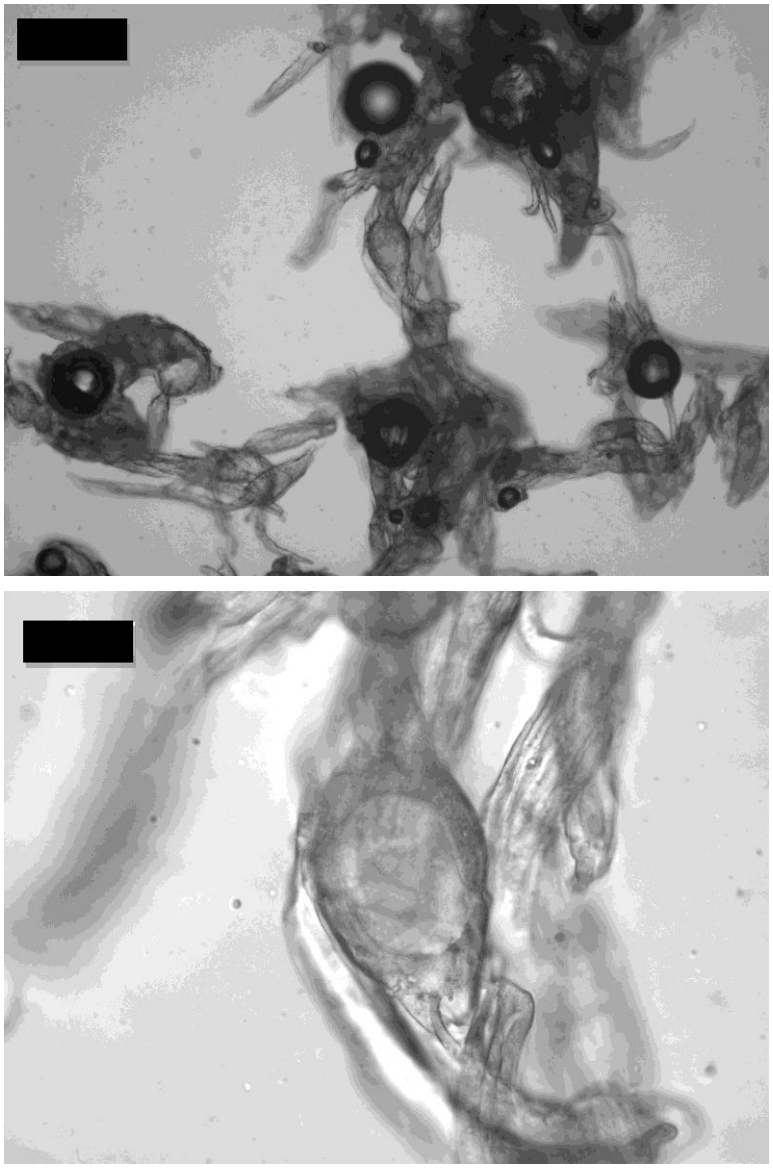

**Figure 8.5. Optical microscopy images of shellac micro-rods containing 40 wt.% tricaprylin. Some of the oil has been encapsulated within the shellac micro-rods but the quality of the micro-rods has been compromised by the possible action of tricaprylin as a co-solvent for shellac along with ethanol. Scale bars for top and bottom images are 100 μm and 25 μm respectively.**

8.2.4. Dimethylsulphoxide as a water-soluble co-solvent

50 wt.% dimethylsulphoxide (BDH Laboratories, GPR range) was added to a 30 wt.% ethyl cellulose in acetone solution to form micro-rod capsules. Many large micro-rods which had a flat, ribbon-like morphology were observed, but no pockets of encapsulated oil were observed. This suggests that the DMSO is acting as a co-solvent with acetone for the ethyl cellulose polymer. Here, the difference from section 8.2.3 is that the DMSO has dissolved in the water phase during the formation of the micro-rods.

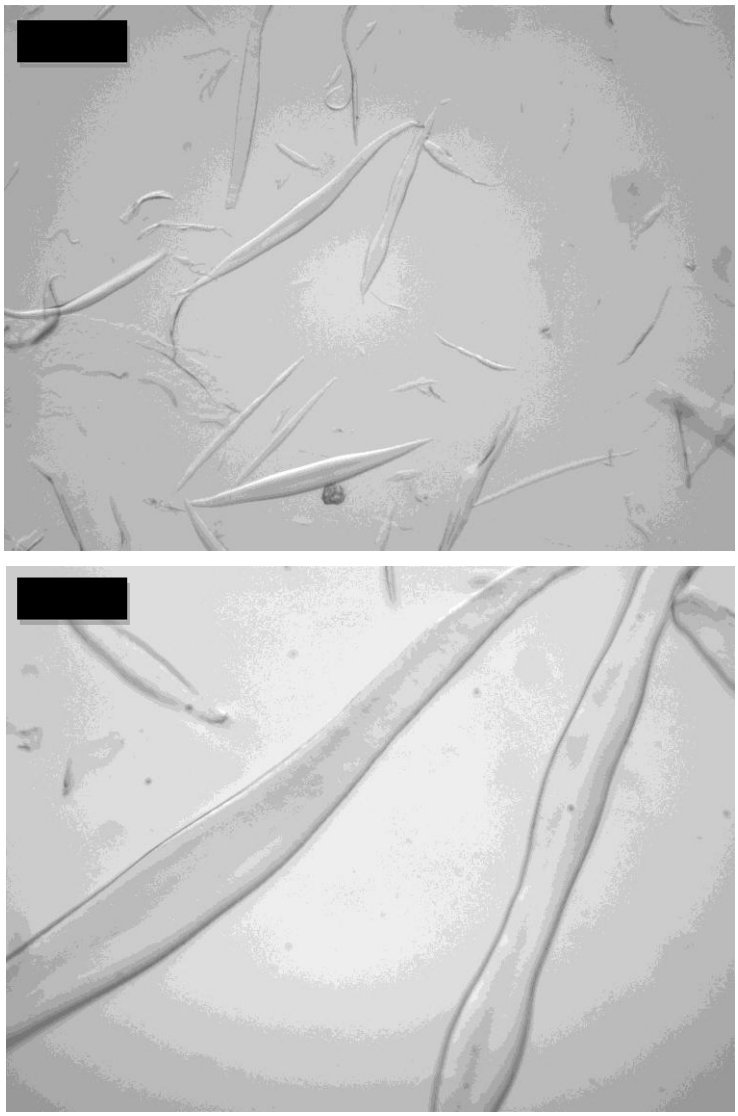

**Figure 8.6. Optical microscopy images of ethyl cellulose micro-rods formed in the presence of DMSO at 50 wt.% in the disperse phase. Micro-rods produced are large and flat – ribbon-like in morphology. In this case, the encapsulated oil, DMSO, is acting as a co-solvent for ethyl cellulose, and is not entrapped within the rods. Scale bars for the top and bottom images are 100 μm and 25 μm respectively.**

### 8.2.5. Isopropyl myristate

25 wt.% isopropyl myristate was added to a 30 wt.% ethyl cellulose in acetone solution to form micro-rod capsules. Fig. 8.7 shows that the oil may be distributed throughout the micro-rods as there is a speckled appearance seen under high magnification. This may indicate a better affinity between the ethyl cellulose and the encapsulated oil.

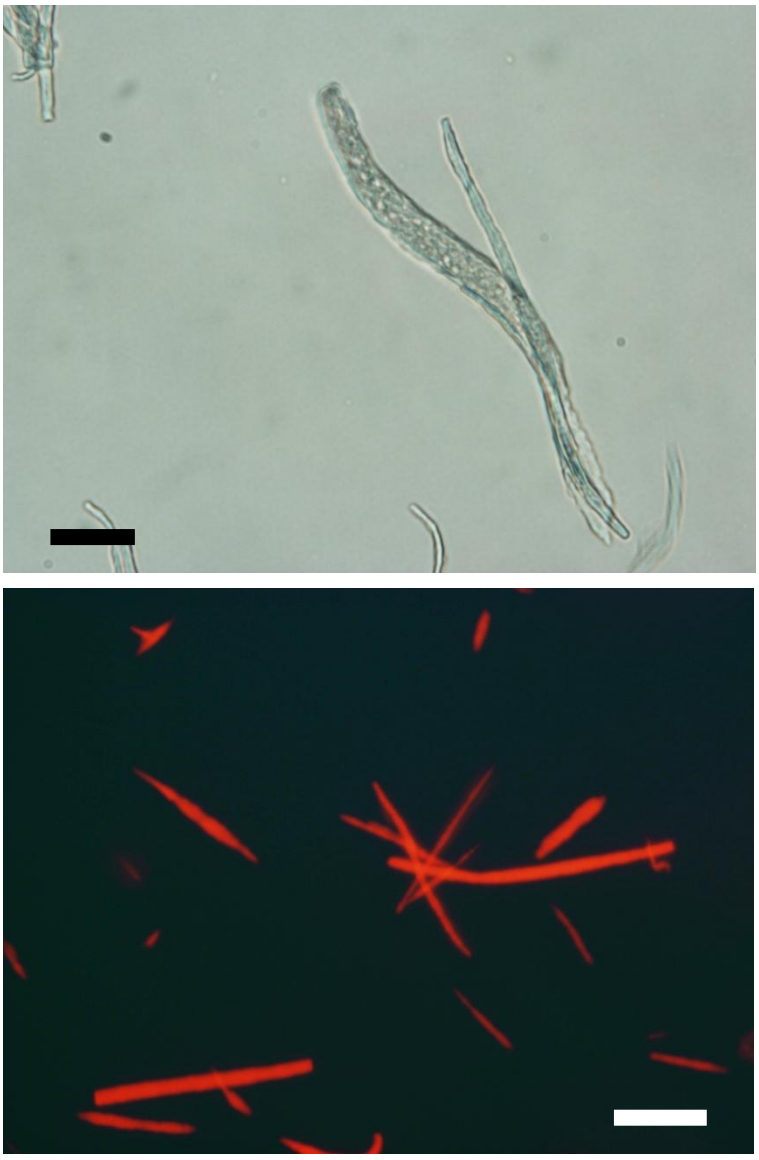

**Figure 8.7. Optical microscopy images of ethyl cellulose micro-rods containing 25 wt.% entrapped isopropyl myristate. The oil is distributed throughout the structure of the micro-rod, suggesting a good affinity between the oil and the micro-rod polymer. Fluorescence microscopy image of the same sample where the EC is stained with Nile Red dye. Scale bars for top and bottom images are 10 µm and 20 µm respectively.**

### 8.2.6. Sunflower oil

Shellac micro-rods containing encapsulated sunflower oil (from the local supermarket) were produced from a dispersed phase comprising shellac in ethanol so as to form micro-rod capsules with 25 wt.% encapsulated sunflower oil. All other production conditions were the same as those described in section 8.1.

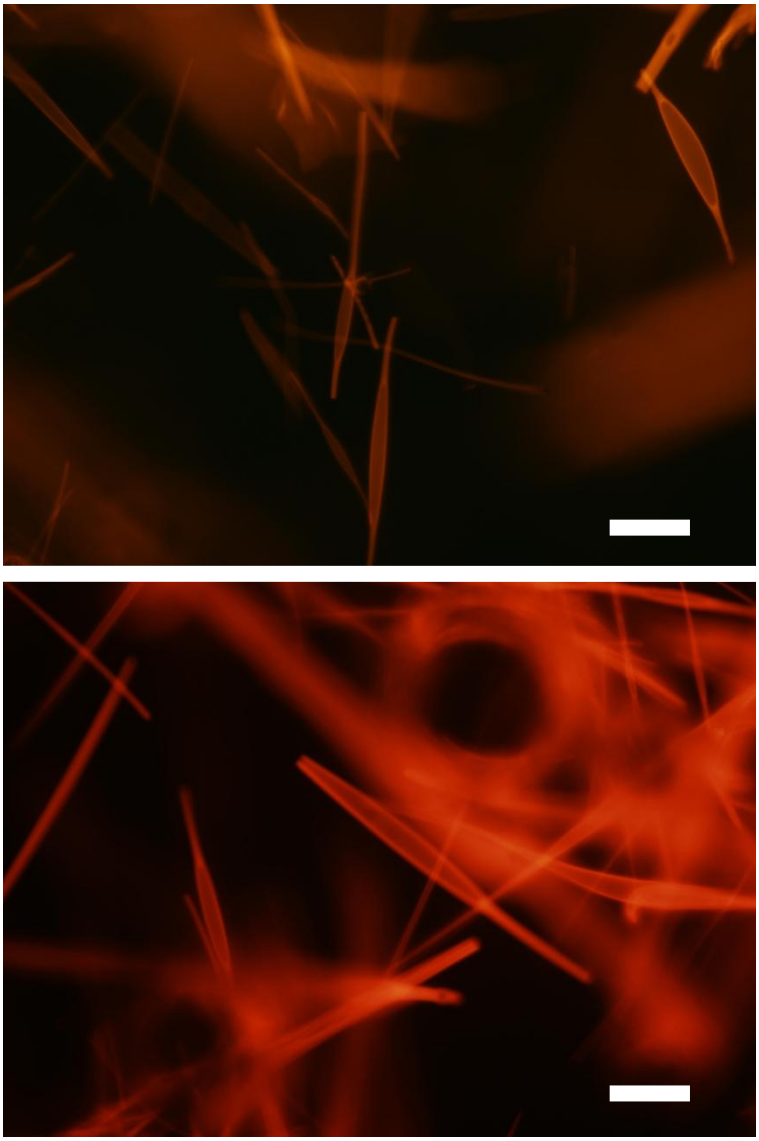

**Figure 8.8. Fluorescence microscopy images of shellac micro-rod capsules containing encapsulated sunflower oil at 25 wt.% with respect to shellac weight. The micro-rods have been stained with a small amount of Nile Red. The micro-rod capsules show slender pockets of entrapped oil in small numbers, suggesting higher interfacial tension between the shellac and the sunflower oil. Scale bars are 20 μm.**

At stirrer speeds below 1,000 rpm, large micro-rods with poor sample uniformity were produced. The main observation at all speeds with the combination of sunflower oil and shellac wax was the smaller number of pockets of encapsulated oil within the micro-rods, and their large size compared with the much smaller pockets of trapped oil seen in other shellac/oil combinations.

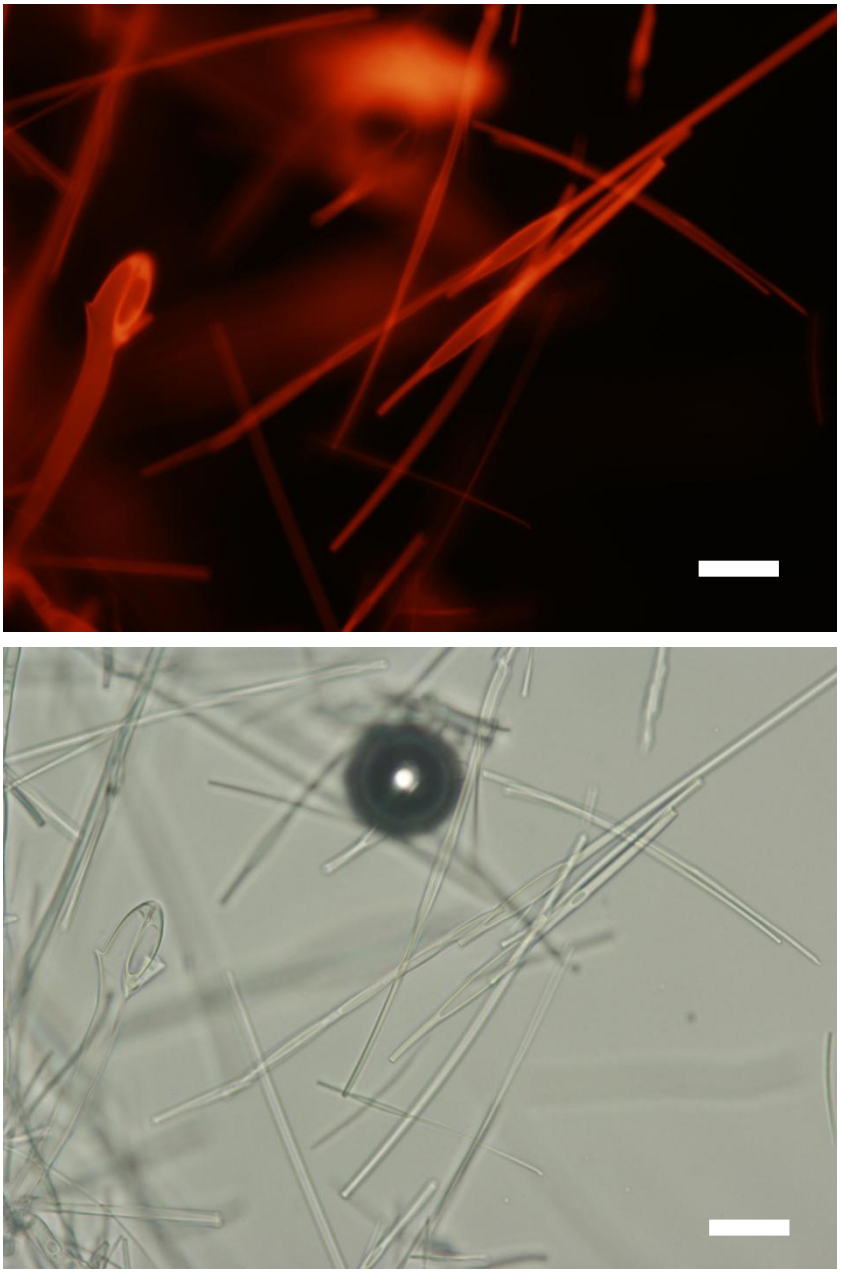

**Figure 8.9. Fluorescence and optical microscopy images of shellac micro-rods containing 25 wt.% added sunflower oil with respect to shellac. For the fluorescence microscopy image the micro-rods have been stained with a small amount of Nile Red. The capsules have very high aspect ratios. Scale bars are equal to 20 µm.**

### 8.2.7. Cod liver oil

Cod liver oil (obtained from a local chemist store) was encapsulated within shellac micro-rod capsules. This is potentially useful for food formulations to mask the unpleasant odour of the cod liver oil and to protect it from oxidation. The oil was added to the disperse phase resulting in micro-rod capsules containing 38 wt.% entrapped oil.

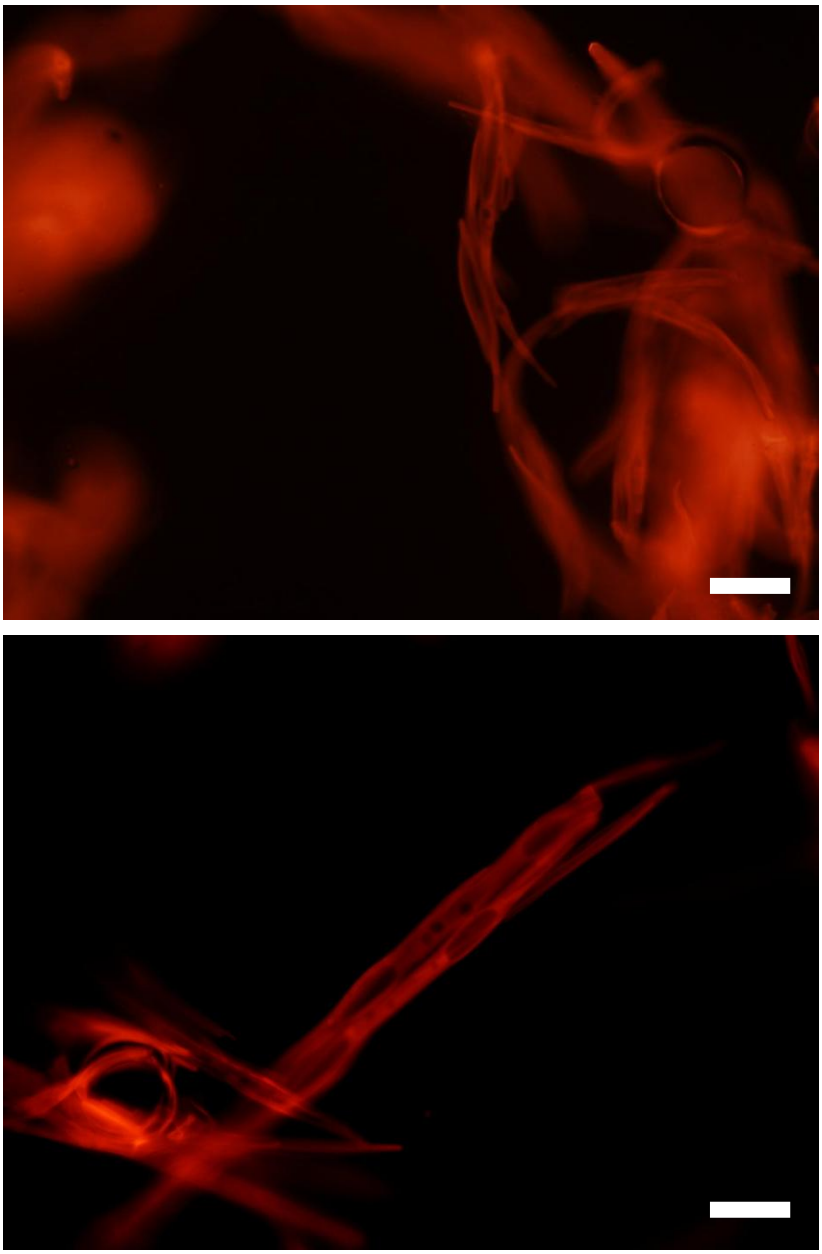

**Figure 8.10. Fluorescence microscopy images of shellac micro-rod capsules containing encapsulated cod liver oil at 38 wt.% with respect to shellac weight. The micro-rods have been stained with a small amount of Nile Red. Scale bars are 25 µm.**

### 8.3. Effect of the oil concentration on the resultant micro-rod capsules

The micro-rod capsules produced so far using ethyl cellulose as a template have resulted in micro-rods where the entrapped oil is spread throughout the structure. They resemble a multi-core-type capsule[2] rather than a conventional one with a single liquid core. Figs. 8.11 and 8.12 show that oil is distributed throughout the micro-rods but also appears to be leaching out. Such characteristics could yield micro-rods of variable wettability by altering the concentration of encapsulated oil, behaviour analogous to a series of silicas of varied hydrophobicity with different levels of surface hydrophobisation by DCDMS (dichloro-dimethyl silane).

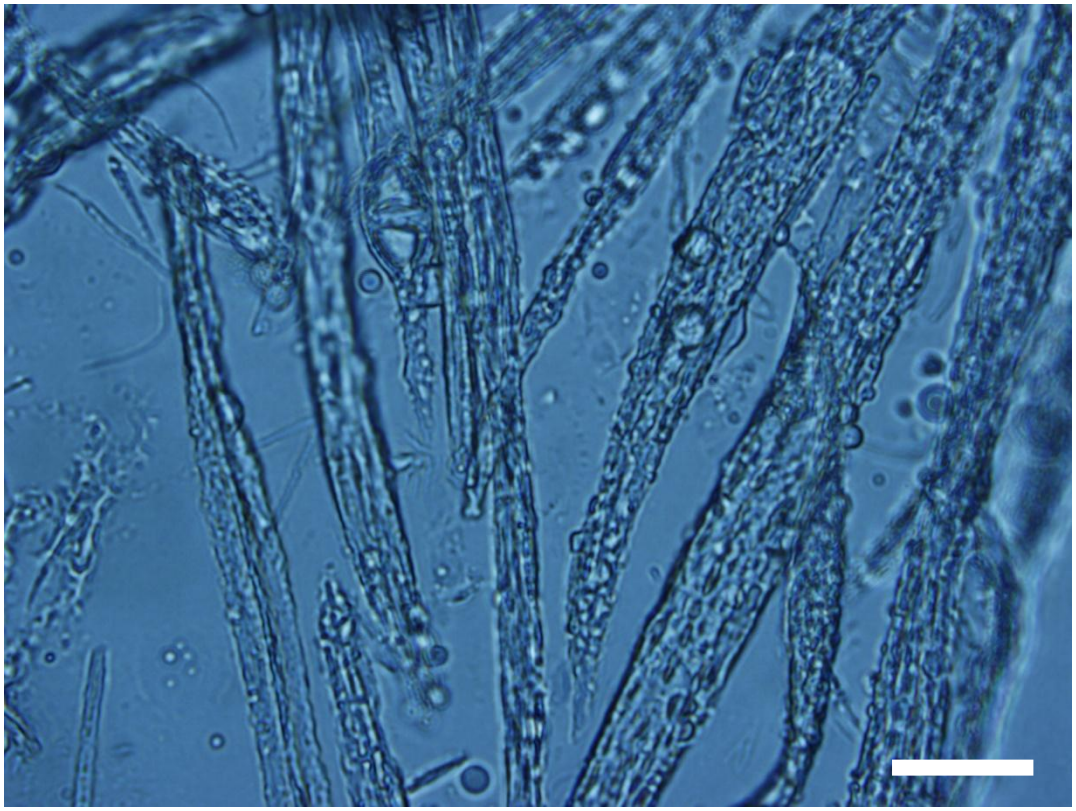

**Figure 8.11. Optical microscopy image of ethyl cellulose micro-rods containing 50 wt.% squalane which is dispersed throughout the micro-rods, rather than as a smaller number of larger encapsulated pockets of oil. The oil can be seen leaching out of the micro-rods, which would potentially increase their hydrophobic character. Scale bar is 20 μm.**

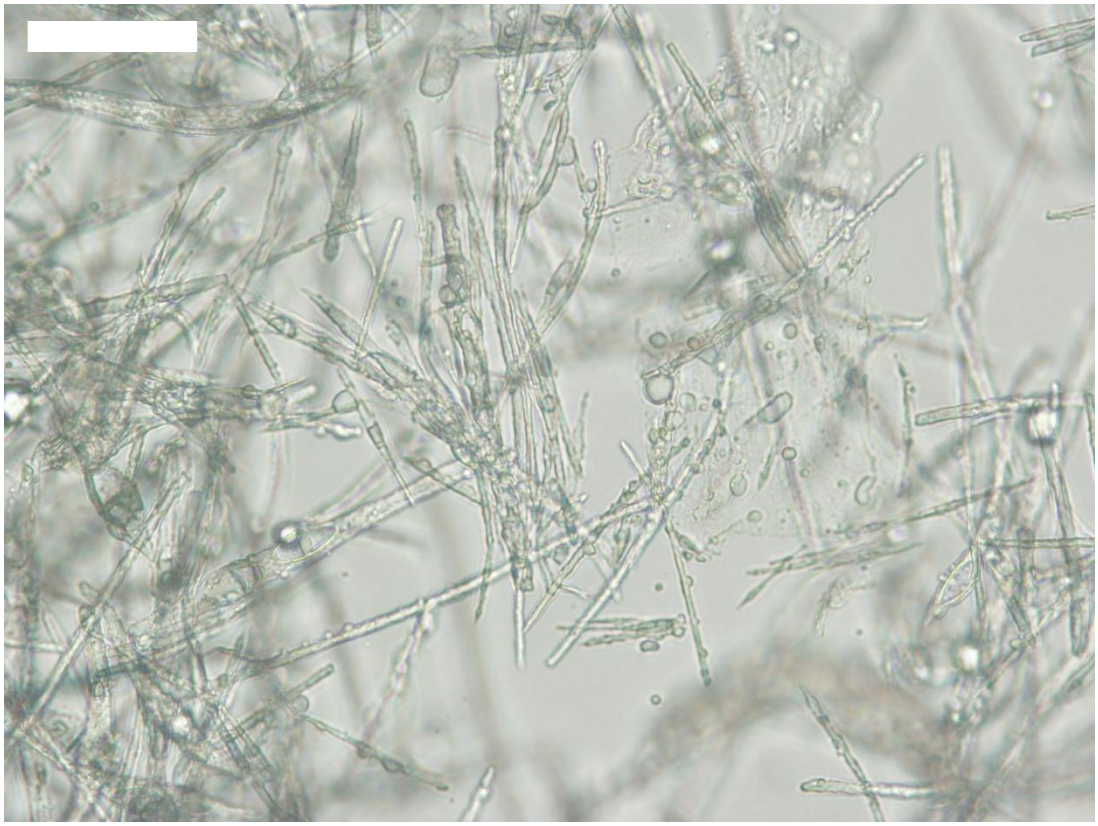

**Figure 8.12. Optical microscopy image of ethyl cellulose micro-rods containing 50 wt.% squalane. Scale bar is 50 µm.**

## 8.4. Effect of addition of surfactants on the properties of the resultant micro-rod capsules

This technique was then extended to examine the effect of the addition of surfactants to the dispersed phase on the resultant micro-rod capsules. The idea is to investigate if the interfacial tension between the capsule polymer and the encapsulated oil was responsible for the interior structure of the micro-capsule. Using the method described in experimental section 2.3.4, 2 batches of shellac micro-rod capsules were produced which contained 25 wt.% encapsulated sunflower oil (w.r.t. shellac weight). To one batch, 10 wt.% Span 85 surfactant was added to the sunflower oil in order to check the affinity between the encapsulated oil and the micro-rod polymer. Span 85 (sorbitan trioleate) is a low HLB (oil soluble) non-ionic surfactant which was chosen as it mixes well with the sunflower oil. Fig. 8.13 shows the micro-rod capsules produced, firstly, with no added surfactant, and then with Span 85 added (fig. 8.14).

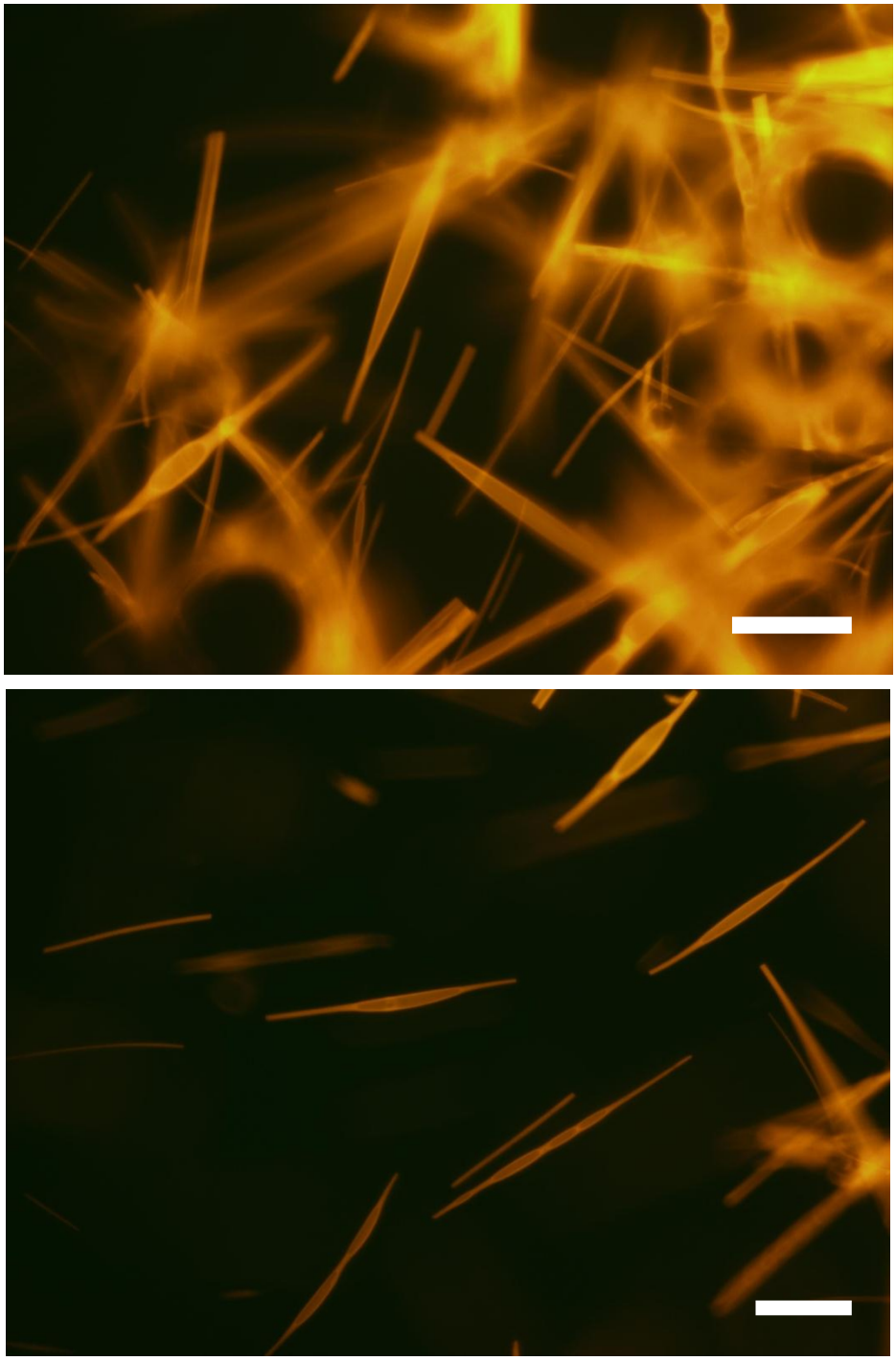

**Figure 8.13. Fluorescence microscopy images of shellac micro-rod capsules containing encapsulated sunflower oil at 25 wt.% with respect to shellac weight. The micro-rods have been stained with a small amount of Nile Red. The sunflower oil is trapped in large pockets within the rods, suggesting that the affinity between the oil and the micro-rod polymer is poor, i.e. the interfacial tension between them is high. Scale bars are equal to 20 μm.**

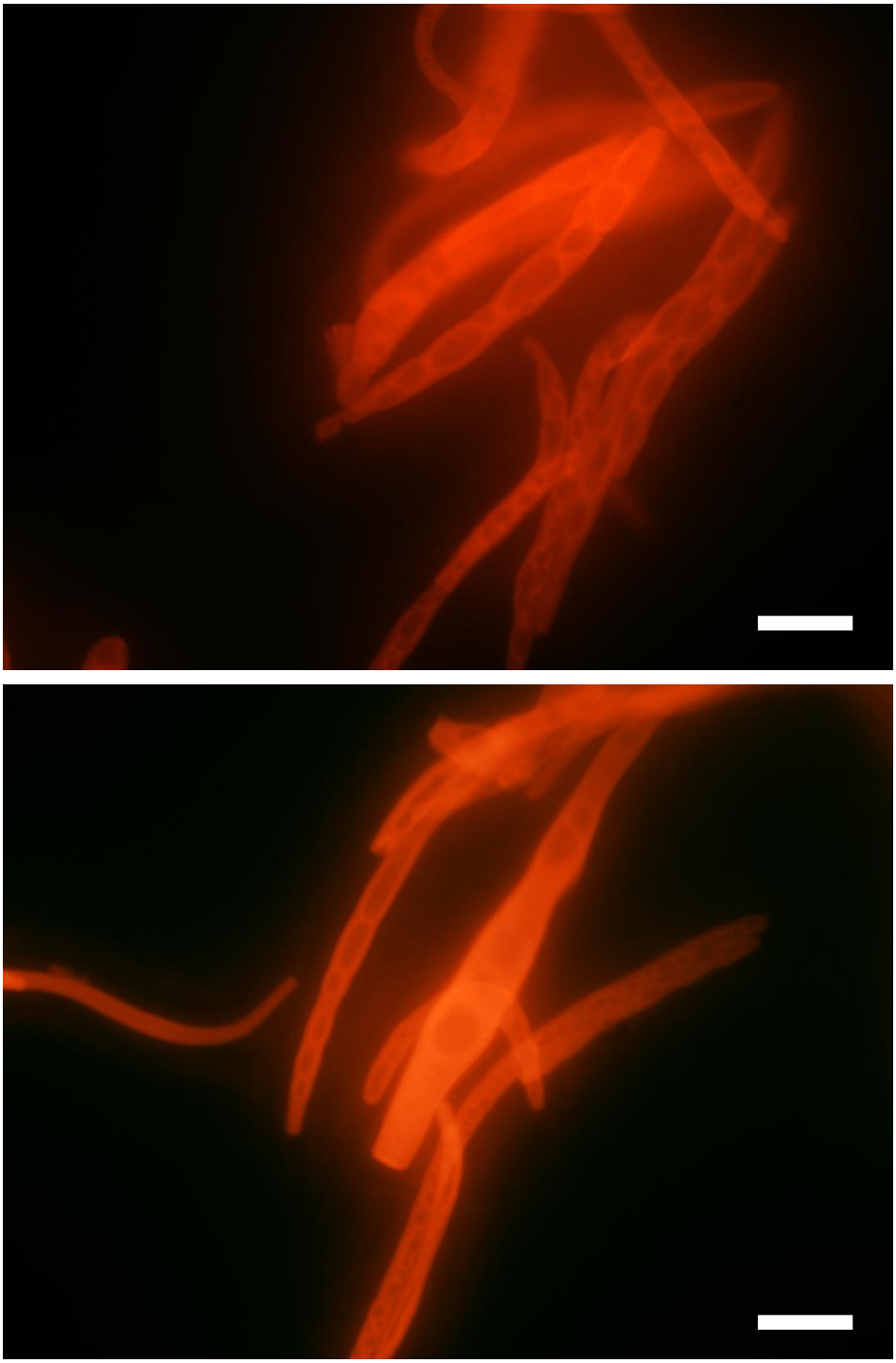

**Figure 8.14. Fluorescence microscopy images of shellac micro-rod capsules containing 25 wt.% encapsulated sunflower oil and Span 85 (at 10 wt.% with respect to the weight of sunflower oil). The micro-rods have been stained with a small amount of Nile Red. The pockets of sunflower oil within the micro-rods are smaller and more numerous than in the capsules with no added surfactant, suggesting that the surfactant may have altered the affinity between the oil and the shellac thus reducing the interfacial tension between them. Scale bars are 20 μm.**

It is apparent that in these examples, added surfactant has led to the formation of an increased number of smaller pockets of oil within shellac micro-rod capsules. This may be due to a lowering of interfacial tension between the capsule wall material (shellac) and the entrapped oil, reducing the tendency of the system to try to minimize the interfacial area between the two phases. Similar experiments were conducted using ethyl cellulose micro-rod capsules and a range of surfactants. Span 85, and also Tween 20 and Tween 60 (polyoxyethylene sorbitan monolaurate and polyoxyethylene sorbitan stearate respectively) were incorporated to investigate any changes in the morphology of the micro-rod capsules due to lowering of interfacial tensions affecting the way in which the entrapped oil was encapsulated. However we did not observe any visible differences in the morphologies of the produced micro-capsules.

### 8.5. Effect of capsule wall polymer on properties of resultant micro-rod capsules

Results presented thus far in this chapter illustrate that the appearance of micro-rod capsules differs greatly depending on the material used as the capsule wall. Ethyl cellulose micro-rod capsules demonstrated a structure with many small pockets of entrapped oil, spread evenly throughout the micro-rods (fig. 8.15) whereas shellac micro-rod capsules have shown larger pockets of encapsulated oil (fig. 8.16).

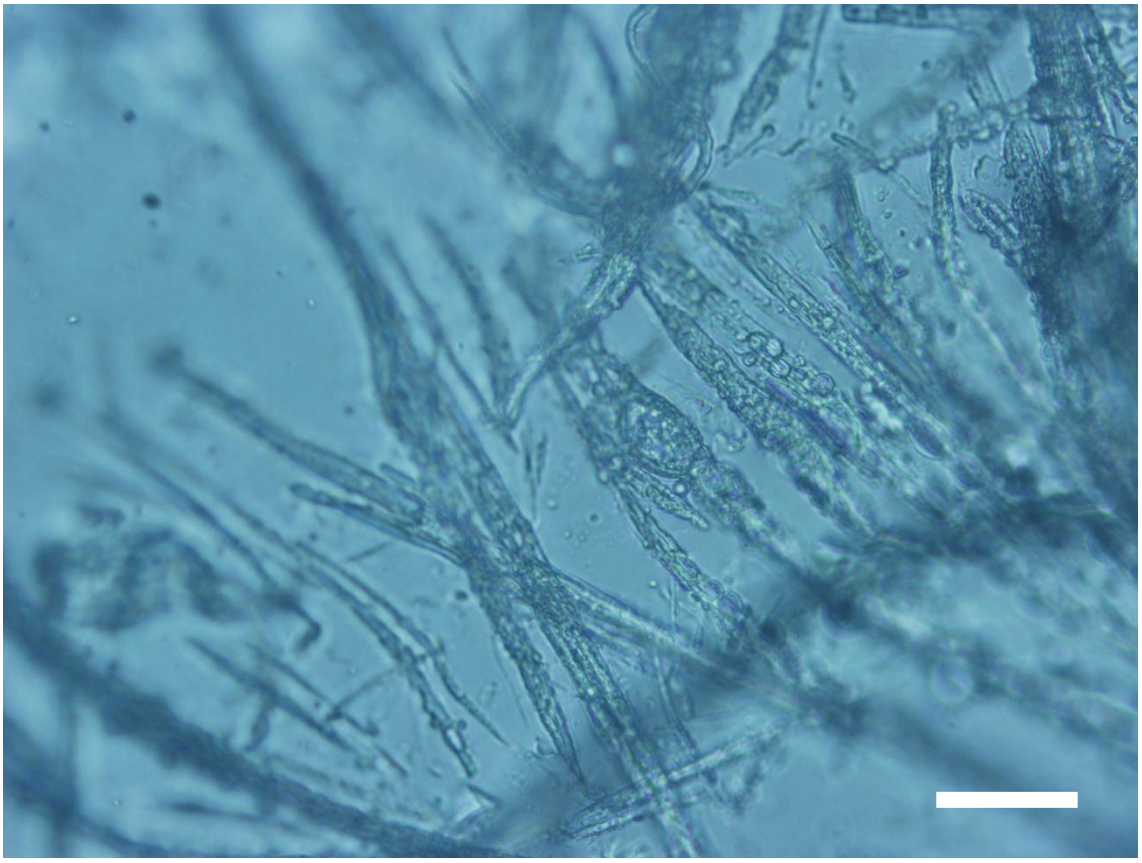

**Figure 8.15. Optical microscopy image of ethyl cellulose micro-rods containing squalane. This figure shows the type of oil entrapment observed in all of the ethyl cellulose based micro-rod capsules, where numerous but small pockets of the oil are spread throughout the structure of the micro-rods. Scale bar is 20 µm.**

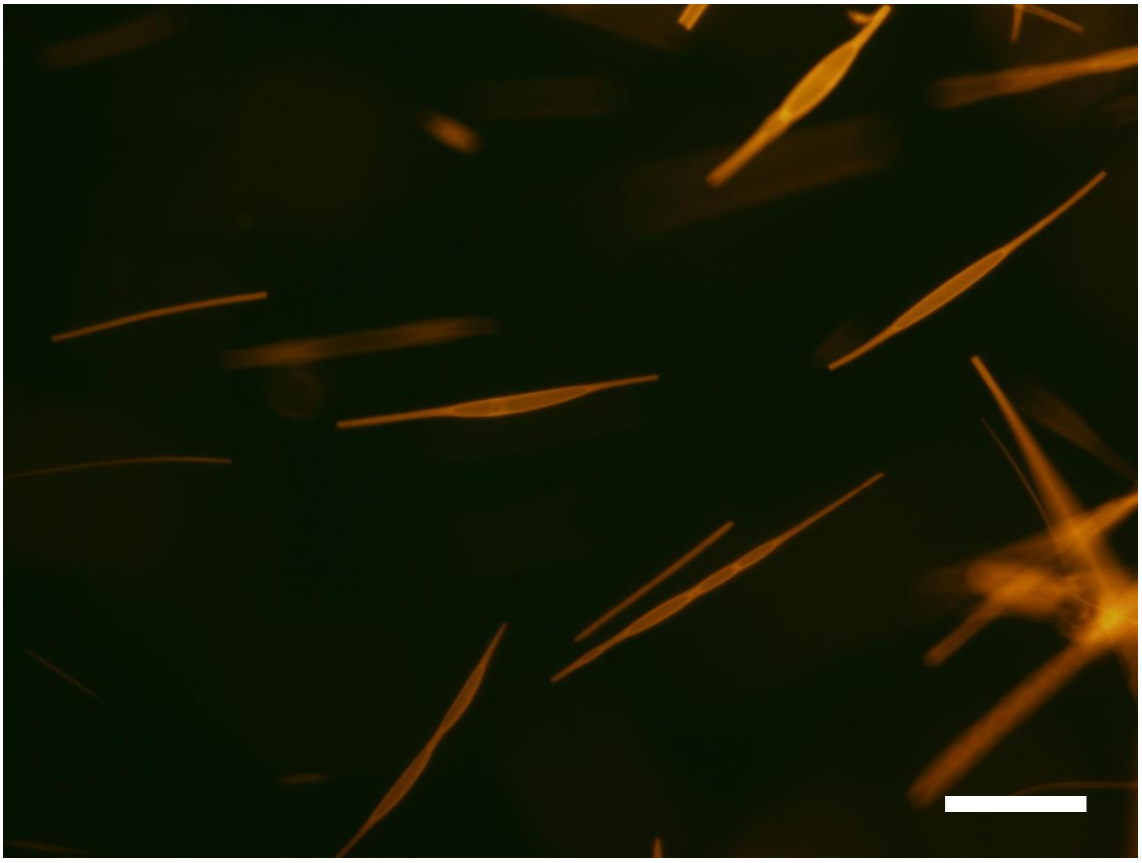

**Figure 8.16. Fluorescence microscopy images of shellac micro-rod capsules containing encapsulated sunflower oil at 25 wt.% with respect to shellac weight. The micro-rods have been stained with a small amount of Nile Red. The sunflower oil is trapped in large pockets within the micro-rods, a contrary situation to that observed with ethyl cellulose micro-rod capsules. Scale bar is 20 μm.**

These two different micro-rod capsule morphologies could be a result of the difference in affinities between ethyl cellulose and the shellac with the encapsulated oils.

### 8.6. Effect of polymer/oil ratio on micro-rod capsule properties

A shellac micro-rod capsule containing encapsulated sunflower oil was chosen as a system to investigate the effect that altering the polymer/encapsulated oil ratio on resultant micro-rod capsule size and morphology. The disperse phase concentration of shellac was varied between 30 and 60 wt.% in ethanol, prior to addition of sunflower oil. Sunflower oil (0.3 g) was added to each 1 mL shellac solution prior to dispersing it in the continuous phase under shear. This gave approximate ratios of shellac to oil of 1:1, 1:1.333, 1:1.667 and 1:2 (30 wt.%, 40 wt.%, 50 wt.% and 60 wt.% respectively). Nile Red fluorescent dopant was included to aid visualisation. Fig. 8.17 shows an optical microscope image of the disperse phase mixture of sunflower oil and shellac in ethanol solution.

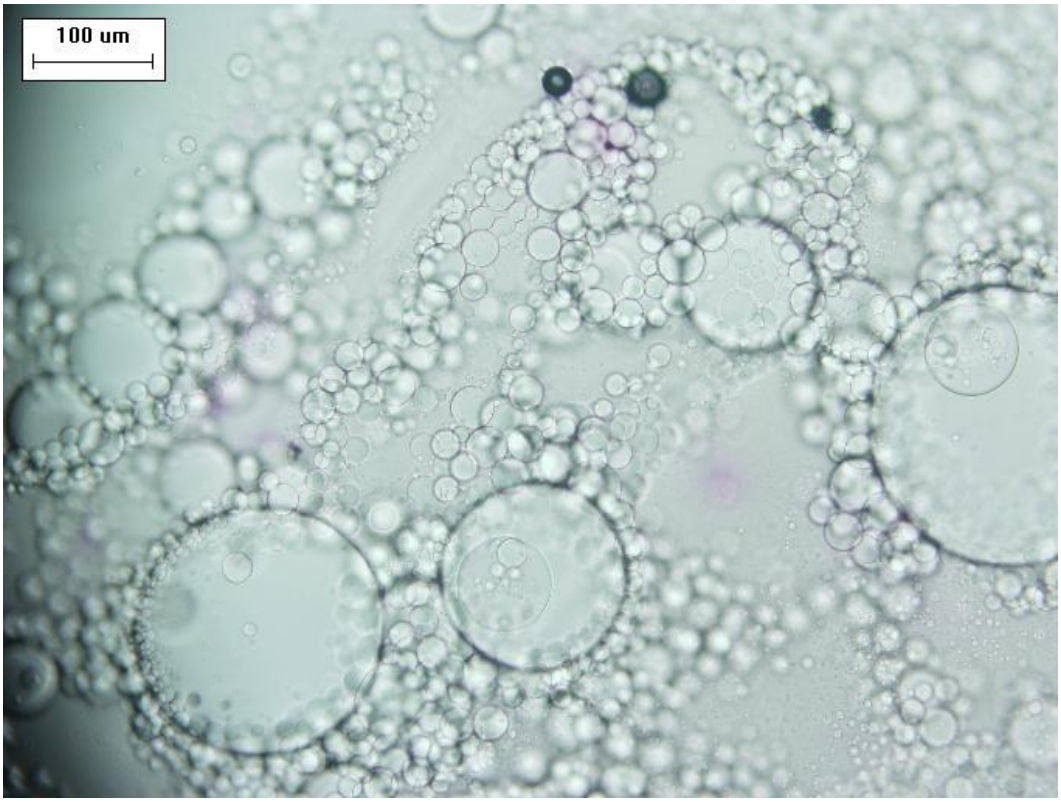


**Figure 8.17. Optical microscopy image of disperse phase mixture used in the production of micro-rod capsules including shellac and sunflower oil. Scale bar is 100 µm.**

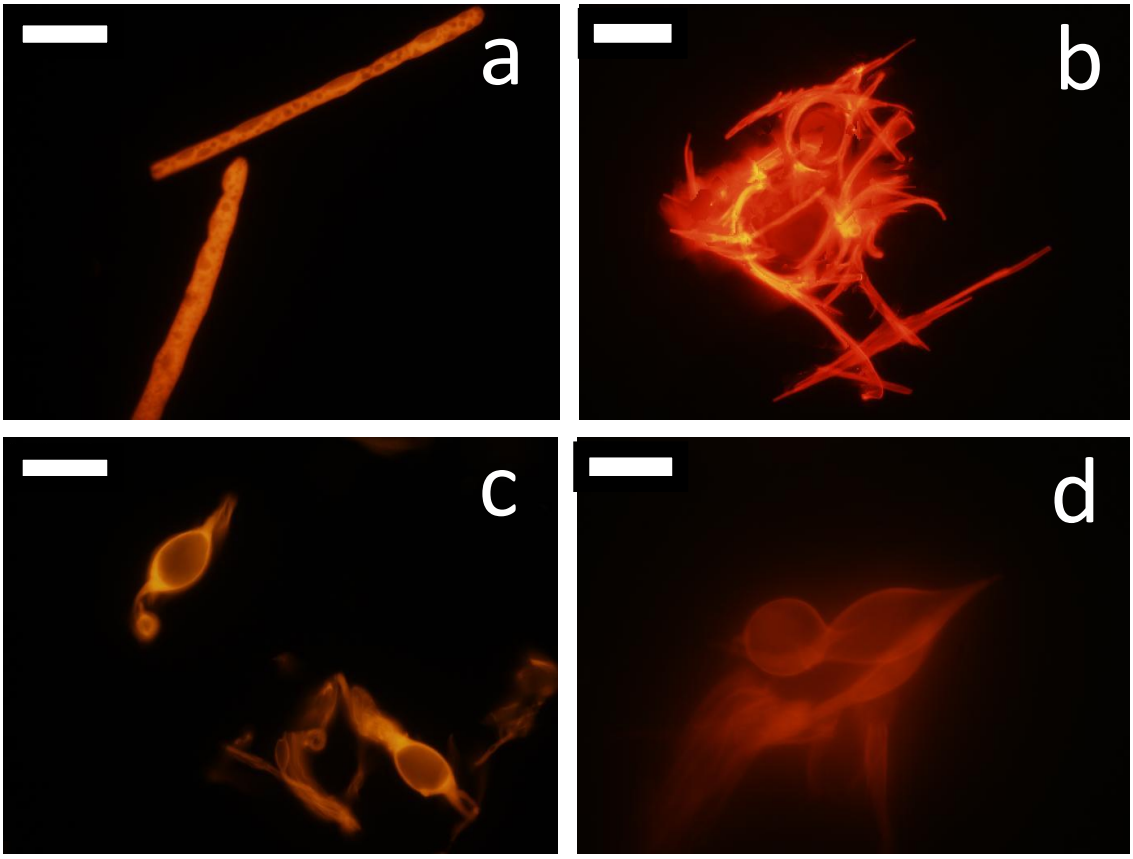


**Figure 8.18. Shellac micro-rod capsules containing approximately 33 wt.% (a), 38 wt.% (b), 43 wt.% (c) and 50 wt.% (d) encapsulated sunflower oil. The morphology of the micro-rod capsules changes from micro-rods to the form of oil drops which appear to be coated in a thin layer of shellac with increasing oil concentration. Scale bars are 25 µm (a – c) and 10 µm (d).**

Fig. 8.18 shows that as the concentration of oil (with respect to shellac) increases, the micro-rod capsules lose their rod-like morphology. Many of the capsules produced in the 50 wt.% oil sample (fig. 8.18d) appear as drops of sunflower oil surrounded by a layer of shellac. This is also observed, although to a lesser extent, in the 43 wt.% oil sample. Figs. 8.18a and b show that when 33 or 38 wt.% oil was used, the capsules obtained were much more rod-like. Fig. 8.19 shows the average lengths of the micro-rod capsules.

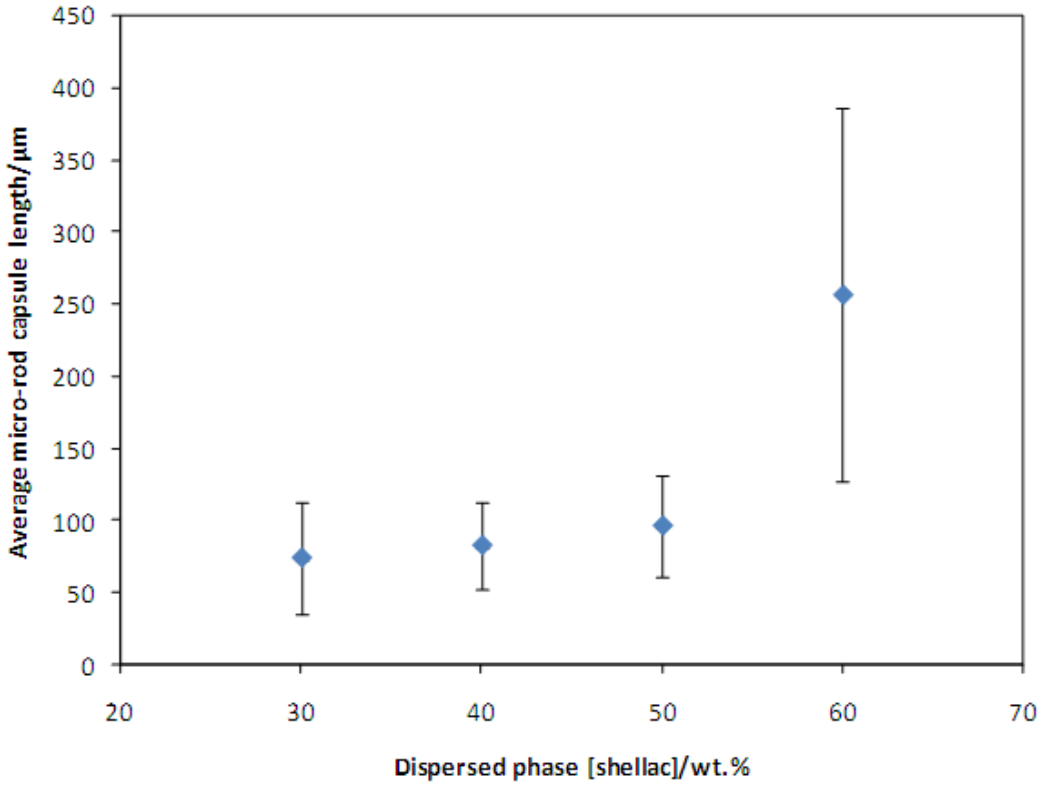


**Figure 8.22. Average micro-rod capsule length with increasing shellac concentration (with respect to sunflower oil loading). Error bars represent one standard deviation either side of the mean micro-rod capsule length. Micro-rod capsules were measured from optical micrographs containing at least 30 micro-rod capsules. Micro-rod capsule polydispersity increases dramatically at 60 wt.% shellac in ethanol concentration. This is probably due to the high viscosity of this solution causing processing problems during micro-rod capsule production.**

## 8.7. Conclusions

This chapter summarizes the author's work on micro-rod capsules. They have been fabricated from shellac and ethyl cellulose using the technique which has been demonstrated throughout this thesis as being highly successful for the production of a range of food-grade or multifunctional micro-rods for potential foam stabilisation use. The capsules were produced simply by mixing the oil desired for encapsulation in with the dispersed phase prior to addition to the continuous phase under shear. As the micro-rods form due to solvent attrition and shear-induced droplet elongation processes, the incorporated oils can become trapped within the rods, giving rise to micro-rod capsules.

A range of oils were incorporated within the dispersed phase for the production of micro-rod capsules. A principle observation of the micro-rod capsules was the tendency to contain few but large pockets of entrapped oil, whereas others contained large numbers of smaller pockets distributed throughout the micro-rods. This appeared to be quite dependent on whether ethyl cellulose or shellac was used as the capsule wall material which could be due to the different affinities of these materials for the entrapped oils. More typically for shellac micro-rod capsules, the size and number of pockets of entrapped oil can be altered with the addition of surfactants, such as Span 85. This suggests that the interfacial tension between the micro-rod polymer solution and the encapsulated oil controls the way in which the oil is distributed within the micro-rod capsules.

Finally, it was also observed that variation in the ratio of encapsulated oil to micro-rod capsule wall polymer gave rise to capsules of different size and morphologies. Capsules with high oil concentrations loose their rod-like shape, and are shorter than those with less entrapped oil.

It should be stressed that this chapter is an introductory work describing multifunctional micro-rod capsules produced in a novel way, which could have potential for encapsulation of food grade materials and for delivering environment-sensitive or unpleasant-tasting/smelling additives in food formulations. They could also serve an additional function of foam stabilising agents. Further studies could include more characterisation and foaming tests, for example a comparison between the foam stabilising abilities of ethyl cellulose micro-rods and oily ethyl cellulose micro-rods containing squalane, and also tests on micro-rod capsule permeability and release of entrapped ingredients.

## 8.8. References


[1] D. Poncelet. In *Surface Chemistry in Biomedical and Environmental Science*, pgs 23 – 34, J.P. Blitz and V.M. Gun'ko (eds.) 2006, Springer.

[2] B.F. Gibbs, S. Kermasha, I. Alli, C.N. Mulligan. *Int. J. Food Sci. Nutr.*, 1999, **50,** 213.

[3] L.S. Jackson, K. Lee. *Lebensm. – Wiss. Technol.*, 1991, **24,** (4), 289.

[4] N. Parris, P.H. Cooke, K.B. Hicks, *J. Agric. Food Chem.*, 2005, **53,** 4788.

[5] A. Gharsallaoui, G. Roudant, O. Chambin, A. Voilley, R. Saurel. *Food Res. Int.*, 2007, **40,** 1107.

[6] C. Theis. *In Microencapsulation. Methods and Industrial Applications*, S. Benita (ed.) 1996, Marcel Dekker, New York.

[7] S. Gouin. *Trends in Food Sci. & Tech.* 2004, **15,** 330.

[8] R.G. Alargova, D.S. Warhadpande, V.N. Paunov, O.D. Velev. *Langmuir*, 2004, **20,** 10371.

[9] R.G. Alargova, K.H. Bhatt, V.N. Paunov, O.D.Velev, *Adv. Mater.*, 2004, **16,** 1653.

[10] R.G. Alargova, V.N. Paunov, O.D.Velev, *Langmuir*, 2006, **22,** 765.

[11] A.L. Campbell, B.L.Holt, S.D. Stoyanov, V.N. Paunov. *J. Mater. Chem*, 2008, **18,** 4074.

# CHAPTER 9 – SUMMARY OF MAIN ACHIEVEMENTS, CONCLUSIONS AND FUTURE WORK

This thesis has focussed on the fabrication and use of anisotropic micro-rods for foam stabilisation with applications in food formulations. We used acidic hydrolysis of Nata de Coco bacterial cellulose to form cellulose nano-rods which were applied as a foam scaffolding material. We also used a combination of in-shear-flow dispersion and solvent attrition techniques to form micro-rods from edible polymeric materials, such as shellac, ethyl cellulose and zein. Characterisation and modification of Nata de Coco nano-rods is described in chapter 3, while chapters 4, 5 and 6 are concerned with the characterisation of the properties of shellac, ethyl cellulose and zein micro-rods respectively as well as their foam stabilisation ability. Chapters 7 and 8 cover some further developments of this approach used to produce polymer micro-rods. Here, novel multi-functional micro-rods with altered morphology for potentially improved foamability and foam stability and micro-rods with encapsulated oil ('micro-ampules') are described. A concise summary of this work is presented below, followed by suggestions for future directions of research.

1. We produced cellulose nano-rods by sulphuric acid hydrolysis of native, gelatinous Nata de Coco and characterised their morphology by SEM, TEM and PCS (for size and ζ-potential evaluation). These nano-rods possessed a negative surface charge, due to grafting of sulphate ester groups deposited during the hydrolysis process. It was found that this charge could be altered by changing the hydrolysis temperature, time and acid concentration, attributable to grafting of more or less sulphate ester groups to the cellulose surface. This was in agreement with behaviour observed in the literature for cotton fibres. The cellulose nano-rods did not foam well, even after coating them with a layer of positively-charged polyelectrolyte. Modest foaming was observed when the cellulose nano-rods were coated in a thin layer of shellac wax via the use of a solvent change technique. Coating of the nano-rods with ethyl cellulose gave superior foamability and foam stability in excess of that observed with foams stabilised by a mixture of cellulose nano-rods and ethyl cellulose nano-particles due to a 'foam scaffolding' effect. The latter is due to hydrogen-bond formation between ethyl cellulose nano-particles on the air-water interface and the hydrophilic cellulose nano-rods in the foams films and channels.

2. Shellac, ethyl cellulose and zein polymer micro-rods were all successfully produced using an in-shear-flow dispersion solvent attrition technique and characterised by optical and fluorescence microscopy. The technique involves injection under shear of a dispersed phase solution of micro-rod polymer dissolved in an appropriate solvent, where the solvent is soluble in the continuous phase, but the polymer itself is not. This leads to drop elongation in the shear field and solvent attrition where the solvent in the drop transfers to the continuous phase in which it is soluble which leads to the formation of a rod-shaped polymeric particle. Control of micro-rod length and diameter was achieved by controlling the shear rate (stirrer speed or disperse phase viscosity) and dispersed phase polymer concentration.

3. We produced surface-active shellac micro-rods which proved to be effective foam stabilisers. When a foam is formed, the stabilising shellac micro-rods adhere strongly to each other, forming a solid matrix structure, which remains indefinitely stable. However, aqueous suspensions of shellac micro-rods have a limited shelf-life due to the tendency of the rods to aggregate.

4. By varying the fabrication parameters and the type of solvent, a range of ethyl cellulose micro-rods of various morphologies were produced, starting from long, thin strings and ending with large, flat ribbons and micro-rods respectively. It was found that the increasing of the salinity or the lowering of the pH gave enhanced foamability and foam stability. Once formed these foams were stable in closed containers for up to several weeks. These micro-rods were also successfully used as emulsion stabilisers, and formed coarse water-in-undecane emulsions that were stable for several days in closed containers at room temperature. Optical microscopy revealed the intertwining of micro-rods adsorbed at the interface. Upon evaporation of the volatile oil phase the ethyl cellulose micro-rods alone can prevent the water drops from coalescing. However, further evaporation of the water phase did not produce free-standing ethyl cellulose supported porous structures.

5. Using the in-shear dispersion and solvent attrition method we produced micro-rods from the maize prolamine zein, the dispersion of which was aided by addition of water to the dispersed phase. Zein micro-rods showed relatively good foamability around the isoelectric point of zein (pH 6.8), and this did not change upon addition

of NaCl. Best foamability was observed when shellac was incorporated into zein fibres at 10 – 20 wt.%. Foamability was improved noticeably, with foams stable for up to several weeks in closed containers.

6. By incorporation of solid micro-particles into the polymer we formed micro-rods with altered morphology which has the potential to potentially increase their foamability. Incorporation of large particles with diameters up to 5 times that of unmodified rods gave varied results but often led to the production of micro-rods with diameters similar to those of the entrapped particles. This behaviour suggests that the large particles have disrupted the shear flow processes during the formation of the micro-rods. The use of smaller micro-particles yielded thinner micro-rods with greater aspect ratios. Lumpy shellac micro-rods containing entrapped yeast cells showed excellent foam stabilising behaviour, with drainage being retarded when yeast cell lumps were present. This suggests that the lumps are enhancing the stability by blocking the Plateau borders within the foam, obstructing foam drainage and improving foam lifetimes. Magnetic micro-rods made from both ethyl cellulose and shellac have been successfully produced by incorporation of hydrophobised magnetic nano-particles, which could have potential for magnetically-targeted delivery. Ballooned micro-rods have also been successfully produced. These have been made in two ways. First, by the entrapment and subsequent thermal degradation of sodium bicarbonate micro-crystals within ethyl cellulose micro-rods, and secondly, by the entrapment of copper micro-particles and microwave radiation mediated localised heating of the ethyl cellulose micro-rods in which they have been trapped.

7. Finally, this technique has been further extended to the formation of micro-rod capsules, which could be used for the encapsulation and delivery of unpleasant tasting/smelling oil additives in food, whilst they can also provide stability for a food formulation. These micro-ampules were formed by mixing the oil desired for encapsulation into the dispersed phase polymer solution prior to injection into the continuous phase for micro-rod production. We produced micro-ampules with sunflower oil and cod liver oil trapped in shellac micro-rod capsules. In this case, the capsules were small, regular in size and shape, and contained a small number (often one) of pockets of oil. The use of ethyl cellulose as a capsule wall material

led to the formation of rods with the entrapped oil distributed throughout the structure in small, but highly numerous compartments. The addition of certain surfactants allowed for the formation of shellac micro-rod capsules with a greater number of smaller encapsulated pockets of oil. This suggests that the distribution of the oil within the micro-rod capsules is influenced by the surface energy of the interface between the polymer and the encapsulated oil phases and that this can be controlled by the use of surface active agents.

## SUGGESTIONS FOR FUTURE WORK

Due to the great number of potential variations for the systems described in this work, many areas of the thesis could be further investigated, and a number of areas exist which have not been explored yet. These include the following:

- Due to the success of coating hydrolysed cellulose nano-rods with ethyl cellulose in improving their foamability, further analysis, specifically TEM to find out how the nano-rods are being coated should be carried out, then further work on these nano-rods could be highly beneficial when used as foaming agents due to the small size of air bubble nano-rods of such dimensions should be able to adsorb to.

- An important area for further research involves characterisation of the foamability of modified ethyl cellulose micro-rods (ballooned rods, lumpy rods etc.) by comparison with standard ethyl cellulose rods. It is hoped that this could yield similar positive results shown by lumpy yeast-shellac micro-rods where drainage of water from aqueous foams formed by hand-shaking appeared to be retarded.

- Ethyl cellulose micro-rods containing encapsulated oil. These micro-rods possessed small pockets of entrapped oil distributed throughout the length of the micro-rods, and also leaching out, suggesting porosity. These properties could lead to the formation of hydrophobic micro-rods of tuneable wettability by

varying the concentration of entrapped oil, analogous to a series of micro-porous silicas with varied surface composition giving a range of hydrophobicities.

- It may be useful to further probe the ethyl cellulose cages produced as a result of drying the ethyl cellulose micro-rod-stabilised water-in-oil emulsions produced in chapter 5. If these micro-rod-stabilised drops could be coated with several layers of polyelectrolyte with alternating positive and negative charge, it may be possible to strengthen them so that they might survive the drying process, forming a new type of micro-capsule.

- Further work is required on producing foams stabilised by a mixture of cellulose nano-rods and ethyl cellulose nano-particles by a so-called 'foam scaffolding' mechanism. It would be beneficial if ethyl cellulose nano-particles of different size produced using a solvent change technique were used. Increasing the control over nano-particle size and concentration in the formulation could increase the synergistic scaffolding effect of the foam stabilisation.

- More detailed investigation on the effect of pH and electrolyte on foams stabilised by micro-rods is required in order to increase their foamability.